AFRL-SR-AR-TR-09-0110

# REPORT DOCUMENTATION PAGE



| 1. REPORT DATE | 2. REPORT TYPE | 3. DATES COVERED *(From - To)* |
|---|---|---|
| 31-01-2009 | Final | 01-01-2006 to 31-12-2008 |

**4. TITLE AND SUBTITLE**

Covert, Intelligent, and Spectrally-Efficient MIMO-Based Noise Radar Networks

**5a. CONTRACT NUMBER**
FA9550-06-1-0029

**5b. GRANT NUMBER**

**5c. PROGRAM ELEMENT NUMBER**

**6. AUTHOR(S)**

Ram M. Narayanan, Wiriyanto Darsono, Kyoung-Deuk Kim, Wei-Jen Chen, Qihe Pan, Shrawan C. Surender

**5d. PROJECT NUMBER**

**5e. TASK NUMBER**

**5f. WORK UNIT NUMBER**

**7. PERFORMING ORGANIZATION NAME(S) AND ADDRESS(ES)**

The Pennsylvania State University
Office of Sponsored Programs
110 Technology Center
The Pennsylvania State University
University Park, PA 16802

**8. PERFORMING ORGANIZATION REPORT NUMBER**

**9. SPONSORING / MONITORING AGENCY NAME(S) AND ADDRESS(ES)**

Air Force Office of Scientific Research/NE
875 North Randolph Street, Suite 325
Arlington, VA 22203
Dr Jon Sjogren

**10. SPONSOR/MONITOR'S ACRONYM(S)**
AFOSR

**11. SPONSOR/MONITOR'S REPORT NUMBER(S)**

**12. DISTRIBUTION / AVAILABILITY STATEMENT**

Distribution A – Approved for Public Release

**13. SUPPLEMENTARY NOTES**

**14. ABSTRACT**

The following tasks were accomplished:

1. Distributed adaptive beamforming using noise waveforms: The use of multiple radars for characterizing the radar cross section (RCS) of the target was investigated, and the RCS enhancement was quantified. A framework for inducing orthogonality in sequences and in polarization was developed to differentiate signals from various transmitters. Generalized Likelihood Ratio Test (GLRT) and Tapped Delay Line (TDL) beamforming were integrated.
2. RF tag approaches: The concept of using notched frequency sub-bands within the ultrawideband (UWB) noise waveform was assessed to identify re-reflections from different tags. Using an array of notched tags around the target, it was possible to infer target orientation. A system design for communication between radar and RF tags using UWB noise waveforms is proposed.
3. MIMO-based networking: A scheme for embedding multi-hop communication mechanism within the MIMO noise radar system was investigated for networking purposes. Orthogonal Frequency-Division Multiplexing (OFDM) was employed for communications, which was then inserted into notched sub-bands of the UWB noise signal. Multi-radar networked operation was proposed.

**15. SUBJECT TERMS**

MIMO, Noise Radar, RF Tag, Beamforming, Networking, OFDM

| 16. SECURITY CLASSIFICATION OF: | | | 17. LIMITATION OF ABSTRACT | 18. NUMBER OF PAGES | 19a. NAME OF RESPONSIBLE PERSON |
|---|---|---|---|---|---|
| a. REPORT | b. ABSTRACT | c. THIS PAGE | | | Ram M. Narayanan |
| Unclassified | Unclassified | Unclassified | None | 158 | 19b. TELEPHONE NUMBER *(include area code)* (814) 863-2602 |

# COVERT, INTELLIGENT, AND SPECTRALLY-EFFICIENT MIMO-BASED NOISE RADAR NETWORKS

# COVERT, INTELLIGENT, AND SPECTRALLY-EFFICIENT MIMO-BASED NOISE RADAR NETWORKS

## 1. OVERVIEW

In this proposal, we had proposed to develop, test, and implement a novel framework for a covert, intelligent, and spectrally-efficient noise radar network based upon multiple-input multiple-output (MIMO) architectures. The basic concept revolves around a covert ad-hoc ultrawideband (UWB) sensor network using random noise waveforms. In this configuration, various transmitters and receivers communicate with each other to form an intelligent, adaptive, optimal system with low probability of detection (LPD) and low probability of intercept (LPI). Our proposal sought to extend and enhance our work on noise radar developed over the past 12 years by incorporating recent advancements in communications theory, such as RF tags and MIMO channel concepts. These include topics such as MIMO networked transmitters and antennas, multiple adaptive polarization using an inverse water filling argument, fractal radar imaging at different levels of detail for different requirements, smart antennas, a radar communications channel using RF tags, which are integrated to form a system that can be termed "covert and intelligent". The minimal cross-interference between the network's uncorrelated noise sources also ensures that the system is "spectrally efficient".

MIMO systems are being increasingly used in radar, wherein multiple transmitters and receivers achieve better spatial resolution in radar images as well as a higher probability of detection. These advantages are often critical in military applications where the probability of missed detection has to be minimized as much as possible, irrespective of cost. Intelligent adaptive control can be implemented in such systems in various manners, including control of polarization and transmit power transmitted by different antennas in the system using the reverse filling argument (that has been successfully used in communications theory for various channels at various frequency levels), and by using spatial and temporal signal processing. Secure and covert node-to-node and node-to-base communication channels would be developed using RF tags, which are devices similar to the radio frequency identification devices (RFIDs) used in consumer applications. This would enable different radar systems to communicate with each other, and build a network which would be the basis for the adaptive control. The low probability of detection and intercept will be achieved using true noise and chaotic transmit waveforms.

The primary significance of this proposed project is to develop a unified force multiplier system for military applications involving target detection, battlespace surveillance, and target/terrain imaging. The order-of-magnitude advantages of the proposed system is that it is simultaneously *covert* (*i.e.*, transmissions undetectable by or unintelligible to hostile forces), *intelligent* (*i.e.*, able to adapt waveform features and allocate resources on-the-fly for enhanced performance), and *spectrally-efficient* (*i.e.*, optimally conserves spectral bandwidth by being able to pack more systems within the same frequency band). The impact of our proposed research are expected to be felt in numerous military theaters that use multiple radar systems, either as being part of a specific radar network or exploiting radars of opportunity.

The major tasks we had proposed to address were:

1. Study and development of waterfilling scheme for networked radar sensing,
2. Study and development of distributed adaptive beamforming using noise waveforms,
3. Study of covert RF tag approaches,
4. Design of noise radar system and MIMO-based network, and
5. Preparation of reports and publications.

## 2. RESEARCH ACCOMPLISHMENTS

### 2. 1. Beamforming and Multiple Beam Approaches

Consider the scenario in the MIMO radar system wherein the radars are collocated. In this case, we use a unique signal (waveform) transmitted by each single radar, and multiple waveforms are obtained from the entire radar set. The justification for multiple waveforms is to ensure that the radar system can reliably detect the target in case one transmitted signal experiences severe distortion, *i.e.*, multipath interference, fading, and so on, while detecting the target. This is implemented if we use more than one signal to illuminate and detect the target.

In this scenario, we need to use orthogonal signals so that the radar can "recognize" its own transmitted signal and cancel out other signals transmitted by other radars. In this case, orthogonality can be performed either in frequency (using different frequency range) by using different orthogonal sets of pulse sequences, or in polarization by using different polarization combinations (horizontal or vertical polarization). For now, we consider the case where we use different orthogonal sets of pulse sequences, *i.e.*, by employing orthogonal noise-like pseudorandom pulses as the transmitted waveforms. Adversaries and others that do not belong to the friendly group will observe these transmitted waveforms as noise. Such a waveform type will induce the covertness in our system and establish a low probability of detection (LPD) capability.

Let us consider a MIMO configuration that employs two radars, *i.e.*, Radar 1 and Radar 2. Each radar (receiver) will then obtain reflected waveforms from the illuminated target that are transmitted by each radar. However, since the transmitted signals are orthogonal to each other, each radar's receiver cancels out the unintended waveform due to orthogonality. This can happen because each radar has knowledge about its own transmitted waveform, and hence can "match-filter" and processes only its own waveform. Fig. 1 shows typical transmit and receive signals for Radars 1 and 2. Although the receive signals have additional noise brought about in the propagation channel, we note that thresholding can help recover the original transmit sequence.

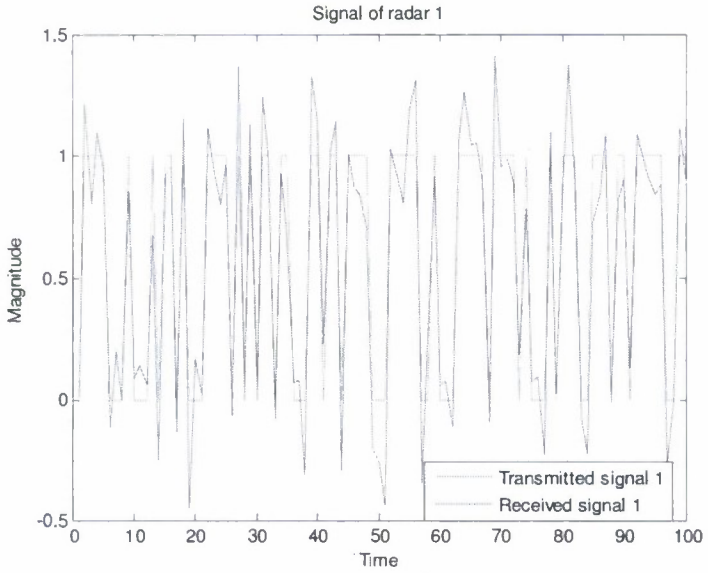


(a)

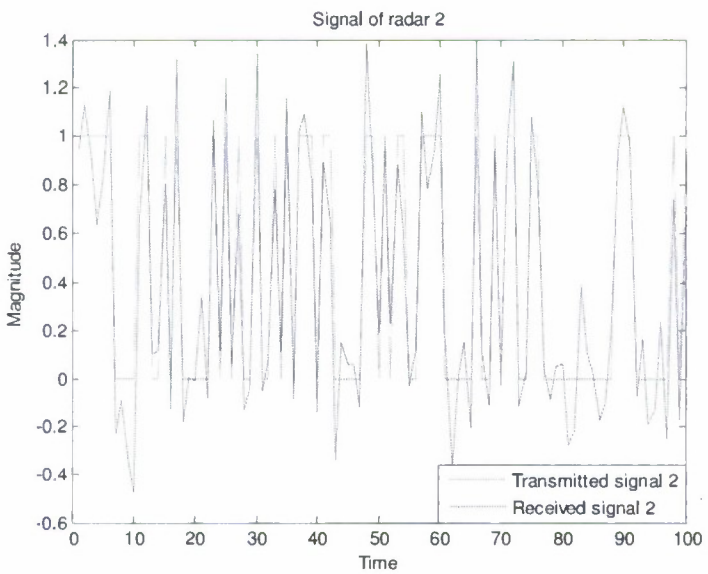


(b)

Fig. 1: Transmitted and received signals by (a) Radar 1 and (b) Radar 2.

Fig. 2 shows that our radars still have the capability to recognize the range to the target through the indicated "peak" of the autocorrelation process. Since the radars are collocated, the delays experienced by the transmitted signals that impinge upon the intended target and are received by the radars are approximately the same between one transmitted signal and the other.

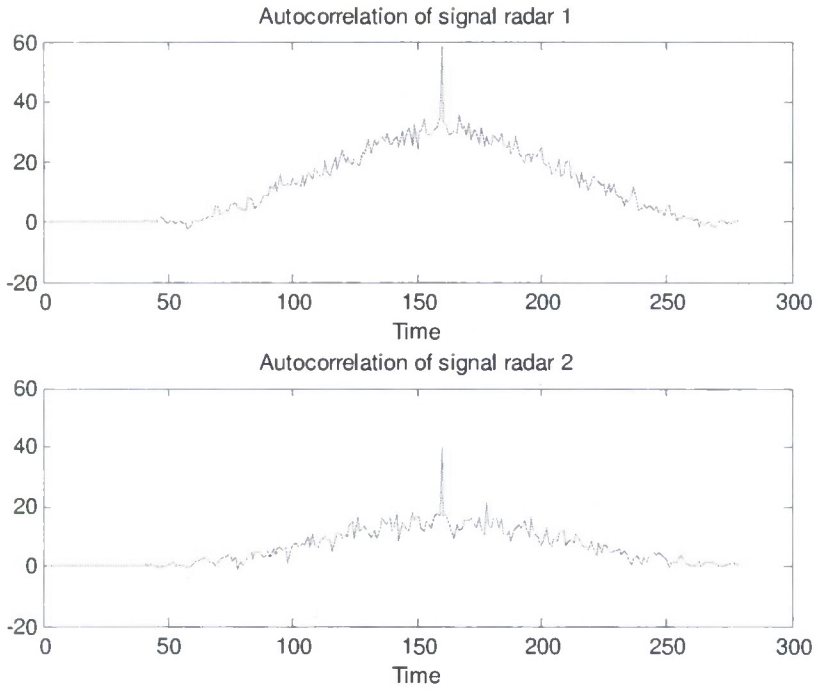


Fig. 2: The autocorrelations of waveforms of Radar 1 (top) and Radar 2 (bottom).

Electromagnetic waves, with any specified polarization, are normally diffracted or scattered in all directions when incident on a target. These scattered waves are broken down into two parts:

1. Waves that have the same polarization as the receiving antenna.
2. Waves that have different polarization, to which the receiving antenna does not respond.

The two polarizations are orthogonal and are referred to as the Principal Polarization (PP) and Orthogonal Polarization (OP) respectively. The intensity of the scattered PP energy is used to define target Radar Cross Section (RCS).

The received power at radar is a function of several parameters[1], *i.e.*, a function of the transmitter system, the propagation path from the transmitter system to the target, the propagation path from the target to the receiving system, and the receiving system. The relationship can be expressed as:

$$P_r = \underbrace{\frac{P_t G_t}{L_t}}_{\text{Transmitting system}} \underbrace{\frac{1}{4\pi r_t^2 L_{mt}}}_{\text{Propagating medium}} \underbrace{\sigma}_{\text{Target}} \underbrace{\frac{1}{4\pi r^2 L_{mr}}}_{\text{Propagating medium}} \underbrace{\frac{G_r \lambda_0^2}{4\pi L_r}}_{\text{Receiving system}} \underbrace{\frac{1}{L_p}}_{\text{Polarization effect}} \quad (1)$$

[1] G. T. Ruck, D.E. Barrick, W.D. Stuart, and C.K. Krichbaum, *Radar Cross Section Handbook*, Vol. 1. New York, NY: Plenum , 1970.

where

$P_r$ = received power,
$P_t$ = transmitter power,
$G_t$ = the gain of the transmitting antenna in the direction of the target,
$L_t$ = numerical factor to account for losses in the transmitting system,
$L_r$ = numerical factor to account for losses in the receiving system,
$r_t$ = range between the transmitting antenna and the target,
$\sigma$ = radar cross section,
$L_{mt}, L_{mr}$ = numerical factors which allow the propagating medium to have loss,
$r$ = range between the target and receiving antenna,
$G_r$ = gain of the receiving antenna in the direction of the target,
$\lambda_0$ = radar wavelength,
$L_p$ = numerical factor to account for polarization losses.

By rearranging (1), the formula for the RCS can be written as:

$$\sigma = \frac{P_r L_r (4\pi)}{G_r \lambda_0^2} \frac{L_t}{P_t G_t} L_{mr} L_{mt} (4\pi)^2 r_t^2 r^2 L_p \tag{2}$$

The RCS fluctuates as a function of radar aspect angle and frequency. For simplicity, isotropic point scatterers are considered. Let us consider the geometry in Fig. 3. Two unity (1-m$^2$) isotropic scatterers are aligned, spaced 1 meter, and placed along the radar line of sight, *i.e.*, zero aspect angle in (a). In other case, radar sees the target with an aspect angle of 45° shown in (b).

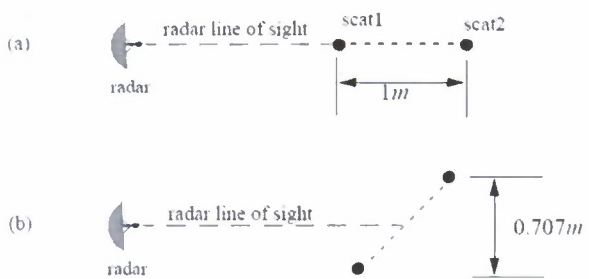


Fig. 3: RCS dependency on aspect angle: (a) 0° aspect angle, (b) 45° aspect angle.

We also characterize the RCS using a multiple-input multiple-output (MIMO) architecture of three different antennas which are spaced to form equilateral triangle with the midpoint of the two scatterer centers (of the target) as the center of the triangle, as shown in Fig. 4. In this case, we assume each of the three radars transmit an uncorrelated noise signal.

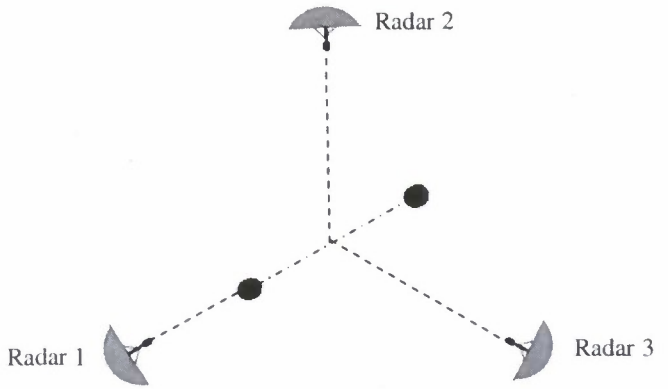


Fig. 4: MIMO radar configuration with three equally spaced radars in azimuth.

In Fig. 4, Radar 1 will receives the scattered signals transmitted by Radar 1 (monostatic or backscattered RCS), and also transmitted by the other two radars, *i.e.*, Radar 2 and Radar 3 (each is considered as a bistatic RCS). Assume that Radar 1 can perfectly differentiate different noise waveforms transmitted by itself, Radar 2 and Radar 3. At any time instant, each radar will experience different RCS for the target since each of them sees the two target scattering centers from different aspect angles. The angle for the bistatic RCS (transmitter-receiver) is the summation of the angles for the transmitter-target and the target-receiver[2].

Similar phenomena occur at Radars 2 and 3. Radar 2 will receive the scattered signals transmitted by itself and, at the same time, transmitted by Radars 1 and 3, while Radar 3 will receive the scattered signals transmitted by itself and also transmitted by Radars 1 and 2.

We can then assume that the RCS caused by the two scatterer centers is the accumulation of the RCS values seen by each radar, where the available transmitted power is distributed among the three radars. This is justified due to the fact that powers (proportional to RCS) add when the signals are uncorrelated. In this case, we can also assume that the accumulated RCS measured by Radar 1 is the same as that measured by Radar 2 or Radar 3.

The RCS dependency on frequency is of interest. Consider two scattering centers are aligned as shown in Fig. 5. Assume that the distance between *scat1* and *scat2* is 0.25 m and that we are using a wideband C-Band noise radar operating over the 4-5 GHz frequency range. The RCS dependency on frequency is shown in Fig. 5. Since we are considering wideband frequency operation, the RCS is calculated based upon single frequency as well as frequency-averaging over a 100 MHz bandwidth for each point on the plot. The advantage of frequency-averaging in reducing RCS variations, especially the deep fades, is clearly seen.

[2] M. I. Skolnik, *Introduction to Radar Systems*, 3rd Edition. New York, NY: McGraw Hill, 2001.

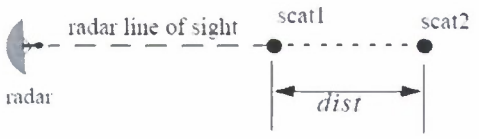


Fig. 5: Scatterer geometry for computing RCS dependency on frequency.

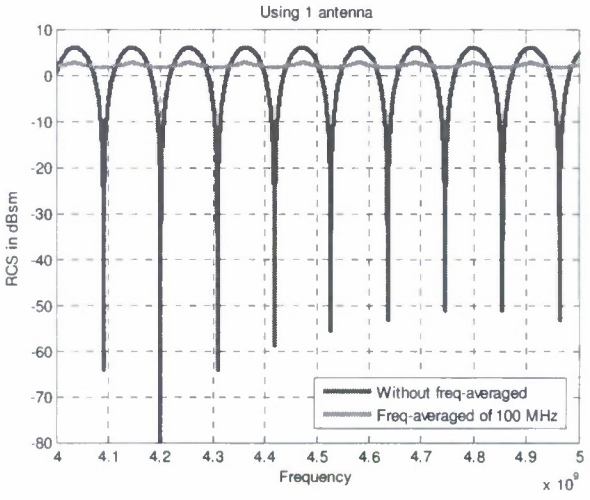


(a)

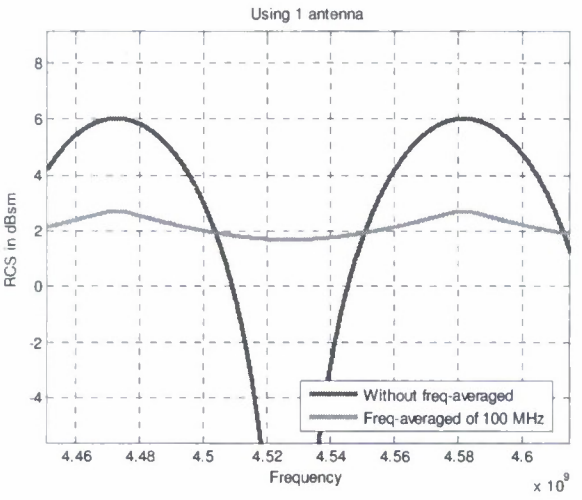


(b)

Fig. 5: RCS in monostatic radar case for (a) single frequency and (b) frequency-averaging.

If we incorporate the MIMO architecture shown in Fig. 4, with the aspect angle is fixed 0° with respect to the Radar 1, we get the RCS dependency on frequency as shown in Fig. 6.

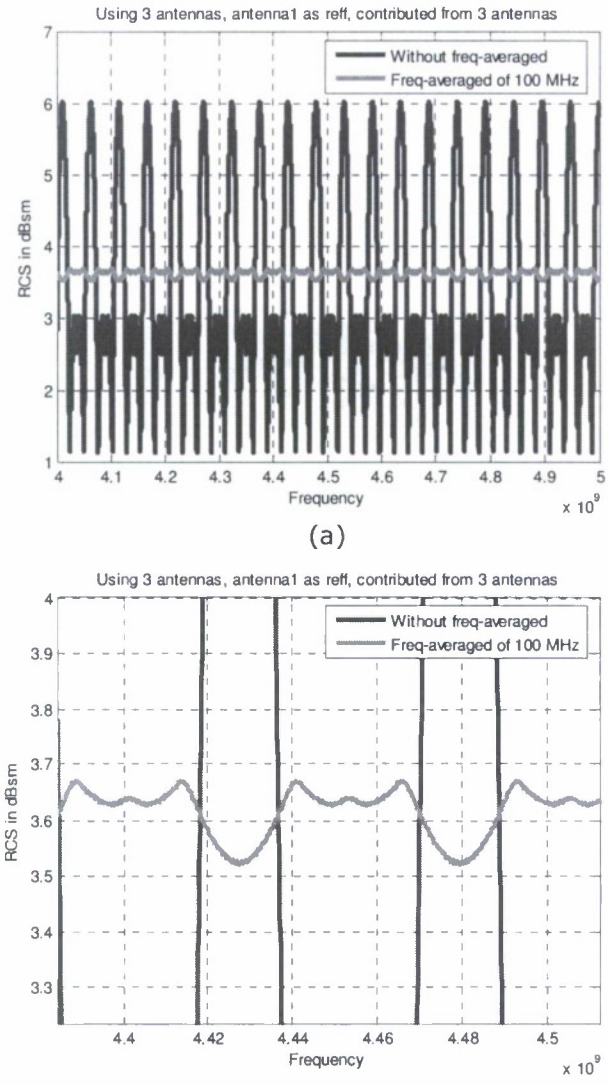


Fig. 6: RCS enhancement with three radars in a MIMO architecture for (a) single frequency, and (b) frequency-averaging.

Comparing Fig. 5 and Fig. 6, we can see that the frequency-averaged RCS for the MIMO architecture is higher than that for the single radar system. Moreover, the fluctuation of frequency-averaged RCS within the frequency range of 4-5 GHz in the MIMO architecture is much less than that in the single radar system. Furthermore, we notice that the single-frequencies RCS in single radar system experiences several very deep fades which is not the case for the single-frequencies RCS in the MIMO architecture.

In the MIMO-based noise radar architecture, we have multiple transmitted signals. Therefore, orthogonality is essential in MIMO-based architecture, in order that the receivers can

differentiate and recognize which signals originate from which transmitter. The orthogonality can take place as orthogonal in sequences, frequency-bands, or polarization.

Orthogonality in sequences means that the transmitters emit orthogonal random sequences (similar to the Code Division Multiple Access or CDMA in the wireless communication system). The receivers have knowledge about the different orthogonal sequences transmitted and know that a particular transmitter only transmit a particular sequence pattern. In order to determine which transmitter that a particular signal originates from, the receiver simply correlates the received signal with the different set of sequences it has. When the correlation result yields a high "peak", it means that the transmitted signal has been recognized.

Orthogonality in frequencies means that each transmitter emits a signal that is orthogonal (unique) in frequency-band to the others. The receivers have different band-pass filters and it has the capability to pass only the signals that has the expected frequency band. In this way, the receiver can recognize from which transmitter this signal comes from.

Another possible orthogonality can be induced in polarization. In this case, the transmitter can transmit either using vertical polarization or horizontal polarization. For example, Radar 1 can use horizontal polarization to transmit its signal, while Radar 2 can use vertical polarization. Thus, if adequate polarization isolation exists, each radar receive antenna will capture only the signal sent from its own transmit antenna that obviously matches it in polarization.

Thus, orthogonality is an important aspect in MIMO radar. By transmitting orthogonal signals, we aim to maximize the probability that radar can distinguish the signals transmitted by different transmitters and in turns to optimize the probability of detection of the target (and to increase the signal to noise ratio (SNR)). Therefore, transmitting orthogonal signals can also be seen as one of the optimization efforts, specifically waveform optimization.

The purpose of the proposed MIMO radar configuration in Fig. 7 is to exploit the redundancy of the transmitted signal. In this kind of configuration, the antennas are collocated or placed close to each other, *i.e.*, as in an antenna array. Therefore, if one "route" for the signal (signal transmitted, target illuminated and rereflected, and signal received) is experiencing a deep fade, there will be other available "good routes" in order to accomplish the radar ranging and imaging purposes. We can certainly use real random noise as the transmitted signal. The receivers need to recognize the frequency dependent transmitted orthogonal signals in order to distinguish the reflected signals (from the target) before we apply the adaptive beamforming process for estimation. The orthogonal signals are separated using appropriate bandpass filters. There are at least two different orthogonality approaches that could be applied, as described in the following. For simplicity, let us assume that there are two transmitters and two receivers.

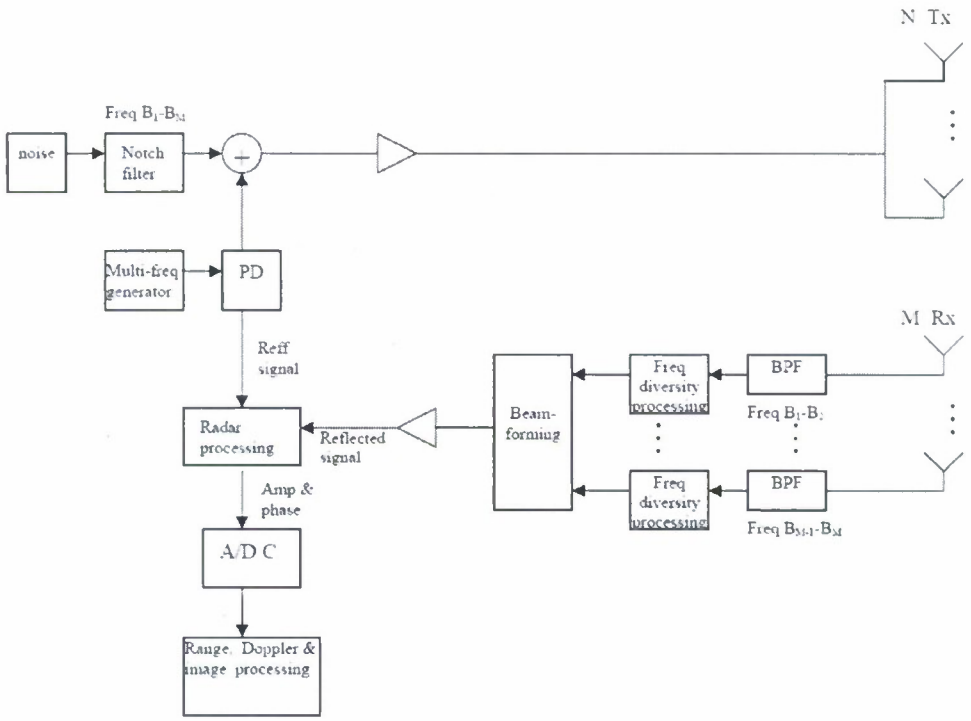


Fig. 7: MIMO radar configuration with collocated antennas with noise transmissions.

*Use of orthogonal sequences:*

This method is shown in Fig. 8. In Fig. 8(a) (transmitter portion), two orthogonal sequences are generated. To generate two or more orthogonal sequences, initial weight vectors were used[3]. These weight vectors are derived directly from the sample covariance matrix of the observed data. The initialization methods considered are based on:

- Gram-Schmidt orthogonalization,
- Eigen decompositon,
- QR decomposition.

All of these methods yield orthogonal, or nearly orthogonal, output signals. In our case, we use QR decomposition method to determine the initial weight vectors.

Each of the two orthogonal sequences is modulated using BPSK modulation with frequency carrier of 5.15 GHz. This signal is "inserted" into the 5.1-5.2 GHz notched band of 5-6 GHz bandlimited noise signal to camouflage the information signal, and thus to introduce the covertness to the system.

[3] T. E. Biedka, "A comparison of initialization schemes for blind adaptive beamforming," *Proceedings of the 1998 IEEE International Conference on Acoustics, Speech, and Signal Processing (ICASSP'98)*, Vol. 3, Seattle, WA, pp. 1665-1668, May 1998.

These two modulated signal are transmitted through the added-white-Gaussian-noise (AWGN) channel that has signal-to-noise ratio (SNR) of 35 dB, and Channel 1 and 2 add up.

In Fig. 8(b) (receiver portion), BPSK demodulator with the passband frequency of 5.1-5.2 GHz is used to recover the notched band and to retrieve the carrier frequency modulated by the orthogonal sequences. The orthogonal sequences are obtained by demodulating these signals using 5.15 GHz frequency carrier. The receiver will be able to distinguish the transmitted sequences by looking at the correlation results (the receiver has knowledge about the transmitted signals) as shown in Fig. 9(a) and Fig. 9(b). Also, after going through the beamforming process, the receiver can determine the estimated transmitted sequences.

In Fig 8, there are two orthogonal random sequences that can be generated using the QR decomposition method. The random sequences take place in the form of bipolar binary number that is orthogonal to each other, as shown in Table I for example.

TABLE I: EXAMPLE OF BIPOLAR ORTHOGONAL SEQUENCES

| Time | 0 | 1 | 2 | 3 | 4 | 5 | 6 | 7 | 8 | 9 |
|---|---|---|---|---|---|---|---|---|---|---|
| s1 | 1 | -1 | 1 | 1 | 1 | 1 | -1 | 1 | -1 | 1 |
| s2 | 1 | -1 | -1 | -1 | -1 | -1 | 1 | 1 | -1 | 1 |

After going through the modulation processes, they are transmitted by antenna Tx1 and antenna Tx2. The receiver will then demodulate the signals. It will be able to distinguish the two sequences, by observing the result of the cross-correlation and auto-correlation process. As noted in Fig. 9(a) and Fig. 9(b), when the sequence is correlated by itself (*i.e.*, auto-correlation), we can see the "obvious peak" compared to when it is correlated with another sequence (*i.e.*, cross-correlation).

However, there is a slight problem here. As we see in Table I, some of the transmitted signals have different "polarity". In the adaptive beamforming process, we need to apply some weights on the receiver outputs to make a decision. The weights combination on the receiver is adaptive (*i.e.*, can change from time to time); however, it should always be the same combination for different transmitted sequences. The beamforming process should be able to solve this if there is some "workable" combination of the two transmitted sequences. However, this will be a difficult task for the beamforming, especially when we have more antennas that transmit different sequences (*i.e.*, if there are s3, s4, and so on). Therefore, we try to come up with a different way of inducing orthogonality for the transmitted signals, such as orthogonality in frequency.

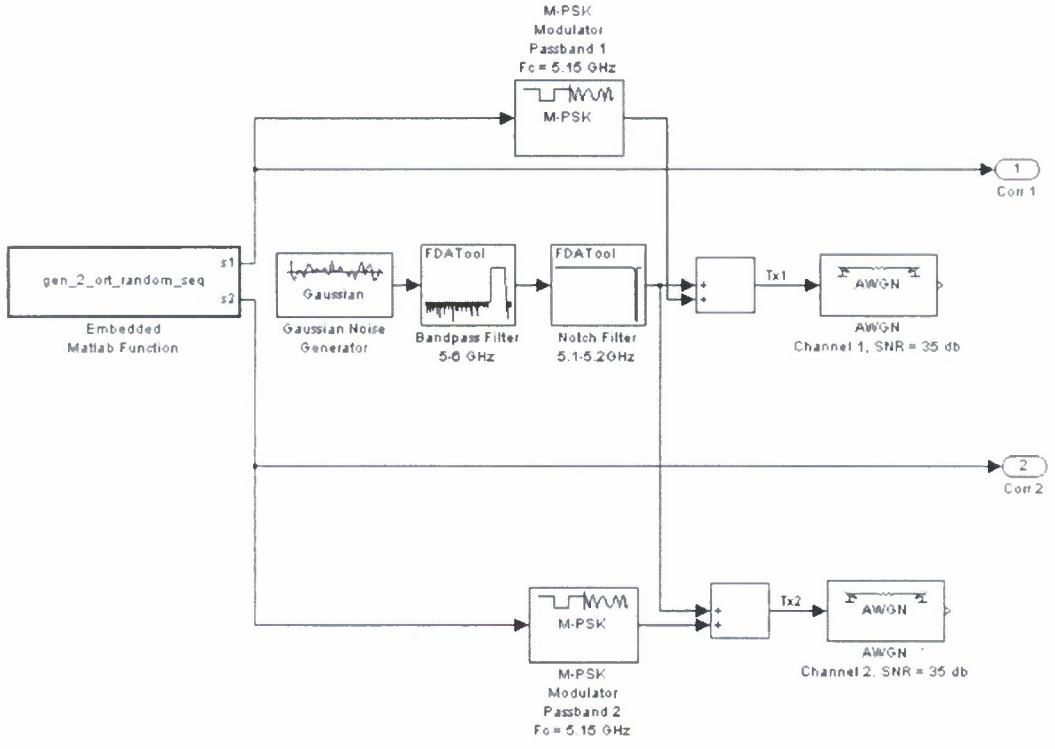


(a)

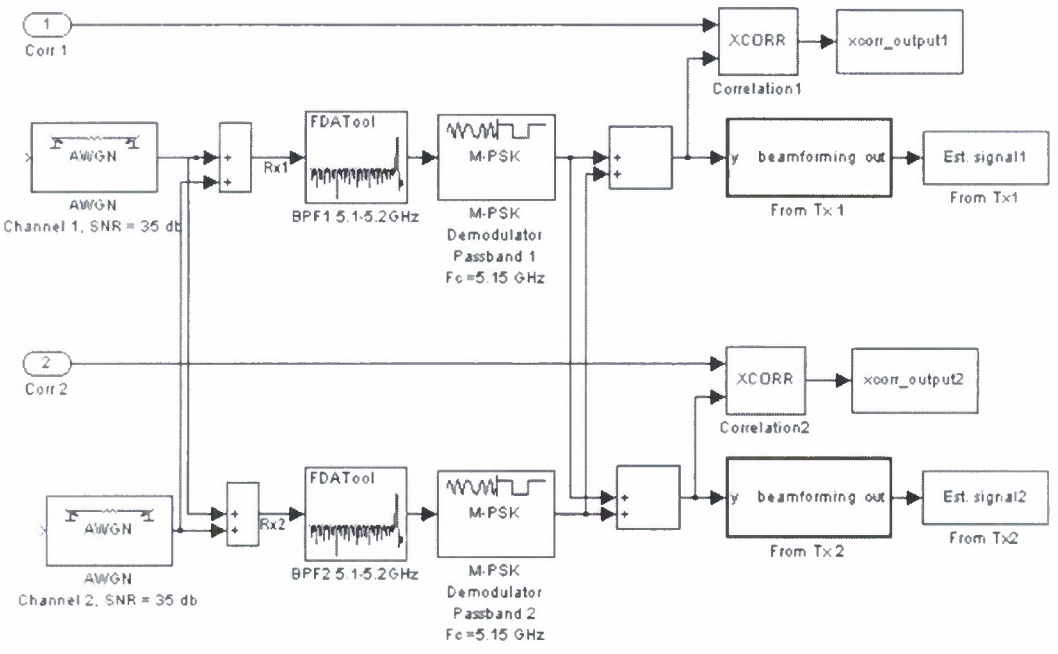


(b)

Fig. 8: MIMO radar using orthogonal sequences:
(a) transmitter portion, and (b) receiver portion.

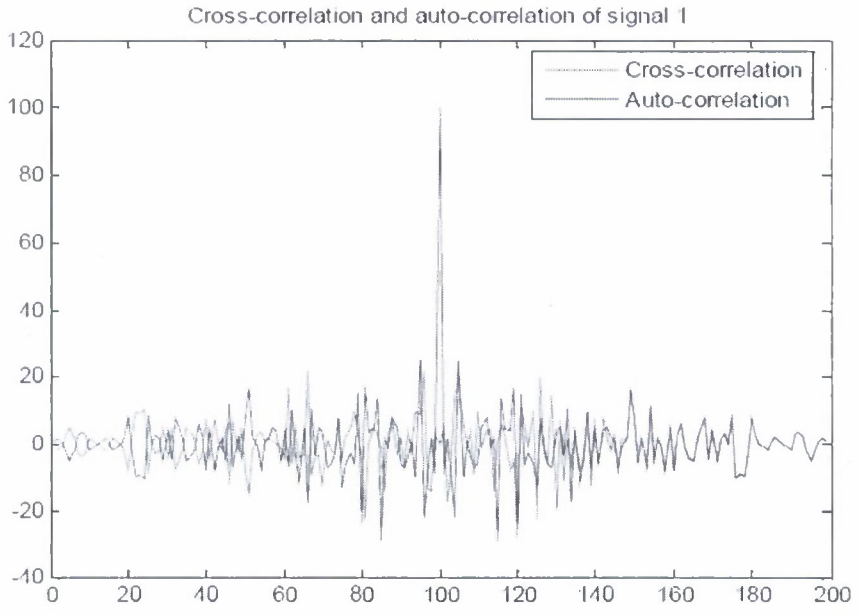


(a)

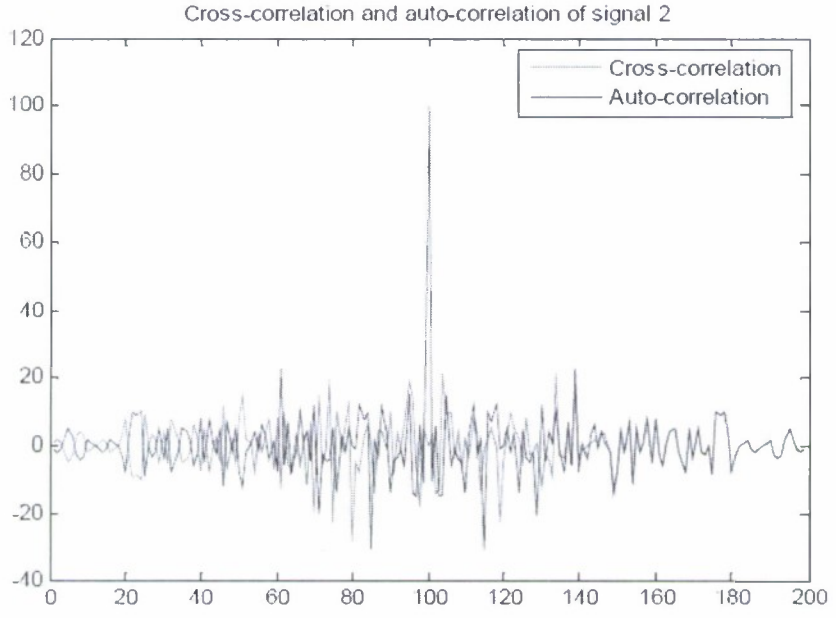


(b)

Fig. 9: The auto-correlation and cross-correlation of (a) transmitted signal 1, and (b) transmitted signal 2.

*Use of orthogonal frequency bands:*

This method is shown in Fig. 10. In this scheme, we generate one random sequence which will modulate different frequency carriers, i.e. 5.15 GHz for Transmitter 1 (we call this s1) and 5.25 GHz for Transmitter 2 (we call this s2). As in the previous method, we have bandlimited noise over 5-6 GHz. However, this time it is notched at two different frequency bands: one at 5.1-5.2 GHz (which is going to be "inserted" by s1) and the other one at 5.2-5.3 GHz (which is going to be "inserted" by s2). The signal s1 is transmitted by antenna 1 and signal s2 is transmitted by antenna 2.

These signals are transmitted through AWGN channel that has signal-to-noise-ratio (SNR) of 35 dB and is combined at the receiver side.

At the receiver side, each Receiver 1 and Receiver 2 obtains the signals that contain both frequency bands (*i.e.*, 5.1-5.2 GHz and 5.2-5.3 GHz). Two BPSK demodulators are used to demodulate the received signals, one at the frequency band of 5.1-5.2 GHz (with carrier frequency of 5.15 GHz), and the other one at the frequency band of 5.2-5.3 GHz (with carrier frequency of 5.25 GHz). The retrieved orthogonal sequences are combined through the adaptive beamforming process to estimate the original transmitted random signals.

In order to observe the advantage and feature that can be obtained using MIMO architecture, we intend to build a testbed for our MIMO-based noise radar system. We can use this testbed as an essential (basic) framework for testing MIMO-based architecture, which can always be expanded on different architectures, especially when we want to incorporate orthogonality within the transmitted signals.

Fig. 11 shows the block diagram for MIMO Radar Testbed. The testbed is designed to demonstrate the MIMO operation for C-Band radar (4-8 GHz frequency range), specifically that operates on 5 GHz frequency. Four antennas are used as transmitters and four other antennas are used as receivers.

To simulate the MIMO operation, each of the four transmitter and four receivers operates consecutively (controlled by a PC). The sequence can be arranged in the form of a transmitter-receiver combination as the following: Tx1-Rx1, Tx1-Rx2, Tx1-Rx3, Tx1-Rx4, Tx2-Rx1, ..., Tx4-Rx4. For every Tx-Rx combination, the target is going to be scanned by variable delay-lines in order to track its exact range location and speed, from the perspective of that particular pair of antennas.

There are a total of 256 stepped 8-bit delay-lines. The exact location and speed of the target from each Tx-Rx perspective can be determined whenever the maximum value of cross-correlation is reached for that particular transmitter-receiver pair (performed by the mixers and I/Q detector). Therefore, the information about the target range location and speed is expected to be more accurate, since it is tracked from 4×4=16 different antenna positions.

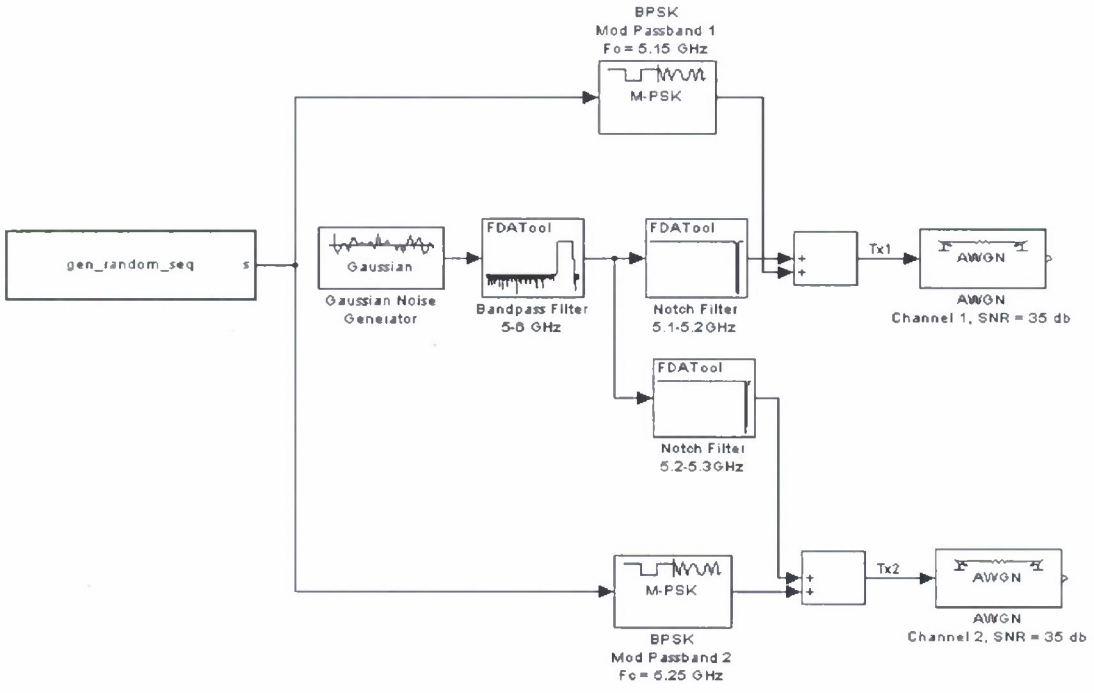


(a)

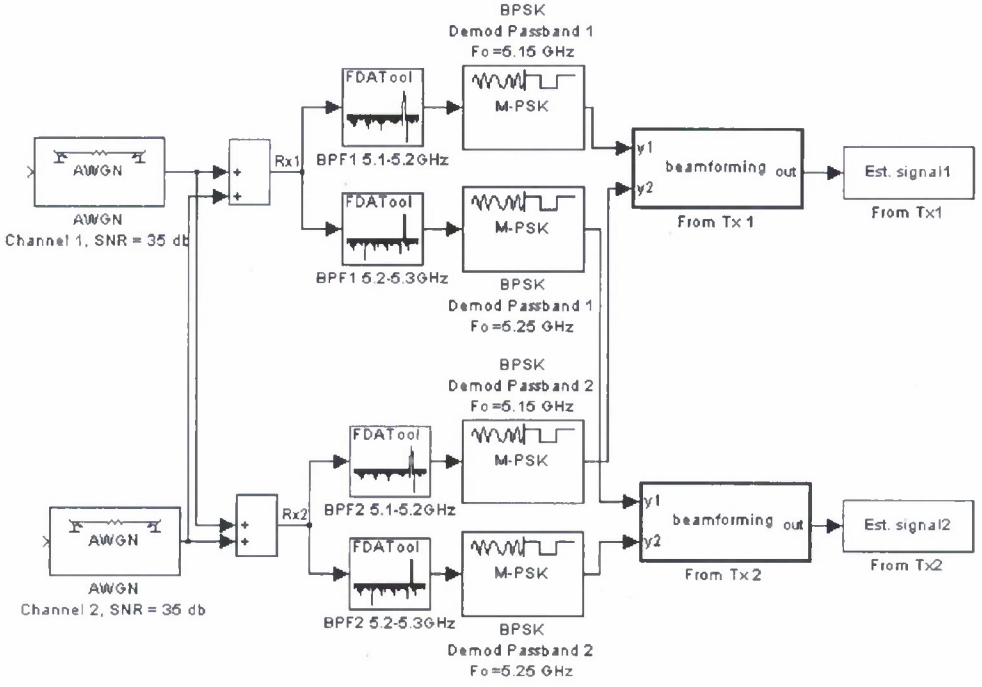


(b)

Fig. 10: MIMO radar using orthogonal frequencies:
(a) transmitter portion, and (b) receiver portion.

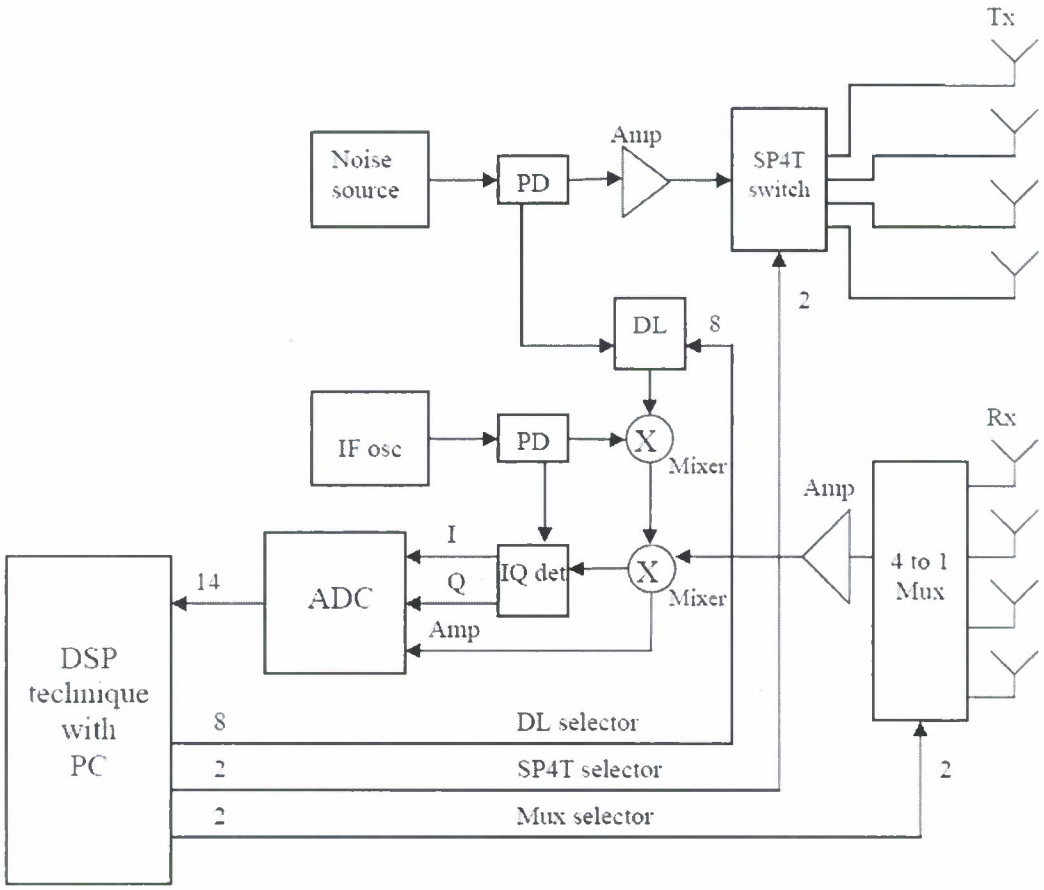


Fig. 11: Block diagram of the proposed MIMO Noise Radar Testbed.

This year, we concentrated on detection performance of multi-input multi-output (MIMO) radar system in a cluttered environment. We were concerned with detecting a target embedded in clutter whose amplitude is described as a correlated K-distribution. We observed that because of one of the characteristics of MIMO, viz. spatial diversity, the receiver operating characteristic (ROC) curve improves as the number of transmitters increases. We also discuss a number of factors of MIMO radar performance.

*Spatial diversity in MIMO radar:*

It is well known that in conventional radar system, fluctuations of the target radar cross section (RCS) degrade radar performance. A novel idea to limit such degradation is by

collecting more spatial samples[4]. Obviously, if those samples are highly correlated, they are helpless for improving the radar performance. For collecting the independent samples and achieving the spatial diversity, there are several requirements. First of all, unlike standard and original phased-array radar only transmitting coherent signals, the multiple probing signals in MIMO may be independent or correlated with each other. Second, transmitters will be separated with sufficient distance. As a result, it makes the signals illuminating at different "aspects" of the target[5]. Here is a brief explanation for the independent samples.

Given that MIMO radar is in its infancy, there is no standard definition of what it is. It is common, although not ubiquitous, that a bistatic radar configuration comes under the purview of MIMO radar. Such a scenario is depicted in Fig. 12. The target consists of multiple scatterers organized in the form of a linear array. There are $M$ elements in the transmitter array and $N$ elements in the receiver array.

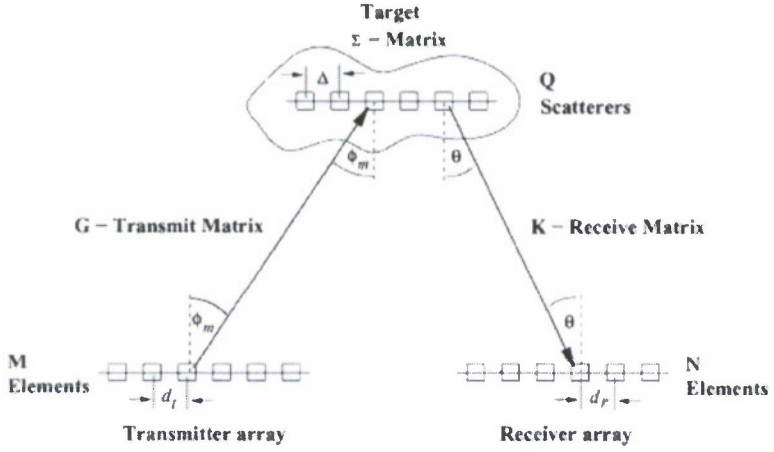


Fig. 12: Bistatic radar scenario. The target consists of multiple scatters organized in the form of a linear array.

Assuming there are $Q$ scatterers in the target, and each of them is independent and identically distributed (i.i.d.) with zero mean and unit-variance. Therefore they can be represented as Gaussian complex random variables $\zeta_q$. So, the target is modeled by the diagonal matrix

$$\sum = \frac{1}{\sqrt{2Q}} \begin{pmatrix} \zeta_0 & 0 & \cdots & 0 \\ 0 & \zeta_1 & \ddots & \vdots \\ \vdots & \ddots & \ddots & 0 \\ 0 & \cdots & 0 & \zeta_{Q-1} \end{pmatrix} \tag{3}$$

[4] E. Fishler, A. Haimovich, R. Blum, D. Chizhik, L. Cimini, and R. Valenzuela, "MIMO radar: an idea whose time has come," *Proc. 2004 IEEE Radar Conference*, Philadelphia, PA, pp. 71-78, April 2004.

[5] N.H. Lehmann, E. Fishler, A. Haimovich, R.S. Blum, D. Chizhik, L.J. Cimini, and R.A. Velenzuela, "Evaluation of transmit diversity in MIMO-radar direction finding," *IEEE Transactions on Signal Processing*, **55**(5), pp. 2215-2225, May 2007.

Then, considering the radiation from transmitters to every scatterer, the signal vector induced by $m^{th}$ transmit antenna is given by

$$g_m = \left[1, e^{-j2\pi \sin\phi_m \Delta_2/\lambda}, \ldots, e^{-j2\pi \sin\phi_m \Delta_{Q-1}/\lambda}\right] \tag{4}$$

Similarly, from scatterers to receivers, the signal vector received by $n^{th}$ receive antenna is given by

$$k(\theta) = \left[1, e^{j2\pi \sin\theta\Delta/\lambda}, \ldots, e^{j2\pi \sin\theta(Q-1)\Delta/\lambda}\right] \tag{5}$$

Last, a plane wave signal arriving at the array at the angle $\theta$ excites the elements of the array with phase shifts given by the vector

$$a(\theta) = \left[1, e^{-j2\pi \sin\theta d_r/\lambda}, \ldots, e^{-j2\pi \sin\theta(N-1)d_r/\lambda}\right] \tag{6}$$

With above definitions, the received signals which originate from $m^{th}$ transmitter and reflected by the target are given by

$$r_m = a(\theta)k^T(\theta)\sum g_m s_m \tag{7}$$

Moreover, since the space of receivers supposed to be smaller than half of wave-length to achieve unambiguous direction finding, without loss of generality, $k(\theta)$ can be replaced with $1_Q = [1,\ldots,1]^T$. Then, we can modify (7) into

$$r_m = a(\theta)1_Q \sum g_m s_m = a(\theta)\alpha_m s_m \tag{8}$$

For achieving independence, $E\{\alpha_m^* \alpha_{m+1}\} = 0$.

$$\begin{aligned} E\{\alpha_m^* \alpha_{m+1}\} &= E\{g_m^H \sum{}^H 1_Q 1_Q^T \sum g_{m+1}\} \\ &= g_m^H E\{\sum{}^H 1_Q 1_Q^T \sum\ \} g_{m+1} = \frac{1}{2Q} g_m^H I_Q g_{m+1} = 0 \end{aligned} \tag{9}$$

$$g_m^H g_{m+1} = \sum_{q=0}^{Q-1} e^{j2\pi[(\sin\phi_{m+1} - \sin\phi_m)q\Delta/\lambda]} = 0 \tag{10}$$

Approximate the difference of sine terms in (10) as follows:

$$\sin\phi_{m+1} - \sin\phi_m \approx d_t / R \tag{11}$$

where $R$ is the distance between target and transmitters. Using this in (10), we get

$$\sum_{q=0}^{Q-1} e^{j2\pi[(d_t/R)q\Delta/\lambda]} = 0 \tag{12}$$

Orthogonality is achieved when

$$\frac{d_t\Delta}{\lambda R} = \frac{1}{Q} \tag{13}$$

However, for large $Q$, (12) is approximately met when

$$\frac{d_t\Delta}{\lambda R} \geq \frac{1}{Q} \tag{14}$$

That means if the distance between transmitters is larger than $\lambda R/\Delta Q = \lambda R/D$ ($D$ is the size of target), the reflected signals from the transmitted signals emanating from different transmitters are independent of each other.

*Advantages of MIMO radar system:*

As we mentioned in last section, the biggest differences between MIMO and phased-array radars are the fact that MIMO radars have independent transmitting waveforms and spatial diversity. In fact, they open the way to a variety of technologies to improve the radar performance, or to outperform over phased array system.

For example, it is shown that the detection probability is dramatically enhanced because of the efforts in stabilizing the reflected power[6]. Because MIMO supports additional dimensions, the Cramer-Rao bound (CRB) of estimating direction of arrival (DOA) is decreased[7]. MIMO systems have been designed for clutter which is much larger than the target[8]. Therefore, the reflected signals from target can be coherently demodulated and its power can be accumulated. However, reflected signals from clutter will be independent, and their power is dispersed. It has also been shown that MIMO has better identifiability than a phased-array system[9]. In other words, under certain acceptable accuracy in estimating DOA, MIMO is able to detect more targets than phased array. Accuracy may depend on algorithms, so they apply CRB to evaluate the achievable accuracy.

---

[6] E. Fishler, A. Haimovich, R.S. Blum, L.J. Cimini, D. Chizhik, and R.A. Valenzuela, "Spatial diversity in radars-models and detection performance," *IEEE Transactions on Signal Processing*, **54**(3), pp. 823-838, March 2006.

[7] S.M. Kay, *Fundamentals of Statistical Signal Processing – Estimation Theory*. Prentice Hall: Upper Saddle River, NJ, 1993.

[8] X.Z. Dai, J. Xu, Y.N. Peng, and X.G. Xia, "A new method of improving the weak target detection performance based on the MIMO radar," *Proc. International Conf. on Radar (CIE'06)*, Shanghai, China, doi: 10.1109/ICR.2006.343265, October 2006.

[9] J. Li and P. Stoica, "MIMO Radar with colocated antennas," *IEEE Signal Processing Magazine*, 24(5), pp. 106-114, September 2007.

Besides the performance improvements mentioned above, there are several techniques that can be applied in MIMO radar which are not suitable for the phased array radar system. This is because MIMO has a very powerful characteristic, viz. orthorgonality between the reflected signals from different transmitters. It guarantees that the covariance matrix of received signals will be full rank. Therefore, it is possible to use adaptive location and detection techniques directly. Actually, we can say it is another significant advantage of MIMO radar system, since adaptive techniques are known to have much better resolution and much better interference rejection. The following sections depict two examples about how we apply such adaptive algorithms in MIMO.

*Multiple signal classification (MUSIC):*

Consider multiple signal classification (MUSIC) algorithm as a first example[10,11]. Without a doubt, the covariance matrix of received signal can be treated as the summation of two matrices. One is for noise, the other is for reflected signal which is a space constructed by the target direction vectors. The idea of MUSIC is to project the potential direction of received signal to the noise subspace. If the test direction belongs to signal subspace, the projection should be zero. This is because the signals and noise subspaces are independent of each other. Therefore, if we take the inverse of the projection, the peaks are caused only by the target directions.

Moreover, for correctly determining the number of targets, a requirement for signal covariance matrix is its rank should be equal to that number. With the features of MIMO, there is no difficulty to achieve that. For detailed formulation, we can rewrite (8) after matched filter and normalization as

$$R_m^{"} = \begin{bmatrix} r_{m,1} \\ r_{m,2} \\ \vdots \\ r_{m,N} \end{bmatrix} = \begin{bmatrix} a(\theta_1) & a(\theta_2)... & a(\theta_P) \end{bmatrix} \begin{bmatrix} \alpha_{m,1} \\ \alpha_{m,2} \\ \vdots \\ \alpha_{m,P} \end{bmatrix} + \begin{bmatrix} Z_1 \\ Z_2 \\ \vdots \\ Z_N \end{bmatrix} \tag{15}$$

Here, $P$ is the number of targets, $Z_n$ is additive white Gaussian noise (AWGN) at the $n^{th}$ receiver. $r_{m,n}$ is the received signal at the $n^{th}$ receiver from the $m^{th}$ transmitter. The covariance is calculated from

$$E\left\{R^{"}R^{"H}\right\} = \frac{\sum_{m=1}^{M} R_m^{"} \times R_m^{"H}}{M} \tag{16}$$

[10] B. Friedlander and A.J. Weiss, "Direction finding using noise covariance modeling," *IEEE Transactions on Signal Processing*, **43**(7), pp. 1557-1567, July 1995.

[11] R. Schmidt, "Multiple emitter location and signal parameter estimation," *IEEE Transactions on Antennas and Propagation*, **34**(3), pp. 276-280, March 1986.

It is easy to tell because of (9) that the rank of signal space in (16) is guaranteed to be full. That means it is equal to the number of targets, $P$.

In Fig. 13, $M = N = 5$, and SNR = 24 dB. From the figure, we conclude from the presence of sharp peaks and deep valleys that good resolution and interference rejection are achieved.

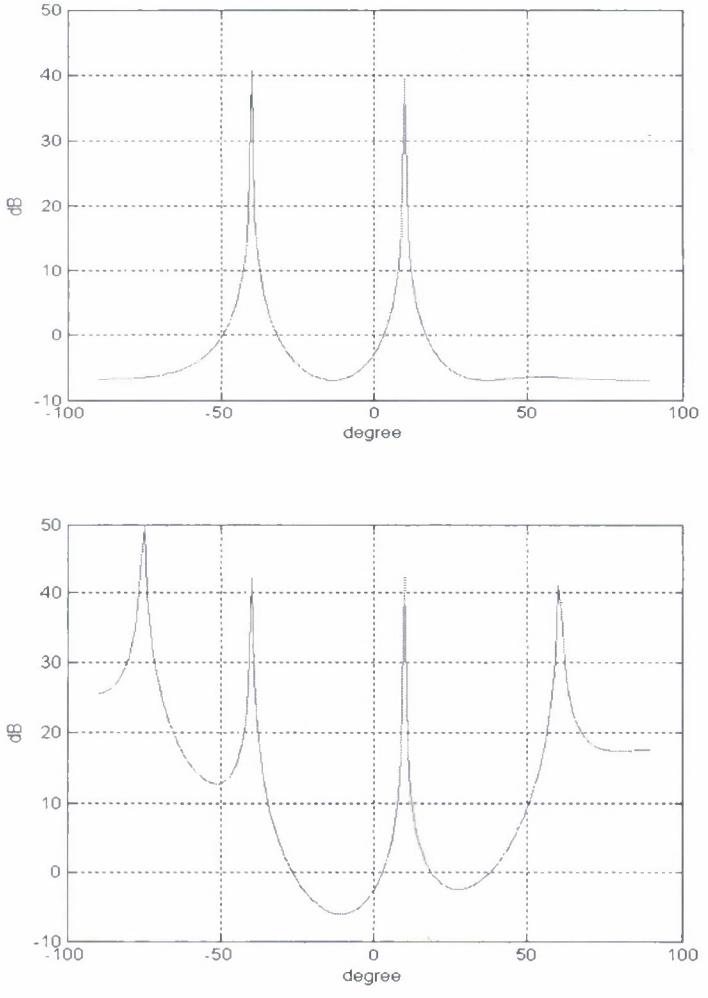


Fig. 13: Receive beam-pattern of MUSIC direction finding algorithm for 2 and 4 targets.

*Capon beamforming:*

For another adaptive technique Capon beamforming[12], the received signals of $n^{th}$ receiver can be represented as

$$R_n = \sum_m r_{m,n} + Z_n = \sum_m a(\theta)\alpha_{ni} s_m + Z_n \qquad (17)$$

[12] L. Xu and J. Li, "Iterative generalized-likelihood ratio test for MIMO radar," *IEEE Transactions on Signal Processing*, 55(6), pp. 2375-2385, June 2007.

For multi-targets, it can be modified in matrix form as

$$R = A(\theta)\alpha S + Z \tag{18}$$

where $R$ is $N\times1$ matrix, $A$ is $N\times P$, $P$ is the number of targets. The $(p,m)^{th}$ element in $\alpha$ is $\alpha_{pm,\theta}$ and $S$ is $M\times1$ represented as signal vector. The covariance matrix of $R$ is $X$ estimated as

$$\widehat{X} = \frac{1}{L} RR^{H} \tag{19}$$

In (19), $L$ is the number of samples.

The goal of Capon beamforming is to maximize the signal to noise ratio (SNR). So, its weights are designed for maintaining the signal power and minimizing the total received power at the same time. Then, it can be formulated as an optimization problem as follows.

$$\min_{W} tr(W^{H} XW) \text{ subject to } W^{H} A(\theta) = I \tag{20}$$

For solving (20), $\widehat{X}^{-1}$ is necessary information. That explains the importance of full rank in $\alpha$ and $S$. We determine the optimal weights, $W$. The received beam pattern is presented below. Obviously, in Fig. 14, it still has sharp peak and deep valleys that are consistent with our previous conclusions, viz. excellent resolution and interference rejection.

*Detecting target in correlated clutter environment:*

In previous sections, from those various approaches that we have seen it is evident that MIMO radar does gather a lot of attention. These developments improve the radar performance in many aspects, such as detection, estimation, and resolution. However, in our opinion, MIMO radar system in correlated clutter environment does not get the sufficient concern that it deserves. In fact, we can't ignore clutter in the real world. So, we choose to further study in this field.

*K*-distributed clutter

Before we move on, the *K*-distributed clutter, one of the most popular models of clutter, it should be introduced first[13,14,15]. The clutter distribution is given by

---

[13] P.F. Sammartino, C.J. Baker, and H.D. Griffiths, "MIMO radar performance in clutter environment," *Proc. International Conf. on Radar (CIE'06),* Shanghai, China, doi: 10.1109/ICR.2006.343554, October 2006.

[14] P.F. Sammartino, C.J. Baker, and H.D. Griffiths, "Adaptive MIMO radar system in clutter," *Proc. IEEE Radar Conference*, Waltham, MA, pp. 276-281, April 2007.

[15] R.S. Raghavan, "A model for spatially correlated radar clutter," *IEEE Transactions on Aerospace and Electronic Systems*, **27**(2), pp. 268-275, March 1991.

$$K[x;a,v]=\frac{2}{a\Gamma(v+1)}\left(\frac{x}{2a}\right)^{v+1}K_v\left(\frac{x}{a}\right)U(x)\;;\; v>-1 \tag{21}$$

where $U(x)$ is the unit step function, $\Gamma(.)$ is the Gamma function, $K_v(.)$ is the modified Bessel function of order $v$.

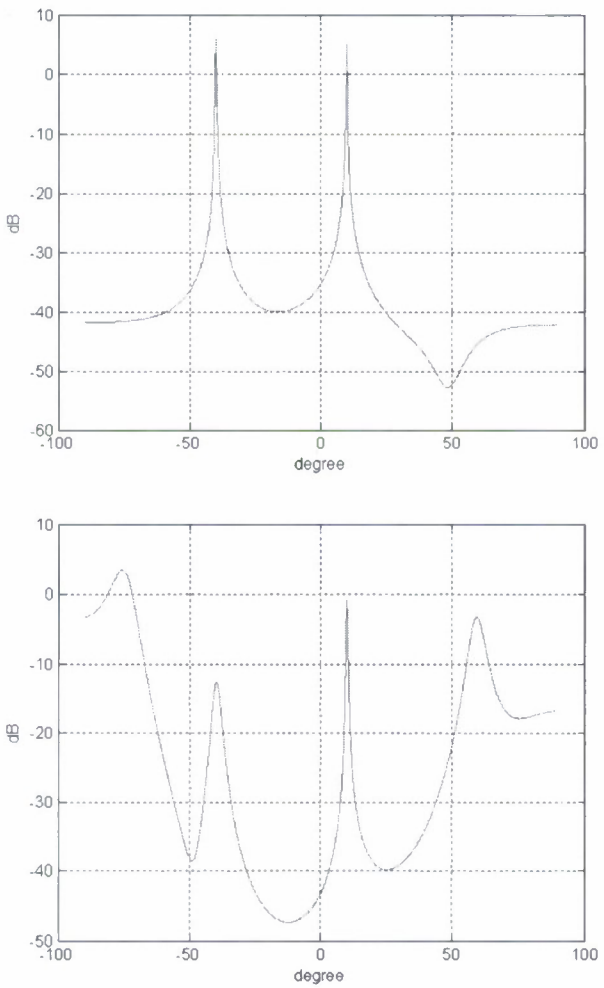


Fig. 14: Receive beam-pattern of Capon beamforming for 2 and 4 targets.

The simplified form (no modified Bessel function), (21) is represented as

$$f_X(x)=K[x;a,v]=\int_0^\infty f_{X/Y}(x\,|\,Y=y)f_Y(y)dy \tag{22}$$

where

$$f_{X/Y}(x \mid Y = y) = R[x; y] \tag{23}$$

and

$$f_Y(y) = G[y; 2a^2, v] \tag{24}$$

Above, the instantaneous envelope from the $i^{th}$ patch ($i$ denotes the spatial position of the patch) or range cell is modeled as two statistically independent random variables (RVs) $X_i$ and $Y_i$. The first RV, $X_i$, often referred to as the "speckle" envelope is described by Rayleigh distribution with parameter $y$, $R[x; y]$. The second RV, $Y_i$, models the local mean power of the speckle element and follows a Gamma distribution, $G[y; 2a^2, v]$. $2a^2$ is the scale parameter, and $v$ is for shape parameter. Lastly, the complex echo signal from clutter is model as $Xe^{j\varphi}$ where $\varphi$ is uniformly distributed in $[0, 2\pi]$. Thus, the complex clutter signal has a complex Gaussian distribution.

*Correlation:*

Definition based on speckle component

Both Ref. 13 and Ref. 14 are the related works about detection performance in a correlated clutter environment. In fact, for these two papers, the correlation is defined based on the speckle component. Furthermore, signals that reflected successively (time), and observed in neighboring range cells (space) may be correlated. Therefore, they can be described as a complex joint Gaussian distribution.

In addition, both of the detection rules in Ref. 13 and Ref. 14 are based on comparing the received power. Since those clutter signals have the same local mean power, if there is a target, the received power suppose being larger than target free case. The problem they try to handle in Ref. 13 is that we may observe strong clutter signals in two neighboring range cells very possibly, because of correlation. Undoubtedly, that is bad for detection. So, they proposed a whitening process to eliminate this correlation. Differently, in Ref. 14, they achieve a more accurate estimate of the local mean power by observing more range cells (gathering more spatial samples).

Definition based on local mean power

In Ref. 15, there is a completely different definition on correlation. In time domain, the correlation period of speckle is much shorter than of local mean power. In space, neighboring range cells, there is no correlation of their speckle, because the author claims that speckle in different range cells are caused by reflections from different aspects of the target. But, the correlation of their local mean power should not be ignored. In simple terms, the correlation is focused on local mean power instead of speckle. It is this definition of correlation that we adopt in our analysis.

So, the joint probability density distribution of $i^{th}$ and $k^{th}$ range cells is described as

$$f_{Y_k Y_i}(y_k, y_i) = \sum_{n=0}^{\infty} p_n G[y_i; b_{ik}, n+v] G[y_k; b_{ik}, n+v] \tag{25}$$

where

$$b_{ik} = 2a^2(1-\rho_{ik}) \tag{26}$$

$$p_n = (1-\rho_{ik})^{v+1} \frac{\Gamma(v+n+1)}{\Gamma(v+1)} \frac{\rho_{ik}^n}{n!};\ n = 0,1,2... \tag{27}$$

Let the correlation coefficient $\rho_{ik}$ be defined as

$$\rho_{ik} = \frac{E\left[\left(Y_i - E[Y_i]\right)\left(Y_k - E[Y_k]\right)\right]}{\sigma_Y^2} \tag{28}$$

For further reference, conditional pdf given $Y_i = y_i$ is

$$f_{Y_k|Y_i}(y_k / Y_i = y_i) = \frac{f_{Y_k Y_i}(y_k, y_i)}{f_{Y_i}(y_i)} \tag{29}$$

Replacing (29) by (24) and (25), the conditional pdf is obtained.

*Signal model and assumptions:*

Assume that there is a large clutter source behind one target. We further assume that clutter covers several range cells while the target covers only one range cell. By Capon beamforming, optimal weights steer the linearly uniform receiver array to scan the whole range cell. In a certain range cell, the received signals can be modeled as

$$r_n(t) = \sum_{m=1}^{M} \alpha t_{m,\theta}(t)\phi_m(t) + \sum_{m=1}^{M} \alpha c_{m,\theta}(t)\phi_m(t) + Z_n \tag{30}$$

where $r_n(t)$ is the received signals of $n^{th}$ receiver, $\alpha t_{m,\theta}(t)$ is the complex reflectivity proportional to the RCS for the $(m, n)^{th}$ transmit and receive pair and for the target at the location $\theta$, $\alpha c_{m,\theta}(t)$ is the complex reflectivity proportional to the RCS for the $(m, n)^{th}$ transmit and receive pair and for the clutter at the location $\theta$, $\phi_m(t)$ is the waveform of $m^{th}$ transmitter (satisfy the orthogonality: $\int \phi_m(t)\phi_k^*(t)dt = \delta_{mk}$), and $Z_n$ is the noise included white noise and maybe jamming signals.

So, after matched filter, equation (30) can be rewritten as

$$r_{n,m}(t) = \alpha t_{m,\theta}(t) + \alpha c_{m,\theta}(t) + Z'_{n,m} \tag{31}$$

where $r_{n,m}(t)$ is the received signal of $n^{\text{th}}$ receiver corresponding to $m^{\text{th}}$ transmit waveform. Furthermore, $Z'_{n,m} = \int Z'_n * \phi_m(t)dt$ is still a normal distributed RV.

Moreover, there are some assumptions for the signal model. First, consistent with the MIMO radar system, $\alpha t_{m,\theta}(t)$ and $\alpha t_{k,\theta}(t)$ will be identical and independent RV, if $m \neq k$. So are $\alpha c_{m,\theta}(t)$ and $\alpha c_{k,\theta}(t)$. $\alpha t_{m,\theta}(t)$ has a complex normal distribution and the envelope of $\alpha c_{m,\theta}(t)$ is *K*-distributed with uniformly distributed phase.

Furthermore, because all range cells are within the correlation length, they are correlated with each other on their local mean power. Moreover, for convenience, we would like to assume the time length of waveform is within the speckle correlation period. Therefore, it will not suffer time selective fading. In other words, for one waveform it will only multiply one reflectivity in whole waveform period.

Finally, clutter in different range cells will satisfy spatially wide sense stationary (WSS). That means the correlation will depends on the distance between range cells only. For simplicity, we assume the $\rho_{ik} = \rho^{d_{i,k}}$.

For answering the question how we detect target in a cluttered environment, we can describe this question in two hypotheses in (32). We can apply Capon to estimate reflectivity in (32). Hypothesis 0, $H_0$, represents the target free case. So, there is only clutter signal. In Hypothesis 1, $H_1$, there is a target, $\alpha t_{m,\theta}(t) \neq 0$.

$$\begin{aligned} H_0 &: x_m = \alpha c_{m,\theta}(t) \\ H_1 &: x_m = \alpha t_{m,\theta}(t) + \alpha c_{m,\theta}(t) \end{aligned} \tag{32}$$

*Likelihood ratio test:*

Parameters estimation for K-distribution

For calculating the likelihood ratio, first of all, we need to glean the parameters of clutter distribution. An algorithm with a simple calculation and with limited samples to earn the reliable estimation results is presented in Fig. 15[16].

[16] R.S. Raghavan, "A method for estimating parameters of *K*-distributed clutter," I*EEE Transactions on Aerospace and Electronic Systems*, **27**(2), pp. 238-246, March 1991.

Of course, correlation coefficient of different range cells needs to be known first. We can observe the clutter signals, and apply (28).

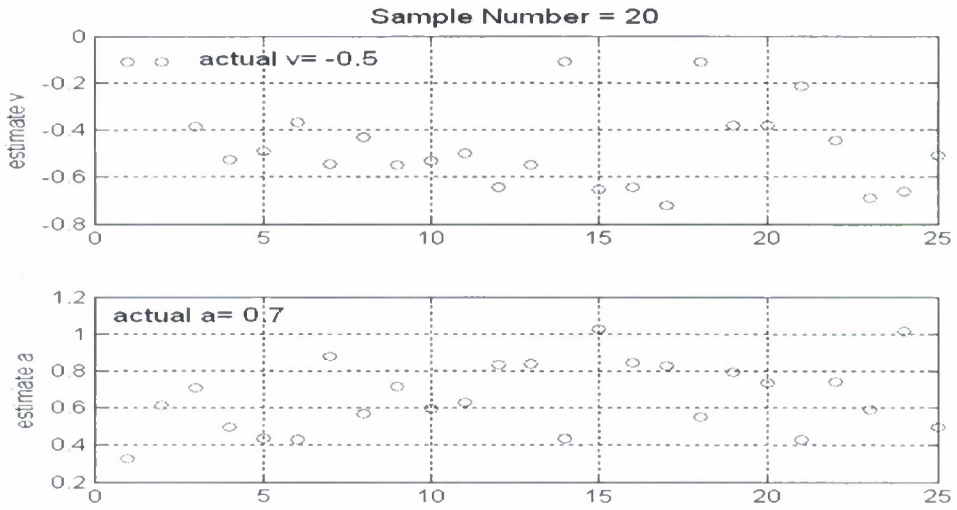


Fig. 15: Independent 20 trials for parameter estimation.

Calculating the likelihood ratio

Once we know the parameters of clutter distribution, referring to (22), the pdf given $H_0$ is

$$f_X(x_m;H_0)=\int_0^\infty f_{X/Y}(x_m|Y=y)f_Y(y)dy \tag{33}$$

Given $y$, $\alpha c_{m,\theta}$ is a complex normal distribution. And, we assume $\alpha t_{m,\theta}$ is complex normal distributed, too. Therefore, their summation is still complex normal distributed RV whose variance is the summation of their individual variance. According to this, given $H_1$, (31) should be modified to (32), where $\sigma_t^2$ is the variance of target reflectivity:

$$f_X(x_m;H_1)=\int_0^\infty f_{X/Y}(x_m|Y=y+\sigma_t^2)f_Y(y)dy \tag{34}$$

So, with (33), and (34), the ratio test can be represented as (35)

$$\frac{f_X(x_m;H_1)}{f_X(x_m;H_0)}=\frac{\int_0^\infty f_{X|Y}(x_m|Y=y+\sigma_t^2)f_Y(y)dy}{\int_0^\infty f_{X|Y}(x_m|Y=y)f_Y(y)dy}>\gamma \tag{35}$$

where $\gamma$ is the threshold. If the ratio is larger than the threshold, we claim to detect a target. Otherwise, it is target free. By using the probability density of $x_m$ further, all possibility of

local mean power is considered, as presented in (35). This idea is similar with the principle of Bayesian ratio test[17].

Obviously, such a ratio test totally wastes the information about correlation. In fact, if we can observe the local mean power of correlated range cells, such additional information will supposedly improve the radar performance. Following this idea, the pdf given $H_0$ should be modified to (36), where $y_i$ is current local mean power in the $i^{th}$ range cell which is correlated with the $k^{th}$. Their correlation coefficient denotes as $\rho_{ik}$.

$$f_X(x_m;H_0)=\int_0^\infty f_{X/Y}(x_m\,|\,Y=y_k)f_{Y_k|Y_i}(y_k\,|\,Y_i=y_i)dy_k \tag{36}$$

Similarly, the pdf, given $H_1$, is

$$f_X(x_m;H_1)=\int_0^\infty f_{X/Y}(x_m\,|\,Y=y_k+\sigma_t^2)f_{Y_k|Y_i}(y_k\,|\,Y_i=y_i)dy_k \tag{37}$$

And (35) should be modified to

$$\frac{f_X(x_m;H_1)}{f_X(x_m;H_0)}=\frac{\int_0^\infty f_{X/Y}(x_m\,|\,Y=y_k+\sigma_t^2)f_{Y_k|Y_i}(y_k\,|\,Y_i=y_i)dy_k}{\int_0^\infty f_{X/Y}(x_m\,|\,Y=y_k)f_{Y_k|Y_i}(y_k\,|\,Y_i=y_i)dy_k}>\gamma \tag{38}$$

For distinguishing (35) and (38), we term (35) as non-conditional, or Gamma based likelihood ratio test, because the local mean power is described by Gamma distribution only. On the other hand, (38) is a conditional likelihood ratio test.

Extending the test to MIMO radar system is not difficult. Since the spatial diversity makes the channel impulse responses met by different radars independent, the joint pdf given $H_0$ and $H_1$ can be represented in (39) and (40)

$$f_{\bar{X}}(x_1,x_2...x_m;H_1)=\prod_{q=1}^{m}f_{\bar{X}}(x_q;H_1) \tag{39}$$

$$f_{\bar{X}}(x_1,x_2...x_m;H_0)=\prod_{q=1}^{m}f_{\bar{X}}(x_q;H_0) \tag{40}$$

From (39), and (40), the hypothesis likelihood ratio test for MIMO become

$$\frac{f_{\bar{X}}(x_1,x_2...x_m;H_1)}{f_{\bar{X}}(x_1,x_2...x_m;H_0)}=\prod_{q=1}^{m}\frac{f_{\bar{X}}(x_q;H_1)}{f_{\bar{X}}(x_q;H_0)}>\gamma \tag{41}$$

[17] S.M. Kay, *Fundamentals of Statistical Signal Processing – Detection Theory*. Prentice Hall: Upper Saddle River, NJ, 1993.

*Numerical example:*

Advantage of correlation and spatial diversity

In the following example, the correlation coefficient between two successive range cells is 0.8. And, the shape and scale factor for Gamma distribution are 0.5 and 2 respectively. For focusing on advantages of spatial diversity and information on correlation, we begin with an ideal case, no noise and no error on estimating reflectivity and target location.

In Fig. 16, the dashed line is for target free case. So, following the detection rule, false alarm happens if the value of likelihood ratio test is larger than $\gamma$. Taking the wider red dashed line as an example, set $\gamma = 2$, the false alarm probability is 0.1.

On the other hand, the solid line represents that there is a target. So, according to the detection mechanism, successful detection happens if the value of likelihood ratio test is larger than $\gamma$. Taking the wider red solid line as an example, set $\gamma = 2$, the detection probability is almost 0.8.

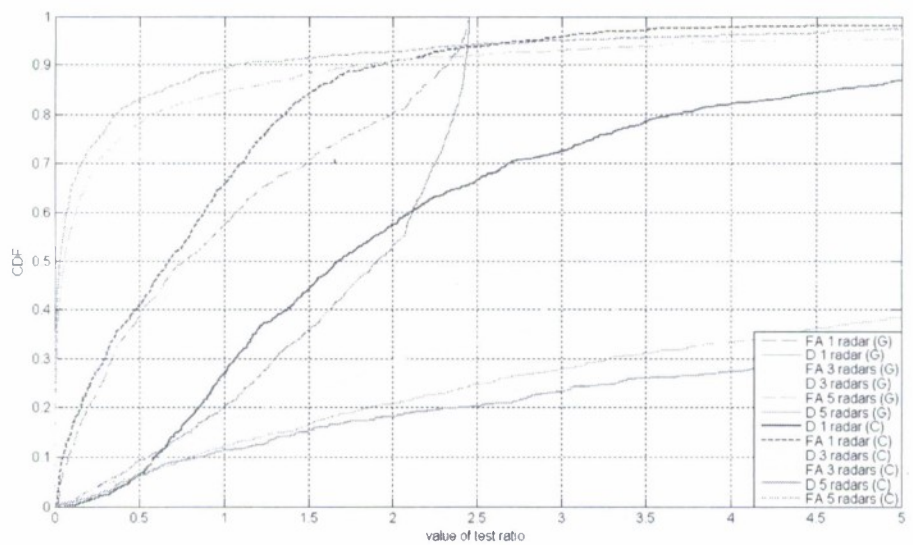


Fig. 16: CDF of Gamma based and of conditional likelihood test ratio in different number of transmitters.

Therefore, by setting the threshold, $\gamma$ to be different values, we can obtain the ROC curve in Fig. 17.

In Fig. 17, the wider and thinner line presents the conditional and Gamma based likelihood ratio test respectively. Clearly, conditional likelihood ratio test does outperform Gamma based. We can also have the same conclusion from Fig. 16, because the distance of wider solid line (detection) and the dashed line (false alarm) is larger than of thinner's.

Moreover, as the number of radars increased, the better the performance is. Similarly, in Fig. 16, there is larger separation between solid and dashed lines of more number of radars.

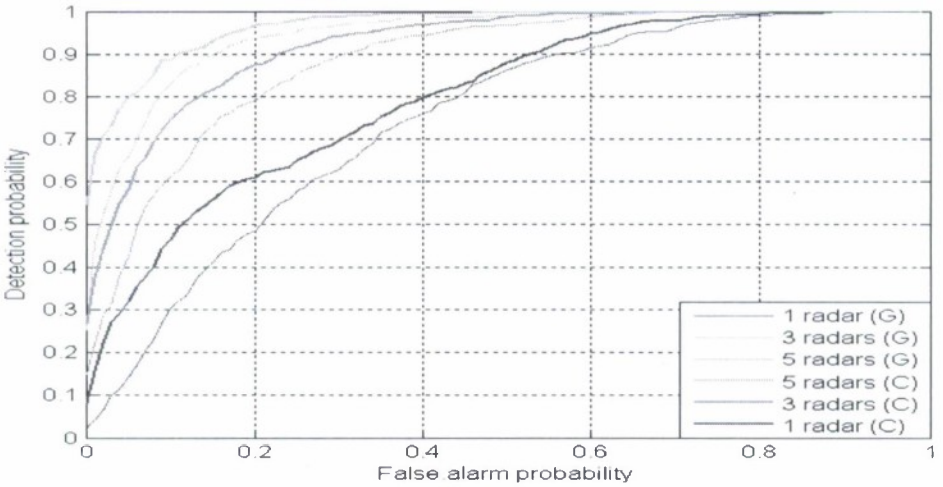


Fig. 17: ROC of Gamma based and of conditional likelihood test ratio in different numbers of radars.

Correlation coefficient

Conditional based likelihood ratio test does take the advantage of information of correlation. However, if there is almost non-correlation between range cells, the conditional likelihood ratio test should degrade to non-conditional one. So, it will be interesting to determine at what correlation level conditional likelihood ratio is still worthy to be applied.

There is a numerical example in Fig. 18. There are five (5) or three (3) radars. We observe if correlation coefficient is equal to 0.2, the system performs similarly with non-conditional based. And if correlation coefficients are equal to 0.6 and 0.8 respectively, their performances are comparable.

Given the related information does help to know clutter signal in concerned range cell better. We try to apply uncertainty measurement to explain the effects of correlation coefficient. The uncertainty values of non-conditional and conditional are equal to (42) and (43) respectively

$$H_Y(y) = -\int_0^{\infty} f_Y(y)\ln(f_Y(y))dy \tag{42}$$

$$H_{Y_k|Y_i}(y_k \mid y_i) = -\int_0^{\infty}\int_0^{\infty} f_{Y_k|Y_i}(y_k \mid y_i)\ln(f_{Y_k|Y_i}(y_k \mid y_i))dy_i dy_k \tag{43}$$

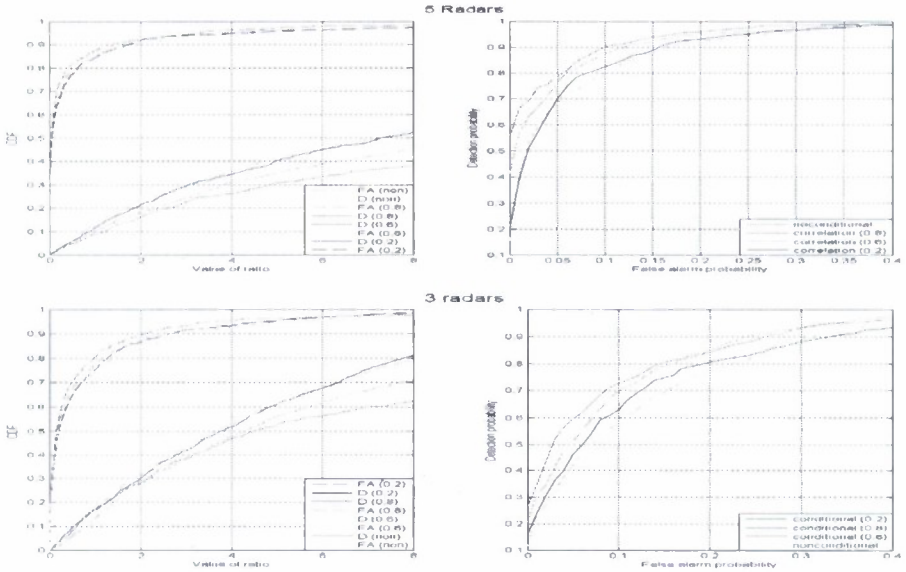


Fig. 18: ROC and CDF of 5 and 3 radars with different correlation coefficient.

Table II shows as correlation coefficient is smaller than 0.4, their uncertainty values are very close to non-conditional situation. So, in this case, the additional information of the correlated local mean power in neighbor range cell does not help us to know the clutter signal in concerned range cell better.

TABLE II: COMPARISON OF UNCERTAINTY IN VARIOUS PARAMETERS

| Correlation coefficient \ Parameters | Shape factor = 0.5; Scale factor = 2 | Shape factor = 0.5; Scale factor = 4 |
|---|---|---|
| 0.01 | 0.7757 (nats) | 1.45255 (nats) |
| 0.2 | 0.7717 (nats) | 1.45255 (nats) |
| 0.4 | 0.75202 (nats) | 1.41447 (nats) |
| 0.6 | 0.63765 (nats) | 1.32678 (nats) |
| 0.8 | 0.48027 (nats) | 1.11952 (nats) |
| Non-conditional | 0.78376 (nats) | 1.4769 (nats) |

Comparison of the performance of Likelihood based detection algorithm with Sammartino's power based detection algorithm

There are not many works discussing MIMO radar performance in clutter environment. We could only find Ref. 14. Even though they apply very different clutter model, after slight modification, it can be changed to another comparable algorithm.

The detection algorithm is

$$\left|x_m(h)\right|^2 - \frac{k}{L}\sum_{\substack{l=1 \\ l\neq h}}^{L}\left|x_m(l)\right|^2 \underset{H_0}{\overset{H_1}{\gtrless}} 0 \tag{44}$$

where $x_m(h)$ is the received signals of the $h^{\text{th}}$ range cell from the $m^{\text{th}}$ transmitter. The first term in (44) is the received power of concerned range cell, and the second one is the summation of received power in neighbor range cells multiplied by a coefficient. Extending this equation to MIMO radar system, the detection algorithm become

$$\sum_{m=1}^{M}\left|x_m(h)\right|^2 - \frac{k}{L}\sum_{m=1}^{M}\sum_{\substack{l=1 \\ l\neq h}}^{L}\left|x_m(l)\right|^2 \underset{H_0}{\overset{H_1}{\gtrless}} 0 \tag{45}$$

Upon assuming $\{x_1, x_2 ... x_m\}$ are i.i.d. RVs, if number of radars, $M$, is sufficiently large, according to law of large number, the first term can be approximated as

$$\sum_{m=1}^{M}\left|x_m(h)\right|^2 \approx M \times E[\left|x_m\right|^2] \tag{46}$$

Moreover, if it is target free, (46) is $m$-times that of the clutter power. If there is a target, (46) is $m$-times of the summation of clutter and target signal power.

Similarly, if the number of spatial samples, $M \times L$, is large enough, the second term can be approximated as

$$\frac{k}{L}\sum_{m=1}^{M}\sum_{\substack{l=1 \\ l\neq h}}^{L}\left|x_m(l)\right|^2 \approx M \times k \times E[\left|x_m\right|^2] \tag{47}$$

So, for a special case, if those $L$ range cells are target free, $k = 1$, and there is a target in concerned range cell, (45) is going to be larger than zero. Even though there are targets in those range cells, we can adjust $k$ to meet the required false alarm probability.

In Fig. 19, we compare its performance with conditional likelihood based detection algorithm. Truly, it functions well when the number of spatial samples, $M \times L$, is large. Therefore, we can conclude the best feature of conditional likelihood ratio test is that less spatial samples are necessary.

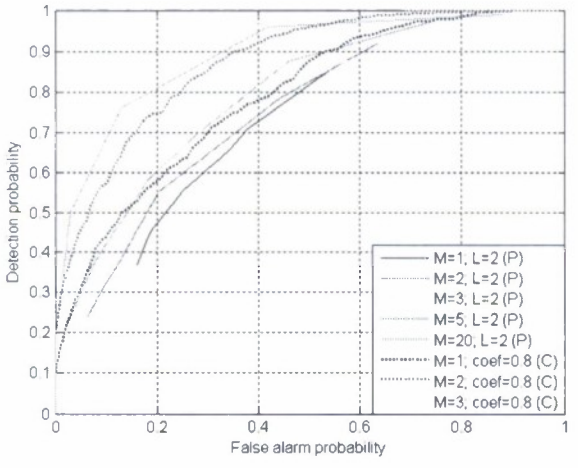


Fig. 19: Comparison of the performance of conditional likelihood based with power based detection algorithm.

Noise effect

Obviously, noise will affect the accuracy of reflectivity estimation. And undoubtedly, the larger the SNR, better is the accuracy. Therefore, with larger SNR, better radar performance can be achieved.

In Fig. 20, we assume there are three (3) transmitters and correct information about target location is available. And, when SNR increases from 0 dB to 5 dB, the mean square estimation error (MSE) in estimating reflectivity reduces from 0.05 to 0.01. That pulls the ROC curve up and is approximated to previous results with perfect reflectivity estimation.

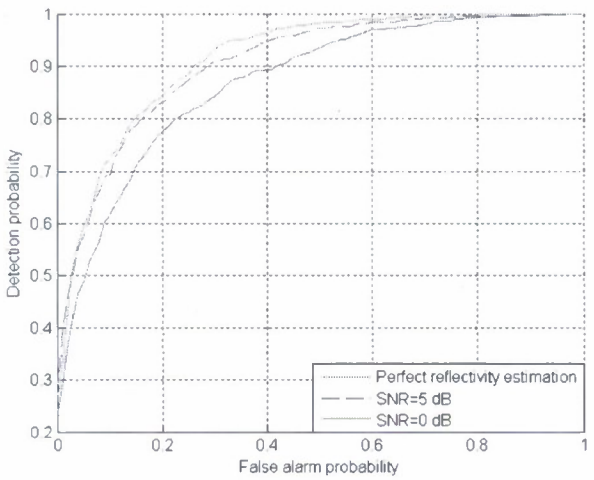


Fig. 20: ROC with 3 radar in different SNR.

In Fig. 21, we show even though the signals are polluted by additive white Gaussian noise, both spatial diversity and correlation information still benefit the performance.

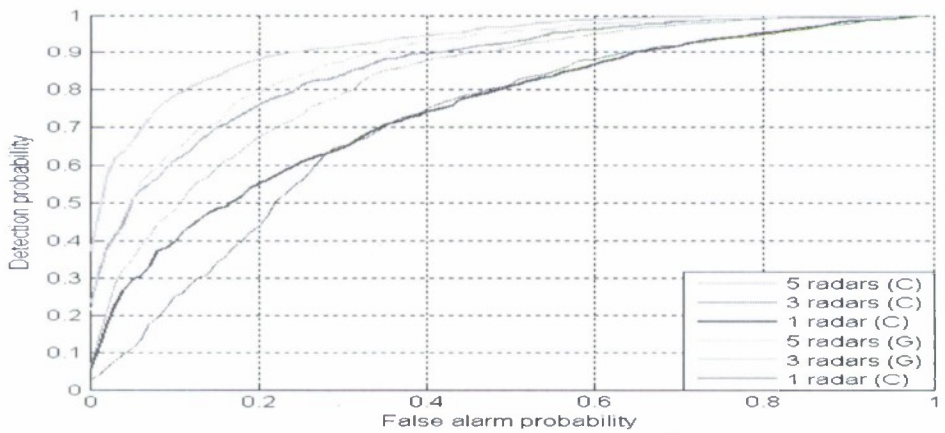


Fig. 21: ROC of Gamma based and of conditional likelihood test ratio in different numbers of transmitters in noisy environment.

*Discussion:*

From the previous results, we show the advantages of spatial diversity and MIMO in detecting target in clutter environment. Information about correlation should be utilized to achieve better performance. And, with limited spatial sample, power based detection algorithm performs much worse than the likelihood based one. More interestingly, we notice smaller uncertainty can increase the distance between detection and false alarm line in CDF, and bigger SNR can provide more accurate reflectivity estimation. Both are very critical to ROC curve.

A distinguishable difference between MIMO and phased array system is the transmitted beam pattern. It has been shown that because of the independence between transmitting signals, the transmitting array cannot compose a transmit beam pattern to focus its power illuminating on certain area[18,19]. So, radar performance will be worse.

Therefore, after gathering some *a priori* information, such as number of targets and their locations, it is necessary to make efforts to redesign transmitting waveforms. For example, in Ref. 9, the transmitted beam pattern generated by new well designed and correlated waveforms, not only do focus on targets' locations, and suppress the interference from other places, but also meet the requirement about 3 dB beamwidth and minimize its sidelobe level. Considering the mean square error (MSE) in estimating the target location, it shows with such modifications, the new system can have 10 dB in SNR gain over the omni-directional one.

There is another interesting work[20]. This combines principles of two very different fields, information and estimation theory, to design waveforms for MIMO radar system. Its goals are to maximize the mutual information between reflectivity and received signals, and minimize the mean square error in estimating target impulse response. They observed that two different criteria reach the same conclusion eventually.

Inspired by these works, we think it should be a good direction to figure out better waveforms for detecting target in clutter environment. Preliminarily, we think re-allocating may be the first step.

In our opinion, since each transmitter owns its waveform which is independent with other's, and even illuminating on same range cell, spatial diversity makes them meet orthogonal channel response, they can be considered as independent channels in communication system. Therefore, with the clutter state information, if we can supply more power on less uncertainty channel, and stop wasting power on channel with large uncertainty, supposedly, the likelihood ratio will be more reliable, and the performance will be more improved. We will investigate this water-filling approach further.

*Generalized Likelihood Ratio Test and Tapped Delay Line Beamforming:*

Multi-input and multi-output (MIMO) radar systems have captured the attention of many researchers in recent years. These systems apply independent probing signals, and sufficiently separated radars to achieve the spatial diversity which is the primary difference between MIMO and phase array radar systems. This unique feature of MIMO radar has been further investigated in various topics and many advantages have been discovered. First, it has been shown that MIMO radar detection performance is dramatically improved which has

---

[18] D.A. Gray, "Multi-channel noise radar," *Proc. 2006 International Radar Symp. (IRS 2006)*, Krakow, Poland, doi: 10.1109/IRS.2006.4338086, May 2006.

[19] D.A. Gray and R. Fry, "MIMO noise radar - element and beam space comparisons," *Proc. 2007 International Waveform Diversity and Design Conf.*, Pisa, Italy, pp. 344-347, June 2007.

[20] Y. Yang and R.S. Blum, "MIMO radar waveform design based on mutual information and minimum mean-square error estimation," *IEEE Transactions on Aerospace and Electronic Systems*, **43**(1), pp. 330-343, January 2007.

contributed to the efforts in stabilizing the reflected power[21]. Second, since spatial diversity provides independent radar cross section (RCS) estimates, the Cramer-Rao bound (CRB) for the direction of arrival (DOA) estimation is effectively reduced[22]. Third, ambiguity function formulation proved that coherent processing over widely dispersed sensors elements may lead to range resolutions higher than supported by the waveform's bandwidth[23]. Finally, the different spatial spread characteristics of a small target and clutter in a spatial diversity MIMO radar can enhance the target detection probability[24].

Since an independent waveform set is necessary for MIMO operation, waveform design is very critical. Early work focused on creating orthogonal waveforms, for which the sidelobe level in the autocorrelation and cross correlation functions are approximately zero. Examples include polyphase orthogonal sequences based on the Hadamard matrix[25] as well as an integration of Genetic Algorithm and the traditional iterative code selection method[26]. Then, the idea that the waveform set should maximize the total radar return or match the illumination to the scene was recognized and developed[27]. Another interesting criterion for designing waveforms, namely, maximizing the conditional mutual information between the random target impulse response and the reflected waveforms, was then developed[28].

Being consistent with the considerations of MIMO radar waveform design, the UWB noise waveform is a great candidate. In addition to previously discussed advantages, the UWB noise waveform has the following benefits. First, the autocorrelation function of noise waveform has only one peak. Second, the ease of generating a set of independent noise waveforms is another significant advantage. Third, it is well known that waveforms with ultra-wide bandwidths improve the range resolution, which is inversely proportional to the bandwidth. Fourth, since random noise waveform is aperiodic, the ambiguity in range/velocity is suppressed[29]. Moreover, noise waveform has potential for further

---

[21] E. Fishler, A. Haimovich, R.S. Blum, L.J. Cimini, Jr., D. Chizhik, and R.A. Valenzuela, "Spatial diversity in radars–models and detection performance," *IEEE Transactions on Signal Processing,* **54**(3), pp. 823–838, Mar. 2006.

[22] N.H. Lehmann, E. Fishler, A.M. Haimovich, R.S. Blum, D. Chizhik, L.J. Cimini, Jr., and R.A. Valenzuela, "Evaluation of transmit diversity in MIMO-radar direction finding," *IEEE Transactions on Signal Processing,* vol. **55**(5), pp. 2215–2225, May 2007.

[23] N.H. Lehmann, A.M. Haimovich, R.S. Blum, and L. Cimini, "High resolution capabilities of MIMO radar," *Proceedings of the 40th Asilomar Conference on Signals, Systems and Computers (ACSSC '06),* Pacific Grove, CA, pp. 25–30, Oct.-Nov. 2006

[24] X.-Z. Dai, J. Xu, Y.-N. Peng, and X.-G. Xia, "A new method of improving the weak target detection performance based on the MIMO radar," *Proc. International Conference on Radar (CIE '06),* Shanghai, China, doi: 10.1109/ICR.2006.343265, Oct. 2006.

[25] H.A. Khan and D.J. Edwards, "Doppler problems in orthogonal MIMO radars," *Proc. IEEE Conference on Radar,* Verona, NY, pp. 244-247, Apr. 2006.

[26] B. Liu, Z. He, J. Zeng, and B. Liu, "Polyphase orthogonal code design for MIMO radar systems," *Proc. International Conference on Radar (CIE '06),* Shanghai, China, doi: 10.1109/ICR.2006.343409, Oct. 2006.

[27] B. Friedlander, "On data-adaptive waveform design for MIMO radar signals," *Conference Record of the 41st Asilomar Conference on Signals, Systems and Computers, (ACSSC '07),* Pacific Grove, CA, pp.187-191, Nov. 2007.

[28] Y. Yang and R.S. Blum, "MIMO radar waveform design based on mutual information and minimum mean-square error estimation," *IEEE Transactions on Aerospace and Electronic Systems,* **43**(1), pp.330-343, Jan. 2007.

[29] S.R.J. Axelsson, "Random noise radar/sodar with ultrawideband waveforms," *IEEE Transactions on Geoscience and Remote Sensing,* **45**(5), pp.1099–1114, May 2007.

developments in MIMO radar system. For example, recently, multichannel and MIMO noise radar architectures have been proposed and theoretically studied[30,31].

Compared to MIMO radar advantages and waveform design, the practical issue of MIMO radar operation in multi-target environment has not received adequate attention it deserves. In one of limited studies in this topic, the authors proposed an iterative generalized likelihood ratio test algorithm (iGLRT) for locating targets[32]. The iGLRT does not only iteratively examine target existences for the whole area, but also exploits the information about observed targets to help detect new targets. As a result, localization accuracy is improving sequentially, and almost reaches the CRB when the iterative procedure is finished. However, since the discussion is restricted to narrow band signals, its extension to MIMO UWB noise radar is advantageous.

Since multiple targets are dispersed in the environment, the beamforming technique must be applied to focus the reflected signals from each of them. However, most discussions about beamforming in radar field are limited in narrow band signals[33,34]. Moreover, the applications of the general broadband beamforming, namely the tapped delay line (TDL) system, used in communications are very different from the radar field[35,36,37].

In the following, we first discuss the necessary modifications to apply the TDL based beamforming to MIMO UWB noise radar. Next, we review GLRT and conditional GLRT (cGLRT) for our radar system. Subsequently, we integrate the GLRT and TDL system and propose an iGLRT mechanism. Finally, we demonstrate the iGLRT procedure and verify that our proposed algorithm can eventually result in an estimation accuracy being very close to CRB via numerical examples.

*System Model:*

Consider a UWB MIMO noise radar system with $N$ transmitters and $M$ identical receivers which are equipped with omni-directional antennas arranged in a linear array. In order to gain the advantages of spatial diversity, the signals transmitted by different transmitters are chosen from a statistically independent UWB noise waveform set, and transmitters are

[30] D.A. Gray, "Multi-channel noise radar," *Proc. International Radar Symposium (IRS 2006)*, Krakow, Poland, doi: 10.1109/IRS.2006.4338086, May 2006.
[31] D.A. Gray and R. Fry, "MIMO noise radar – element and beam space comparisons," *Proc. International Waveform Diversity and Design Conference*, Pisa, Italy, pp. 344-347, June 2007.
[32] L. Xu and J. Li, "Iterative generalized-likelihood ratio test for MIMO radar," *IEEE Transactions on Signal Processing*, **55**(6), pp. 2375–2385, Jun. 2007.
[33] I. Bekkerman and J. Tabrikian, "Target detection and localization using MIMO radars and sonars," *IEEE Transactions on Signal Processing*, **54**(10), pp. 3873–3883, Oct. 2006.
[34] D.R. Fuhrmann and G. San Antonio, "Transmit beamforming for MIMO radar systems using signal cross-correlation," *IEEE Transactions on Aerospace and Electronic Systems*, **44**(1), pp. 171-186, Jan. 2008.
[35] V.V. Mani and R. Bose, "Smart antenna design for beamforming of UWB signals in Gaussian noise," *Proc. International ITG Workshop on Smart Antennas (WSA 2008)*, Vienna, Austria, pp. 311-316, Feb. 2008.
[36] W. Liu, "Adaptive broadband beamforming with spatial-only information," *Proc. 15th International Conference on Digital Signal Processing*, Cardiff, U.K., pp. 575-578, July 2007.
[37] O.L. Frost, III, "An algorithm for linearly constrained adaptive array processing," *Proceedings of the IEEE*, vol. **60**(8), pp. 926-935, Aug. 1972.

sufficiently separated. Moreover, the receivers are suitably spaced for achieving direction unambiguity. We assume that the transmitters, receivers, and targets are all static. Since the transmit signals are UWB, it is indeed possible to resolve the scatterers on the target. Therefore, a target is modeled as the combination of several independent scatterers, and convolution operation is applied to describe the target reflection. The received signals at the $m$ th receiver from the $q$ th target reflection can be represented as

$$X_{m,q}(t) = \sum_{n=1}^{N} \int_0^{T_h} h_{n,q}(\tau) S_n(t - \tau_{r_m,q} - \tau_{t_n,q} - \tau(\theta_{n,q}, \theta_{rq}))d\tau . \tag{48}$$

In above equation, $h_{n,q}(t)$ is the $q$ th target impulse response met by the $n$ th transmitted band-limited noise waveform, $S_n(t)$, and $T_h$ is the duration of $h_{n,q}(t)$. Moreover, the propagation path is separated into three parts. First of all, $\tau_{t_n,q}$ is the common propagation time from the $n$ th transmitter to all scatterers in the $q$ th target and $\tau_{r_m,q}$ is the common propagation time from all scatterers to the $m$ th receiver, as shown in Figure 22(a). Secondly, the propagation time differences to individual scatterers is denoted as $\tau(\theta_{n,q}, \theta_{rq})$, shown as the solid lines in Figure 22(b), which depends on the $q$ th target direction to the $n$ th transmitter, $\theta_{n,q}$, and the direction to the receiver array, $\theta_{r,q}$.

Since the receivers are close to each other, the relation of arrival times to different receivers is easy to describe. We assume the distances between target scatterers and between receivers are much smaller than the distance between the target and the receiver array. This is the well known criterion for the far field assumption. Therefore, one target reflection arrives at all receivers at the same angle, $\theta_{r,q}$. Moreover, since the receivers are arranged in a linear array as shown in Figure 22(c), the relationship between $\tau_{r_{m1},q}$ and $\tau_{r_{m2},q}$ is given by

$$\tau_{r_{m2},q} = (m2 - m1)\, d_r \sin(\theta_{r,q}) / c + \tau_{r_{m1},q} \tag{49}$$

where $d_r$ and $c$ denote the distance between two successive receivers, and the speed of light, respectively.

Since it is easier to develop our discussion in matrix form, we also express the convolution operation in (48) in discrete-time form as

$$\overline{X}_{m,q} = \sum_{n=1}^{N} s_{n,m,q} h_{n,q} . \tag{50}$$

In (50), $\overline{X}_{m,q} \in R^{L_o \times 1}$ and $h_{n,q} \in R^{P \times 1}$ respectively denote the received signal vector and the target impulse response, $s_{n,m,q} \in R^{L_o \times P}$ is the $n$ th transmitted signal to the $q$ th target and received by the $m$ th receiver, where $P$ is the number of scatterers in the $q$ th target, and $L_o$

is the number of observed samples. Moreover, the $p$ th column of $s_{n,m,q}$ is collected by sampling $S_n(t-\tau_{r_m,q}-\tau_{t_n,q}-\tau_p(\theta_{n,q},\theta_{rq}))$ where $\tau_p(\theta_{n,q},\theta_{rq})$ represents the specific response time for the $p$ th scatter. Since the propagation time is considered in $L_o$, it is larger than the number of samples in the transmitted impulse duration, $L$.

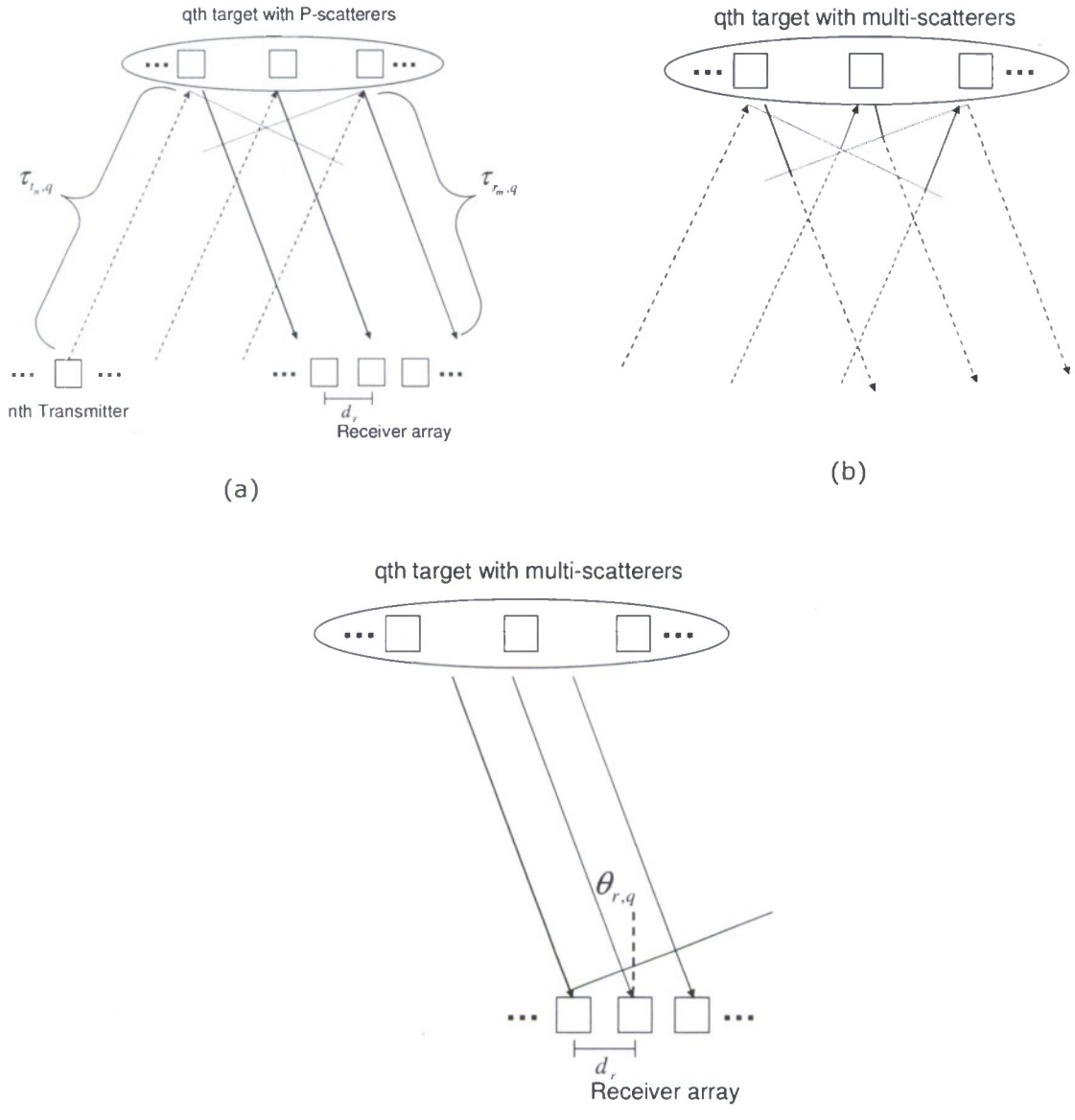


Fig. 22: Various geometric configurations. (a) Common propagation time in the channel model, (b) Different scatterer response times in the channel model, (c) Different receiver arrival times in the channel model.

Then, we consider $Q$ static targets, a single jammer, and thermal noise in our model. As a result, the received signal of the $m$ th receiver is

$$X_m(t) = \sum_{q=1}^{Q} \sum_{n=1}^{N} \int_0^{T_h} h_{n,q}(\tau) S_n(t - \tau_{r_m,q} - \tau_{t_n,q} - \tau(\theta_{n,q}, \theta_{r,q})) d\tau + j\left(t - \tau_{j,m}(\theta_j)\right) + z_m(t), \quad (51)$$

where $j\left(t - \tau_{j,m}(\theta_j)\right)$ is the jamming signal, which is independent of the transmitted signals, and its relative delay $\tau_{j,m}(\theta_j)$ to the $m$ th receiver depends on the direction of jammer. Moreover, jamming signals are usually band-limited white noise or multi-tone[38]. In a UWB radar system, partial band noise affects the system performance more seriously than multi-tone does. Therefore, we prefer considering the worst case, and assume that the jamming signal is partial band noise in following discussions. The thermal noise at the input of the $m$ th antenna is denoted as $z_m(t)$. Since thermal noise terms in different receivers are generated by different but identical antenna elements, we can simply assume they are uncorrelated to each other, and have equal power.

We further simplify the calculation by assuming the scatters are isotropic, as per Ref. 23. Therefore, different transmitted signals will meet the same target impulse response. Thus, (51) can be rewritten as

$$X_m(t) = \sum_{q=1}^{Q} \int_0^{T_h} h_q(\tau) \sum_{n=1}^{N} S_n(t - \tau_{r_m,q} - \tau_{t_n,q} - \tau(\theta_{n,q}, \theta_{r,q})) d\tau + j\left(t - \tau_{j,m}(\theta_j)\right) + z_m(t). \quad (52)$$

This equation can also be expressed in discrete-time form as

$$\vec{X}_m = \sum_{q=1}^{Q} \sum_{n=1}^{N} s_{n,m,q} h_q + \vec{j}_{m,\theta_j} + \vec{z}_m, \quad (53)$$

where $\vec{j}_{m,\theta_j}, \vec{z}_m \in R^{L_0 \times 1}$, and the number of observed samples for (53) needs to be large enough to cover the delays of all target reflections.

*TDL-Based Beamformer*:

If a narrow band signal is transmitted, the target reflection obtained by different receivers will have equal amplitude and different phases. Therefore, the principle of beamformer design is to compensate the phase differences and guarantee observed signals in different receivers are coherently summed up. This constructive summation efficiently increases not only the power of the target reflection, but also the probability of detecting the target. However, if a randomly wideband signal such as UWB noise is transmitted, received signals at different receivers are very possibly uncorrelated to each other. As a result, constructive

[38] R.L. Peterson, R.E. Ziemer, and D.E. Borth, *Introduction to Spread Spectrum Communications*. Englewood Cliffs, NJ: Prentice Hall, 1995.

summation is not achievable using only one weight, and we need a more complex beamforming structure.

We apply the widely studied TDL based beamformer to our MIMO UWB noise radar system whose structure is presented in Figure 23 [see Ref. 35-37]. Received signals at each antenna are fed into a tapped-delay line which consists of $K$ taps and $K$ adjustable weights. Then, we sum up the outputs of all TDLs.

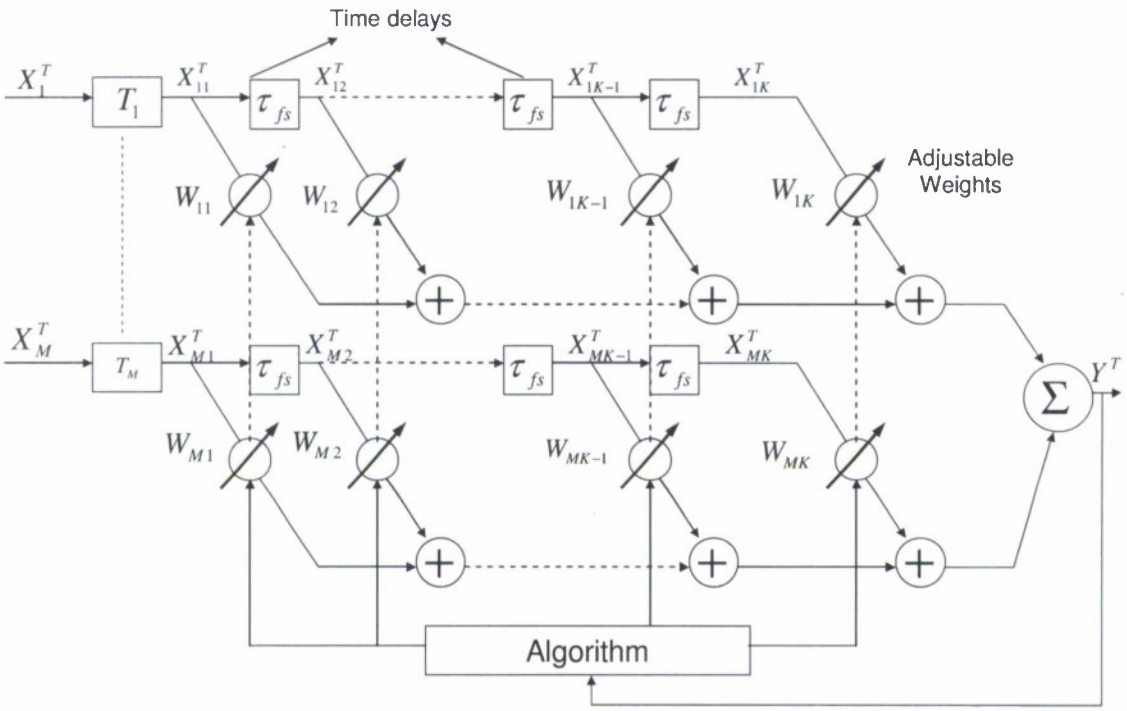


Fig. 23: TDL beamformer structure.

In the first tap, the amount of time advance for the $m$ th receiver is denoted as $T_m$. The values of $T_m$, $m \in [1,...,M]$ are jointly designed for receivers to coherently receive the reflection from a pre-steered direction, $\theta_{pre}$. Therefore, considering our system model, the outputs of the $m1$ th and the $m2$ th receiver's first tap outputs are $X_{m1,1}(t) = X_{m1}(t + (m1-1)d_r \sin(\theta_{pre})/c)$, and $X_{m2,1}(t) = X_{m2}(t + (m2-1)d_r \sin(\theta_{pre})/c)$, respectively. From (51), we note that if $\theta_{pre}$ is equal to one of the target direction angles, $\theta_{r,q}$, the $q$ th target reflection appears at the first tap outputs simultaneously. Since the signals in each receiver are coherent, it is akin to creating a beam pattern for a certain direction. Therefore, repeatedly processing the received signals with all possible $\theta_{pre}$ values is similar to steering the receiver beam pattern over the whole area. We call a cycle of this process in the TDL beamformer, a complete 'scan'.

The delay time for the rest $K-1$ taps, $\tau_{fs}$, is equal to $1/fs$ where $fs$ is the sample frequency. All in all, the output signal of the $k$ th tap in the $m$ th receiver can be represented as

$$\begin{aligned} X_{m,k}(t) &= X_m(t+(m-1)d_r\sin(\theta_{pre})/c-(k-1)\tau_{fs}) \\ &= \sum_{q=1}^{Q}\int_0^{T_h} h_q(\tau)\sum_{n=1}^{N} S_n\left(t-\tau_{r_m,q}+(m-1)d_r\sin(\theta_{pre})/c-(k-1)\tau_{fs}-\tau_{t_m,q}-\tau(\theta_{n,q},\theta_{rq})\right)d\tau \\ &+ j\left(t+(m-1)d_r\sin(\theta_{pre})/c-\tau_{im}(\theta_i)-(k-1)\tau_{fs}\right) \\ &+ z_m\left(t+(m-1)d_r\sin(\theta_{pre})/c-(k-1)\tau_{fs}\right) \end{aligned} \quad . \quad (54)$$

The summation of the product of all TDL outputs with different weight is the output of the overall TDL based beamformer. Therefore, it can be represented as $Y=WX$ where $X=\left[\vec{X}_{1,1},\vec{X}_{1,2},\ldots,\vec{X}_{1,K},\vec{X}_{2,1},\ldots,\vec{X}_{M,K}\right]^T\in R^{MK\times L_w}$ in which the element $\vec{X}_{m,k}$ is the output signal vector of the $k$ th tap in the $m$ th receiver, and $W=\left[W_{11},W_{12},\ldots,W_{1K},W_{21},\ldots,W_{MK}\right]\in R^{1\times MK}$ is the vector for the adjustable weights. The expected power of the TDL outputs is given by

$$E\left[YY^T\right]=E\left[WXX^TW^T\right]=WR_XW^T. \quad (55)$$

This beamforming problem can be formulated as a linearly constrained minimum-variance (LCMV) optimization problem as

$$\min_W WR_XW^T \qquad \text{subject to } C^TW^T=F. \quad (56)$$

The purpose of constraint function is to guarantee that the reflected signals from pre-steered directions has a response similar to that of a finite impulse filter (FIR) with parameter vector $F\in R^{K\times 1}$. As we mentioned in previous discussion, the reflections from the pre-steered direction appear after the first set of taps synchronously. Therefore, the reflection is processed by a FIR which is unified by all the tapped delay lines. In order to make the parameters of this FIR to be equal to $F$, the summation of the $k$ th vertical column weights must be equal to the $k$ th element of vector $F$, while $C$, the constraint function, is given by $C=\left[I,\ldots,I\right]^T\in R^{MK\times K}$ to formulate the above equality, where $I$ is a $K\times K$ identity matrix.

The cost function in (56) is to minimize the total output power. If we follow the assumptions in Ref. 35-37 that the received signals consist of one target reflection, jamming signals and noise, and they are independent to each other, $R_X$ is the summation of the covariance matrices of the target reflection $R_d$, jamming signals $R_j$, and thermal noise $R_z$. Moreover, $F$ in the constraint function could be designed as an almost ideal bandpass filter to limit the power loss of target reflection. Since the power of desired signals is maintained, minimizing the total power $R_X$ equally reduces the jamming and noise power as much as possible.

However, the cost function formulation is quite different in a multi-target environment. Since every target reflection is caused by the combination of all transmitted signals, they are correlated to each other. If we still apply (56), even though the weights still meet the requirement of the constraint function, the correlation between reflections will be utilized, and the signals in pre-steered directions will possibly be eliminated to minimize the total output power. Therefore, the cost function must be modified, and only the power of interference from other directions and thermal noise should be minimized, as given by

$$\min_{W} W\left(R_i + R_j + R_z\right)W^T \text{ subject to } C^T W^T = F. \tag{57}$$

where $R_i$ is the covariance matrix of target reflections from other directions.

According to the discussion in the system model, thermal noise terms at each receiver are independent of each other and have equal power. Therefore, $R_z$ is a scaled identity matrix, $\sigma_z^2 I$, where $\sigma_z^2$ is the unknown noise power variance.

Since jamming signals are band-limited white noise, each element of its covariance matrix $R_j$ is a sinc function and its value depends on the jamming signal's bandwidth, power, and time shift. Moreover, the time shift depends on the arrival time at different receivers which is related to the jammer direction. In order to collect the information about jamming signal's bandwidth, strength, and direction, we employ a spectrum analyzer to measure the power of the TDL outputs in each $\theta_{pre}$. We can collect the approximate bandwidth and strength, when the receiver's look direction correctly steers to the jammer's direction. Therefore, we are able to estimate $R_j$ by applying these parameters to determine the correlation between different tap outputs in the TDL.

As defined before, the covariance matrix of target reflections from other directions is denoted as $R_i$. Other reflections also interfere with the desired signals. Therefore, they should be efficiently suppressed to make the desired signals even more obvious. Moreover, these reflections consist of independent transmitted signals. Therefore, in order to estimate $R_i$, we have to consider each transmitted signal strength and arrival time individually. It may be a little more complicated. We will discuss arrival time and strength estimation in the next section.

Finally, we apply the Lagrange multiplier to solve the optimal weights for (57) and they are given by [Ref. 35]

$$W_{opt} = \left(R_i + R_j + R_z\right)^{-1} C\left(C^T\left(R_i + R_j + R_z\right)^{-1} C\right)^{-1} F. \tag{58}$$

All in all, the weights resulting from (58) lead the TDL beamformer to restrain the influences from unwanted signals without damaging the desired signals.

*Generalized Likelihood Ratio Test Formulation:*

The GLRT is one of the most popular hypothesis tests for target detection. We will review, in order, the GLRT and cGLRT for the TDL output signals in our MIMO wideband noise radar.

Generalized Likelihood Ratio Test

The TDL based beamformer sequentially processes received signals with different advance times in the first set of taps. Therefore, the hypothesis problem is formulated as determining whether a target exists in the concerned direction. Moreover, since we do not have any *a priori* environment information and the TDL based beamformer can maintain the reflection power from the look direction, hypothesis $H_0$ implies that only thermal noise feeds in the TDL beamformer while hypothesis $H_1$ implies that both a target reflection and noise enter the TDL beamformer. Referring to (50), we write the hypothesis problem as

$$\begin{aligned} H_0 &: Y = Z \\ H_1 &: Y = f_w\left(\sum_{n=1}^{N} s_{n,1,q}h_q, \sum_{n=1}^{N} s_{n,2,q}h_q, \ldots, \sum_{n=1}^{N} s_{n,M,q}h_q\right) + Z = f_w\left(\tilde{s}_{1,q}h_q, \tilde{s}_{2,q}h_q, \ldots, \tilde{s}_{M,q}h_q\right) + Z \end{aligned} \quad (59)$$

Firstly, we simplify the notation by using $\tilde{s}_{m,q}h_q$ to represent $\sum_{n=1}^{N} s_{n,m,q}h_q$. Moreover, $f_w\left(x_1, \ldots, x_M\right)$ is a function that describes the operation of TDL beamformer and it represents the output of the TDL beamformer when $x_1, \ldots, x_M$ are the inputs at the $M$ receivers. In order to represent the beamformer output in a more succinct form and develop the estimator for $h_q$, we further study $f_w\left(\tilde{s}_{1,q}h_q, \tilde{s}_{2,q}h_q, \ldots, \tilde{s}_{M,q}h_q\right)$ which can be expanded as

$$f_w\left(\tilde{s}_{1,q}h_q, \tilde{s}_{2,q}h_q, \ldots, \tilde{s}_{M,q}h_q\right) = \begin{bmatrix} W_{11} \\ W_{12} \\ \vdots \\ W_{1K} \\ W_{21} \\ \vdots \\ W_{MK} \end{bmatrix}^T \begin{bmatrix} J_1^T J_{11} \tilde{s}_{1,q}h_q \\ J_2^T J_{11} \tilde{s}_{1,q}h_q \\ \vdots \\ J_K^T J_{11} \tilde{s}_{1,q}h_q \\ J_1^T J_{21} \tilde{s}_{2,q}h_q \\ \vdots \\ J_K^T J_{M1} \tilde{s}_{M,q}h_q \end{bmatrix} = \tilde{S}_q h_q \quad (60)$$

where $J_{m,1}$ and $J_k$ are matrices representing the time advance of the first tap and time delay of the $k$ th tap respectively. They are given as

$$J_k = \begin{bmatrix} \overbrace{1 \quad \cdots}^{k-1} & 0 \\ & 1 \\ 0 & \end{bmatrix} \quad k \in \{1,\ldots,K\}, \tag{61a}$$

$$J_{m,1} = \begin{bmatrix} \overbrace{1 \quad \cdots}^{\lceil (m-1)d_r \sin(\theta_{pre})/c \rceil} & 0 \\ & 1 \\ 0 & \end{bmatrix} \quad m \in \{1,\ldots,M\}. \tag{61b}$$

Furthermore, we introduce the compact notation $\tilde{S}_q$ defined as

$$\tilde{S}_q = \sum_{m=1}^{M} \sum_{k=1}^{K} W_{m,k} J_k^T J_{m1} \tilde{S}_{m,q} . \tag{62}$$

According to (60-62), the hypothesis test can be recast more compactly as

$$\begin{aligned} H_0 &: Y = Z \\ H_1 &: Y = \tilde{S}_q h_q + Z \end{aligned} . \tag{63}$$

First of all, we investigate the probability density function (PDF) of $Y$ given $H_0$, $f(Y \mid H_0)$. Even though each sample of thermal noise is an independent Gaussian random variable, the delay and addition operation in the TDL system establish the correlation between noise samples at the TDL outputs. The correlation is determined by the known weights, length of TDL, and unknown power of input noise. Moreover, we assume mean value of the noise is zero. Therefore, if noise has unit variance, $f(Y \mid H_0)$ is denoted as $N \sim (0, C_z)$ where $C_z \in R^{L_o \times L_o}$. According to this conclusion, for unknown noise variance, $f(Y \mid H_0)$ is $N \sim (0, \sigma_z^2 C_z)$ where $\sigma_z^2$ is an unknown scaling term that makes $\sigma_z^2 C_z$ represent the exact noise covariance matrix. We can similarly argue that $f(Y \mid H_1)$ is $N \sim \left(\tilde{S}_q h_q, \sigma_z^2 C_z\right)$.

We apply the GLRT to determine which hypothesis is more possible. The GLR is defined as [Ref. 32]

$$\rho_\theta = 1 - \frac{\max_{\sigma_z^2} f(Y \mid H_0)}{\max_{\sigma_z^2, h_q} f(Y \mid H_1)} . \tag{64}$$

The maximum likelihood estimate (MLE) for $\sigma_z^2$ in the numerator is[39]

$$\hat{\sigma}_{z0}^2 = \frac{1}{L_o} Y^T C_z^{-1} Y . \tag{65}$$

For the denominator, it will be much easier to estimate $h_q$ if we know $\tilde{S}_q$ . $\tilde{S}_q$ is a matrix determined by known transmitted signals and their unknown arrival times at the receivers. In order to collect the arrival times, we apply $N$ correlators with $N$ signals which are the outputs of $N$ independent transmitted signals processed by the FIR with parameter vector, $F$ of the TDL beamformer. Since the TDL beamformer has effectively suppressed the unwanted signals, and its linear combination will not at all affect the statistical independence between UWB noise waveforms, it is possible to observe and estimate the arrival times. As a result, $\tilde{S}_q$ can be generated with these estimated arrival times, and the MLE for $\sigma_z^2$ and $h_q$ in $H_1$ hypothesis are then given by [Ref. 39]

$$\hat{\sigma}_{z1}^2 = \frac{1}{L_0}\left(Y - \tilde{S}_q \hat{h}_q\right)^T C_z^{-1}\left(Y - \tilde{S}_q \hat{h}_q\right), \tag{66a}$$

$$\hat{h}_q = \left(\tilde{S}_q^T C_z^{-1} \tilde{S}_q\right)^{-1} \tilde{S}_q^T C_z^{-1} Y . \tag{66b}$$

Conditional Generalized Likelihood Ratio Test

We extend the GLRT discussion to a multi-target environment. In the following discussion, $Q$ targets have been observed in the estimated directions $\left\{\hat{\theta}_q\right\}_{q=1}^{Q}$ and we want to determine if an additional target lies in a concerned direction. Since $Q$ targets have been detected, their influences on the desired signal should be included in formulating the hypothesis problem. The hypothesis problem can be illuminated as

$$\begin{aligned} H_Q &: Y = f_w\left(\sum_{q=1}^{Q}\tilde{s}_{1,q}\hat{h}_q, \sum_{q=1}^{Q}\tilde{s}_{2,q}\hat{h}_q, \ldots, \sum_{q=1}^{Q}\tilde{s}_{M,q}\hat{h}_q\right) + Z \\ H_{Q+1} &: Y = f_w\left(\tilde{s}_{1,Q+1}h_{Q+1}, \ldots, \tilde{s}_{M,Q+1}h_{Q+1}\right) \\ &\quad + f_w\left(\sum_{q=1}^{Q}\tilde{s}_{1,q}\hat{h}_q, \sum_{q=1}^{Q}\tilde{s}_{2,q}\hat{h}_q, \ldots, \sum_{q=1}^{Q}\tilde{s}_{M,q}\hat{h}_q\right) + Z \end{aligned} , \tag{67}$$

where $\hat{h}_q$ represents the estimated target impulse response of the $q$ th target. Following the previous discussion, the hypothesis problem can be further simplified as

[39] S.M. Kay, *Fundamentals of Statistical Signal Processing, Volume II: Detection Theory*. Upper Saddle River, NJ: Prentice Hall PTR, 1993.

$$H_Q : Y = \sum_{q=1}^{Q} \tilde{S}_q \hat{h}_q + Z = \bar{S}_Q \bar{\hat{h}}_Q + Z$$
$$H_{Q+1} : Y = \tilde{S}_{Q+1} h_{Q+1} + \bar{S}_Q \bar{\hat{h}}_Q + Z \tag{68}$$

where $\bar{S}_Q = \left[\tilde{S}_1, \tilde{S}_2, \ldots, \tilde{S}_Q\right] \in R^{L_y \times QP}$, and $\bar{\hat{h}}_Q = \left[\hat{h}_1, \hat{h}_2, \ldots, \hat{h}_Q\right]^T \in R^{QP \times 1}$. Moreover, the PDF of received signal given different hypothesis, $f\left(Y \mid H_Q\right)$ is $N \sim \left(\bar{S}_Q \bar{\hat{h}}_Q, \sigma_z^2 C_z\right)$, and $f\left(Y \mid H_{Q+1}\right)$ is $N \sim \left(\tilde{S}_{Q+1} h_{Q+1} + \bar{S}_Q \bar{\hat{h}}_Q, \sigma_z^2 C_z\right)$. The GLR given the $Q$ targets is defined as [Ref. 32]

$$\rho_{\theta\{\hat{\theta}_q\}_{q=1}^{Q}} = 1 - \frac{\max_{\sigma_z^2} f(Y \mid H_Q)}{\max_{\sigma_z^2, h_{q+1}} f(Y \mid H_{Q+1})} \tag{69}$$

The MLE parameters for the likelihood ratio test are

$$\hat{\sigma}_{zQ}^2 = \frac{1}{L}\left(Y - \bar{S}_Q \bar{\hat{h}}_Q\right)^T C_z^{-1} \left(Y - \bar{S}_Q \bar{\hat{h}}_Q\right), \tag{70}$$

$$\hat{\sigma}_{z(Q+1)}^2 = \frac{1}{L}\left(Y - \bar{S}_Q \bar{\hat{h}}_Q - \tilde{S}_{Q+1} \hat{h}_{Q+1}\right)^T C_z^{-1} \left(Y - \bar{S}_Q \bar{\hat{h}}_Q - \tilde{S}_{Q+1} \hat{h}_{Q+1}\right), \tag{71a}$$

$$\hat{h}_{Q+1} = \left(\tilde{S}_{Q+1}^T C_z^{-1} \tilde{S}_{Q+1}\right)^{-1} \tilde{S}_{Q+1}^T C_z^{-1} \left(Y - \bar{S}_Q \bar{\hat{h}}_Q\right). \tag{71b}$$

Moreover, another given condition is $Q$ targets and a strong jammer. For one jamming source, the hypothesis problem is

$$H_{Q;J} : Y = \bar{S}_Q \bar{\hat{h}}_Q + J\left(\hat{\theta}_J\right) + Z_n$$
$$H_{Q+1;J} : Y = \tilde{S}_{Q+1} h_{Q+1} + \bar{S}_Q \bar{\hat{h}}_Q + J\left(\hat{\theta}_J\right) + Z_n \tag{72}$$

where $J\left(\hat{\theta}_J\right)$ represents the band-limited noise jamming signals from the estimated direction $\hat{\theta}_J$. Thus, $f(Y \mid H_{Q;J})$ is $N \sim \left(\bar{S}_Q \bar{\hat{h}}_Q, \hat{C}_J + \sigma_z^2 C_z\right)$ and $f(Y \mid H_{Q+1;J})$ is $N \sim \left(\tilde{S}_{Q+1} h_{Q+1} + \bar{S}_Q \bar{\hat{h}}_Q, \hat{C}_J + \sigma_z^2 C_z\right)$, where $C_J$ is the covariance matrix of jammer TDL outputs. $C_J$ depends on the jamming source direction, jamming signal power, and bandwidth. These parameters can be collected by employing the spectrum analyzer as mentioned in previous section to estimate $\hat{C}_J$.

In order to calculate the GLR given by,

$$\rho_{\theta\{\hat{\theta}_q\}_{q=1}^{Q};J} = 1 - \frac{\max_{\sigma_z^2} f(Y \mid H_{Q;J})}{\max_{\sigma_z^2, h_{q+1}} f(Y \mid H_{Q+1;J})} \tag{73}$$

we have to find the value of $\sigma_z^2$ which maximizes $f(Y \mid H_{Q;J})$. Differentiating $\ln f(Y \mid H_{Q;J})$ with respect to $\sigma_z^2$ and setting it equal to zero, we have[40]

$$\frac{\partial \ln f(Y \mid H_{Q;J})}{\partial \sigma_z^2} = 0$$

$$\Rightarrow -\frac{1}{2} tr\left[\left(\hat{C}_J + \sigma_z^2 C_z\right)^{-1} C_z\right] + \frac{1}{2}\left(Y - \bar{S}_Q \bar{\hat{h}}_Q\right)^T \left(\hat{C}_J + \sigma_z^2 C_z\right)^{-1} C_z \left(\hat{C}_J + \sigma_z^2 C_z\right)^{-1} \left(Y - \bar{S}_Q \bar{\hat{h}}_Q\right) = 0 . \tag{74}$$

The solution to (74) is the MLE $\hat{\sigma}_z^2$. Since it is difficult to directly find the solution, we apply a numerical approach, namely the Newton-Raphson iteration, to solve for MLE $\hat{\sigma}_z^2$ [Ref. 40]. Note that maximizing $\ln f(Y \mid H_{Q+1;J})$ is somewhat different from maximizing $f(Y \mid H_{Q;J})$. First of all, maximizing $\ln f(Y \mid H_{Q+1;J})$ with respect to $h_{Q+1}$ is equal to minimizing the exponential term in $f(Y \mid H_{Q+1;J})$. Taking the first differential to the exponential term with respect to $h_{Q+1}$, we obtain the MLE $\hat{h}_{Q+1}$, which is function of $\sigma_z^2$ as given by

$$\hat{h}_{Q+1} = \left(\tilde{S}_{Q+1}^T \left(\hat{C}_J + \sigma_z^2 C_z\right)^{-1} \tilde{S}_{Q+1}\right)^{-1} \tilde{S}_{Q+1}^T \left(\hat{C}_J + \sigma_z^2 C_z\right)^{-1} \left(Y - \bar{S}_Q \bar{\hat{h}}_Q\right). \tag{75}$$

Secondly, differentiating $\ln f(Y \mid H_{Q;J})$ with respect to $\sigma_z^2$ and setting it equal to zero yields

$$\frac{\partial \ln f(Y \mid H_{Q+1;J})}{\partial \sigma_z^2} = 0$$

$$\Rightarrow -\frac{1}{2} tr\left[\left(\hat{C}_J + \sigma_z^2 C_z\right)^{-1} C_z\right] \tag{76}$$

$$+\frac{1}{2}\left(Y - \tilde{S}_{Q+1} h_{Q+1} - \bar{S}_Q \bar{\hat{h}}_Q\right)^T \left(\hat{C}_J + \sigma_z^2 C_z\right)^{-1} C_z \left(\hat{C}_J + \sigma_z^2 C_z\right)^{-1} \left(Y - \tilde{S}_{Q+1} h_{Q+1} - \bar{S}_Q \bar{\hat{h}}_Q\right) = 0$$

Replacing the $h_{Q+1}$ in (76) with (75), we apply the Newton-Raphson iteration to solve for the MLE $\hat{\sigma}_z^2$ first. Then, the MLE $\hat{\sigma}_z^2$ are substituted for $\sigma_z^2$ in (28) to compute the MLE $\hat{h}_{Q+1}$.

[40] S.M. Kay, *Fundamentals of Statistical Signal Processing, Volume I: Estimation Theory*. Upper Saddle River, NJ: Prentice Hall PTR, 1993.

*Iterative Generalized Likelihood Ratio Test:*

Our iterative generalized likelihood ratio test (iGLRT) not only calculates the GLR, but also utilizes the results from the GLRT and the spectrum analyzer to update the weights in the TDL based beamformer. Both GLRT and spectrum analyzer provide the environment information. The GLRT confirms the target locations while the spectrum analyzer detects the jammer directions. Moreover, the TDL based beamformer applies the information provided by the GLRT and the spectrum analyzer to efficiently suppress the unwanted interferences in the environment. Since more and more interferences are suppressed during the iterations, this mechanism is able to sequentially enhance the detection probability and improve the estimation accuracies of the target directions and the target impulse responses. The detailed procedure is listed in Table III.

TABLE III: iGLRT AND TDL WEIGHTS UPDATE PROCEDURE

Step I: Start first 'scan'

I.1 Set up initial $W$ in TDL

I.2. 'Scan' the whole area

– Apply GLRT to calculate $\rho_\theta$ and measure the power $p_\theta$ to each direction.

I.3 If $\rho_\theta < \rho_0$ and $p_\theta < p_0$ for all directions, then stop;

Otherwise orderly denote them $\hat{\theta}_{\rho_v}$, $v = 1,2,\ldots$ $\rho_{\hat{\theta}_{\rho_1}} > \rho_{\hat{\theta}_{\rho_2}} > \ldots$ and $\hat{\theta}_{p_v}$, $v = 1,2,\ldots$ and $p_{\hat{\theta}_{p_1}} > p_{\hat{\theta}_{p_2}} > \ldots$

I.4 If 2 or more than 2 directions in $\hat{\theta}_{\rho_v}$ or $\hat{\theta}_{p_v}$ were observed, go to Step II; otherwise go to Step III.

Step II: Start another 'scan' from previously observed target directions

II.1 Update the weights

II.2 Re-'scan' the previously noticed directions and its neighbors with new weights for refining the estimated parameters and apply cGLRT to calculate their $\rho_{\theta\{\hat{\theta}_q\}_{q=1}^{Q}}$ or $\rho_{\theta\{\hat{\theta}_q\}_{q=1}^{Q};J}$

II.3 Go to Step III to finish 'scanning'.

Step III: Finish 'scanning'

III.1 Re-'scan' the rest of the directions, and apply cGLRT to calculate their $\rho_{\theta\{\hat{\theta}_q\}_{q=1}^{Q}}$ or $\rho_{\theta\{\hat{\theta}_q\}_{q=1}^{Q};J}$

III.2 If no additional direction whose $\rho_{\theta\{\hat{\theta}_q\}_{q=1}^{Q}} > \rho_0$ is found, then stop;

Otherwise, orderly denote them $\hat{\theta}_v$, $v = 1,2,\ldots$ and $\rho_{\hat{\theta}_1\{\hat{\theta}_q\}_{q=1}^{Q}} > \rho_{\hat{\theta}_2\{\hat{\theta}_q\}_{q=1}^{Q}} > \ldots$ and repeat the iteration from Step II until no more subject is found.

At the very beginning, we start the first 'scan'. As mentioned before, each 'scan' is achieved by processing the received signals with all possible time advances in the first taps. In other words, this is a signal processing procedure rather than mechanical steering.

In Step I.1, we set up the initial weights. Without any *a priori* information about the environment, the weights are designed to minimize $WR_zW^T$. Since thermal noise at every tap output is independent of each other and has equal power, $R_z$ is a scaled identity matrix. Therefore, minimizing $WR_zW^T$ is equal to minimizing $WW^T$. Another special point to be noted in the first 'scan' is that in addition to calculating the GLR, the power of the TDL beamformer outputs is also measured for detecting strong jammers.

If multiple sources (*i.e.*, targets or jammers) are noticed in Step I, we refine their parameters in Step II. We choose one of the observed sources, and adjust the weights to suppress the influences from the rest to collect more precise parameters on the concerned source. The refining procedure will repeat until all observed sources have been chosen.

Determining weights to suppress the influences from other sources is very different from weights determination in the first 'scan'. In the second 'scan', since we already have some knowledge about the environment, the weights are the solution for the LCMV problem in (57). Therefore, $R_z$, $R_j$, and $R_i$ need to be investigated. First, we utilize the estimated thermal noise power of TDL outputs in the first 'scan' to calculate the thermal noise power in each receiver and $R_z$. Second, $R_j$ is determined by applying the observation from the spectrum analyzer. Third, the arrival times are obtained from the correlators and the estimated target impulse responses provide us with the reflection strength. These two parameters are sufficient to determine $R_i$. Finally, the updated weights are calculated in (58). Moreover, $R_j$ and $R_i$ also change with the time advance values of the first tap in the TDL beamformer. Therefore, when the TDL beamformer is 'scanning', weights should also be modified.

In Step III, the rest of the scan area is re-checked. The weights are designed to suppress the observed interferences, and are determined according to the latest parameters collected in Step II.

*Numerical Examples:*

In this section, we first demonstrate the iGLRT and TDL integration mechanism. Then, we investigate the CRB of our signal model. Last, we compare our system's performance with CRB in localization and target impulse response estimation accuracy.

Demonstration the Procedures of iGLRT

In our simulation, we assume four targets located at −5, 10, 17, and 25 degree angles. We have 5 transmitters and 10 receivers. The transmitters are sufficiently separated. Transmitted

noise waveforms of different transmitters are independent of each other. The noise signal bandwidth is 1 GHz and its center frequency is 1.5 GHz. In order to satisfy the Nyquist sampling condition, the sampling frequency is chosen to be twice the highest frequency. The transmitted pulse duration is 250 ns. Moreover, the variance of transmitted signals summation is normalized to 1. If the desired angular resolution is $\Delta\theta$, the distance between two successive receivers $d_r$ must be designed to guarantee that the arrival times for the reflections from directions $\theta$ and $\theta+\Delta\theta$ are separated by at least one sample interval. Therefore, $d_r$ should satisfy the inequality $1/f_s \le d_r[\sin(\theta+\Delta\theta)-\sin(\theta)]/c$. For a small $\Delta\theta$ requirement, $\sin(\Delta\theta)\approx\Delta\theta$ and $\cos(\Delta\theta)\approx 1$. This approximation simplifies the inequality and it can be rewritten as $d_r \ge c/[\Delta\theta f_s \cos\theta]$. If the maximum value of the angle over which the scan in performed is $\theta_{\max}$, then a value of $d_r = c/[\Delta\theta f_s \cos\theta_{\max}]$ will both satisfy the above inequality and yet maintain minimum possible receiver spacing for a compact sized array. For the case wherein $f_s$, $\theta_{\max}$, and $\Delta\theta$ are 2 GHz, 40 degrees, and 1 degree respectively, $d_r$ is computed as 11.22 m.

The parameter vector $F$ in equation (57) is designed to be the parameter vector of a FIR bandpass filter from 1 GHz to 2 GHz, and a Hamming window is applied to determine its exact value[41]. Moreover, the length of the parameter vector is 100. It also means that we have 100 taps in each TDL. Finally, each target consist of 10 independent scatterers, and the reflectivity of each scatterer is modeled as a Gaussian random variable with zero mean and variance is equal to $1/\sqrt{10}$. We will demonstrate the iGLRT procedure in a multi-target environment, as well as in a jammer and a multi-target environment, in order below.

We consider a multi-target environment without a jammer. In Figure 24, we set the signal to noise power ratio (SNR) to 0 dB. After the first 'scan', we apply (64) to calculate the GLR and observe two targets which are located at −5 and 10 degree angles, if the threshold for GLR is set to be 0.25 as shown in Figure 24(a). The second 'scan' starts from refining the parameters of these two targets and calculating their new GLR using (69). The weights are designed to suppress the reflection power from the other one. Then, we adjust the time advance in the first tap to check the rest of the directions by calculating their GLR, with weights designed to efficiently suppress the interferences from two detected targets. As a result, the GLRs for the other two targets obviously increase as shown in Figure 24(b). After another 'scan' which also begins from refining the target parameters, their GLRs are even larger and no additional target are detected as shown in Figure 24(c).

We now add a jammer to the environment. Its power is 40 dB stronger than the received signals, and it is located at −15 degree angle. The SNR is still maintained at 0 dB. Moreover, we assume the worst case scenario in that the bandwidth of jamming signal is also 1-2 GHz. Therefore, when the pre-steered direction steers towards the direction of the jammer, the power of the jamming signals will completely pass through the designed bandpass filter and we can directly measure the variance of the TDL outputs for estimating the jamming power.

[41] S.J. Orfanidis, *Introduction to Signal Processing*. Englewood Cliffs, NJ: Prentice Hall International, 1996.

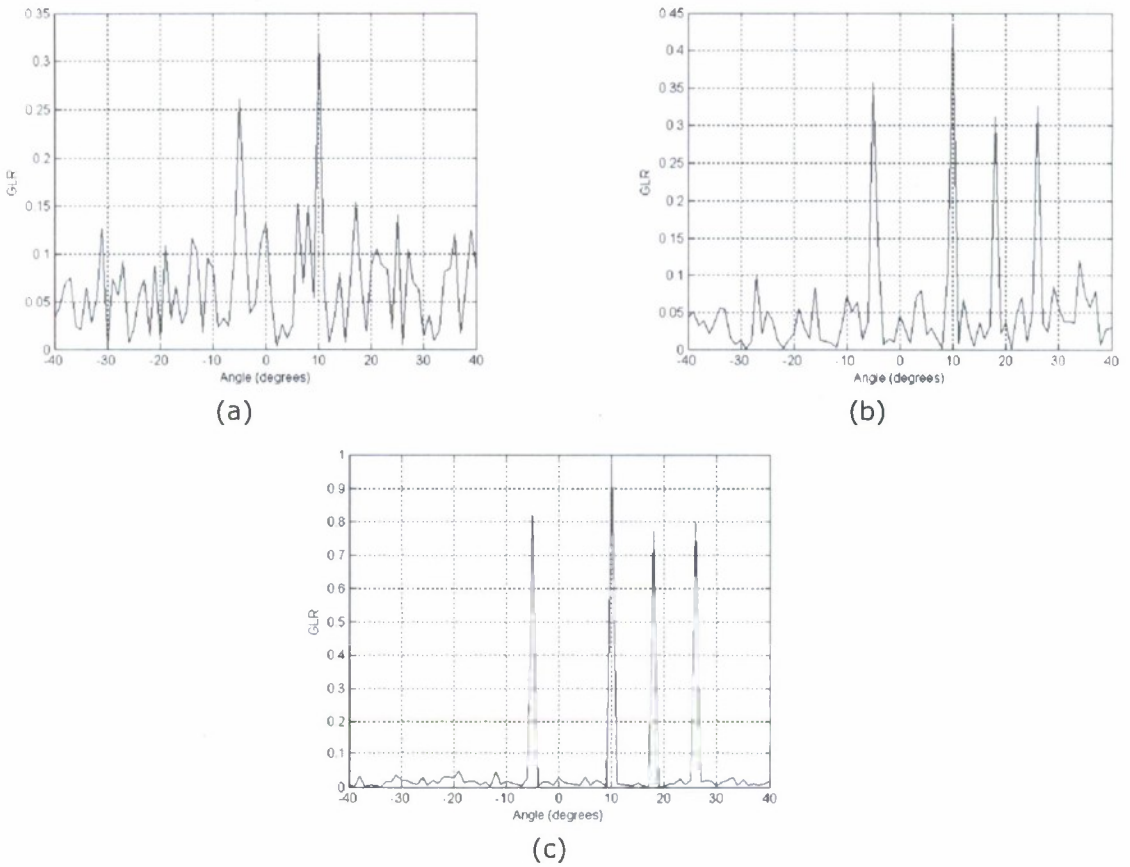


Fig. 24: Various GLRs for multi-target environment without jammer. (a) After first 'scan', (b) After second 'scan', (c) After third 'scan'.

After the first scan, no obvious peak is observed in Figure 25(a). It is due to the fact that under such powerful interference, it is too hard to collect approximate target parameters. However, in Figure 25(b), we noticed a strong power arriving from an angle of −15 degree. Its GLR is small, but power is large. Therefore, it is treated as a jammer. Since only one jamming source was detected, we skip Step II and prepare to start another 'scan'. Moreover, weights are updated to limit the power from estimated jammer direction. As shown in Figure 25(c), we observe two targets in the second scan. In the third scan, we refine the target parameters first. Then, weights are designed to reduce the influences from the jammer and the two target reflections. Since most of the interferences are suppressed, two more targets are detected as shown in Figure 25(d). Figure 25(e) illustrates the results after the fourth scan, and it is easy to note that the GLRs are further increased. Upon comparing this result with the noise-only situation, we note that the powerful interference leads the values of GLRs in jamming environment to be smaller than in a noise-only environment.

Cramer-Rao Bound

Before we apply the CRB to evaluate the estimation accuracy of our iGLRT mechanism, we develop the CRB of our signal model first.

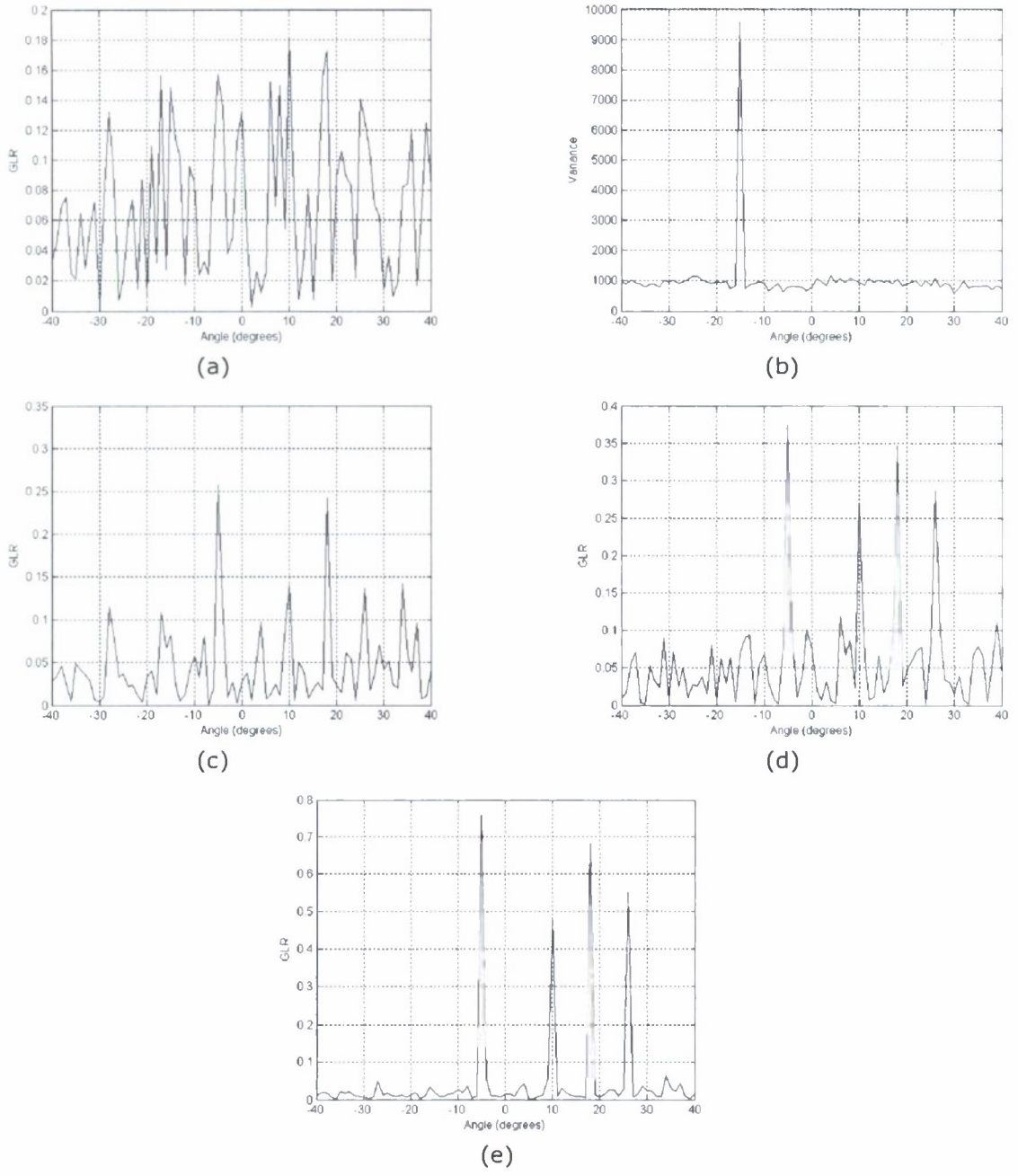


Fig. 25: Various GLRs for multi-target environment with jammer. (a) After first 'scan', (b) Variance of TDL outputs for different directions, (c) After second 'scan', (d) After third 'scan', (e) After fourth 'scan'.

According to the previous discussion in the signal model, the received signals for all receivers can be written as

$$X = \begin{bmatrix} \vec{X}_1 \\ \vec{X}_2 \\ \vdots \\ \vec{X}_M \end{bmatrix} = \begin{bmatrix} \sum_{q=1}^{Q}\sum_{n=1}^{N} s_{n,1,q} h_q \\ \sum_{q=1}^{Q}\sum_{n=1}^{N} s_{n,2,q} h_q \\ \vdots \\ \sum_{q=1}^{Q}\sum_{n=1}^{N} s_{n,M,q} h_q \end{bmatrix} + \begin{bmatrix} \vec{j}_{1,\theta_j} \\ \vec{j}_{2,\theta_j} \\ \vdots \\ \vec{j}_{M,\theta_j} \end{bmatrix} + \begin{bmatrix} \vec{z}_1 \\ \vec{z}_2 \\ \vdots \\ \vec{z}_M \end{bmatrix} \tag{77}$$

where $X \in R^{L_n M \times 1}$. Moreover, $\vec{j}_{1,\theta_j}$, $\vec{j}_{2,\theta_j}$, ..., $\vec{j}_{M,\theta_j}$ are jointly Gaussian random variables, $\vec{z}_m$ is also Gaussian and mutually independent of each other. We also assume that the jammer signal and the thermal noise are uncorrelated. Therefore, the probability density function of $X$ is given by

$$\begin{aligned} X \sim N & \left( \begin{bmatrix} \sum_{q=1}^{Q}\sum_{n=1}^{N} s_{n,1,q} h_q \\ \sum_{q=1}^{Q}\sum_{n=1}^{N} s_{n,2,q} h_q \\ \vdots \\ \sum_{q=1}^{Q}\sum_{n=1}^{N} s_{n,M,q} h_q \end{bmatrix}, \begin{bmatrix} E\left[\vec{j}_{1,\theta_j}\vec{j}^{T}_{1,\theta_j}\right] & E\left[\vec{j}_{1,\theta_j}\vec{j}^{T}_{2,\theta_j}\right] & \cdots & E\left[\vec{j}_{1,\theta_j}\vec{j}^{T}_{M,\theta_j}\right] \\ E\left[\vec{j}_{2,\theta_j}\vec{j}^{T}_{1,\theta_j}\right] & E\left[\vec{j}_{2,\theta_j}\vec{j}^{T}_{2,\theta_j}\right] & \cdots & E\left[\vec{j}_{2,\theta_j}\vec{j}^{T}_{M,\theta_j}\right] \\ \vdots & \vdots & \ddots & \vdots \\ E\left[\vec{j}_{M,\theta_j}\vec{j}^{T}_{1,\theta_j}\right] & E\left[\vec{j}_{M,\theta_j}\vec{j}^{T}_{2,\theta_j}\right] & \cdots & E\left[\vec{j}_{M,\theta_j}\vec{j}^{T}_{M,\theta_j}\right] \end{bmatrix} + \begin{bmatrix} \vec{z}_1 \\ \vec{z}_2 \\ \vdots \\ \vec{z}_M \end{bmatrix} \right) \\ & = N\left(\tilde{r}, Z_{j,w}^{-1}\right) \end{aligned} \tag{78}$$

Referring to the discussion in Ref. 32, since only the exponential term in this normal distribution relates to CRBs of the target impulse response $h$, and target directions $\theta_r$, the Fisher information matrix (FIM) with respect to $h$, and $\theta_r$, can be written as

$$FIM = \begin{bmatrix} F(\theta_r, \theta_r) & F(\theta_r, h) \\ F(h, \theta_r) & F(h, h) \end{bmatrix}. \tag{79}$$

The $[i, j]$ element in block $F(\theta_r, \theta_r)$ in (79) is given by

$$F(\theta_{ri}, \theta_{rj}) = 2\left\{ \frac{\partial[\tilde{r}]^T}{\partial \theta_{ri}} Z_{j,w}^{-1} \frac{\partial[\tilde{r}]}{\partial \theta_{rj}} \right\}. \tag{80}$$

The signal part in $\tilde{r}$ is function of arrival times which depend on target directions. Therefore,

$$\frac{\partial[\tilde{r}]}{\partial\theta_{ri}}=\begin{bmatrix}\sum_{n=1}^{N}\int_0^{T_h}h_i(\tau)\dfrac{\partial\left[S_n\left(t-\tau_{r_1,q}(\theta_{ri})-\tau_{t_n,q}(\theta_{n,i})-\tau(\theta_{n,i},\theta_{ri})\right)\right]}{\partial\theta_{ri}}d\tau\\ \vdots\\ \sum_{n=1}^{N}\int_0^{T_h}h_i(\tau)\dfrac{\partial\left[S_n\left(t-\tau_{r_M,q}(\theta_{ri})-\tau_{t_n,q}(\theta_{n,i})-\tau(\theta_{n,i},\theta_{ri})\right)\right]}{\partial\theta_{ri}}d\tau\end{bmatrix}. \tag{81}$$

Since $\theta_{n,i}$ is related to $\theta_{ri}$, we can write $\theta_{n,i}=g(\theta_{ri})$. Using the definition of the differential, the partial derivative term in (34) can be represented as

$$\begin{aligned}&\frac{\partial\left[S_n\left(t-\tau_{r_m,q}(\theta_{ri})-\tau_{t_n,q}(\theta_{n,q})-\tau(\theta_{n,q},\theta_{ri})\right)\right]}{\partial\theta_{ri}}\\ &=\lim_{\Delta\theta_{ri}\to 0}\frac{S_n\left(t-\tau_{r_m,q}(\theta_{ri}+\Delta\theta_{ri})-\tau_{t_n,q}\left(g(\theta_{ri}+\Delta\theta_{ri})\right)-\tau\left(g(\theta_{ri}+\Delta\theta_{ri}),\theta_{ri}+\Delta\theta_{ri}\right)\right)}{\Delta\theta_{ri}}\\ &\quad-\frac{S_n\left(t-\tau_{r_m,q}(\theta_{ri})-\tau_{t_n,q}\left(g(\theta_{ri})\right)-\tau\left(g(\theta_{ri}),\theta_{ri}\right)\right)}{\Delta\theta_{ri}}\end{aligned}. \tag{82}$$

In our target model, each target consists of $P$ independent scatterers. Therefore, they should be studied separately, and the $\left[i,(q-1)P+p\right]$ element in $F(\theta_r,h)$ is the result of taking the differential corresponding to the $p$ th scatterer of the $q$ th target, i.e.,

$$F(\theta_{ri},h_{q,p})=2\left\{\frac{\partial[\tilde{r}]^T}{\partial\theta_{ri}}Z_{j,w}^{-1}\frac{\partial[\tilde{r}]}{\partial h_{q,p}}\right\}. \tag{83}$$

Similarly, the $\left[(q_{i1}-1)P+p_{j1},(q_{i2}-1)P+p_{j2}\right]$ element in $F(h,h)$ is

$$F(h_{q_{i1},p_{j1}},h_{q_{i2},p_{j2}})=2\left\{\frac{\partial[\tilde{r}]^T}{\partial h_{q_{i1},p_{j1}}}Z_{j,w}^{-1}\frac{\partial[\tilde{r}]}{\partial h_{q_{i2},p_{j2}}}\right\}. \tag{84}$$

Applying (80)-(84) to calculate (79), then CRB can be derived as

$$CRB(\theta)=\left[F_{\theta_r,\theta_r}-F_{\theta_r,h}F_{h,h}^{-1}F_{h,\theta_r}\right]^{-1}, \tag{85}$$

or

$$CRB(h)=F_{h,h}^{-1}+F_{h,h}^{-1}F_{h,\theta_r}\left(F_{\theta_r,\theta_r}-F_{\theta_r,h}F_{h,h}^{-1}F_{h,\theta_r}\right)^{-1}F_{\theta_r,h}F_{h,h}^{-1}. \tag{86}$$

Since the CRBs are functions of the transmitted waveforms and the target impulse responses, they will be random variables. In order to evaluate the performance in a meaningful way, the average CRB is a more relevant parameter [Ref. 22].

Comparison between CRBs and iGLRT Performance

Thermal noise in receivers is assumed to be independent of each other. However, the correlations between jamming signals in different receivers are determined by their arrival times. Therefore, thermal noise and noise jammer affect the performance very differently, and should be discussed separately. Moreover, in order to make the difference more obvious, we assume that the jammer is located at 0 degree angle, and all other parameters are the same as in the previous discussion.

In Figures 26 and 27, we compare the mean square error (MSE) of target impulse response estimation resulting from iGLRT with the average CRB. In Figure 26, the noise power is equal to the signal power (SNR = 0 dB), and we increase the jamming power to achieve different signal to jammer and noise power (SJNR). In Figure 27, the jammer power is equal to signal power (SJR = 0 dB), and signal to noise power ratio (SNR) is varied.

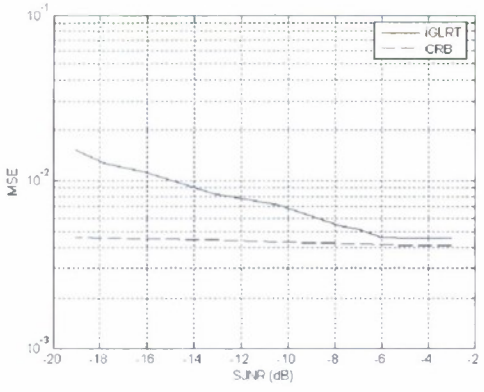


Fig. 26: iGLRT and CRB comparison of target impulse response estimation when SNR is fixed at 0 dB and SJR is varied.

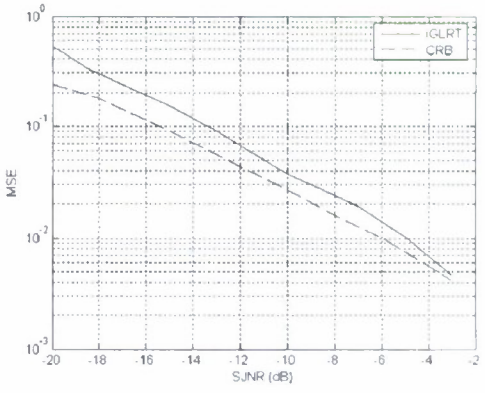


Fig. 27: iGLRT and CRB comparison of target impulse response estimation when SJR is fixed at 0 dB and SNR is varied.

Both figures show iGLRT results are close to CRBs especially when the SJNR is large. Moreover, when the SJR is varied, the CRBs and iGLRT lines are flatter and values are smaller than when caused by varying the SNR. It proves that the jammer and thermal noise do affect the performance differently, and the TDL based beamformer performs better in eliminating jamming signals better than thermal noise.

In Figures 28 and 29, the target location MSE resulting from iGLRT and CRB are compared. We can infer similar conclusions with above discussion.

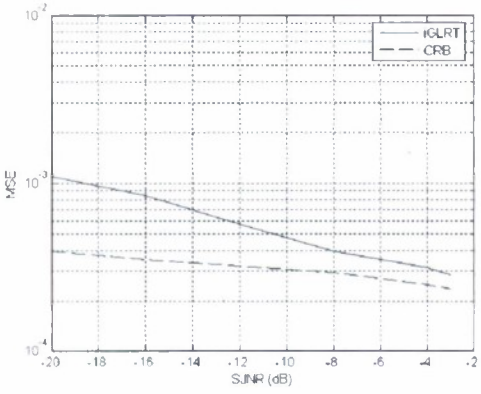


Fig. 28: iGLRT and CRB comparison of target location estimation when SNR is fixed at 0 dB and SJR is varied.

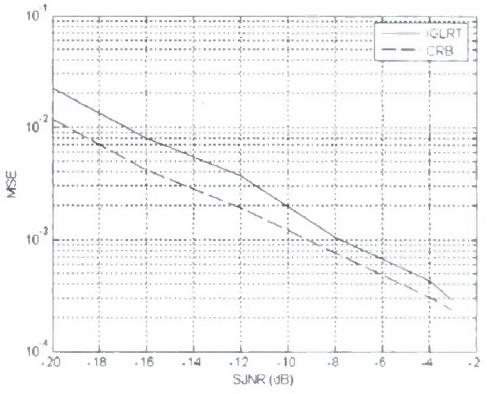


Fig. 29: iGLRT and CRB comparison of target location estimation when SJR is fixed at 0 dB and SNR is varied.

## 2. 2. RF Tags

*Noise Radar Tag Basics*:

Radio frequency (RF) technology is used in many different applications, such as television, radio, cellular phones, radar, and automatic identification systems. RFID stands for radio frequency identification and describes the use of radio frequency signals to provide automatic identification[42]. RFID is similar in concept to bar coding. Bar code systems use a reader and coded labels that are attached to an item, whereas RFID uses a reader and special RFID devices that are attached to an item. Bar code uses optical signals to transfer information from the label to the reader; RFID uses RF signals to transfer information from the RFID device to the reader. These RFID systems are composed of two main components – an interrogator (reader) and a tag (passive, active, or semi-active).

A tag contains information and a reader queries the tag for the information. A tag is sometimes called a transponder. The word transponder comes from the words transmitter and responder. It is an identifier affixed to a certain item or an object holding its identification information. The tag responds to a reader's request by transmitting the information. The tag consists of a microchip connected to an antenna and sometimes a battery. The tag's antenna is physically attached to the chip and is used to draw energy from the reader to energize the tag. Active tags generate energy from its battery and passive tags receive energy from the reader that generates a radio frequency (RF) field. A major requirement for tagging and sensor systems is that the remote devices show long battery life which corresponds to a low power consumption. Due to limitations of power consumption, the use of a local RF source is not acceptable on the remote devices. Backscatter modulation is therefore well suited for such a kind of system[43].
The interrogator or reader transmits an unmodulated RF carrier which is modulated on the tag by a backscatter modulator. In passive backscatter modulator case, it consists of an RF diode which changes the impedance of an antenna terminal such that the incident RF carrier from the interrogator is either reflected or absorbed. Usually, periodic fluctuations in the amplitude of the carrier used to transmit data back from the tag to the reader. There is only one transmitter – the passive tag (semi-active) is not a transmitter or transponder in the purest definition of the term, yet bidirectional communication is taking place through backscatter modulations. When the backward link is active, the base station (reader) transmits a CW carrier. By changing the tag's impedance, the electromagnetic wave scattered back by the antenna is modulated. This modulated backscattered signal is used for reverse link from tag to base station (reader). The concept is shown in Fig. 30.

---

[42] R. Weinstein, "RFID: a technical overview and its application to the enterprise," *IT Professional*, Vol. 7, No. 3, pp. 27-33, May-June 2005.

[43] M. Kossel, H.R. Benedickter, R. Peter, and W. Bachtold, "Microwave backscatter modulation systems," *IEEE 2000 Microwave Symposium Digest*, Vol. 3, Boston, MA, pp. 11-16, June 2000.

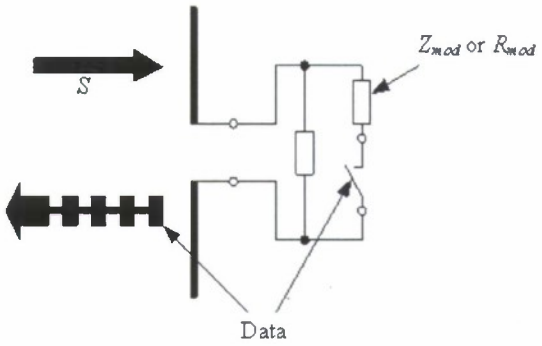


Fig. 30: Generation of the modulated backscatter by the modulation of the tag impedance $Z_{mod}$ or $R_{mod}$.

Modulation of the backscattered wave is achieved by changing the tag's impedance between two different states, $Z_1 = R_1 + jX_1$ and $Z_2 = R_2 + jX_2$.

Antenna scattering mechanisms are divided into structural and antenna mode scattering. Structural mode occurs owing to the antenna's given shape and material, and is independent of the fact that the antenna is specifically designed to transmit or receive RF energy. Antenna mode has to do directly with the fact that the antenna is designed to radiated or receive RF energy with a specific pattern.

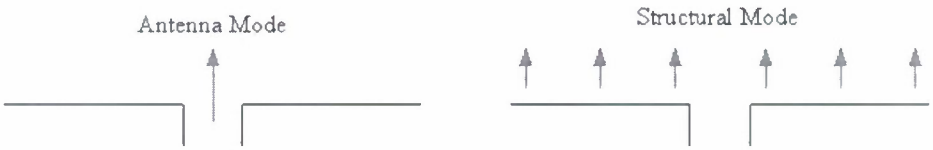


Fig. 31: Antenna scattering: Antenna mode (left) and Structural mode (right).

From Fig. 31, we obtain:

$$I = \frac{V}{\sqrt{\left(R_r + R_{Loss} + R_{Load}\right)^2 + \left(X_A + X_{Load}\right)^2}} \tag{87}$$

The power delivered from antenna to its load is:

$$P_{Ant \to Load} = I^2 R_{Load} \tag{88}$$

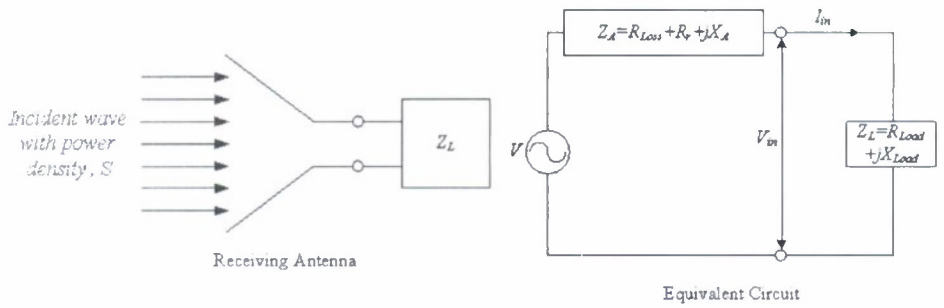


Fig. 32: Antenna equivalent circuit.

Substituting (87) into (88), we get:

$$P_{Ant\to Load}=\frac{V^2R_{Load}}{\left(R_r+R_{Loss}+R_{Load}\right)^2+\left(X_A+X_{Load}\right)^2} \tag{89}$$

In an ideal case, the power delivered from an antenna to its load impedance is equal to the total power the antenna absorbs from the incident field, *i.e.*,

$$P_{Absorbed}=SA_{eff} \tag{90}$$

where $S$ is field density at the antenna location and $A_{eff}$ is the antenna effective area. From (89) and (90), we have:

$$A_{eff}=\frac{V^2R_{Load}}{S\left[\left(R_r+R_{Loss}+R_{Load}\right)^2+\left(X_A+X_{Load}\right)^2\right]} \tag{91}$$

When the antenna load is matched to the antenna impedance, $A_{eff}$ for the lossless case is:

$$A_{eff}=\frac{V^2}{4SR_r}. \tag{92}$$

When the antenna is short circuited, $A_{eff}$ is:

$$A_{eff,SC}=\frac{V^2}{SR_r}. \tag{93}$$

When the antenna is open circuited, $A_{eff}$ is:

$$A_{eff,OC}=0. \tag{94}$$

The RCS, $\sigma$, of the tag antenna is given by:

$$\sigma = \frac{1}{\pi}\left|\frac{2\pi R E_{struct}}{E_{inc}} - (1-\Gamma_a)\frac{\pi R E_{ant}}{E_{inc}}\right|^2 \tag{95}$$

where

$R$ is the distance between the transmitting and the receiving antenna, $E_{struct}$ is the E-field at the receiver in the short circuit case, $E_{inc}$ is the E-field incident at the tag antenna, $\Gamma_a$ is the tag antenna reflection coefficient from load to antenna, and $E_{ant}$ is the E-field strength of antenna mode at the receiver antenna.

We can show that

$$\sigma = \left|(1-\Gamma_a)\sqrt{\pi}R\sqrt{\frac{S_{ant}}{S_{inc}}}\right|^2 = \left|2\sqrt{\pi}R\sqrt{\frac{S_{struct}}{S_{inc}}} - 2\sqrt{\pi}R\sqrt{\frac{S_{scar}}{S_{inc}}}\right|^2. \tag{96}$$

The power densities at the tag's and the reader's locations are, respectively:

$$S_1 = \frac{G}{4\pi R^2}P_1 = S_{inc} \tag{97}$$

and

$$S_2 = \frac{G_{tag}}{4\pi R^2}P_2 = \frac{4\pi}{\lambda^2 G}P_3 = S_{scat} \tag{98}$$

where

$G$ is the reader antenna gain, $G_{tag}$ is the tag antenna gain, $S_1$ is the power density at the tag's location (during forward link), $S_2$ is the power density at the reader's location (during backward link), $P_2$ is the power received by the tag, and $P_3$ is the backscattered power received by the reader.

As an RFID tag changes its antenna matching to form the modulation during backscattering, four different load cases come into play, as follows:

1. short circuit case
2. open circuit case
3. resistor load case
4. IC loaded case

We propose RF tags that comprise of notched filters wherein each unique tag has a unique set of notch frequencies. The brief descriptions of the operation of the band-limited noise signal with notched filters are as follows:

- Radar transmits band-limited UWB noise signal to RF Tags
- RF Tags receive the signal and notch it suitably and retransmit to Radar
- Radar receives signal from RF Tags and correlates with the reference signal to distinguish RF Tags

A zero mean white Gaussian noise signal is generated and passed through a band-pass filter to obtain a band-limited UWB noise signal in the 1-2 GHz range. (This frequency range has been selected for simulation purpose. In actual practice, the frequency may be different). Fig. 33 shows the simulated waveforms of the Gaussian noise and the output of the transmitter after band-limited operation. This band-limited noise signal is notched over a sub-band, and it can be noted that the notched noise transmissions will not be detected by hostile receivers because the waveform appears random and noise-like, as shown in Fig. 34. Therefore, the two requirements of LPI and LPD are clearly met by this method.

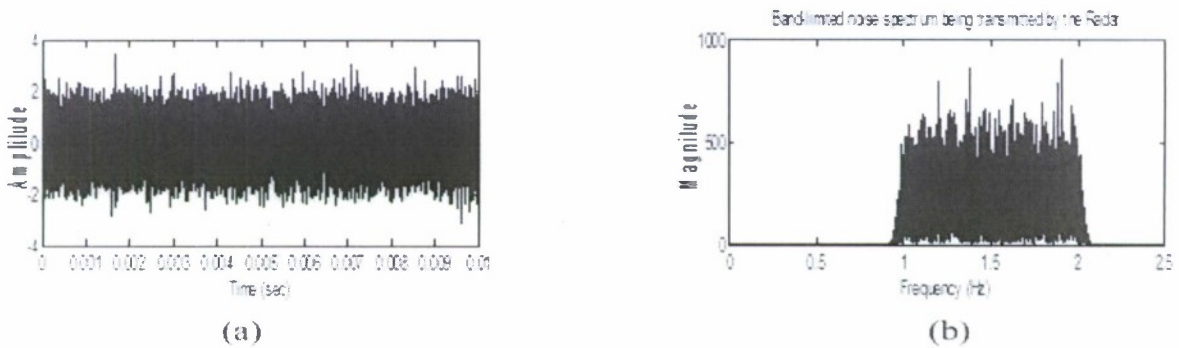


Fig. 33: Band-limited noise in the (a) time domain, and (b) frequency domain.

It is imperative that the radar system has appropriate information of the different notch frequencies (unique IDs for each tag) and uses this information to distinguish returns from multiple tags using correlation processing.

During communications, losses are indispensable. Among the losses, channel noise will be presented in this section. To simulate channel, WGN is added to the channel as shown in Fig. 35.

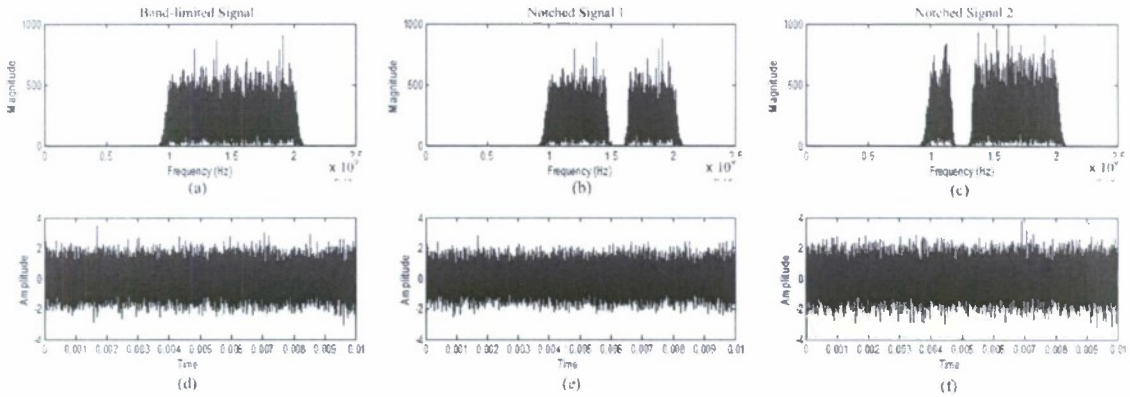


Fig. 34: Signals in time domain (top) and frequency domain (bottom): (a) and (d) Original band-limited signal, (b) and (e) Notched signal 1, and (c) and (f) Notched signal 2.

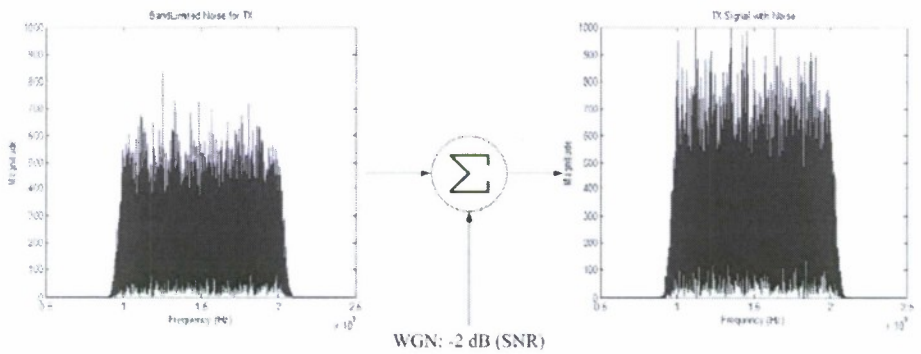


Fig. 35: Simulation of channel noise.

Once the RF tags receive the signals from the radar, they notch the received signals based on their pre-designed configurations. Initially, single notch frequencies with different percentage of notching in a whole frequency band (1%, 10%, and 20%) were simulated. Later, to have better flexibility, two single notch frequencies are cascaded to make two notch frequencies in each tag.

When the tags receive the band-limited noise signal, they notch it and retransmit to the radar. Every tag will have its own notch filters, which have different stopband characteristics, as depicted in Fig. 36. The stopband information has been pre-agreed and stored at the radar for correlation with received signals from each tag. The radar will correlate the received signals with stored notched signals to distinguish tags. Using this method, the numbers of tags appears to be very limited. Therefore, an alternate method of using two notch frequencies was also explored.

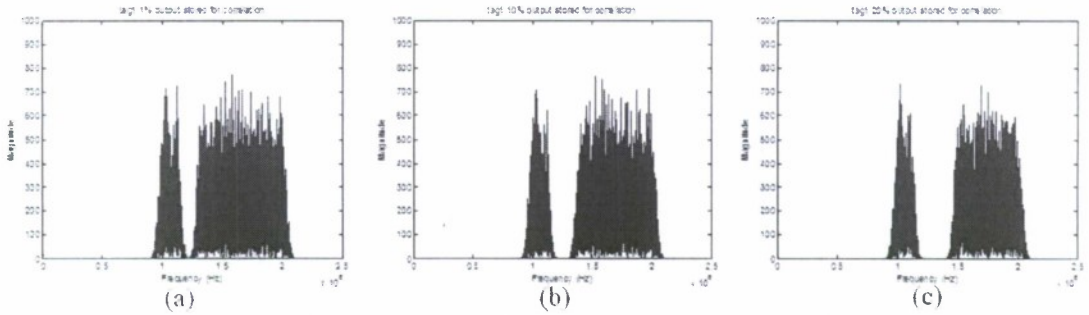


Fig. 36: Single notch with different notch percentages: (a) 1%, (b) 10%, and (c) 20%.

The frequency band was 1–2 GHz and 8 main bands were created based on the notch filter specification shown in Fig. 37. Several such tags were designed to simulate various tags with various cascaded notch filters, as shown in Fig. 38.

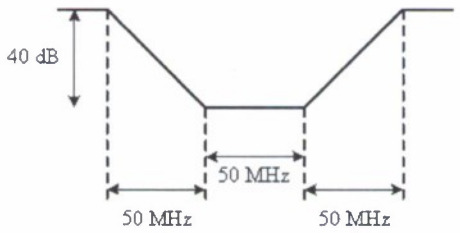


Fig. 37: Single notch filter characteristics.

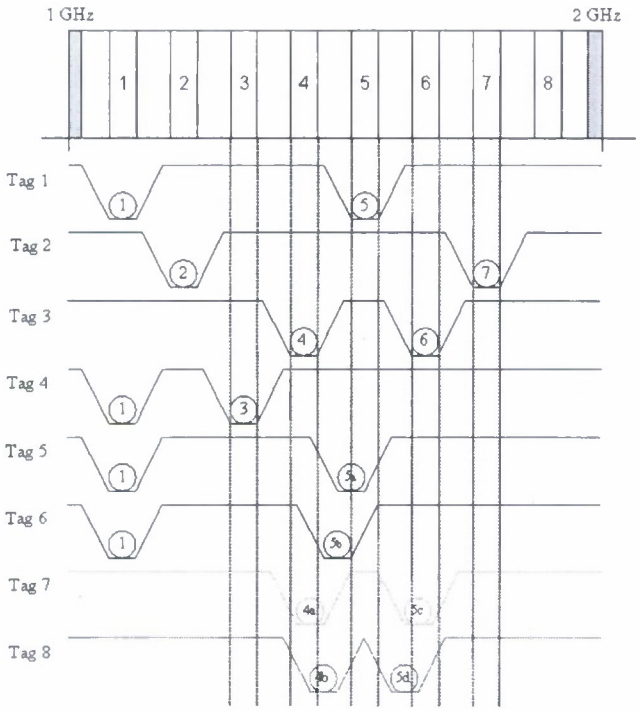


Fig. 38: Various Tags with different dual notch frequencies.

The characteristics of each tag are as follows:

| | |
|---|---|
| (a) Tag 1: | Reference |
| (b) Tag 2 & Tag 3: | No overlapping with a reference signal |
| (c) Tag 4: | Overlapping only one band |
| (d) Tag 5 & Tag 6: | Overlapping one and some of the 2nd band |
| (e) Tag 3, Tag 7, & Tag 8: | Different overlapping with one band |

Fig. 39 shows additional severe overlapping cases:

| | |
|---|---|
| (a) Tag 1a & Tag 2a: | Different references |
| (b) Tag 9 & Tag 10: | Different overlapping with Tag 1a |
| (c) Tag 11: | Overlapping with Tag 2a |

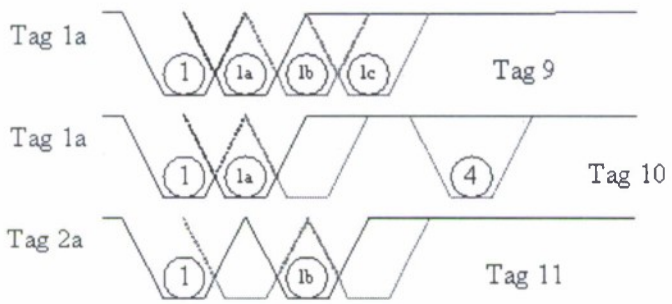


Fig. 39: Additional tags to simulate severe overlapping.

Fig. 40 shows the three different sample tag configurations.

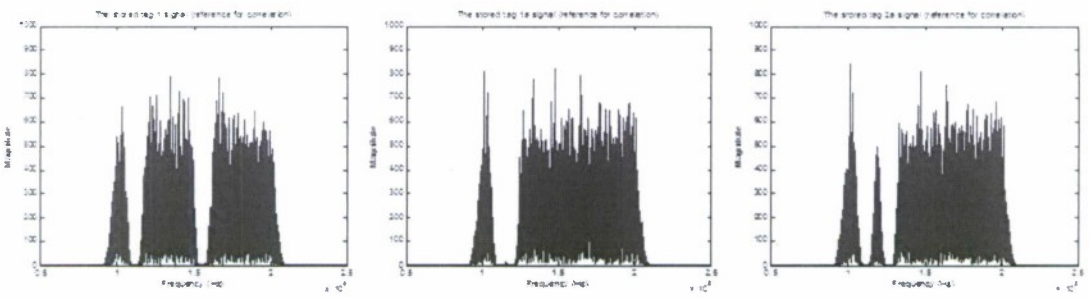


Fig. 40: Three different tag configurations:
(a) Tag 1 (Reference 1), (b) Tag 1a, and (c) Tag 2a.

Fig. 41 shows some of the tags which have different dual notch frequencies.

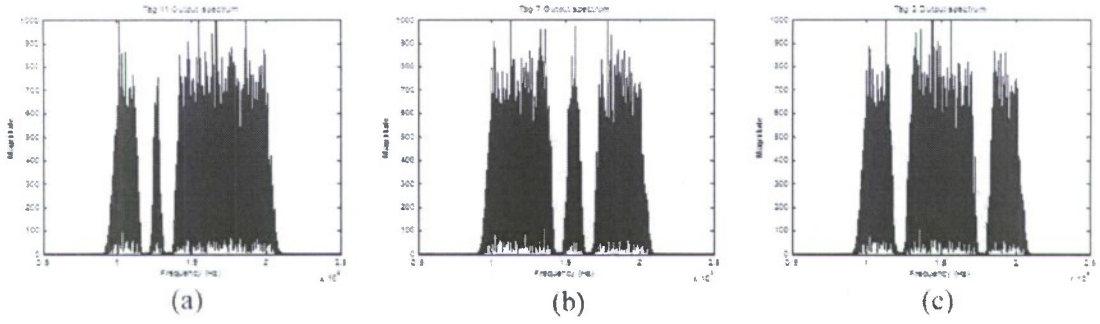


Fig. 41: Three tags with different dual notch frequencies:
(a) Tag 11, (b) Tag 7, (c) Tag 2.

We now look at the results of identifying returns from tags using the correlation method. The summary of operations shown in Fig. 42 is as follows:

1. Radar transmits band-limited noise signal to tags,
2. Radar stores all the pre-agreed tag information (notch frequencies),
3. Tags notch the received signal and re-transmit to Radar,
4. Radar correlates the received signals with the stored tag information.

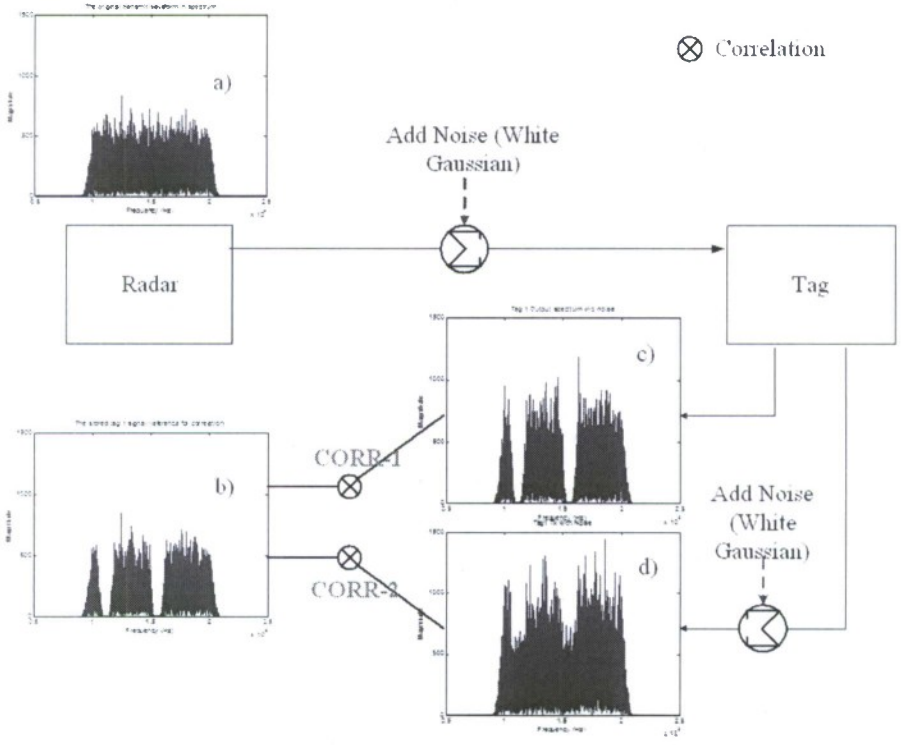


Fig. 42: Multi-tag operations with correlations:
(a) Band-limited noise signal, (b) Stored signal ID, (c) Received signal from tags without WGN, and (d) Received signal from tags with WGN.

Fig. 43 shows the changes to the received signals with added WGN. The correlation results are shown in Fig 44 and a description is provided in Table IV.

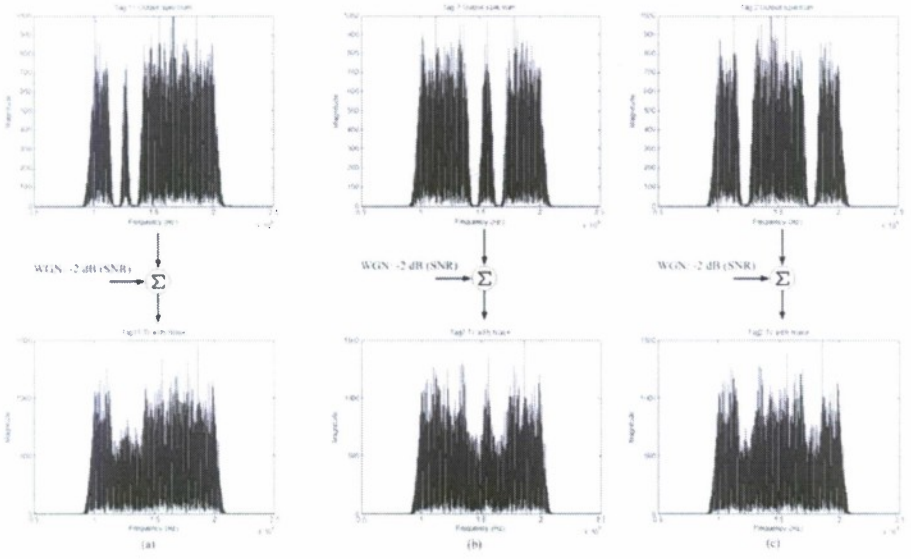

Fig. 43: Received signals with and without WGN:
(a) Tag 11, (b) Tag 7, (c) Tag 2.

TABLE IV: DESCRIPTION FOR FIGURE 44

| Figure Ref. | Description | Remark |
|---|---|---|
| (a) | Reference Signal ⊗ Tag 1 | Auto Correlation |
| (b) | Reference Signal ⊗ Tag 1 Noisy | Added WGN |
| (c) | Reference Signal ⊗ Tag 2 | |
| (d) | Reference Signal ⊗ Tag 2 Noisy | Added WGN |
| (e) | Reference Signal ⊗ Tag 3 | |
| (f) | Reference Signal ⊗ Tag 3 Noisy | Added WGN |
| (g) | Reference Signal ⊗ Tag 4 | |
| (h) | Reference Signal ⊗ Tag 4 Noisy | Added WGN |
| (i) | Reference Signal ⊗ Tag 5 | |
| (j) | Reference Signal ⊗ Tag 5 Noisy | Added WGN |
| (k) | Reference Signal ⊗ Tag 6 | |
| (l) | Reference Signal ⊗ Tag 6 Noisy | Added WGN |
| (m) | Reference Signal ⊗ Tag 7 | |
| (n) | Reference Signal ⊗ Tag 7 Noisy | Added WGN |
| (o) | Reference Signal ⊗ Tag 8 | |
| (p) | Reference Signal ⊗ Tag 8 Noisy | Added WGN |

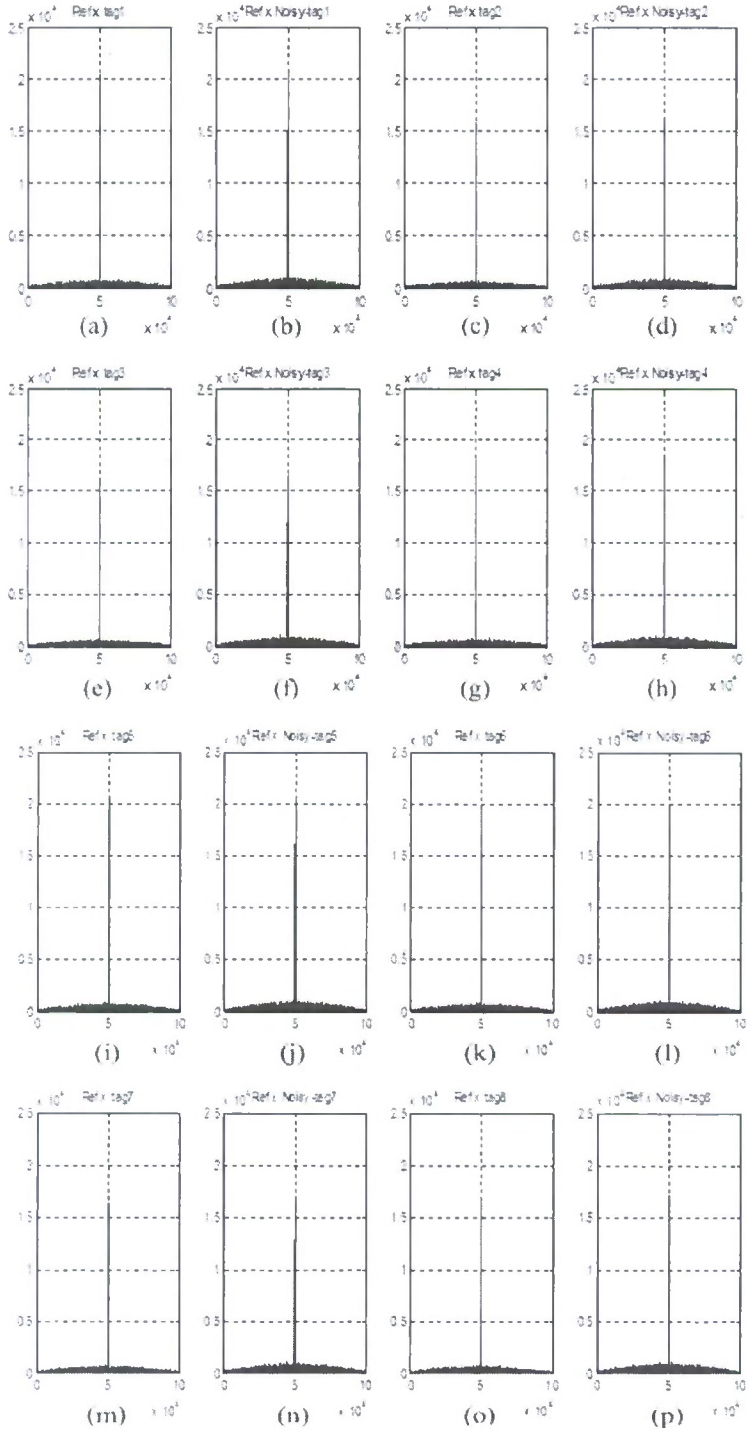


Fig. 44: Correlation results.

Simulation results show the added White Gaussian Noise does not affect the correlation. Figure 45 shows more detail.

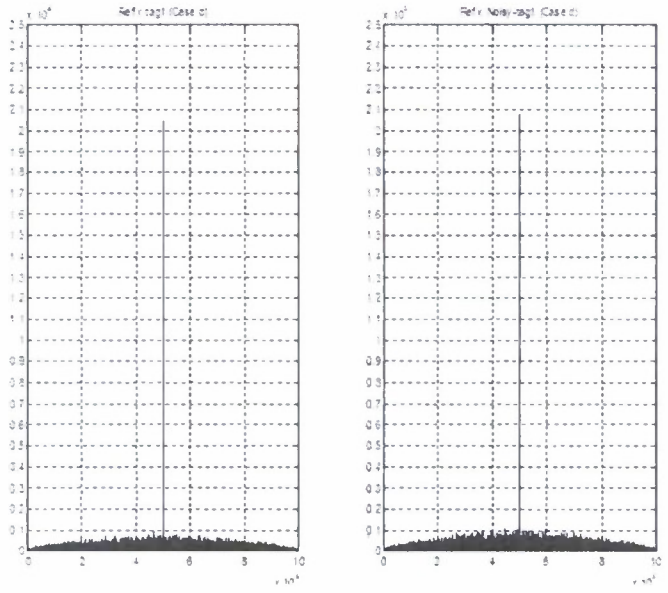

Fig. 45: Comparison between (a) and (b) of Table IV.

The previous simulation results show that the suggested correlation method to distinguish Tags in multi-tag environment is quite robust against channel noise.

In addition to the channel noise, there are other losses (attenuations) which might affect the communications and are investigated. Since tags are different than any other transponders especially because of the limitation of power, the attenuation will be a major issue for communications. The attenuation coefficient is the attenuation per unit distance along the path in a given medium, usually expressed in dB/km. It is usually expressed as a two-way value in the radar case.

The Friis free space equation is given by

$$P_r = P_t G_t G_r \left(\frac{\lambda}{4\pi d}\right)^2 = P_t \left(\frac{\lambda}{4\pi d}\right)^2, \text{ with } G_t = G_r = 1. \tag{99}$$

The path loss is defined as

$$\mathrm{PL(dB)} = 10\log\left(\frac{\lambda}{4\pi d}\right)^2 = 20\log\left(\frac{c}{4\pi fd}\right). \tag{100}$$

The path loss effect is more pronounced for wideband and UWB waveforms. Equation (100) shows that the path loss per octave is 6 dB for a fixed distance. The power received for a

uniform PSD 1-2 GHz random noise waveform is shown in Fig. 46. In the two-way tag communications, the total path loss will be 12 dB per octave. In our simulations, $f_1$ is 1 GHz and $f_2$ is 2 GHz. Therefore, path loss at 2 GHz will be 12 dB higher compared to 1 GHz. The following results in Fig. 47 show the path loss simulations. The SNR is −2 dB and the two-way path loss varies from 0 to 12 dB from 1 to 2 GHz (i.e., 12 dB/octave).

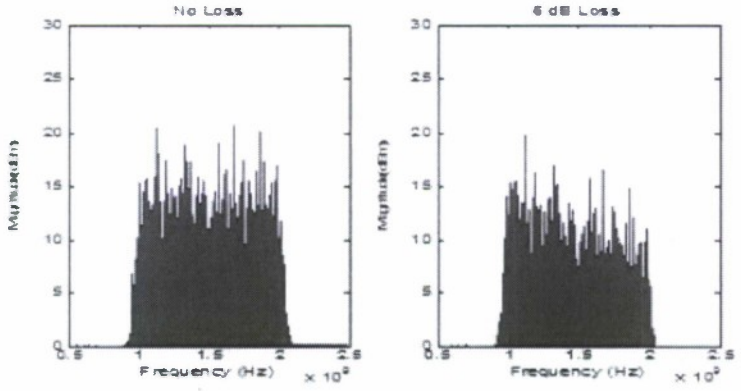


Fig. 46: Received power for a one-way path loss (6 dB/octave).

Simulations indicate that channel noise (SNR of −2 dB) with free space path loss do not affect performance too much. Various factors which can affect communications have been simulated, such as channel noise and path losses. According to simulations, the suggested method which applying correlation to distinguish tags was very strong against to those factors. However, as Table V shows, in order to distinguish between tags, the receiver processor should have the capability to distinguish differences less than 20% of the peak auto-correlation value. This might require a complicated receiver design.

TABLE V: SUMMARY OF PATH LOSS SIMULATIONS (WITH AWGN)

| Figure Ref. | Description | Difference |
|---|---|---|
| (a) | Reference Signal ⊗ Tag 1 (Auto-Correlation) | 0 |
| (b) | Reference Signal ⊗ Tag 2 | 21 % |
| (c) | Reference Signal ⊗ Tag 3 | 21 % |
| (d) | Reference Signal ⊗ Tag 4 | 12 % |
| (e) | Reference Signal ⊗ Tag 5 | 0 % |
| (f) | Reference Signal ⊗ Tag 6 | 4 % |
| (g) | Reference Signal ⊗ Tag 7 | 21 % |
| (h) | Reference Signal ⊗ Tag 8 | 16 % |

It has thus been demonstrated through simulations that the suggested method of using correlation to distinguish RF tags is indeed valid.

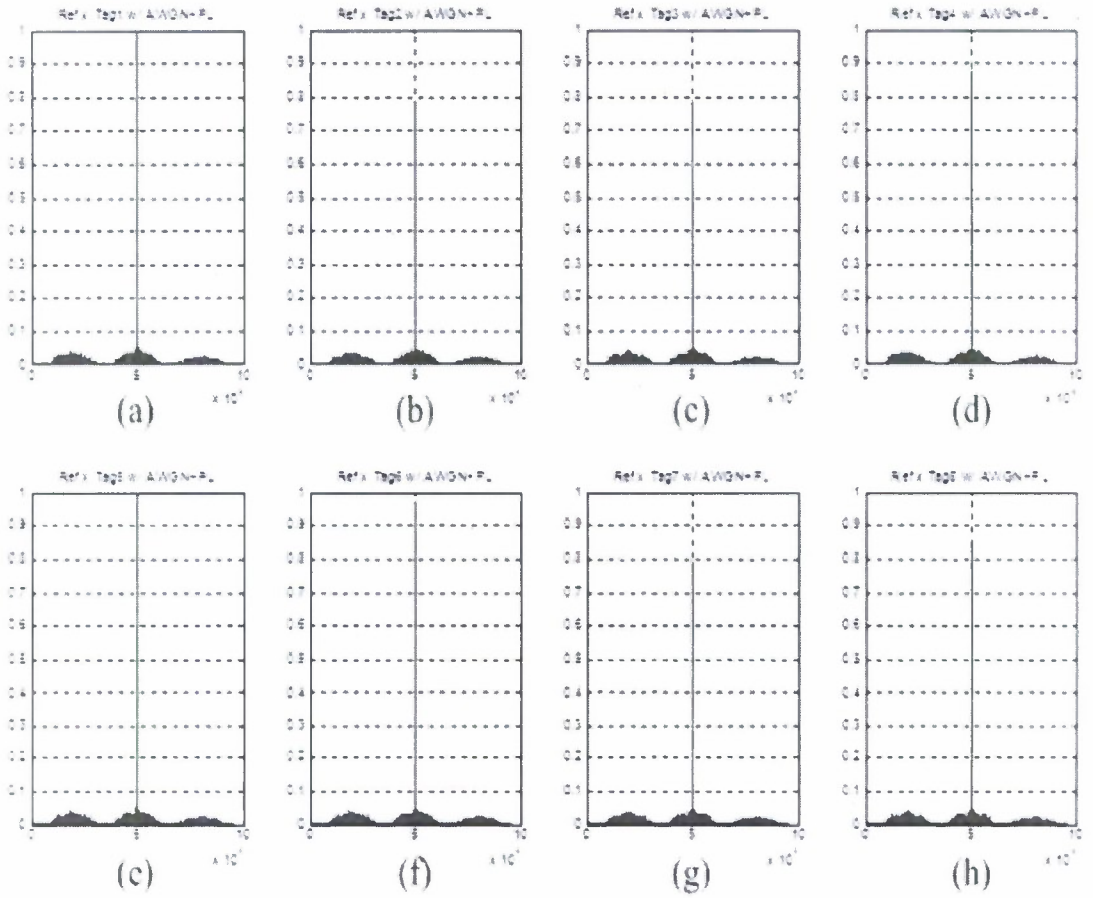


Fig. 47: Correlation results with channel noise (SNR = -2 dB) and two-way path loss (12 dB per octave).

*RF tags for Detecting Target Orientation:*

We now explore a newly suggested application of using RF tags to detect target orientation. First, a sphere will be used as a target for developing a general approach of RCS and then a simulated tank will be used as a target for further analysis. Consider a sphere as shown in Fig. 48 whose scattering RCS simulation results are shown in Fig. 49.

Fig. 49 shows the RCS variations with different $k_0a$ values, where $a$ is the radius of the sphere. It shows that forward scattering RCS is bigger than backscattering RCS. Fig. 50 shows backscattering RCS from 1–2 GHz with FEKO software and Fig. 51 shows the bistatic RCS at 1.45 GHz and 2 GHz. It shows that the forward scattering RCS ($\theta$ : 180°) is the highest.

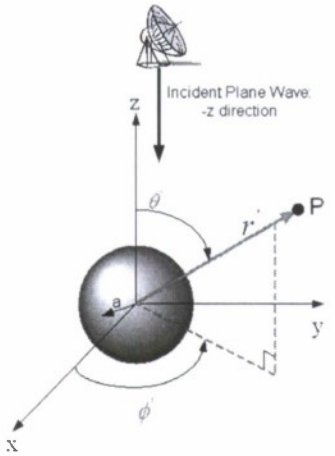


Fig. 48: Scattering geometry for a sphere.

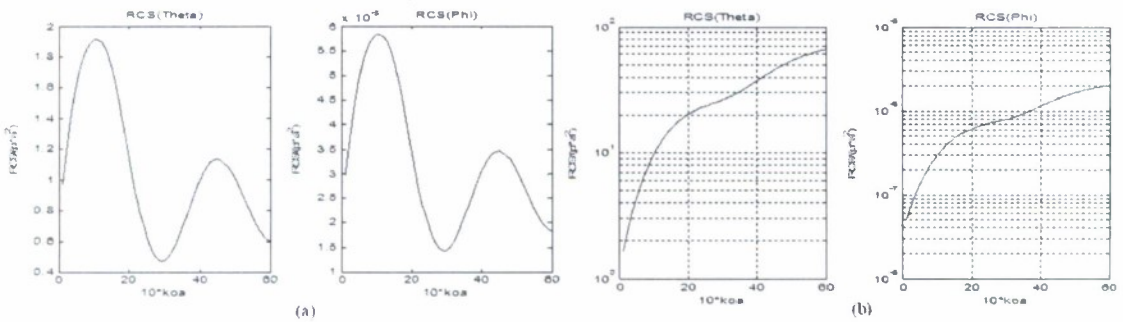


Fig. 49: Backscattering (a) and forward scattering (b) of sphere.
(a) ($\theta'$ : 0.01°, $\phi'$ : .01°, Iterations: 10), (b) ($\theta'$ : 179.9°, $\phi'$ : .01°, Iterations: 10)

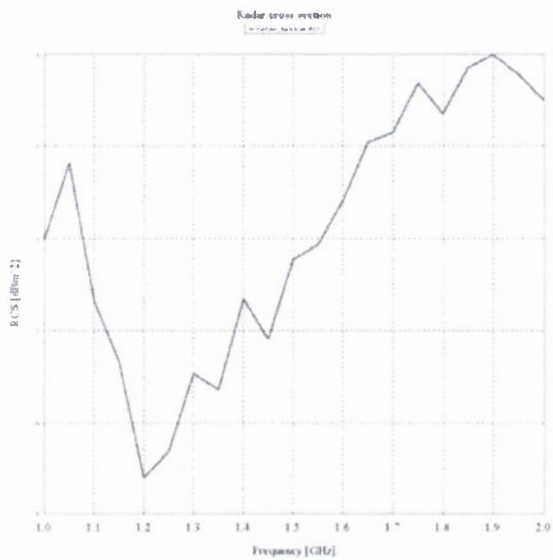


Fig. 50: Backscattering RCS from 1–2 GHz using FEKO software.

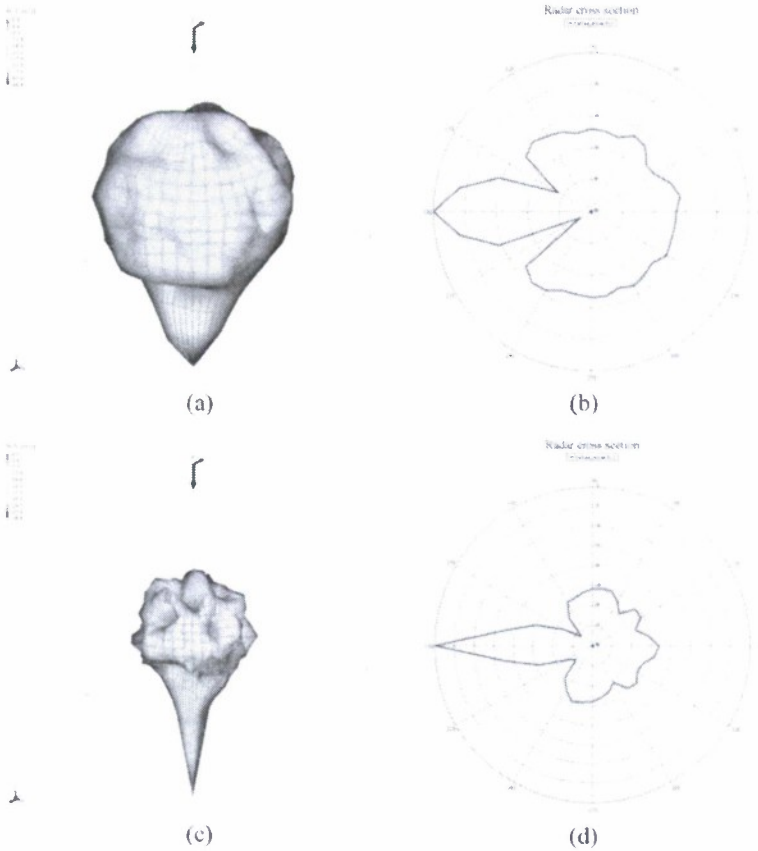


Fig. 51: Bistatic RCS of a sphere: (a) and (b) 1.45 GHz, (c) and (d) 2 GHz.

Let us assume that a tag is located at position $P'$ in Fig. 52. Therefore, scattered field at the point $P'$ will be an incident field for the tag. The scattering fields are given as follows. For simplified analysis, a sphere-shape tag is assumed. As stated before, a new RCS will be generated with the scattered field at $P''$ to detect the target orientation.

To detect target orientation using tag RCS, we use the following assumptions:

- Nine incident plane waves will be used as excitations (simulate target orientations),
- Tags are positioned around the target,
- Target is a perfect electric conductor (PEC).

The geometry of the simulated tank target is shown in Fig. 53. As is seen in Fig. 54, nine (9) incident plane waves are used for simulations that are related to various target orientations. The different angles of incidence simulate different target orientations as shown in Fig. 55.

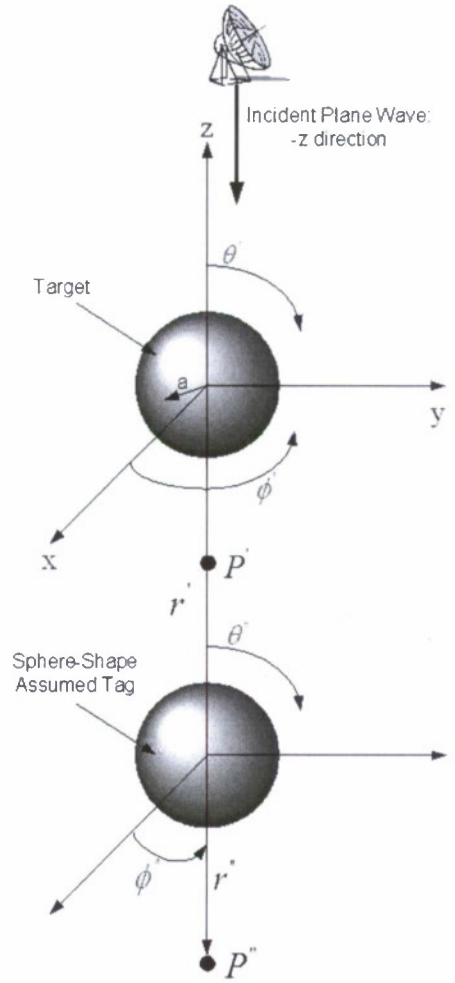


Fig. 52: Sphere-shaped tag configuration.

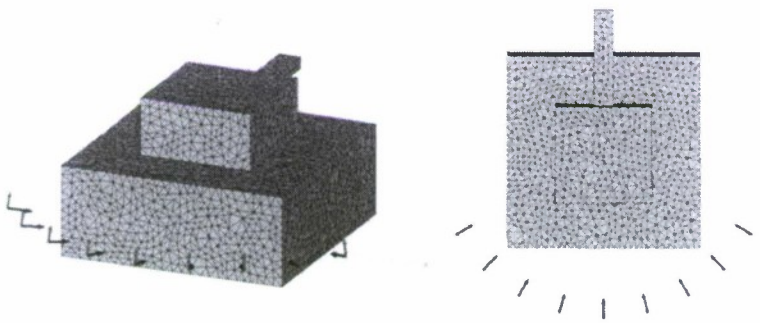

Fig. 53: Simulated tank target and directions of incident plane waves.

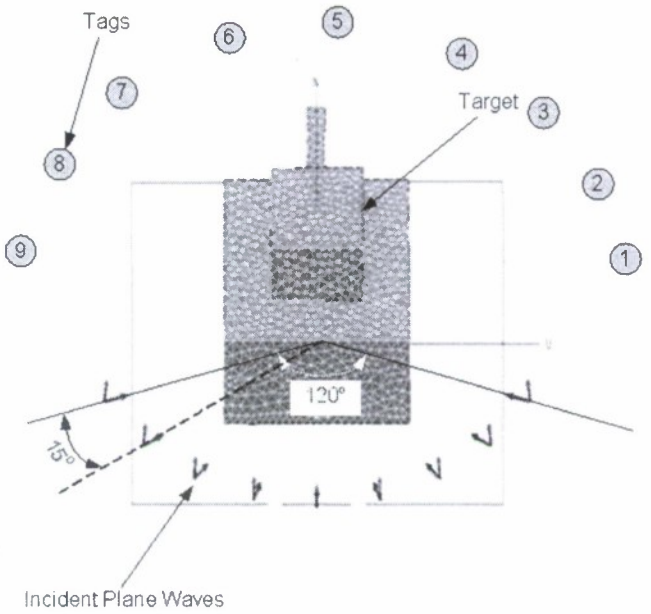


Fig. 54: Simulated tank target with tags.

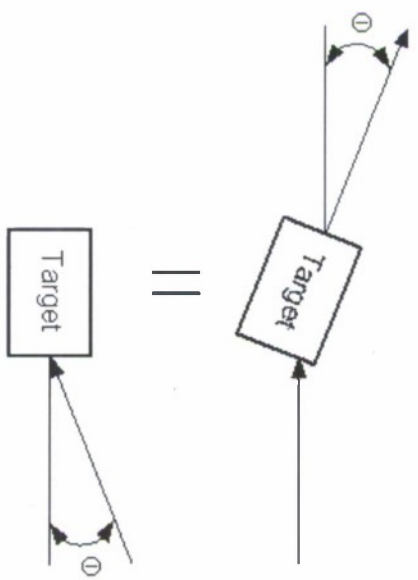


Fig. 55: Incident plane waves and target orientations.

Target RCS (scattered field) will vary depending upon the angle (i.e., its orientation). In addition, since tags are passive (or semi-passive) devices, the scattered field amplitude from a target greater than the threshold level will activate the tags. Therefore, tags which are located in the area where target RCS (scattered field) is above the threshold level will be activated, and as a result, the tags can be used to identify the target orientation. This is

important for military targets such as tanks, as this can provide clues to where the gun barrel is pointed, for example.

As Fig. 56 shows, tags at locations □ and □ will respond because of the scattered field from target is significantly higher at these corresponding scattered angles.

Furthermore, in wideband systems, the target will have its unique RCS pattern at certain angles for each frequency with different amplitudes as shown in Fig. 57 and Fig. 58 (polar plots). Therefore, using an arbitrary threshold level (−10 dB), tags located in the hatched region will respond, and from this information the target orientation can be detected.

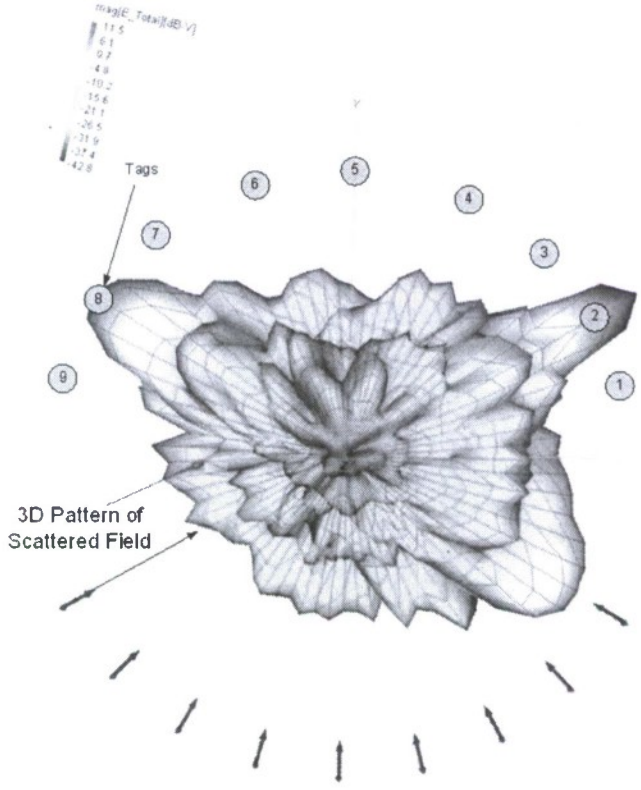


Fig. 56: Detecting target orientation with tags (3D pattern).

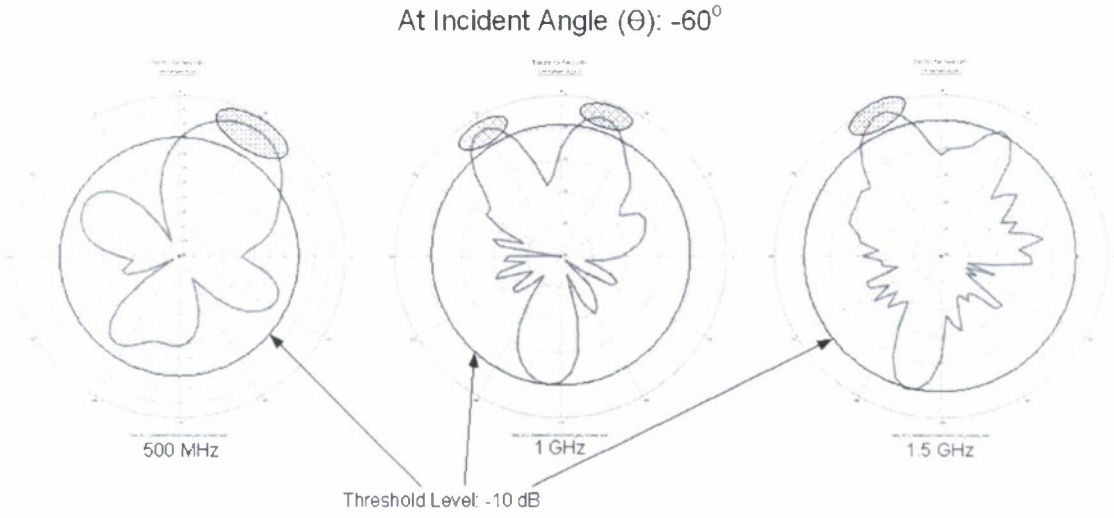


Fig. 57: Detecting target orientation with tags (2D polar pattern) using a threshold level (Incident angle θ = −60°).

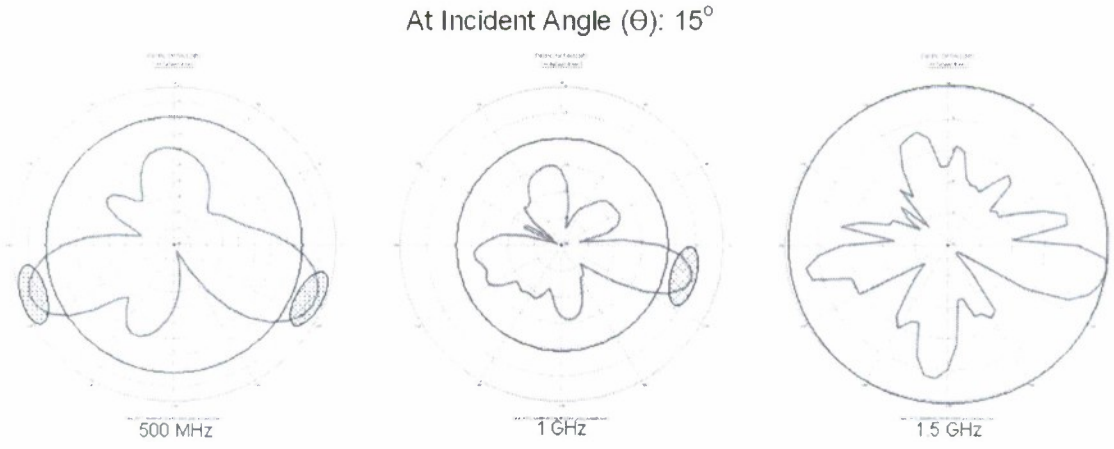


Fig. 58: Detecting target orientation with tags (2D polar pattern) using a threshold level (Incident angle θ = 15°).

*Radar Tag Operating Scenario:*

The Radar—RF tag communication scenario is shown in Fig. 59. Radars are distributed to cover a large area where the RF tags are roaming in a way that less coverage range overlapping occurs. Each radar interrogates the RF tags within its range using a broadcast command. Several radars work collaboratively to communicate with the tags in the whole region.

We assume that the radar transmits bandlimited UWB noise signal to the tags. Upon receiving the radar's signal, the tags within its range wake up and respond to the radar with simple messages such as "I'm OK", "I need help", etc. by modulating the radar signal. Although the tags are passive in that they answer queries using the power transmitted by the radar, it is also possible to increase the range by using an auxiliary power source. The radar detects the responsive RF ID numbers and corresponding tag messages from the tag returns.

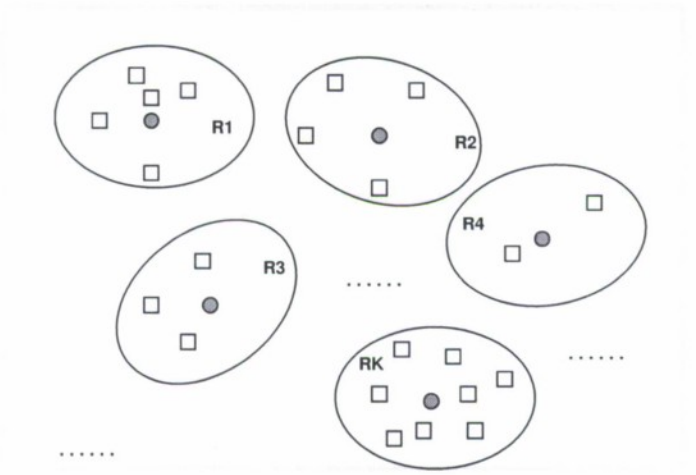


Fig. 59: Radar—RF tag communication scenario.

Tag System Structure

The Radar—RF tag communication system structure is proposed in Fig. 60.

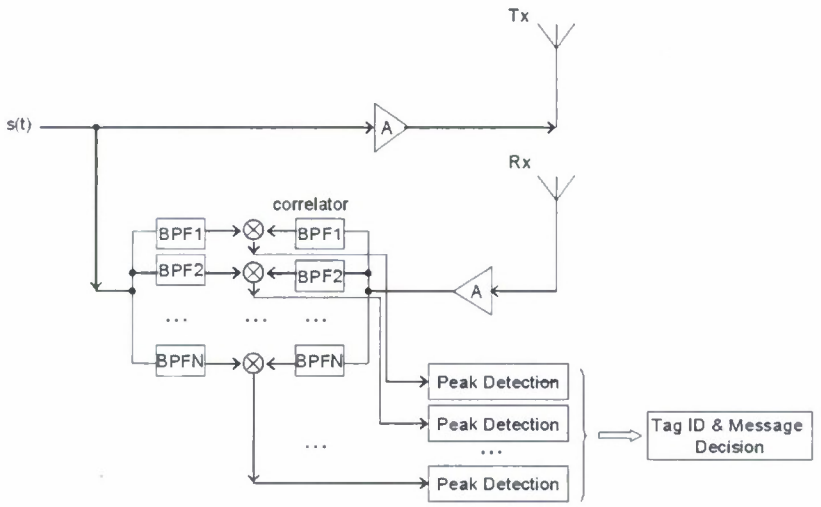


Fig. 60: Radar-RF tag communication structure.

To illustrate the procedure, take the communication between radar and Tag 1 for example.

*Step 1:*

Bandlimited UWB noise signal $s(t)$, shown in Fig. 61, is transmitted to the tags in region $j$ after amplification by the Radar $j$ at time $t$. A replica of signal $s(t)$ is preserved at the radar as reference for tag and message detection.

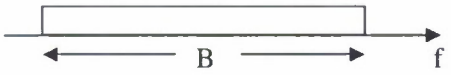


Fig. 61: Bandlimited UWB noise signal spectrum.

*Step 2:*

Each tag filters the received radar signal to a certain frequency band according to the tag ID number. The radar signal frequency band is divided into several non-overlapping sub-bands occupied by different tags, as shown in Fig. 62. Band gap is kept to avoid the interference between the signals of different tags.

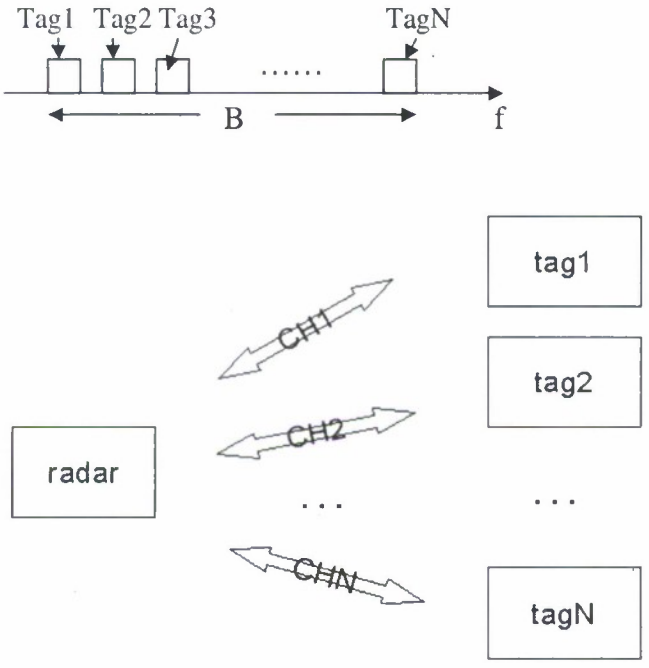


Fig. 62: Nonoverlapping subband interrogation scheme for RF tags.

Tag messages are modulated onto the received radar signal through weighted delays and transmitted back to the radar by the tags. The structure of the tag is shown in Fig. 63.

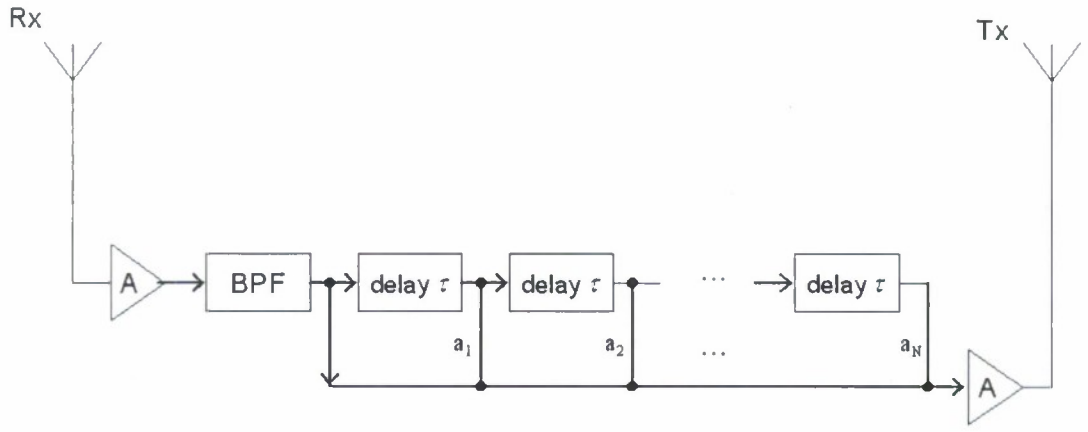


Fig. 63: RF tag structure.

The radar signal arriving at the tag receiver front is given by

$$r(t) = \alpha \cdot s(t - \tau_1) + n(t), \tag{101}$$

where α is signal attenuation, $n(t)$ is white Gaussian channel noise, and $\tau_1$ is the path delay. After passing through the bandpass filter, the received signal becomes

$$y(t) = \alpha \cdot s_1(t - \tau_1) + n(t). \tag{102}$$

The modulated signal at the tag transmitter is

$$y'(t) = y(t) + \sum_{i=1}^{L} a_i y(t - i\tau) = \alpha \cdot [s_1(t - \tau_1) + \sum_{i=1}^{L} a_i s_1(t - \tau_1 - i\tau)] + n(t) \tag{103}$$

where $\tau$ is the unit modulation delay, and the weights $a_i$, $i = 1,2,\ldots,L$ are chosen as either 1 or 0. This enables the tag to transmit $2^L - 1$ kinds of messages, wherein $a_1$ is the first bit of the message, $a_2$ is the second bit, and so on.

*Step 3:*

The tag returned signal at the radar receiver front is

$$y_1(t) = \alpha \cdot y'(t - \tau_1) + n(t) = \alpha^2 \cdot [s_1(t - 2\tau_1) + \sum_{i=1}^{L} a_i s_1(t - 2\tau_1 - i\tau)] + n(t) \tag{104}$$

with the assumption that the channel delay and the signal attenuation are the same as the radar-to-tag link, and that multipath propagation is not taken into consideration.

The tag returned signal $y_1(t)$ is passed through a bank of bandpass filters which are the same as their counterparts used in the RF tags. If only RF Tag 1 responds to the radar, then the output of bandpass filter 1, $y_{11}(t)$, is

$$y_{11}(t) = \alpha^2 \cdot [s_1(t-2\tau_1) + \sum_{i=1}^{L} a_i s_1(t-2\tau_1 - i\tau)] + n(t) \tag{105}$$

and the output of the rest of the bandpass filters are colored noise $n(t)$.

The reference radar signal $s(t)$ is passed through the same bank of bandpass filters. The corresponding outputs are $s_1(t)$, $s_2(t)$, ... $s_N(t)$.

The outputs of the same bandpass filter from the tag returned signal and the reference radar signal cross-correlated. The window used in cross correlation when detecting the tag ID and its corresponding messages at radar receiver is shown in Fig. 64.

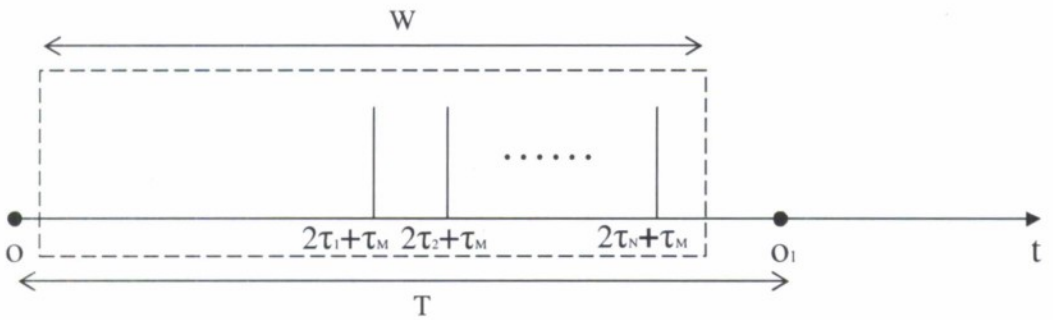


Fig. 64: Cross correlation window.

In the above, $\tau_1 \sim \tau_N$ is single path delay for RF Tag1 ~ RF TagN; $\tau_M = L \cdot \tau$ is the maximum modulation delay, since $L$ and $\tau$ are both known by the radar in advance, thus $\tau_M$ is also known *a priori* at the radar. $W$ is the window length of cross correlation, and it can be calculated as $W = 2\tau_{\max} + \tau_M$. $\tau_{\max}$ is estimated maximum single path delay, $\tau_{\max} = R_{\max}/v$. $R_{\max}$ is the estimated maximum radar range from the radar equation, $R_{\max} = \left[\frac{P_t G A_e \sigma}{(4\pi)2S_{\min}}\right]^{1/4}$, where $S_{\min}$ is the minimum radar detectable signal, $\sigma$ is the RF tag's radar cross section, $P_t$ is the radar transmitted power, $G$ is the transmit antenna gain, and $A_e$ is the receiving antenna aperture area. Also, $T$ is the radar pulse period.

The cross correlation result from bandpass filter 1 is

$$r_{s_1 y_{11}}(k) = E\{s_1(t+k) \cdot y_{11}(t)\} = \alpha^2 \cdot [\delta(-2\tau_1) + \sum_{i=1}^{L} a_i \delta(-2\tau_1 - i\tau)] \tag{106}$$

since the information bearing signal is a noise waveform, and it is uncorrelated with the channel and other noise. The first peak of the cross correlation result is located at $2\tau_1$, which is the round path delay of the tag. If $a_i \neq 0$ for some $i$ = 1,2,...,$L$, then other tag message bearing peaks can be observed at $2\tau_1 + i\tau$, from which te information on whether the tag is responsive as well as which message was sent can be determined.

If the tag message peaks exist, then the tag is responsive, and the tag ID can be detected according to the mapping from the bandpass filter number to the tag ID. To detect the kind of tag message, it needs to capture the modulation delay weight $a_i$, $i$ = 1,2,...,$L$ of that tag. The distances between the first peak and following peaks divided by $\tau$ gives the non-zero bit index, and since the message length $L$ is also known, therefore the message sequence can be decoded. The cross correlation results from the rest bandpass filters are almost zero, which is because the radar signal is uncorrelated with channel noise and other noise.

Simulation Setup

Suppose there are three tags within the range of Radar $j$, and there are a total of three delay taps at each tag.

Subband Width = 0.32 GHz = 320 MHz, Band Gap = 0.02 GHz = 20 MHz;

Tag1 band: 1 GHz~1.32 GHz,
Tag2 band: 1.34 GHz~1.66 GHz,
Tag3 band: 1.68 GHz~2 GHz;

Sampling frequency: 6 GHz;

Tag1's round path delay: 16000 sample intervals,
Tag2's round path delay: 10000 sample intervals,
Tag3's round path delay: 6000 sample intervals,

The corresponding round path delay to the radar's range: $4\times10^{-4}$ sample intervals;

Tag1's message: 101 (msg#5),
Tag2's message: 100 (msg#4),
Tag3's message: 011 (msg#3);

SNR: −3 dB;

Signal attenuation factor $k = 1$;

Modulation unit delay: 90 sample intervals;

The effects of amplifiers and the multipath signals are not considered in the simulation.

Simulation Results

Radar transmitted noise signal over the 1-2 GHz frequency band is shown in the time domain and frequency domain in Fig. 65 and Fig. 66 respectively.

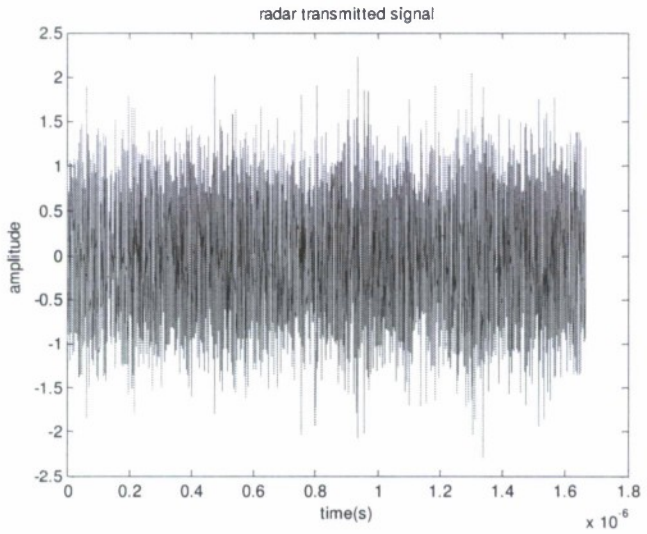


Fig. 65: Time domain representation of 1-2 GHz noise signal.

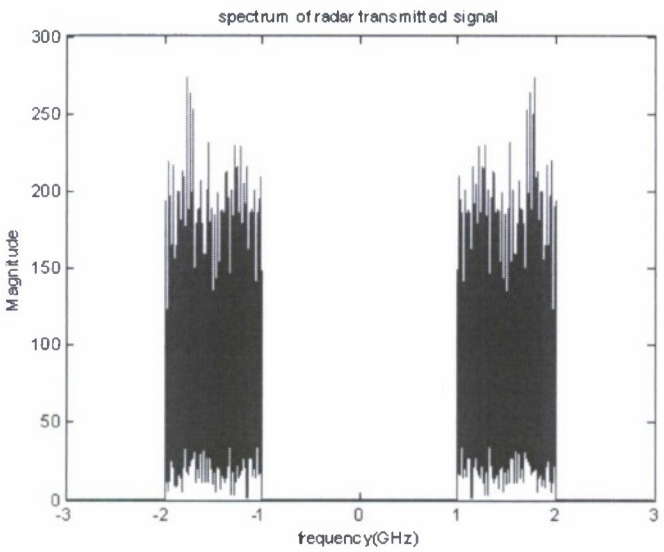


Fig. 66: Frequency domain representation of 1-2 GHz noise signal.

The radar signal is filtered to occupy nonoverlapping frequency bands at different tags. The spectra of the filtered signals at Tag1, Tag2, and Tag3 are shown in Fig. 67.

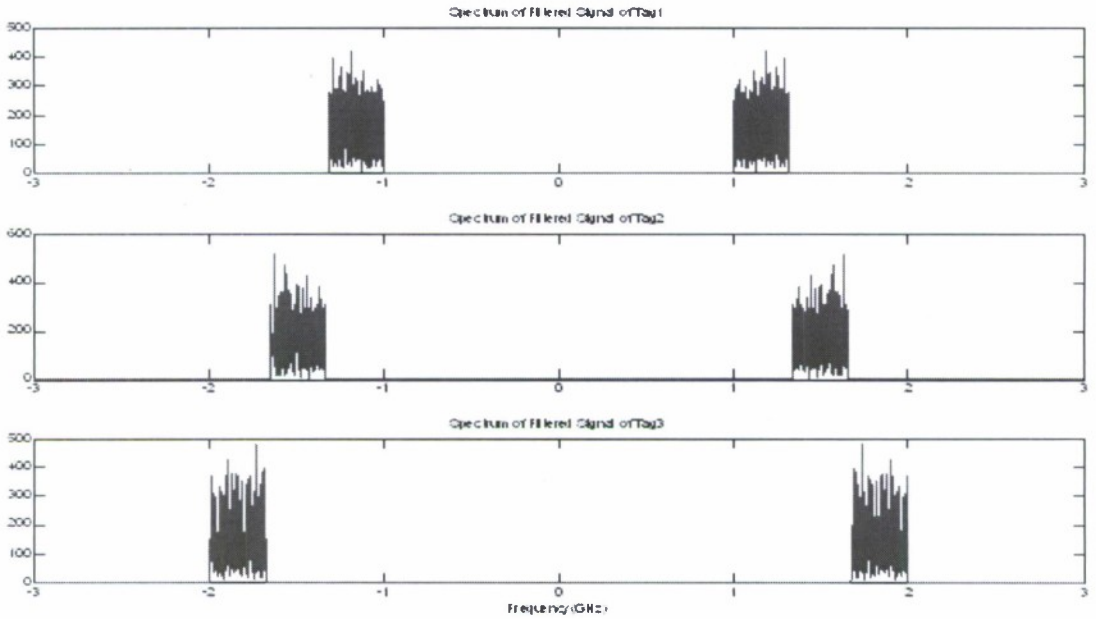

Fig. 67: Spectra of filtered signals at Tag1, Tag2, and Tag3.

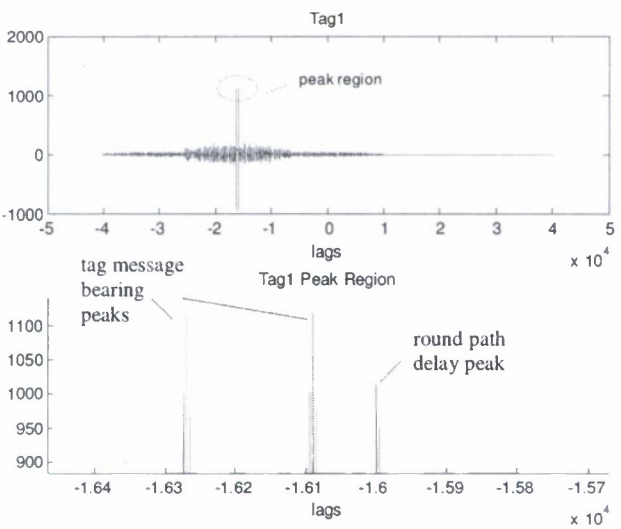


Fig. 68: Cross-correlation results for Tag1 detection.

The cross correlation outputs at the radar receiver for Tag1 detection are shown in Fig. 68. We note that there are three peaks in the cross correlation result for the detection of Tag1. The first peak is located at $-1.6\times10^4$ lags, which is consistent to the round path delay of Tag1 returned signal as in the simulation setup. The following two peaks are located at $-1.609\times10^4$ lags and $-1.627\times10^4$ lags respectively, which are one modulation delay and three modulation delay from the first peak. So Tag1 is responsive to the radar's interrogation. It is also known that there are three delay taps at each tag, that is, the length of tag message is three bits. Then

it can be determined that Tag1 message is 101. The decoded Tag1 message at the radar matches the original message sent by Tag1.

The detection results for Tag2 and Tag3 are shown in Fig. 69 and Fig. 70 respectively. Tag2's message is decoded as 100, and Tag3's message is decoded as 011, and both agree with the original messages sent by Tag2 and Tag3 respectively.

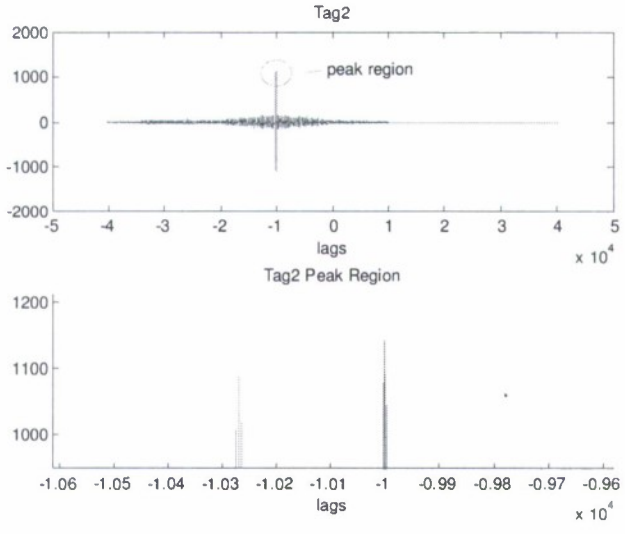


Fig. 69: Cross-correlation results for Tag2 detection.

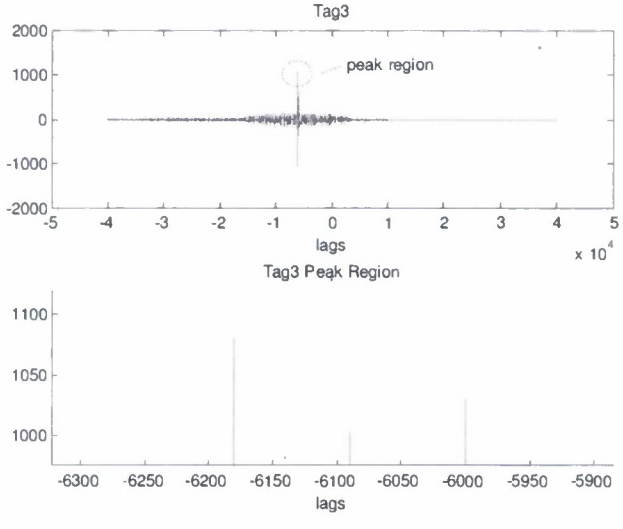


Fig. 70: Cross-correlation results for Tag3 detection.

Role of multipath signals

Multipath signals of the radar transmitted signal and the RF tag returned signal can degrade the detection performance of the radar, since they can be viewed as undesired delay

modulated signals, as shown in Fig. 71. It can be assumed that the multipath signals have very low power compared to the tag direct returns, and their cross correlation outputs with the replica of the radar transmitted signal also have so low peak values relatively that the multipath signals can be differentiated from the tag direct returned signals. Additionally, the tag direct returns at time $2\tau_i + k\tau$, $k = 1,2,...L$, should have almost the same power if the tag is static. If the tag is moving, they may have different powers but their powers should still be much higher than that of the multipath signal.

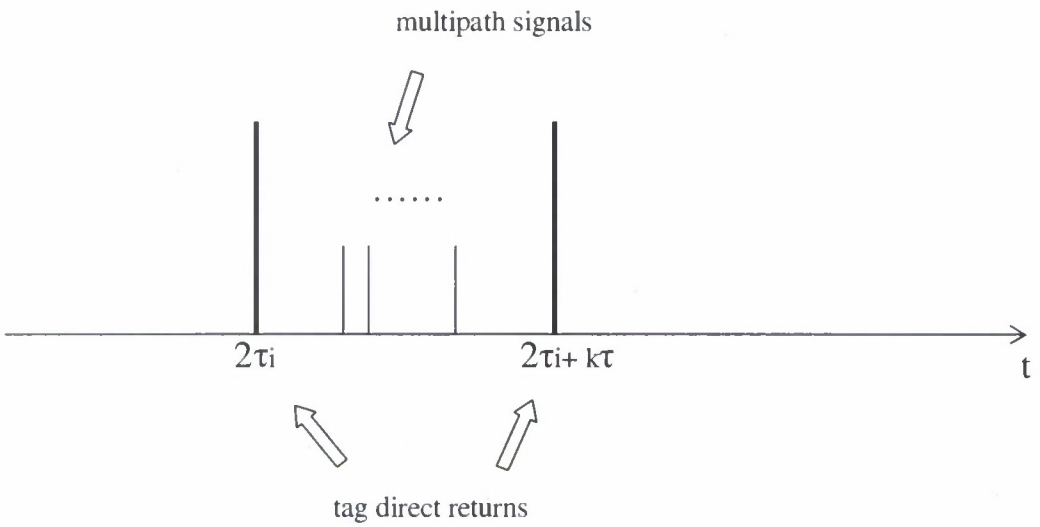


Fig. 71: Multipath interference signals.

Channel

The following factors which make the practical situations more complex are needed to be considered in the radar—RF tag channel.

For RF propagation with link ranges < 500 meters, VHF/UHF, with antenna elements placed near the ground, the path loss can be predicted as follows[44]:

(a) Free space path loss

Free space path loss is given by $\frac{P_r}{P_t} = G_{tx}G_{rx}\left(\frac{c}{4\pi fd}\right)^2$, and expressed in decibels as $L_f = 10\log G_{tx} + 10\log G_{rx} - 20\log f - 20\log d + k$, where $k = 147.6$.

(b) Propagation over a reflecting surface

[44] M. Dapper, J.S. Wells, T. Schwallie, and L. Huon, "RF propagation in short-range sensor communications," *Proc. SPIE Conf. on Unattended Ground Sensor Technologies and Applications V*, Orlando, FL, pp. 330-340, September 2003.

Two-ray model is used for the propagation over a flat surface, as shown in the Fig. 72. The signal at the receiver is the vector sum of the direct and reflected rays.

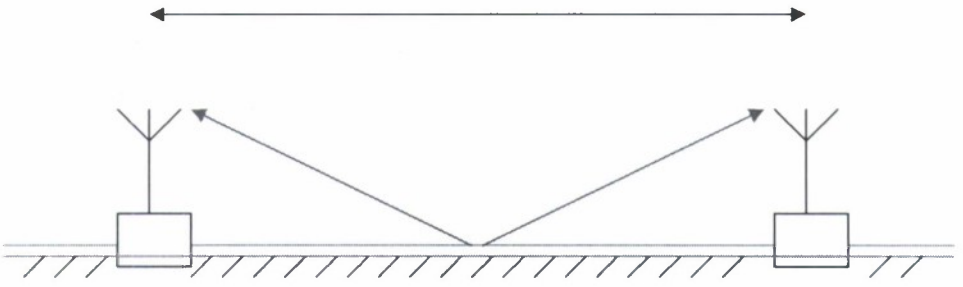

Fig. 72: Two-ray model of propagation over a flat surface.

The reflection coefficient can be calculated as a function of the incident angle $\psi$, as

$$\rho = \frac{(\varepsilon_r - jx)\sin\psi - \sqrt{(\varepsilon_r - jx)\cos^2\psi}}{(\varepsilon_r - jx)\sin\psi + \sqrt{(\varepsilon_r - jx)\cos^2\psi}} \tag{107}$$

where $x = \frac{18\times10^9\sigma}{f}$, $\psi = \tan^{-1}\left(\frac{h_{tx}}{d_{tx}}\right)$, $h_{tx}$ is height of transmitting antenna, $d_{tx}$ is distance between the transmitting and receiving antennas, $\psi$ is the angle of incidence, and $\sigma$ is conductivity.

The total received field strength $E$ is given by

$$E = \left\{G_{tx}G_{rx}\left[\frac{c}{4\pi fd}\right]^2\right\}\left\{1 + \rho\exp\left(1 - j\frac{2\pi}{\lambda}\Delta R\right)\right\} \tag{108}$$

where $\Delta R = \frac{2h_t'h_r'}{d}$, $h_t'$ is the transmit antenna height above the earth's tangent plane through the point of reflection, $h_r'$ is the receive antenna height above the earth's tangent plane through the point of reflection, $G_{tx}$ is the transmit antenna gain, $G_{rx}$ is the receive antenna gain, $\rho$ is the earth reflection coefficient, and $\lambda$ is wavelength.

Some typical values of dielectric constants $\varepsilon_r$ and conductivity $\sigma$ are listed in Table VI.

TABLE VI: DIELECTRIC CONSTANTS AND CONDUCTIVITIES OF VARIOUS SURFACES

| Surface Type | Conductivity $\sigma$ (Siemens) | Dielectric Constant $\varepsilon_r$ |
|---|---|---|
| Sea Water | 5 | 81 |
| Fresh Water | $1\times10^{-2}$ | 81 |
| Good Ground (wet) | $2\times10^{-2}$ | 25-30 |
| Average Ground | $5\times10^{-3}$ | 15 |
| Poor Ground (dry) | $1\times10^{-3}$ | 4-7 |

c) Short range foliage loss

When the propagation rays are blocked by dense and leafy trees, the following equations can be applied:

— For ranges from 14 m to 400 m, the foliage loss in decibels can be modeled as $L_f = 1.33 f^{0.284} d_f^{0.588}$;

— For ranges less than 14 m, the foliage loss is given by $L_f = 0.45 f^{0.284} d_f$

where $d_f$ is the distance through the foliage in meters and $f$ is the frequency in GHz.

d) Propagation over terrain obstacles

For close range communication where transmitter and receiver pairs are relatively local to each other (<1000 meters), the terrain model can be generated as shown in Fig. 73.

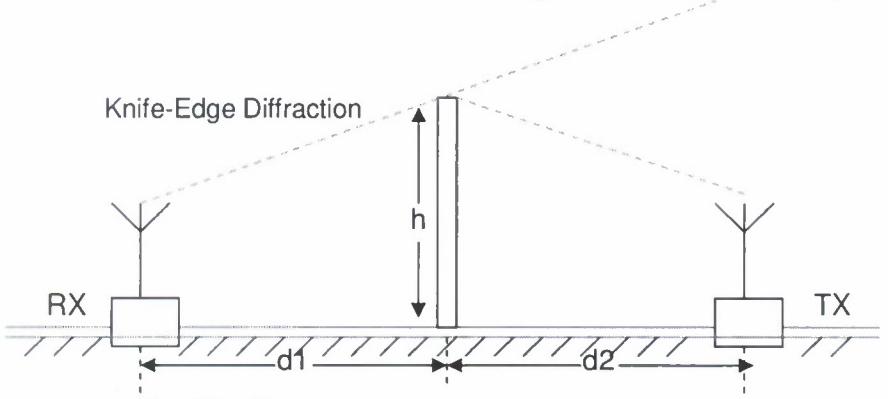


Fig. 73: Short range propagation over obstacles.

This model is based on the "knife-edge" model, in which any obstruction is replaced with an absorbing plane normal to the direct path between the transmitter and the receiver. In addition, the obstacles within the terrain area that blocks the propagation rays are modeled as a single obstruction with a height of $h$, where $h$ is the maximum height of those obstacles. The diffraction parameter, known as the Fresnel-Kirchoff diffraction parameter, is calculated as

$$v = h\sqrt{\frac{2(d_1 + d_2)}{\lambda d_1 d_2}}. \tag{109}$$

The path loss in decibels can then be computed using

$$L_{diff} = 20\log_{10}\left|\frac{(1+j)}{2}\left[\frac{1}{2} - j\frac{1}{2} - \left(C(v) - jS(v)\right)\right]\right| \tag{110}$$

where $d_1$ and $d_2$ are the distances from the obstacle to the transmitter and the receiver in meters, $h$ is the height of the obstacle in meters, and $C(\cdot)$ and $S(\cdot)$ are the cosine and sine integrals.

The total short range path loss in decibels with antennas near ground can be predicted as

$$L_{total} = L_p + L_f + L_{diff}. \tag{111}$$

Modification of the signal form

To make the radar—RF tag communication system more intelligent, some modification of the signal form needs to be done to inform the tags whether the incoming signal is friendly interrogation or interference signals from the enemy, and to enable the radar to differentiate the tag returns from other hostile signals. One way to do this is to append an indication header to the signals communicated between the radar and the tags, as shown in Fig. 74(a). The header is thus an indication of the radar. That is, the signals from the same radar have the same header. The tags know the header information of the radar in advance and have stored a replica of the headers. When a signal arrives at a tag, the signal is made cross correlation with the header replicas. If a peak happens, then the tag knows that the radar wants its data, starts to operate the signal, and responds with the modulated signal with the header. If no peak is observed, then it is interference signal, and the tag does not response. The structure of the tag response is shown in Fig. 74(b).


(a) Transmitted waveform (b) Received waveform

Fig. 74: Header and signal structure

At the radar receiver, cross correlation is used to detect the tag signal header in a similar way.

Operation of the system with modified signal

*Step 1:* Radar transmits interrogation signal with its ID header in front of the signal.

*Step 2:* Upon receiving radar's signal, RF tag first detects the radar header through cross correlation. If a peak is observed, then the signal part after the header is processed through the bandpass filter, etc. The message modulated signal is made up with the same radar header in its front and transmitted back to the radar. If header is undetected, the tag will not respond.

*Step 3:* At the radar receiver, the radar header needs to be detected in the first place as well. If the radar header is detected, then the radar processes the signal part after the header. Otherwise, the radar will not act on the received signal.

Header Recognition Results

Fig. 75(a) and (b) show the header detection results at the RF tag and the radar in the two cases when the signal is with the header and when it is without the header. When the signal is with the header, the detection results at both the RF tag and the radar are much higher value compared to the latter case. Thus, the header can be successfully recognized.

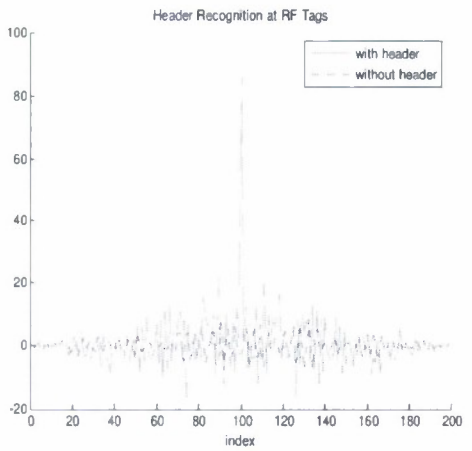


(a) At RF Tags.

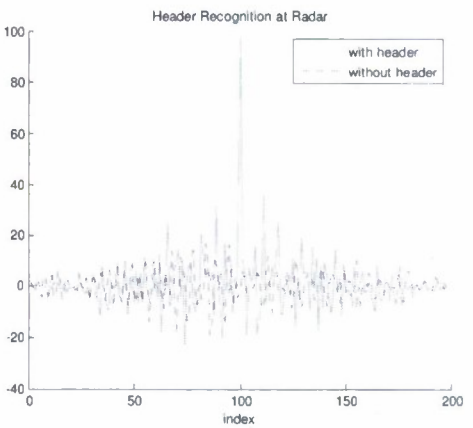


(b) At Radar.

Fig. 75: Header recognition results.

*Radiation pattern of densely distributed RF tags:*

The scenario under consideration is illustrated in the Fig. 76. A lot of RF tags are densely distributed in a small region. The one in red is the tag with feed, the grey ones around it are identical parasitic elements.

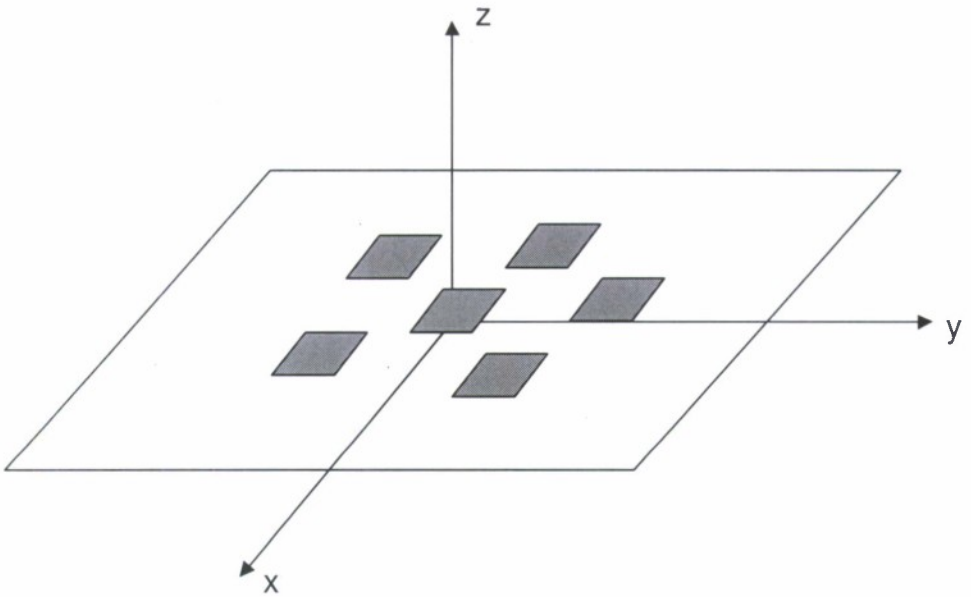


Fig. 76: Scenario of densely distributed RF tags.

Analysis

The analysis focuses primarily on the role of antenna, and the load effect is not taken into account at this time. The simple case is that the retransmission occurs at the same frequency as the impinging wave. The case when the actual device transmits signals at offset frequencies can be viewed by postulating an equivalent *LC* resonant circuit load at each element, which is a special case of the assumed scenario. Thus, the analysis below in general also applies to the practical case at the antenna level.

The parasitic elements come to work through coupling with the active one and each other. The coupling can happen through the active element's radiation or its near-zone fields. In the case that the parasitic elements are densely deployed within a small region surrounding the active one, the near field coupling approach is applicable. To evaluate the new pattern, the near fields should be calculated first, from which the induced current on the elements can be calculated, and then the radiation pattern of the "array" can be calculated. However, it is very difficult to predict those parameters directly using formulas, since there are higher order mutual interactions between the elements and a number of different coupling modes are present, which makes the problem very complex. The problem is approached through simulations using the High Frequency Structure Simulator (HFSS) software package.

How much the pattern is affected by the parasitic elements depends on the type of the element, the way current flows within the elements, and the configuration of the deployment. Placement of the parasitic elements can be found from the direction the current flows on the element to get better induced current, or some loads can be put at the parasitic ones to help form the induced current to a favorable shape, and improve the whole performance consequently. The gap or spacing between the elements also affects the pattern.

Simulation Results

The simulation model is a printed dipole working at 3 GHz sitting on substrate of material Rogers RT/duroid 5880™ on the infinite ground. The dimensions are shown in Fig. 77 and Fig. 78.

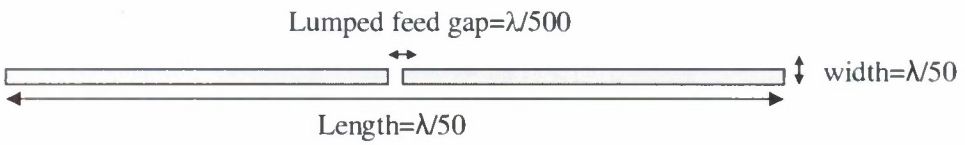


Fig. 77: Printed dipole geometry.


Fig. 78: Substrate side view.

Simulation results are shown in Fig. 79 – Fig. 89, and discussion follows afterwards.

1) Case I: Single Element

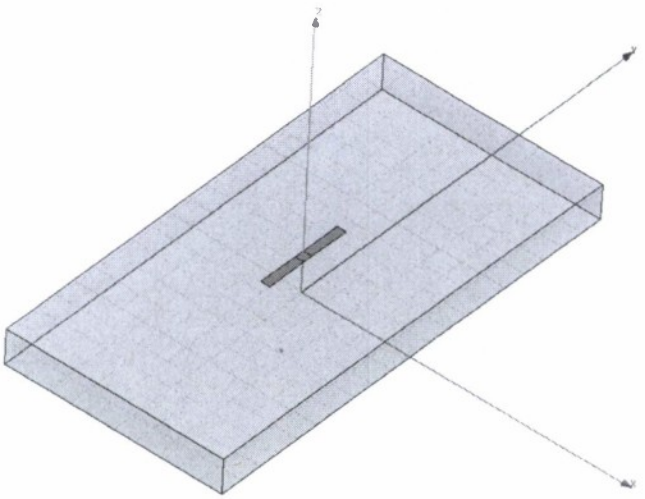

Fig. 79: Case I geometry.

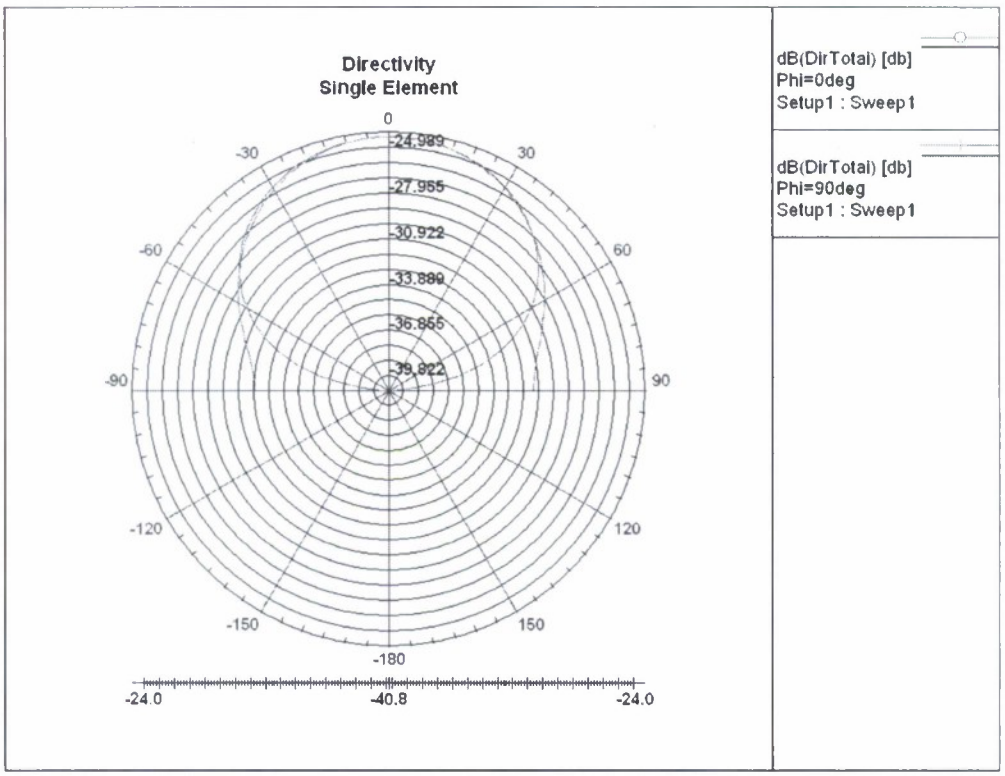


Fig. 80: Case I directivity.

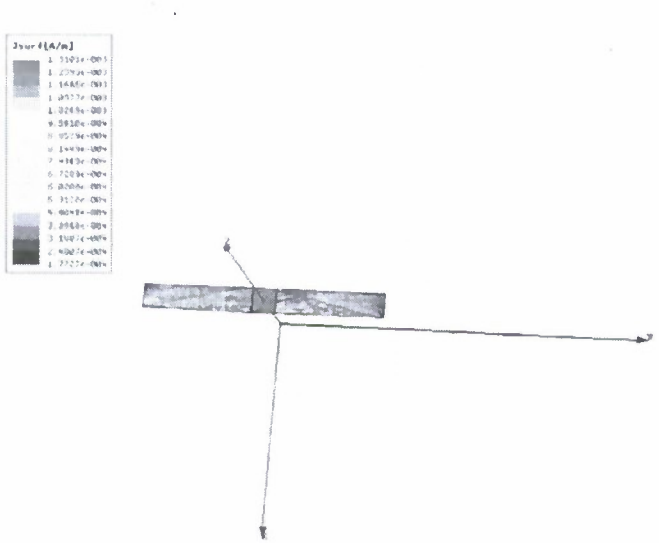

Fig. 81: Case I current distribution.

Case II: 8 Element Uniform Deployment, Gap = $\lambda/5000$

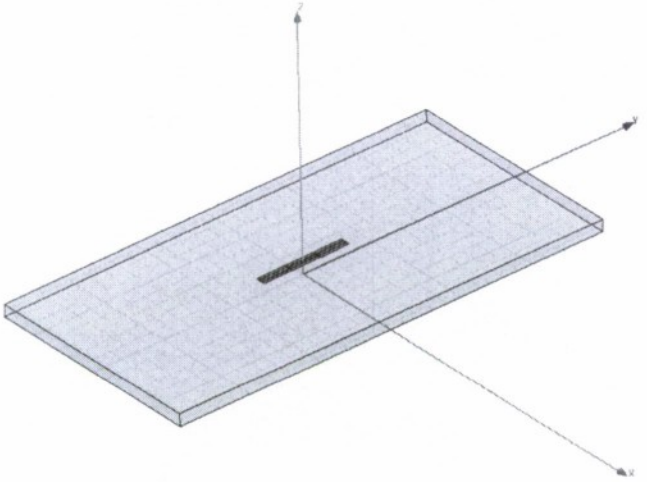

Fig. 82: Case II geometry.

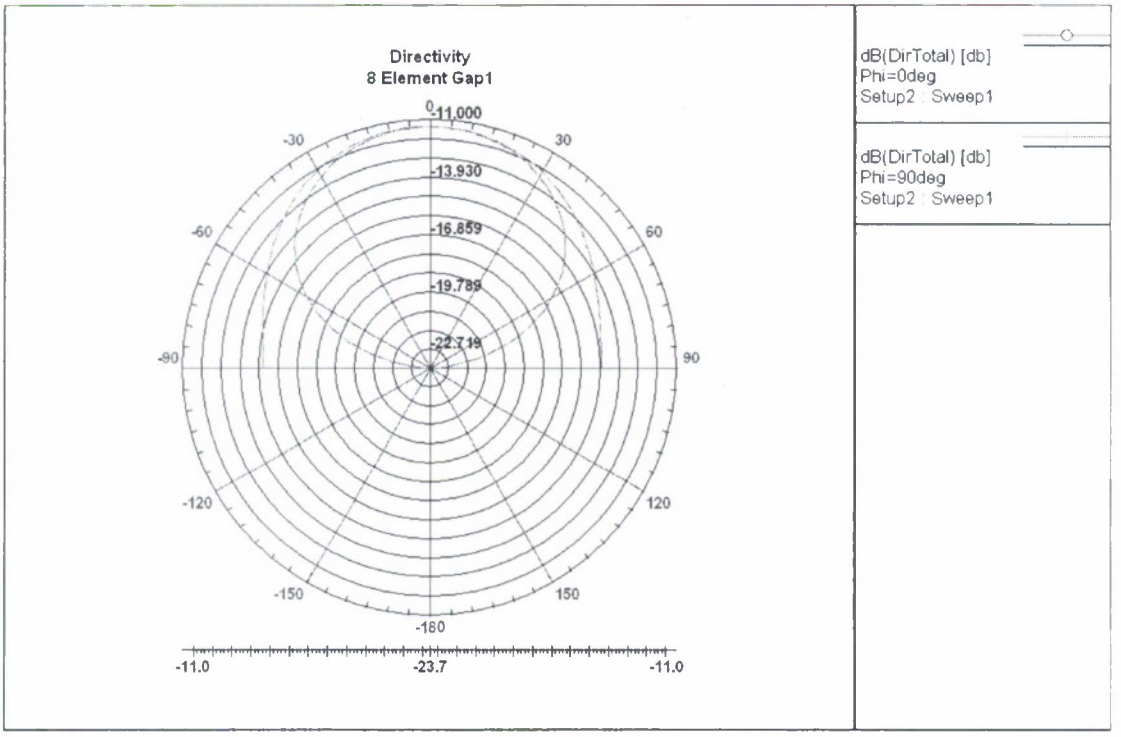


Fig. 83: Case II directivity.

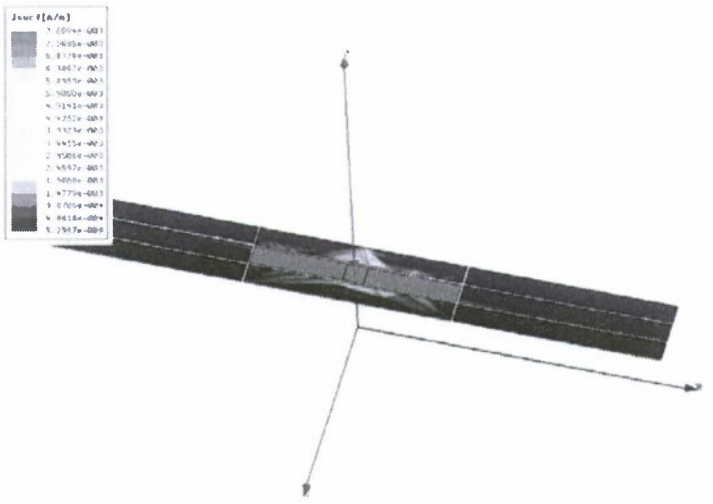

Fig. 84: Case II induced current distribution.

Case III: 8 Element Uniform Deployment, Gap = $\lambda/1000$

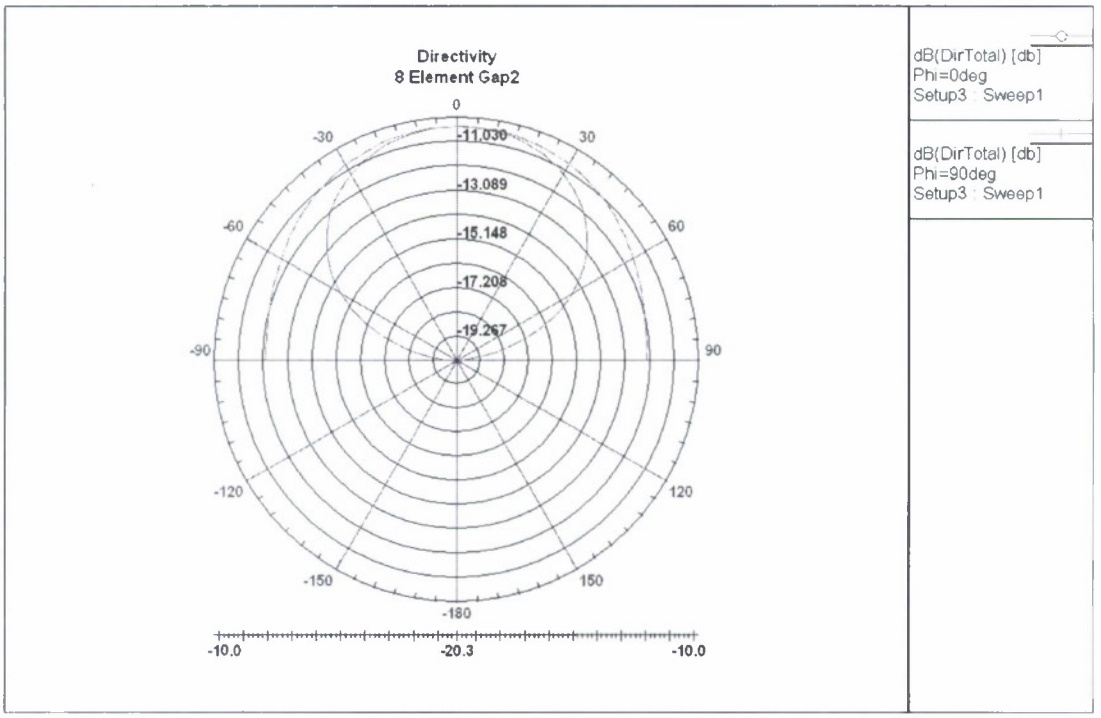


Fig. 85: Case III directivity.

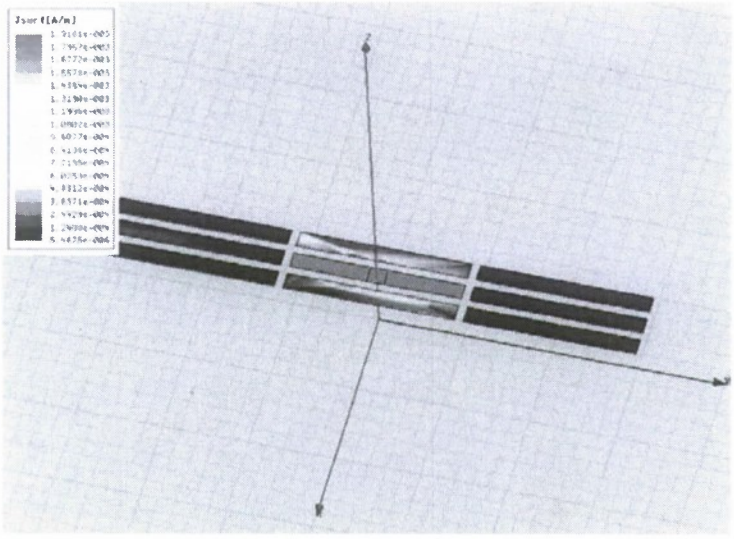

Fig. 86: Case III induced current distribution.

Case 1V: 33 Element Uniform Deployment, Gap = $\lambda$/1000

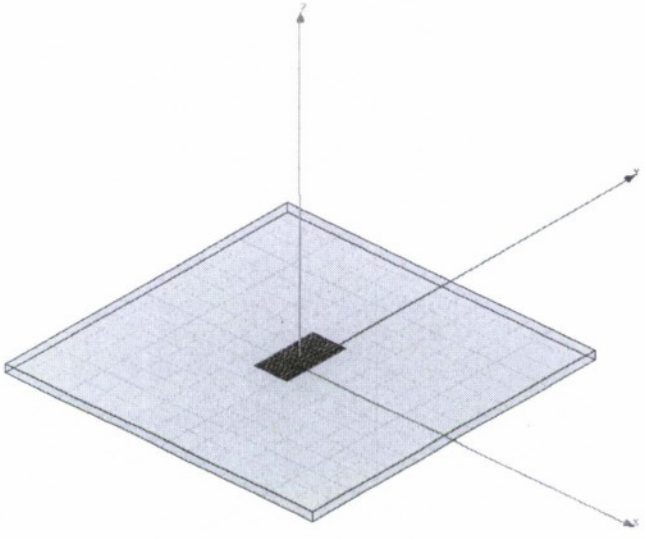

Fig. 87: Case IV geometry.

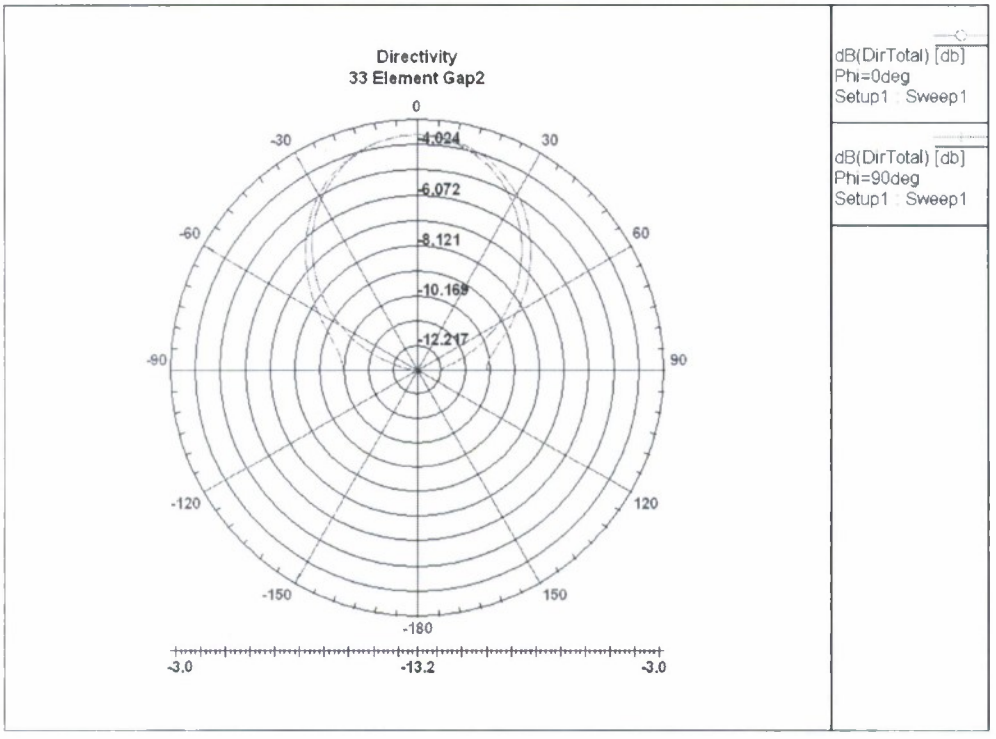


Fig. 88: Case IV directivity.

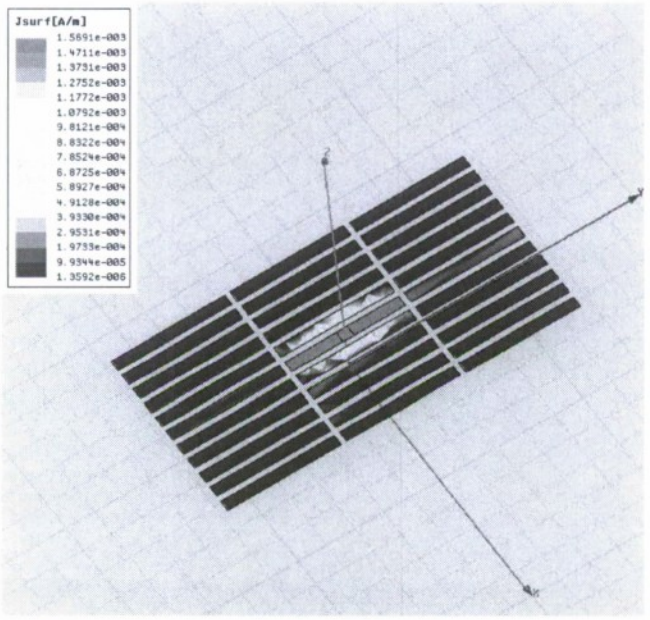


Fig. 89: Case IV induced current distribution.

The above results show that parasitic elements placed closed to the active one improve the directivity. The gap between elements affects the directivity. Though Gap1 is smaller than Gap2, the directivity in the Cap2 case is better. As the number of parasitic elements within the small region of active tag increases, the directivity also increases. Only the nearest neighbors of the active one have apparent induced current; the currents on the rest parasitic elements are very small, and although these elements do not radiate much, they help form the shape of the current on the nearest neighbor of the active tag, and therefore help improve the directivity.

In all the above cases, the elements are uniformly distributed; in the case below (Fig. 90 and Fig. 91), the parasitic elements are randomly placed within a very small region of the active one. This is more realistic in the case of airborne dispersed tags. It can be seen that the directivity is also improved in this case, though not as much in Case II and Case III.

Case V: 8 Elements, Random Deployment

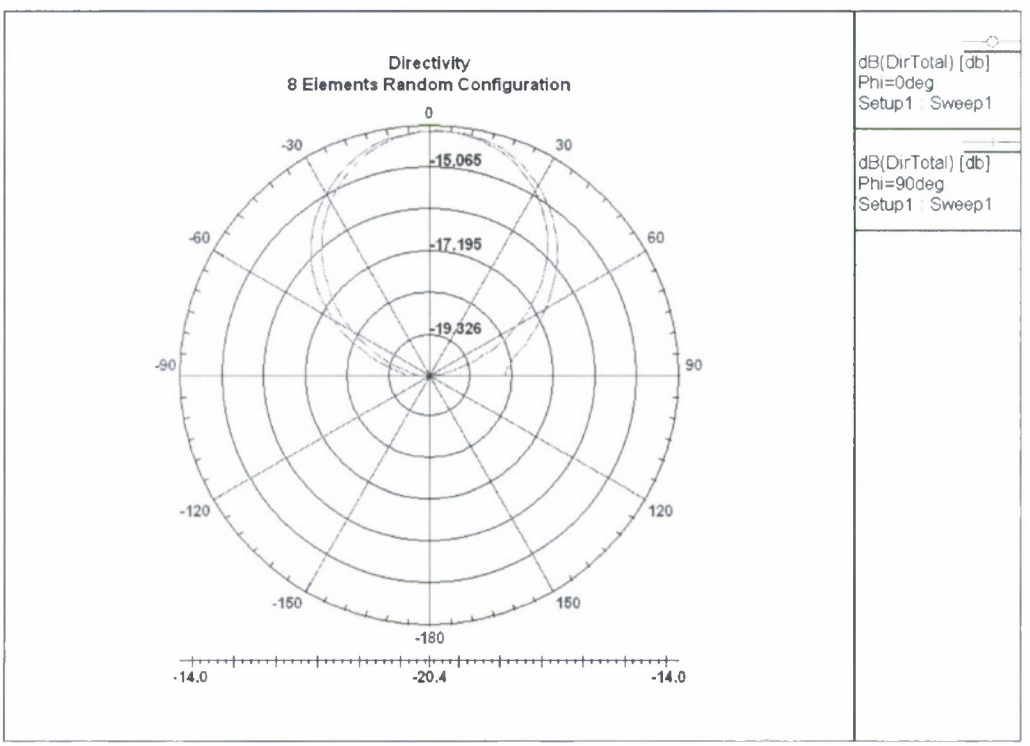


Fig. 90: Case V directivity.

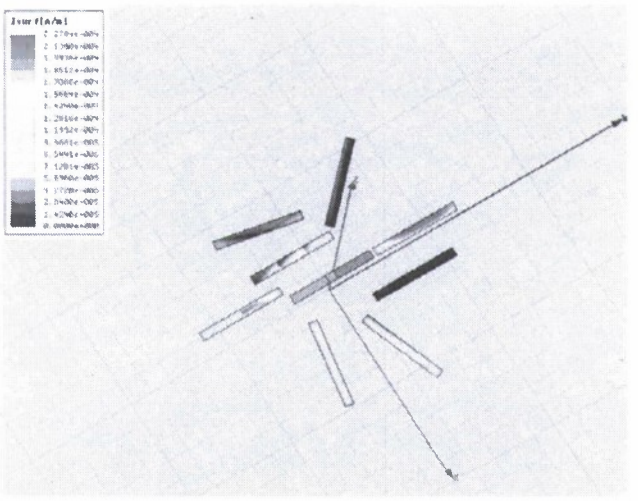

Fig. 91: Case V induced current distribution.

*Proposed RF Tag System Using Ultrawideband Noise Waveforms:*

We propose the architecture of a communication system that uses active RF tags to communicate simple messages with radar using noise signals, inspired by results of recent research[45,46] wherein tag convolvers appropriately modify an incoming radar signal and retransmit the same to the radar. In our approach, an ultrawideband (UWB) noise waveform is chosen as the probing signal for its low probability of detection and interception capabilities as well as its immunity from interference and jamming. It has been established that such waveforms are ideal solutions to combat detection and exploitation since the transmitted signals have unpredictable random-like behavior and do not possess repeatable features for signal identification purposes[47].

System Model

*RF tag structure:* The composite transmitted UWB noise radar signal is represented as a vector of the form $[h(t)\ \ x(t)]$, where $h(t)$ is the radar header appearing in time before $x(t)$, the bandlimited UWB white Gaussian noise (WGN) radar waveform operating over the frequency range $[\omega_L, \omega_H]$. The header signal $h(t)$ is the sum of two components, i.e. $h(t) = h_0(t) + s(t)$, where $s(t) = a\sin\omega_0 t$ is the wake-up signal for the tags within the radar's range, and $h_0(t)$ is also a bandlimited (also over $[\omega_L, \omega_H]$) UWB WGN signal whose sole purpose is to conceal $s(t)$. The wake-up signal $s(t)$ is a single-tone waveform of amplitude $a$ and frequency $\omega_0$, which lies within the frequency band of the noise signal $h_0(t)$. Thus,

[45] P. Bidigare and M. Nayeri, "RF tags: radar as a communications channel," *Proceedings of the 10th Adaptive Sensor Array Processing (ASAP) Workshop*, Lexington, MA, March 2002,

[46] P. Bidigare, "The Shannon channel capacity of a radar system," *Record of the Thirty-Sixth Asilomar Conference on Signals, Systems, and Computers*, Pacific Grove, CA, pp. 113-117, November 2002.

[47] L. Turner, "The evolution of featureless waveforms for LPI communications," *Proc. IEEE National Aerospace and Electronics Conference (NAECON'91)*, Dayton, OH, pp. 1325-1331, May 1991.

$h_0(t)$ is used to mask this radar wake-up signal. The amplitude $a$ of the wake-up signal $s(t)$ should be chosen small enough so that the spectrum of $h(t)$ still appears to be flat over the frequency band, so that it cannot be easily discovered by the unwanted parties. In our simulations, we use a UWB noise signal operating over the 1-2 GHz frequency range and the wake-up signal at 1.5 GHz. Fig. 92 shows the individual components of the radar header signal, while Fig. 93 shows its PSD. Since the radar wake-up signal is a sinusoidal signal embedded in white noise, it can be recognized at the RF tag front end using the well-known multiple-signal classification (MUSIC) algorithm.

The RF tag functional block diagram is shown in Fig. 94. It consists of two parts: a passive receiver, and an active receiver/transmitter. The passive receiver is merely a listening device which uses very little power and is always on in order to sense the radar signal. The active receiver/transmitter is turned on once it gets an indication signal from the passive receiver output that a radar wake-up signal is detected. Upon receiving this wake-up call, it begins to receive and process the rest of the incoming signal, embeds the appropriate RF tag message, and retransmits the message bearing RF tag signal back to the radar.

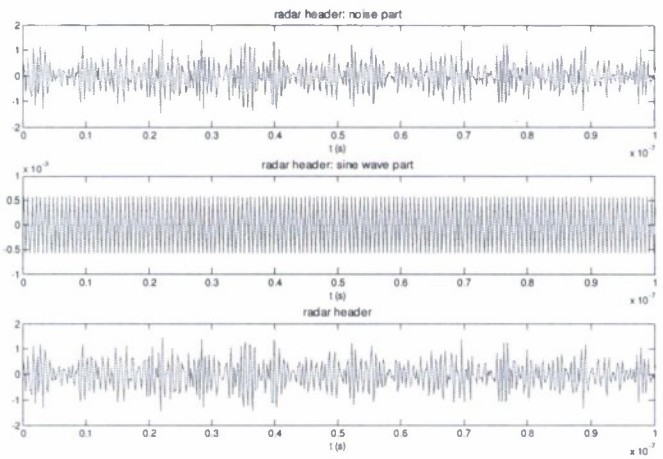


Fig.92: Radar header waveform and its components.

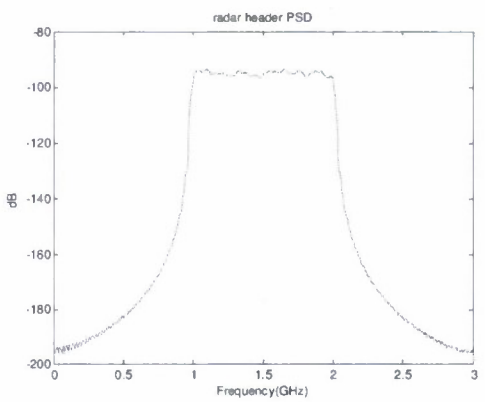


Fig. 93: Power spectral density (PSD) of the radar header signal.

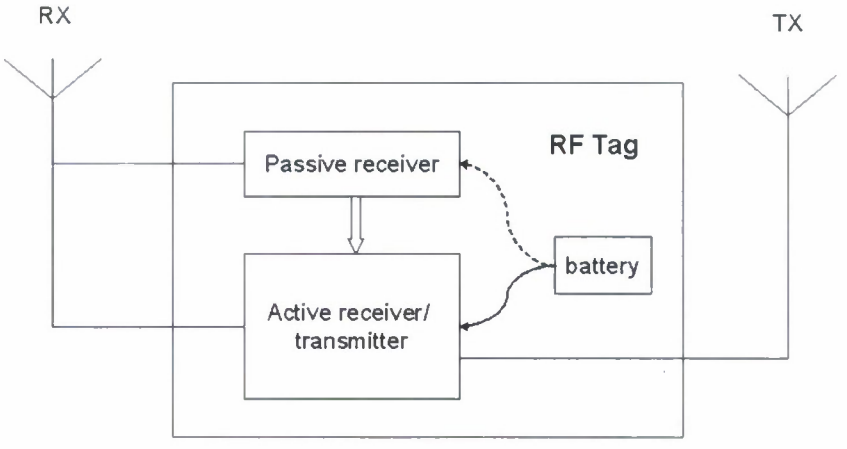


Fig. 94: RF tag functional block diagram.

The passive receiver functional block diagram is depicted in Fig. 95. The low power narrowband filter is centered at the (known) frequency of the radar wake-up signal. Its output feeds the tone detector, which applies the MUSIC algorithm to detect the radar wake-up signal $s(t)$. The results of applying the MUSIC algorithm to the composite radar header signal of Figure 92 is shown in Fig. 96, from which we note that the wake-up signal has been recognized.

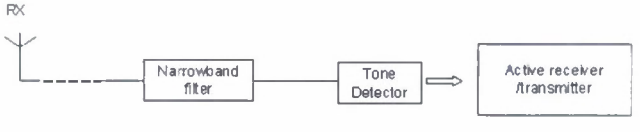


Fig. 95: RF tag passive receiver.

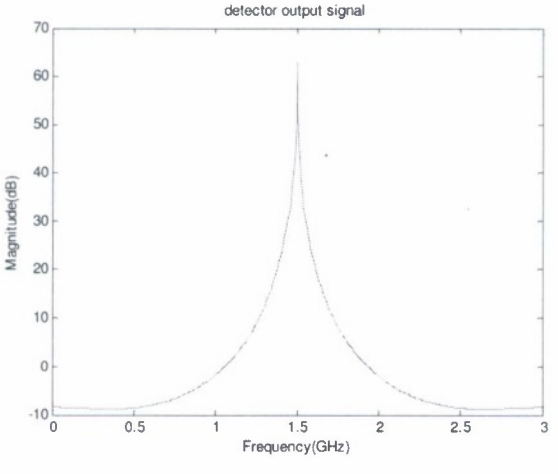


Fig. 96: Frequency estimation of the tone detector output signal.

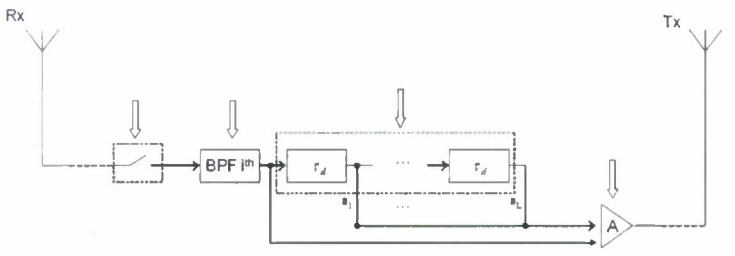


Fig. 97: RF Tag active receiver/transmitter.

The RF tag active receiver/transmitter functional block diagram is shown in Fig. 97. If and only if the radar wake-up signal is detected by the RF tag passive receiver, then the RF tag active receiver/transmitter is enabled. The remaining portion of the radar signal, namely, the radar information bearing signal $x(t)$, is intercepted at the RF tag. First this signal goes through a bandpass filter with bandwidth $\Delta\omega$ and center frequency $\omega_i$, which covers part of the entire bandwidth of radar signal $x(t)$. This frequency index $i$ represents the index of the $i$-th RF tag. We assume that there is a fixed number of RF tags within the radar's range during one interrogation duration. The entire bandwidth of the radar signal is divided into several subbands without mutual overlap by the RF tags, all of the same bandwidth $\Delta\omega$, with center frequencies ranging from $\omega_1$ to $\omega_N$, where $N$ is the total number of RF tags. The output of the bandpass filter at each RF tag can be shown to be uncorrelated with each other. Next, one branch of the bandpass filter output $x_i(t)$ is passed through a weighted tapped delay line to embed the RF tag message. The length of the tapped delay line $L$ denotes the number of bits of the tag message, where each weight $a_j$ is chosen to be either 0 or 1; thus the RF tag is able to transmit a total of $2^L - 1$ kinds of messages. The delay between adjacent taps $\tau_d$ should satisfy the condition $\tau_d \gg (\Delta\omega)^{-1}$ so as to reduce the interference between signals from adjacent delay taps. The other branch of the bandpass filter output, which is used as the indicator of RF tag message's arrival, goes directly to the amplifier and is retransmitted to the radar. Following this signal is the output of the weighted tapped delay line, which also goes through the amplifier and is transmitted back to the radar. Thus, the retransmitted signal for the $i$-th RF tag has the vector form $\left[ x_i(t) \sum_{j=1}^{L} a_j x_i(t - j\tau_d) \right]$.

*Radar detector structure:* The radar detector functional block diagram is depicted in Fig. 98. To detect the $i$-th RF tag's message, the radar received signal $y(t)$ first goes through a bandpass filter whose frequency band corresponds to the $i$-th RF tag. The bandpass filter selects the signal in the desired bandwidth, $y_i(t)$, and thus enhances the signal-to-noise ratio by eliminating out-of-band energy. The electronically controlled single-pole double-throw (SPDT) switch is always connected to terminal 1 if it is not enabled. It switches to terminal 2 only if it is enabled by the output of the threshold detector. The output of the bandpass filter $y_i(t)$ then goes to correlator 1 where it is correlated with $x(t)$, a replica of the UWB noise radar signal saved at the radar. Correlator 1 is used to detect $x_i(t)$, which is the initial portion

of the RF tag signal form. The integration time of correlator 1 is $T_1$. If its output exceeds a threshold at some time, then it determines that the $i$-th RF tag's message is coming in and triggers the SPDT switch. The switch then switches to terminal 2 and the remaining portion of the incoming signal $y_i(t)$ flows to correlator 2.

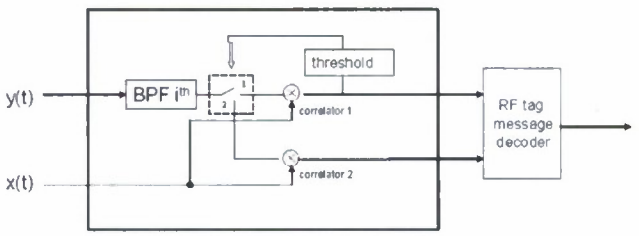


Fig. 98: Radar detector block.

Correlator 2 is used to decode the RF tag's message. Compared to correlator 1, correlator 2 has a longer integration time, denoted by $T_2$. The outputs of correlator 1 and correlator 2 both go to the RF tag message decoder, which knows the length of the weighted tapped delay line of the RF tag and the delay between its adjacent taps. By observing the amplitudes at different time lags, the RF tag message can be decoded. The output of correlator 1 can help in decoding the RF tag message especially in the multipath channel case, which will be discussed later.

Fig. 99 illustrates the implementation of the correlator. The received signal is mixed with a time delayed version of the transmit signal $x(t-\tau)$. The correlation integration is performed by the low-pass filter. The bandwidth of the low-pass filter determines the cross-correlation integration time.

If there are multiple RF tags to be interrogated by the radar, we can connect several of the above detectors at the radar receiver in parallel, with each bandpass filter tuned to the corresponding RF tag's center frequency.

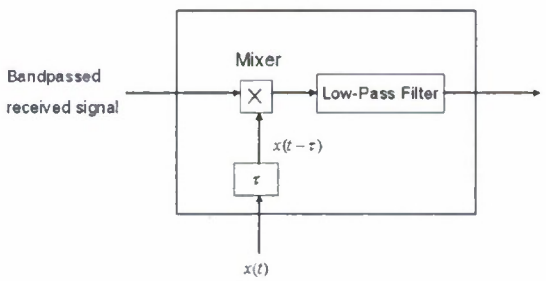


Fig. 99: Implementation of correlator.

Channel Considerations

*AWGN Channel:* In this case, the additive white Gaussian noise introduced by the channel and the propagation delay are considered. The effects of radar clutter are not included, which may be known or estimated *a priori*, and subtracted from the radar received signal. We consider the link between the radar and RF tag 1 as an example to show how the designed system works.

As stated before, to interrogate the RF tags, the radar transmits the signal $[h(t)\ \ x(t)]$. If the RF tag passive receiver successfully captures the radar wake-up signal, then the RF tag responds to the radar with message modulated signals. Suppose the channel propagation delay is denoted by $\tau_0$ and the channel additive noise in the radar-to-RF tag link is denoted by $n_{f1}(t)$, then the output of the bandpass filter of the RF tag is $x_1(t-\tau_0)+n_{f1}(t)$. The output of the weighted tapped delay line after power compensation by the amplifier is $\sum_{j=1}^{L} a_j x_1(t-\tau_0-j\tau_d)+n_{f2}(t)$, where $n_{f2}(t)$ is noise added by the tag. RF tag 1 thus transmits the signal $\left[ x_1(t-\tau_0)+n_{f1}(t) \quad \sum_{j=1}^{L} a_j x_1(t-\tau_0-j\tau_d)+n_{f2}(t) \right]$ back to the radar. At the radar receiver, the received signal after the bandpass filter $y_1(t)$ is given by

$$\begin{aligned} y_1(t) &= \left[ x_1(t-2\tau_0)+n_{f1}(t-\tau_0)+n_{b1}(t) \quad \sum_{j=1}^{L} a_j x_1(t-2\tau_0-j\tau_d)+n_{f2}(t-\tau_0)+n_{b2}(t) \right] \\ &= \left[ x_1(t-2\tau_0)+n_1(t) \quad \sum_{j=1}^{L} a_j x_1(t-2\tau_0-j\tau_d)+n_2(t) \right]. \end{aligned} \tag{112}$$

where $n_{b1}(t)$ and $n_{b2}(t)$ are uncorrelated additive white Gaussian noise in the RF tag-to-radar link. We also define $n_1(t)=n_{f1}(t-\tau_0)+n_{b1}(t)$ and $n_2(t)=n_{f2}(t-\tau_0)+n_{b2}(t)$

The output of correlator 1 is derived as

$$\begin{aligned} c_1(\tau) &= \int_0^{T_1} \left[ x_1(t-2\tau_0)+n_1(t) \right] x(t-\tau)dt \\ &= \int_0^{T_1} x_1(t-2\tau_0) \left[ x_1(t-\tau)+\sum_{i=2}^{N} x_i(t-\tau) \right] dt + \int_0^{T_1} n_1(t)x(t-\tau)dt \\ &= \int_0^{T_1} x_1(t-2\tau_0)x_1(t-\tau)dt + \int_0^{T_1} x_1(t-2\tau_0)\sum_{i=2}^{N} x_i(t-\tau)dt + \int_0^{T_1} n_1(t)x(t-\tau)dt. \end{aligned} \tag{113}$$

Since $x_1(t)$ and $n_1(t)$ are both uncorrelated with $x_i(t)\forall i=2,\cdots,N$, the last two terms of equation (113) are noise terms. A peak whose amplitude is the energy of $x_1(t)$ should be observed at time lag $\tau=2\tau_0$ of the correlator 1 output, if RF tag 1's signal exists.
Similarly, the output of correlator 2 is given by

$$\begin{aligned} c_2(\tau) &= \int_0^{T_2}\left[\sum_{j=1}^{L} a_j x_1(t-2\tau_0-j\tau_d)+n_2(t)\right]x(t-\tau)dt \\ &= \sum_{j=1}^{L} a_j \int_0^{T_2} x_1(t-2\tau_0-j\tau_d)x_1(t-\tau)dt + \int_0^{T_2}\sum_{j=1}^{L} a_j x_1(t-2\tau_0-j\tau_d)\sum_{i=2}^{N} x_i(t-\tau)dt \\ &\quad + \int_0^{T_2} n_2(t)x(t-\tau)dt. \end{aligned} \tag{114}$$

To retrieve the RF tag message, we need to observe the amplitudes of the output of correlator 2 at time lags $\tau=2\tau_0+j\tau_d\forall j=1,\cdots L$. If a peak is observed at time lag when $j$ equals $l$, then the $l$-th bit is 1, otherwise it is 0.

Fig. 100 shows the simulation results of RF tag 1 message decoding in the AWGN channel case. Radar transmits 1 GHz – 2 GHz noise signal to the RF tags. Suppose there three RF tags within the radar's range. The frequency band allocation for the RF tags is: RF tag 1 occupies 1 GHz - 1.32 GHz, RF tag 2 occupies 1.34 GHz - 1.66 GHz, and RF tag 3 occupies 1.68 GHz – 2 GHz. The guard bandwith is 200 MHz. The channel SNR is –3 dB, and the channel round propagation delay is $1.6\times10^{-4}$ time lags. The length of the weighted tapped delay line at the RF tag is 3, and the delay between adjacent taps is 90 time lags. RF tag 1 transmits message 101 to the radar.

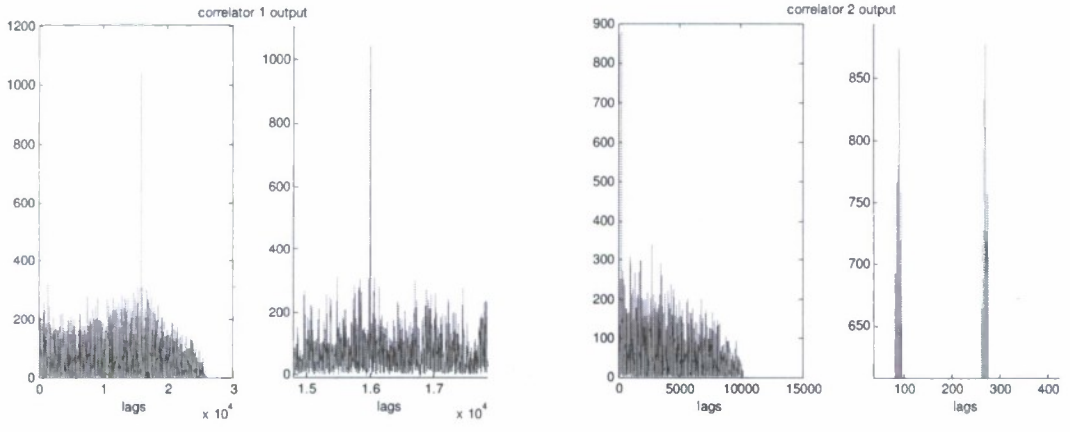


Fig. 100: RF tag decoding in AWGN channel (magnitude).

The output of correlator 1 has a peak at a lag of $1.6\times10^{-4}$, which indicates RF tag 1's message exists. In the output of correlator 2, we observe two peaks at time lags 90 and 270,

which equal $\tau_d$ and $3\tau_d$, respectively, away from lag $1.6\times10^{-4}$. No peak is observed at time lag 180, which equals $2\tau_d$. Thus, this RF tag's message is correctly interpreted as 101.

*Multipath Channel:* Consider the RF tag-to-radar link. The multipath channel response is simply modeled by a finite set of delay and attenuation pairs $\{\alpha_i, \tau_{mi}\}$,

$$h_m(t) = \sum_{i=1}^{M} \alpha_i \delta(t - \tau_{mi}) . \tag{115}$$

The interference from other RF tags is not considered. Thus, the radar received signal out of the bandpass filter which flows to correlator 1 is given by

$$\begin{aligned} x_{1c1}(t) &= h(t) \otimes \left[ x_1(t - 2\tau_0) + n_{f1}(t - \tau_0) \right] + n_{b1}(t) \\ &= \sum_{i=1}^{M} \alpha_i x_1(t - 2\tau_0 - \tau_{mi}) + \sum_{i=1}^{M} \alpha_i n_{f1}(t - 2\tau_0 - \tau_{mi}) + n_{b1}(t) \\ &= \sum_{i=1}^{M} \alpha_i x_1(t - 2\tau_0 - \tau_{mi}) + n_{m1}(t) \end{aligned} \tag{116}$$

where $n_{m1}(t) = \sum_{i=1}^{M} \alpha_i n_{f1}(t - 2\tau_0 - \tau_{mi}) + n_{b1}(t)$ represents the noise term of $x_{1c1}(t)$.

Similarly, the branch of the radar bandpass filter to correlator 2 is given by

$$\begin{aligned} x_{1c2}(t) &= h(t) \otimes \left[ \sum_{j=1}^{L} a_j x_1(t - 2\tau_0 - j\tau_d) + n_{f2}(t - \tau_0) \right] + n_{b2}(t) \\ &= \sum_{j=1}^{L} a_j \sum_{i=1}^{M} \alpha_i x_1(t - 2\tau_0 - j\tau_d - \tau_{mi}) + \sum_{i=1}^{M} \alpha_i n_{f2}(t - 2\tau_0 - \tau_{mi}) + n_{b2}(t) \\ &= \sum_{j=1}^{L} a_j \sum_{i=1}^{M} \alpha_i x_1(t - 2\tau_0 - j\tau_d - \tau_{mi}) + n_{m2}(t) \end{aligned} \tag{117}$$

where $n_{m2}(t) = \sum_{i=1}^{M} \alpha_i n_{f2}(t - 2\tau_0 - i \cdot \tau_m) + n_{b2}(t)$ represent the noise term of $x_{1c2}(t)$.

The output of correlator 1 is calculated as

$$
\begin{aligned}
c_1(\tau) &= \int_0^{T_1} x_{1c1}(t)x(t-\tau)dt \\
&= \int_0^{T_1} \sum_{i=1}^{M} \alpha_i x_1(t-2\tau_0-\tau_{mi}) \left[ x_1(t-\tau) + \sum_{k=2}^{N} x_k(t-\tau) \right] dt + \int_0^{T_1} n_1(t)x(t-\tau)dt \\
&= \sum_{i=1}^{M} \alpha_i \int_0^{T_1} x_1(t-2\tau_0-\tau_{mi})x_1(t-\tau)dt + \sum_{i=1}^{M}\sum_{k=2}^{N} \int_0^{T_1} \alpha_i x_1(t-2\tau_0-\tau_{mi})x_k(t-\tau)dt \\
&\quad + \int_0^{T_1} n_1(t)x(t-\tau)dt
\end{aligned}
\tag{118}
$$

The output of correlator 2 output is calculated as

$$
\begin{aligned}
c_2(\tau) = &\sum_{j=1}^{L} a_j \sum_{i=1}^{M} \alpha_i \int_0^{T_2} x_1(t-2\tau_0 - j\tau_d - \tau_{mi})x_1(t-\tau)dt + \\
&\sum_{j=1}^{L} a_j \sum_{i=1}^{M} \alpha_i \sum_{k=2}^{N} \int_0^{T_2} x_1(t-2\tau_0 - j\tau_d - \tau_{mi})x_k(t-\tau)dt + \int_0^{T_2} n_2(t)x(t-\tau)dt
\end{aligned}
\tag{119}
$$

If the output of correlator 1 has a peak above the threshold at some time lag $\tau^*$, then the radar starts to decode this RF tag's message with the outputs of correlator 2, $c_2(\tau)$, and correlator 1, $c_1(\tau)$.

The first step of tag message decoding is to suppress the noise floor of $c_1(\tau)$ and $c_2(\tau)$. We denote $c_1'(\tau)$ and $c_2'(\tau)$ as the denoised versions of $c_1(\tau)$ and $c_2(\tau)$, respectively. The noise can be reduced by method of wavelets. The denoising procedure contains three stages: (1) wavelet transformation of the signal; (2) thresholding of wavelet coefficients; and (3) inverse wavelet transformation[48]. One threshold $\lambda$ that is easy to implement is given by[49]

$$
\lambda = \sigma\sqrt{2\log(n)/n}\,, \tag{120}
$$

where $n$ is the number wavelet coefficients to be thresholded and $\sigma = \tilde{m}/0.6745$, $\tilde{m}$ being the median of the wavelet transform coefficients.

The next step is to apply the information obtained from $c_1'(\tau)$ to $c_2'(\tau)$ in order to decode the RF tag message. The procedure is described as follows:

(1) Intercept the part of $c_1'(\tau)$ from time lag $\tau^*$, which is denoted as $c_{1r}'(\tau)$.

---

[48] D.L. Donoho, "De-noising by soft-thresholding," *IEEE Transactions on Information Theory*, vol. 41, no. 3, pp. 613-627, May 1995.

[49] W. Zhang and X.H. Zhao, "Wavelet thresholding using higher-order statistics for signal denoising," *Proc. 2001 International Conference on Info-Tech and Info-Net (ICII 2001)*, Beijing, China, vol. 1, pp. 363-368, October-November 2001.

(2) Check the first bit of the RF tag's message by observing the amplitude of $c_2'(\tau)$ at time lag $\tau_d$ away from $\tau^*$. If the corresponding amplitude is above the threshold, then the first bit is decoded as 1.

(3) Intercept the part of $c_2'(\tau)$ from time lag $\tau^* + \tau_d$, denoted as $c_{21}'(\tau)$, and subtract $c_{1r}'(\tau)$ from $c_{21}'(\tau)$. If the first bit is decoded as 0, then check the next bit at time lag $\tau^* + 2\tau_d$.

.....

(4) Do the above operation on the resulting signal iteratively at time lag $\tau^* + i \cdot \tau_d$ for all $i = 1,2,\ldots,L$.

The following is a simulation validation for this method. The channel impulse response used is shown in Fig. 101. The RF tag transmits message 101 to the radar. The length of RF tag's weighted tapped delay line is 3. Channel SNR is −3 dB. The wavelet used in the test is the Daubechies-4 (db4) wavelet. The simulation results are listed in Figs. 102(a)-(d). The plot on the left in Fig. 102(c), which is an enlarged view of the output of correlator 2 after noise suppression using wavelets, shows that there is high peak value at around 90 lags which equals $\tau_d$, so the first bit is decoded as 1. The first multipath signal removal is operated from this bit occurrence. The plot on the left in Fig. 102(d), which is an enlarged view of the output of correlator 2 after one multipath signal removal iteration, shows that there is no high peak value observed at 180 lags which equals $2\tau_d$, so the second bit is decoded as 0, while there exists a high peak value occurring at about 270 lags which equals $3\tau_d$, so the third bit is determined as 1. Since the length of the delay line at the RF tag is known by the radar, the message is interpreted as 101 by the radar. The plot on the right in Fig. 102(d) shows the output of correlator 2 after two multipath signal removal iterations. It shows that the multipath interferences are reduced significantly.

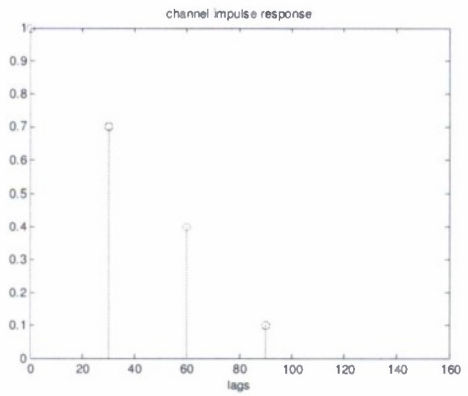


Fig. 101: Channel impulse response used.

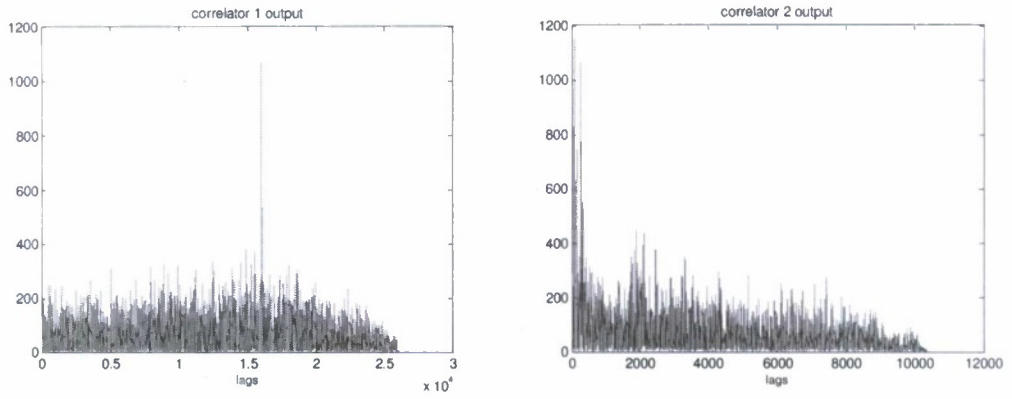
correlator 1 output
correlator 2 output
lags
x 10^4

(a)

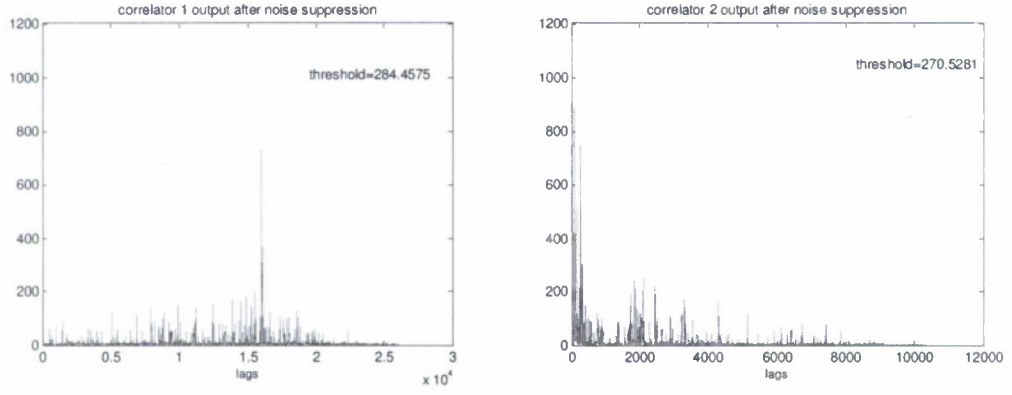
correlator 1 output after noise suppression
threshold=284.4575
correlator 2 output after noise suppression
threshold=270.5281
lags
x 10^4

(b)

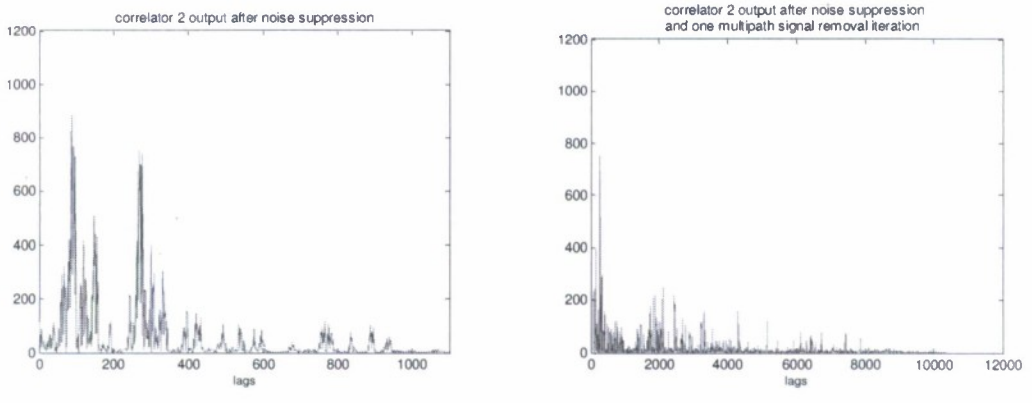
correlator 2 output after noise suppression
correlator 2 output after noise suppression
and one multipath signal removal iteration
lags

(c)

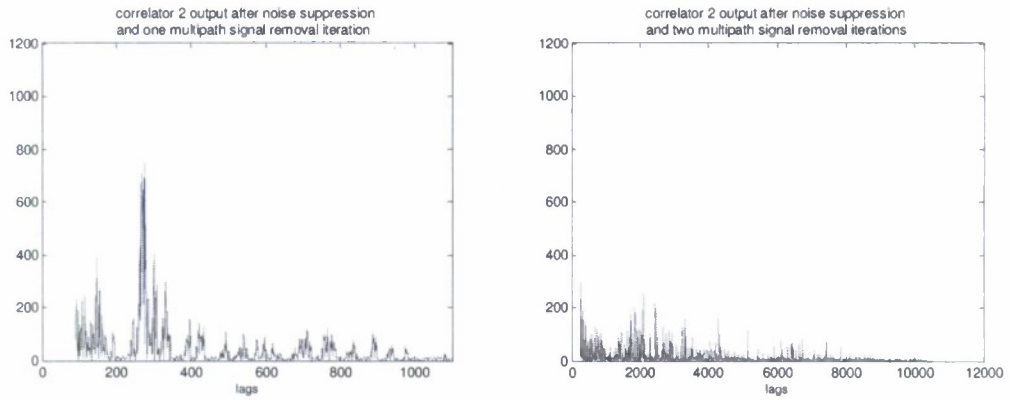


(d)

Fig. 102: Multipath channel results (a) Correlator output in multipath channel case (magnitude), (b) Correlator output after noise suppression (magnitude), (c) RF tag message decoding after 1st multipath signal removal iteration (magnitude), (d) RF tag message decoding after 2nd multipath signal removal iteration (magnitude).

*Performance Analysis:*

The performance of the system is evaluated in term of the bit error probability, also known as the bit error ratio (BER)[50]. Consider the AWGN channel case. Whether the RF tag's message can be correctly decoded or not depends on the outputs of both the correlator 1 and correlator 2. The header has to be detected at first. Consider the header detection. The bit error probability for header detection can be written as

$$p_b(e) = p_b(e|c_1)p(c_1) + p_b(e|\bar{c}_1)p(\bar{c}_1) = p_b(e|c_1)p(c_1) + p(\bar{c}_1) \tag{121}$$

where $p(c_1)$ denotes the probability that correlator 1 output is correctly decoded, $p(\bar{c}_1)$ denotes the probability that the output of correlator 1 is incorrectly decoded, $p_b(e|c_1)$ denotes the bit error probability under the condition that correlator 1 output is correctly decoded, and $p_b(e|\bar{c}_1)$ denotes the bit error probability under the condition that correlator 1 output is incorrectly decoded. Clearly, $p_b(e|\bar{c}_1) = 1$.

The output of correlator 1 gives an indication whether this RF tag responds to the radar irrespective of the condition whether an amplitude exceeding the threshold exists or not in the correlator 2 output.

The probability $p(\bar{c}_1)$ that correlator 1 gives a wrong indication is calculated as follows:

[50] Q. Pan and R.M. Narayanan, "An RF tag communication system model for noise radar," *Proc. SPIE Conference on Wireless Sensing and Processing III*, Orlando, FL, vol. 6980, pp. 698007-1–698007-12, doi:10.1117/12.777394, March 2008.

$$c_1(2\tau_0) = \int_0^{T_1} x_1^2(t-2\tau_0)dt + \int_0^{T_1} x_1(t-2\tau_0)\sum_{i=2}^{N} x_i(t-2\tau_0)dt + \int_0^{T_1} n_1(t)x(t-2\tau_0)dt$$
$$= U_{x11} + n_{e1}(t) \tag{122}$$

where, upon invoking the stationarity property for $x_1(t)$, we have

$$U_{x11} = \int_0^{T_1} x_1^2(t-2\tau_0)dt = \int_0^{T_1} x_1^2(t)dt\,, \tag{123}$$

while

$$n_{e1}(t) = \int_0^{T_1} x_1(t-2\tau_0)\sum_{i=2}^{N} x_i(t-2\tau_0)dt + \int_0^{T_1} n_1(t)x(t-2\tau_0)dt. \tag{124}$$

represents the noise term.

Fig. 103 is a simulation check on distribution of the noise term $n_{e1}(t)$. The simulation data concentrate along the red line, which means the data are almost Gaussian distributed. Thus, we can approximate $n_{e1}(t)$ as Gaussian distributed with mean zero and variance $\sigma_{e1}^2$ in the BER derivation.

The signal component of $c_1(2\tau_0)$ is either 0 or $U_{x11}$. Thus, the average signal strength is $\frac{1}{2}U_{x11}$ assuming each value is equally probable. The optimal threshold can thus be shown to be

$$\chi_1 = \frac{1}{2}U_{x11}. \tag{125}$$

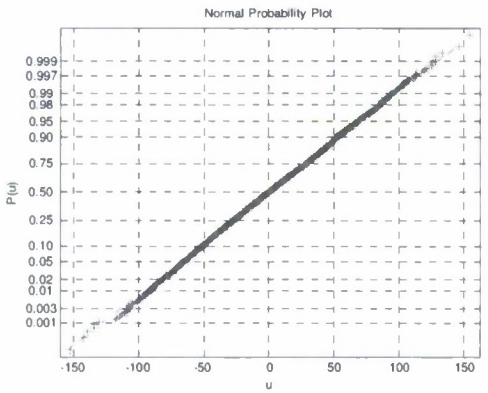


Fig. 103: Noise term distribution check for $n_{e1}(t)$.

The noise variance is $\sigma_{e1}^2$, which can be shown to be equal to the power spectral density $N_0/2$ for a Gaussian distribution. The distance $d_{12}$ between the two signal values is $U_{x11}$. The average probability of error is calculated to be[51]

$$P(\overline{c}_1) = Q\left[\sqrt{\frac{d_{12}^2}{2N_0}}\right] = Q\left[\frac{1}{2}\frac{U_{x11}}{\sigma_{e1}}\right], \tag{126}$$

where the Q-function is given by $Q(x) = \frac{1}{\sqrt{2\pi}}\int_x^\infty e^{-t^2/2}dt, \ x \geq 0$.

The probability $p(c_1)$ that correlator 1 correctly detects the header is then given by

$$p(c_1) = 1 - p(\overline{c}_1) = 1 - Q\left[\frac{1}{2}\frac{U_{x11}}{\sigma_{e1}}\right]. \tag{127}$$

Under the condition that correlator 1 at the radar receiver correctly detects whether the RF tag signal exists or not, the bit error probability for the message detection is calculated as follows.

To determine the $k$-th bit, we look at the amplitude of the output of correlator 2 output at time lag $2\tau_0 + k\tau_d$. The amplitude at the corresponding time lag is given by

$$\begin{aligned} c_2(2\tau_0 + k\tau_d) &= a_k \int_0^{T_2} x_1^2(t - 2\tau_0 - k\tau_d)dt + \sum_{j=1, j\neq k}^{L} a_j \int_0^{T_2} x_1(t - 2\tau_0 - j\tau_d)x_1(t - 2\tau_0 - k\tau_d)dt \\ &\quad + \int_0^{T_2} \sum_{j=1}^{L} a_j x_1(t - 2\tau_0 - j\tau_d) \sum_{i=2}^{N} x_i(t - 2\tau_0 - k\tau_d)dt + \int_0^{T_2} n_2(t)x(t - 2\tau_0 - k\tau_d)dt \\ &= a_k U_{x12} + n_{e2}(t) \end{aligned} \tag{128}$$

where

$$U_{x12} = \int_0^{T_2} x_1^2(t - 2\tau_0 - k\tau_d)dt = U_{x11} \tag{129}$$

and $n_{e2}(t)$ represents the noise terms, given by

[51] J. G. Proakis, *Digital Communications* (4th ed.). New York, NY: McGraw-Hill, 2001.

$$n_{e2}(t) = \sum_{j=1, j\neq k}^{L} a_j \int_0^{T_2} x_1(t-2\tau_0 - j\tau_d)x_1(t-2\tau_0 - k\tau_d)dt$$
$$+\int_0^{T_2} \sum_{j=1}^{L} a_j x_1(t-2\tau_0 - j\tau_d)\sum_{i=2}^{N} x_i(t-2\tau_0 - k\tau_d)dt + \int_0^{T_2} n_2(t)\cdot x(t-2\tau_0 - k\tau_d)dt \tag{130}$$

Similarly, we can show that $n_{e2}(t)$ can be approximated as Gaussian distributed with mean zero, and variance $\sigma_{e2}^2$.

The signal component of $c_2(2\tau_0 + k\tau_d)$ is either 0 or $U_{x12}$ since the coefficient $a_k$ is either 0 or 1. Thus, the average signal strength is $\frac{1}{2}U_{x12}$ assuming each value is equally probable. The optimal threshold in this case is then

$$\chi_2 = \frac{1}{2}U_{x12}. \tag{131}$$

The noise variance is $\sigma_{e2}^2$. The average probability of error for the message, assuming that the header is correctly decided, is calculated to be

$$p_b(e|c_1) = Q\left[\frac{1}{2}\frac{U_{x12}}{\sigma_{e2}}\right]. \tag{132}$$

Therefore, we can write the overall bit error probability as

$$p_b(e) = Q\left[\frac{1}{2}\frac{U_{x11}}{\sigma_{e2}}\right]\left(1-Q\left[\frac{1}{2}\frac{U_{x11}}{\sigma_{e1}}\right]\right)+Q\left[\frac{1}{2}\frac{U_{x11}}{\sigma_{e1}}\right] \tag{133}$$

upon substituting equations (126), (127), and (133) into equation (121).

The bit error probability is simulated in Fig. 104(a)-(b). The bit error probability is simulated as function of the channel signal-to-noise ratio in Fig. 104(a) under the conditions that the length of the delay line at the RF tag is 3. It shows that when the channel SNR is low as –4 dB, the system can still achieve a bit error probability less than $10^{-4}$. The bit error probability is simulated as function of the length of delay line at the RF tag in Fig. 104(b) under the condition that the channel signal-to-noise ratio is –3 dB. It shows that to get a bit error probability less than $10^{-4}$, the length of the delay line at the RF tag can go up to 6.

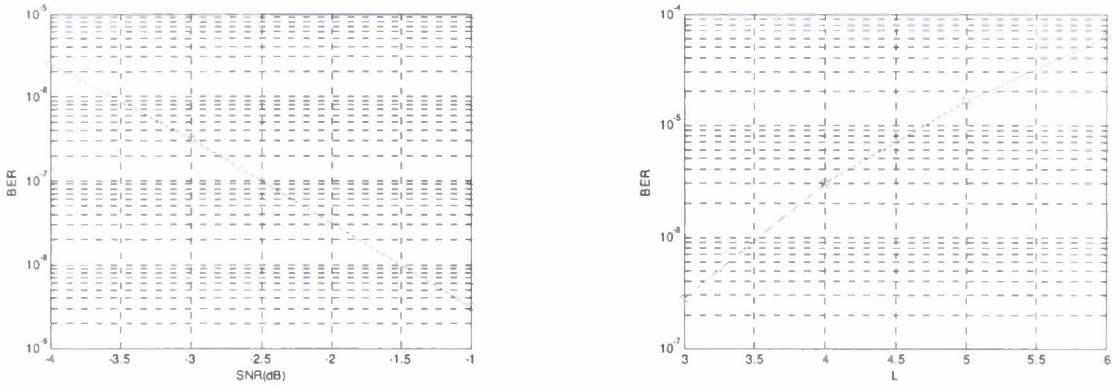


(a) (b)

Fig. 104: Bit error ratio (BER) performance. (a) BER vs. channel SNR for a 3-tap delay line, (b) BER vs. length of RF tag delay line for SNR of −3 dB.

The symbol error probability or the symbol error ration (SER) of the system is defined as the probability that the entire $L$-bit tag message is wrongly received by the radar. It depends upon the BER as well as on the number of delay taps $L$, and is given by

$$p_s(e) = p_s(e|c_1)p(c_1) + p_s(e|\overline{c}_1)p(\overline{c}_1). \tag{134}$$

Note that $p_s(e|\overline{c}_1) = 1$ due to the fact that the header is not correctly detected. On the other hand, if the header is correctly detected, we can show that for an $L$-bit sequence, the probability of all bits being correct is given by the product of the (identical) probabilities of the individual bits, which is simply the individual correct probability raised to the $L$-th power. Thus, we have

$$p_s(e) = \left(1-\left(1-p_b(e|c_1)\right)^L\right)p(c_1) + p(\overline{c}_1). \tag{135}$$

The symbol error probability is simulated as function of the channel SNR and the length of the delay line at the RF tag in Fig. 105(a) and Fig. 105(b), respectively. The plots show that to get a symbol error probability less than $10^{-4}$, the length of the delay line at the RF tag can go up to 5 when the channel SNR is –3 dB. The total number of distinct messages that can be sent in given by $2^L - 1$. Thus, at this symbol error probability level, a total of $2^5 - 1 = 31$ distinct messages can be sent by the tag.

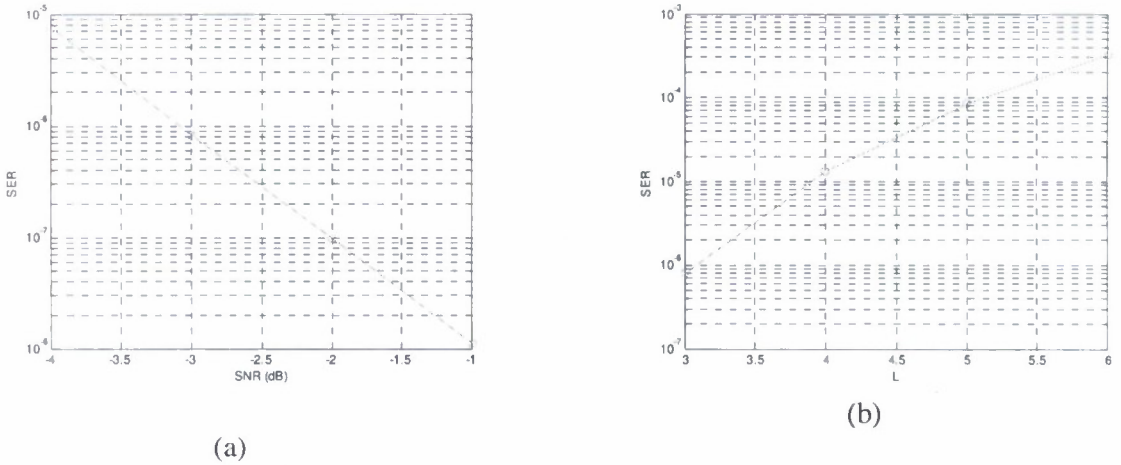


(a) (b)

Fig 105: Symbol error ratio (SER) performance. (a) SER vs. channel SNR for a 3-tap delay line, (b) SER vs. length of RF tag delay line for SNR of −3 dB.

## 2. 3. Noise Radar Networking

A conceptual diagram of our proposed Netted Covert MIMO Radar System is shown in Fig. 106. The netted radar sensor can be divided into two subsystems: tracking and communications. Every radar sensor in this system contains a transmitter and a receiver. Each radar sensor performs two specific functions: (1) target detection and tracking, and (2) data-communication with other radar sensors. The communication subsystem block diagram is shown in Fig. 107. The transmitter section is common to both the subsystems mentioned above. It is only in the receiver, where there is a branch-off between the subsystems. The signal being received by the receiving antenna is passed through a power divider. The two outputs from here are sent to the communication-subsystem-receiver and the tracking-subsystem-receiver respectively.

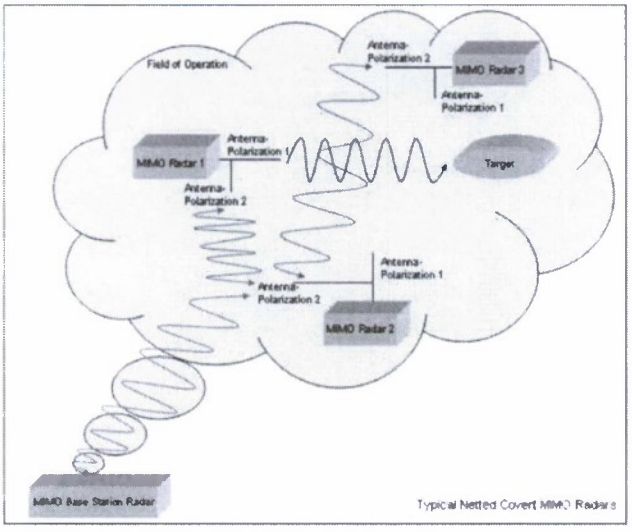


Fig.106: Proposed Netted Covert MIMO Radar System.

Transmitter

A zero mean white Gaussian noise signal is generated and passed through a bandpass filter to generate a band-limited UWB noise signal in the 1–2 MHz range. (In the actual implementation of the system, a frequency range of 1–2 GHz is used. The frequency scaling by a factor of $10^{-3}$ eases memory requirements during simulations). This band-limited noise signal is then notch (band-stop)-filtered within the range of 1.2–1.3 MHz. Intra-sensor communications is achieved by utilizing this sub-band for network communication among different radars. Our earlier studies have shown that spectral fragmentation of the radar frequency band causes no essential distortion to the main-lobe of the point spread function (PSF) if the fragmented gap portion is not too excessive, *i.e.*, $\leq$30%.

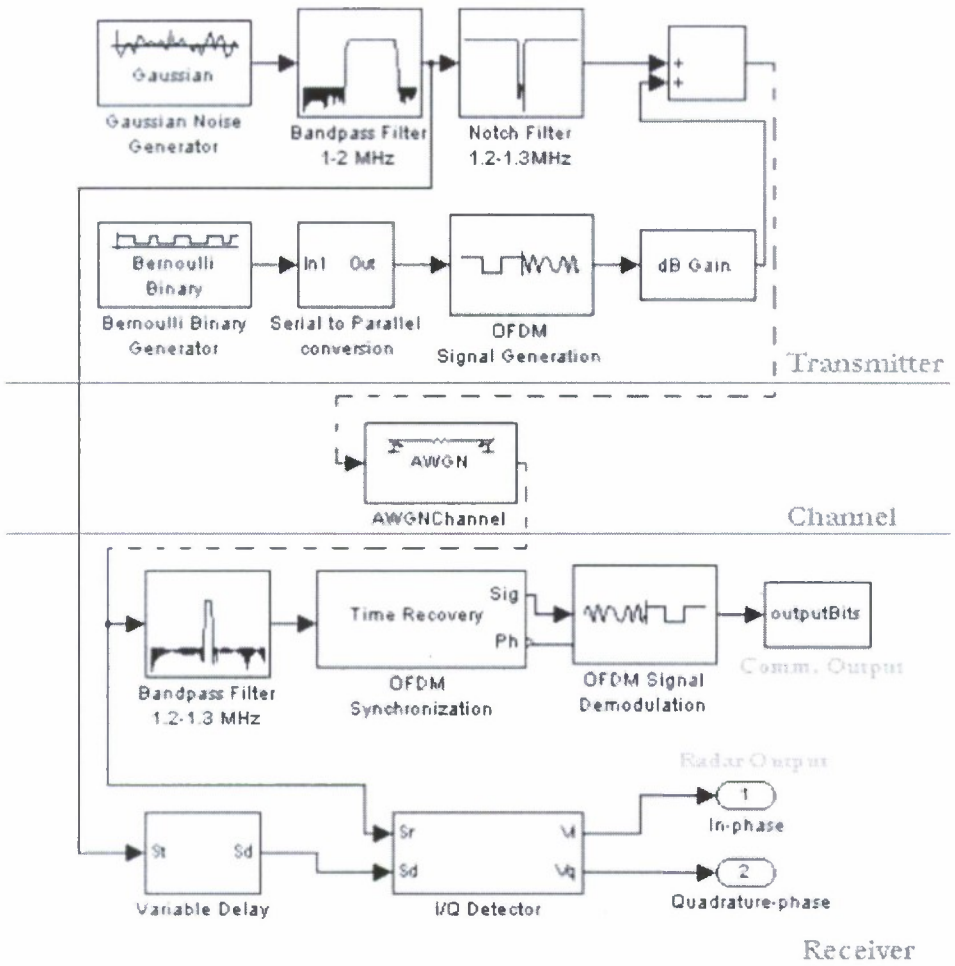


Fig. 107: Communication subsystem block overview.

Thus, the basic performance of the radar is essentially unaffected, even though we have a notch embedded within its transmitted signal. The remainder of the radar's transmit signal is the data signal, that will fill the notch in the spectrum of our band-limited noise signal. A Bernoulli binary number generator is used to generate the digital data that needs to be communicated. In the actual implementation, this data can be either target data or network control packets. This data are then modulated onto a continuous carrier sinusoid whose frequency lies within the notched portion of the band-limited UWB noise signal. BPSK and OFDM were considered for this modulation and the resulting performance is shown later. The modulated signal is then added in the time domain to the notched band-limited noise signal to produce our noise-data radar transmit signal. As seen by any hostile receivers, the transmitted waveform appears random and noise-like. However, for the other radar sensors in its vicinity, the waveform is construed as data plus noise. A simulation-based proof to the above two statements is given later in this report. The transmit signal is assumed to travel to the target and return as an echo to the transmitting radar sensor in the same way as a conventional noise radar. This echo is processed by the tracking-subsystem-receiver by the known correlation methods for obtaining the range information.

We assume a time-invariant additive white Gaussian channel (AWGN) in our system. AWGN gets added to the noise-data signal in the channel. Due to the Omni directional nature of the transmit antenna, it is possible that this noise-data signal is picked up by all radar sensors in the neighborhood of the transmitting radar. These sensors then pass this signal to their communication subsystem.

Communication-subsystem-Receiver

On this side, the incoming signal from a UWB antenna is passed through a narrow band-pass filter designed to pass only the data-carrier spectrum and attenuate all other frequencies. We assume that the data-carrier frequency allocated to each radar is known to all radar sensors within the system, allowing them to demodulate it and thereby retrieve the digital data concealed within. Thus, what appears as noise to the hostile forces actually contains useful information for the friendly radar sensors. In this manner a successful camouflaged communication platform is established between the radar sensors using the noise-data signal.

Let us consider a discrete band-limited UWB noise signal, as follows[52]:

$$bl\_noise[n] = A\,z[n]\exp\{j\omega_o n\} \tag{136}$$

where $z[n]$ is a sample function of a discrete, zero-mean, stationary Gaussian process, $\omega_o = 2\pi f_o$, $f_o$ is the center frequency of the band-pass noise. Fig. 108 shows the plot of this band-limited noise signal. This signal is passed through an ideal notch (band-stop) filter, which can is designed by the addition of an ideal low-pass filter and an ideal high-pass filter. Their cut-off frequencies $(\omega_1, \omega_2)$ are equal to the notch band's start and stop frequencies. The impulse response of such a filter is given by

$$h_{BS}[n] = \partial[n] + \frac{\sin(\omega_1 n)}{\pi n} - \frac{\sin(\omega_2 n)}{\pi n} \tag{137}$$

where $\partial[n]$ is the Kronecker delta function. When the band-limited noise signal is passed through this ideal band-stop filter, a notched band-limited UWB noise signal is generated, which can be represented as

$$ntch\_noise[n] = Az_1[n]\exp\{j\omega_{01} n\} + Bz_2[n]\exp\{j\omega_{02} n\} \tag{138}$$

[52] A.R.S. Bahai and B.R. Saltzberg, *Multi-Carrier Digital Communications: Theory and Applications of OFDM.* New York, NY: Kluwer, 2002.

where $z_1[n]$ and $z_2[n]$ are sample functions of zero-mean independent Gaussian processes, and ( $\omega_{01}$ , $\omega_{02}$ ) are the center frequencies of the noise bands on either side of the notch band in our notched band-limited noise signal.

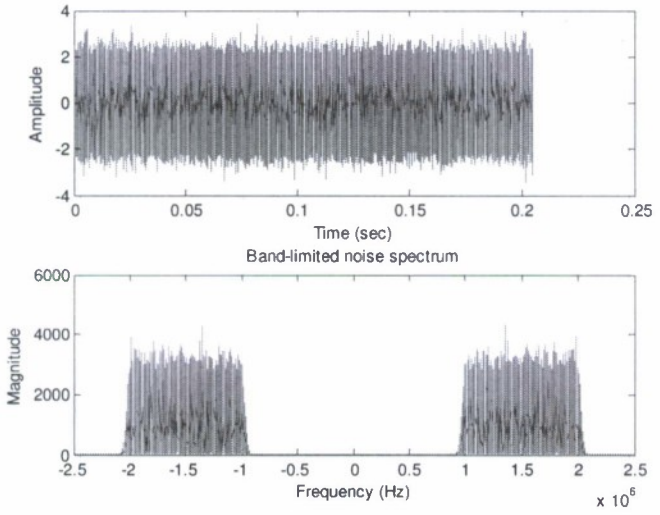


Fig. 108: UWB band-limited noise signal (time and frequency domain) over 1–2 MHz.

Now, in parallel we must generate the modulated data signal. This signal will then be embedded into the notched noise signal shown in (138) above. Various options are available for modulating the digital data onto a carrier. Based on the requirements of covertness and reliability, we believe that Orthogonal Frequency Division Multiplexing (OFDM) forms the most appropriate modulation technique for this system of noise radars. In addition to the advantages that OFDM provides for wireless broadband communications, it has a very desirable frequency spectrum behavior. It is also seen that for low SNR regimes and power-limited channels having sufficiently large bandwidth, orthogonal carrier modulation works the best [Ref. 51]. Our system is inherently low SNR by nature, as we need to operate it close to the noise floor of the receiver. And our operating bandwidth is large due to the UWB nature of the noise radar. Through our simulations, we verified that the frequency spectrum of OFDM-modulated data is best suited to fill in the frequency notch created within the band-limited noise signal, and it makes the composite spectrum of the resultant signal look very strikingly similar to a simple UWB band-limited noise signal. This provided the necessary covertness to our communication channel.

OFDM modulation in the noise radar

Binary data in terms of 1s (ones) and 0s (zeros) are randomly generated. This serial data are converted to a parallel form based on the number of carriers used in the OFDM signal. The number of carriers can be dynamically changed, according to the width available in the notched spectrum of our band-limited noise signal. Differential phase modulation is used to port the incoming bits onto the orthogonal carriers. Once these carriers are ready, an inverse Fourier transform is performed to put the different frequencies together and generate the

time-domain OFDM symbol. Based on the number of bits available for transmission at a time and the number of orthogonal carriers, the number of symbols required can be known. Thus, the required symbols are generated and this complete OFDM signal is then added to the notched band-limited noise signal, for transmission. Appropriate gain is provided to the data signal before it is added to the noise signal, so that it is compatible with the power level of the band-limited noise signal. This is to ensure that the transmit signal looks similar to a simple random noise signal. Digital Signal Processing is one of the important tools to be used for the implementation for this system. DSP hardware and software makes multi-carrier modulation possible. On the receiving side, the incoming signal from a UWB antenna is passed through a narrow band-pass filter designed to pass only the OFDM spectrum and attenuate all other frequencies. This OFDM signal so obtained is Fourier transformed to get the individual frequency components present in the signal. Differential phase de-modulation is performed to retrieve the original data bits from this signal. In our simulations, we compared these bits to the transmitted bits with channel SNR being the variant, to plot the BER curve for our system. This curve shown in the next section proved the reliability associated with our OFDM-based noise radar system.

Therefore, using OFDM to modulate our data we obtain the following signal, which is then embedded into (138):

$$d[n]=\sum_{k=0}^{N-1} m[k]\exp\{j\frac{2\pi}{N}kn\} \tag{139}$$

where $m[k]$ is the $k^{\text{th}}$ symbol in the message symbol sequence for $k$ in [0, $N-1$], $N$ is the number of carriers and $T$ is the active symbol period. Upon simplifying (139), we can write:

$$d[n]=\sum_{k=0}^{N-1} m[k]\exp\{j\omega_k n\} \tag{140}$$

where $\omega_k=\frac{2\pi k}{N}$ is the orthogonal carrier frequency set.

Therefore, our transmitted signal is now is as given by

$$S_t[n]=Az_1[n]\exp\{j\omega_{01}n\}+Bz_2[n]\exp\{j\omega_{02}n\}+\sum_{k=0}^{N-1} m[k]\exp\{j\omega_k n\} \tag{141}$$

Let us assume that our transmitting radar (Radar1) sends this signal towards the target. The echo from the target comes back to Radar1. This transmit signal is also received by another radar (Radar2), which is in the vicinity of Radar1. The two received signals at the two radars are therefore, respectively:

$$S_{r1}[n]=K_1 S_t[n-n_d]+\xi_1[n]\exp\{j\omega_o n\} \tag{142}$$

and

$$S_{r2}[n] = K_2 S_t[n - n_r] + \xi_2[n]\exp\{j\omega_o n\} \tag{143}$$

where $n_d$ is the round-trip time delay, $n_r$ is the propagation delay from Radar1 to Radar2. The second term in (142) and (143) is due to the AWGN channel, which is uncorrelated with $z_1[n]$ or $z_2[n]$. In the above development, $A'$, $A$, $B$, $K_1$, and $K_2$ are the amplitude scaling coefficients.

*Ranging in Radar1:* To find its distance to the target, the receiver in Radar1 will try to estimate the time delay '$n_d$'. It uses correlation techniques to do so. The transmit signal is delayed it by some time $n_\tau$ and then it is cross-correlated with the incoming echo to give $R_{SS}[n, n - n_\tau]$ given by

$$R_{SS}[n, n - n_\tau] = \mathrm{E}\{S_{r1}[n]S_t^*[n - n_\tau]\} \tag{144}$$

Invoking the zero mean and independence properties of $z_1[n]$, $z_2[n]$, $\xi_1[n]$, and $\xi_2[n]$, the cross-correlation results in:

$$\begin{aligned} R_{SS}[n_\tau - n_d] = \mathrm{E}\{&A^2 K_1 z_1[n - n_d]z_1^*[n - n_\tau]\exp\{j\omega_{01}(n_\tau - n_d)\} \\ &+ B^2 K_1 z_2[n - n_d]z_2^*[n - n_\tau]\exp\{j\omega_{02}(n_\tau - n_d)\} \\ &+ K_1 \sum_{k_1=0}^{N-1}\sum_{k_2=0}^{N-1} m[k_1]m^*[k_2]\exp\{j\omega_c(n_\tau - n_d)\}\} \end{aligned} \tag{145}$$

A peak or maximum of the cross-correlation amplitude results when $n_\tau = n_d$. The location in time of this peak is observed and $n_\tau$ is estimated, thus yielding $n_d$. By knowing $n_d$, the target's distance is estimated using the well-known radar equation: $d = n_d c/2$, where $c$ is the velocity of light.

Therefore, using the fact that $n_\tau = n_d$, (145) reduces to:

$$R_{SS}[0] = A^2 K_1 \sigma_{z1}^2 + B^2 K_1 \sigma_{z2}^2 + K_1 \sum_{k_1=0}^{N-1}\sum_{k_2=0}^{N-1} m[k_1]m^*[k_2] \tag{146}$$

where $\sigma_{z1}^2$ and $\sigma_{z2}^2$ are the variances of $z_1[n]$ and $z_2[n]$ respectively. From the third term in equation (146), it is clearly observed that the addition of data to the UWB noise has only changed the amplitude of the peak in the cross-correlation. It has no effect on the location of the peak which is the prime parameter used in estimating the target's distance. We will however try to evaluate this third term in (146) to see how much it affects the amplitude of the cross-correlation.

For this, we need to consider the modulations used on the sub-carriers of an OFDM symbol. In the usual case, the sub-carriers in an OFDM symbol is modulated individually by either BPSK, MPSK, QAM or any other modulation technique. Based on the channel characteristics and the amount of data that we need to transmit, we can decide which one suits the best. In most systems, QAM is used as the modulation technique for the sub-carriers. So, we will continue to analyze our system assuming that we modulate our sub-carriers using a MQAM constellation.

An $M$-ary quadrature amplitude modulation ($M$-QAM) signal can be defined by

$$s(t) = \begin{cases} A_i \cos(2\pi f_c t + \theta_i), & 0 \le t \le T \\ 0, & \text{elsewhere} \end{cases} \tag{147}$$

for $i = 0, 1, \ldots, M - 1$. Here, $A_i$ is the amplitude, $f_c$ is the carrier frequency, $\theta_i$ is the phase angle, and $T$ is the symbol duration. It has a power $P_i = A_i^2/2$, so that $A_i = \sqrt{2P_i}$ [53].

Now each symbol in the 16-QAM constellation diagram can be represented by the 2-tuple $(\sqrt{E_i}\cos\theta_i, \sqrt{E_i}\sin\theta_i)$, where $E_i = P_iT$ is the energy of $s(t)$ contained in a symbol duration for $i = 0, 1, \ldots, M - 1$. From this 2-tuple, it is now easy to find the amplitude and phase of each symbol. We need the amplitude and phase, so that we can substitute them in (28) above to evaluate its third term.

Therefore, for our 2-tuple symbol, we now find its magnitude and phase as follows:

$$\text{Magnitude} = \sqrt{s_{11}^2 + s_{12}^2} = \sqrt{(\sqrt{E_i}\cos\theta_i)^2 + (\sqrt{E_i}\sin\theta_i)^2} = \sqrt{E_i} \tag{148a}$$

and

$$\text{Phase} = \tan^{-1}\frac{s_{12}}{s_{22}} = \tan^{-1}\frac{\sqrt{E_i}\sin\theta_i}{\sqrt{E_i}\cos\theta_i} = \theta_i \tag{148b}$$

Therefore, we can now represent the two-dimensional $M$-QAM symbol as:

$$s_i = \sqrt{E_i}e^{j\theta_i} \tag{149}$$

In (147), we saw that $m[k]$ is a complex symbol from the modulation constellation of the sub-carriers of the OFDM symbol. It appears in the third term on the right-hand-side. We are currently concerned with evaluating this term. This term can be separated as follows:

[53] F. Xiong, *Digital Modulation Techniques*. Boston, MA: Artech House, 2000.

$$\sum_{k_1=0}^{N-1}\sum_{k_2=0}^{N-1} m[k_1]m^*[k_2] = \sum_{k_1=0}^{N-1} m[k_1]\sum_{k_2=0}^{N-1} m^*[k_2] \tag{150}$$

Now, any $m[k]$ is equal to one of the symbols in the $M$-QAM constellation, *i.e.*,

$$m[k] = s_i\big|_{i=0,1\ldots,M-1} = \sqrt{E_i}e^{j\theta_i}\Big|_{i=0,1\ldots,M-1} \tag{151}$$

We can see that based on the incoming data, this $m[k]$ can take any of the $M$ values from the $M$-QAM constellation. That is, this $m[k]$ is a complex random variable.

We now consider each of the summations in (150) separately. Varying $k$, in actuality means that the symbol is going onto the $N$ different frequencies of the complete OFDM symbol. But we have this $m[k]$ as random variable. Therefore each summation is (150) can be seen to be $N$ times the average or expected value of $m[k]$. That is:

$$\sum_{k=0}^{N-1} m[k] = N\mathrm{E}\{s_i\} = N\mathrm{E}\{\sqrt{E_i}e^{j\theta_i}\} \tag{152}$$

Assuming equal probability of occurrence of the $M$ symbols (equiprobable), we can expand (152) as follows.

$$\sum_{k=0}^{N-1} m[k] = N\sum_{i=0}^{M-1} p_i s_i = N\sum_{i=0}^{M-1} p_i\sqrt{E_i}e^{j\theta_i} \tag{153}$$

where $p_i$ is the probability of occurrence of the $i^{\text{th}}$ symbol. We already assumed that this is equiprobable, then $p_i = 1/M$.

$$\sum_{k=0}^{N-1} m[k] = \frac{N}{M}\sum_{i=0}^{M-1} s_i = \frac{N}{M}\sum_{i=0}^{M-1}\sqrt{E_i}e^{j\theta_i} \tag{154}$$

Thus, equation (150) reduces to

$$\sum_{k_1=0}^{N-1}\sum_{k_2=0}^{N-1} m[k_1]m^*[k_2] = \sum_{k_1=0}^{N-1} m[k_1]\sum_{k_2=0}^{N-1} m^*[k_2] = \frac{N^2}{M^2}\sum_{i_1=0}^{M-1} s_{i_1}\sum_{i_2=0}^{M-1} s^*{}_{i_2} \tag{155}$$

and

$$\sum_{k_1=0}^{N-1}\sum_{k_2=0}^{N-1} m[k_1]m^*[k_2] = \sum_{k_1=0}^{N-1} m[k_1]\sum_{k_2=0}^{N-1} m^*[k_2] = \frac{N^2}{M^2}\sum_{i_1=0}^{M-1}\sum_{i_2=0}^{M-1}\sqrt{E_{i_1}}\sqrt{E_{i_2}}e^{j(\theta_{i_1}-\theta_{i_2})} \tag{156}$$

The right hand side of (156) has to be solved individually for every set of incoming data. But we find that our equi-probable symbol assumption helps us in solving this more easily. For example, let us consider $M$ = 4. For a 4-QAM constellation, $\sqrt{E_i}$ remains the same for all the symbols, only the angle changes. We use this property and simplify the double summation in the RHS of (37). On simplification, we see that all the components cancel each other and the result is zero. That is, for an 4-QAM constellation

$$\sum_{k_1=0}^{N-1}\sum_{k_2=0}^{N-1} m[k_1]m^*[k_2] = 0 \tag{157}$$

Upon observing the constellation, we can see that for every constellation that is symmetric about the x-y axis, this average value comes to zero. Hence for any value of $M$, the $M$-QAM's expected value is zero.

Therefore, for our system we can now see that the cross-correlation between the incoming echo and the radar's transmit signal is

$$R_{SS}[0] = A^2K_1\sigma_{z1}^2 + B^2K_1\sigma_{z2}^2 + 0 = A^2K_1\sigma_{z1}^2 + B^2K_1\sigma_{z2}^2 \tag{158}$$

Thus, we see that adding $M$-QAM-based OFDM data to the noise radar's transmit signal does not affect the performance of the noise radar with respect to target identification and tracking. This implies perfect mutual exclusivity between radar and communication operations. Simulation results for this proof are also present further down in this report.

*Data retrieval in Radar2:* The receiver of Radar2 detects the incoming signal (143) from Radar1 and passes it through an ideal band-pass filter with cut-off frequencies ($\omega_1, \omega_2$). All other frequencies are attenuated. This signal is then passed through an OFDM demodulator section to successfully extract the digital bits transmitted by radar1. A measure of any communication subsystem's performance is the probability of bit error ($P_e$). The theoretical expression for $P_e$ in BPSK modulation is:

$$P_e = Q\left(\sqrt{\frac{2E_b}{N_o}}\right) \tag{159}$$

where $\frac{2E_b}{N_o}$ is the signal to noise ratio ($SNR_o$) after the demodulator and before the decision circuit. Simulations results are presented next.

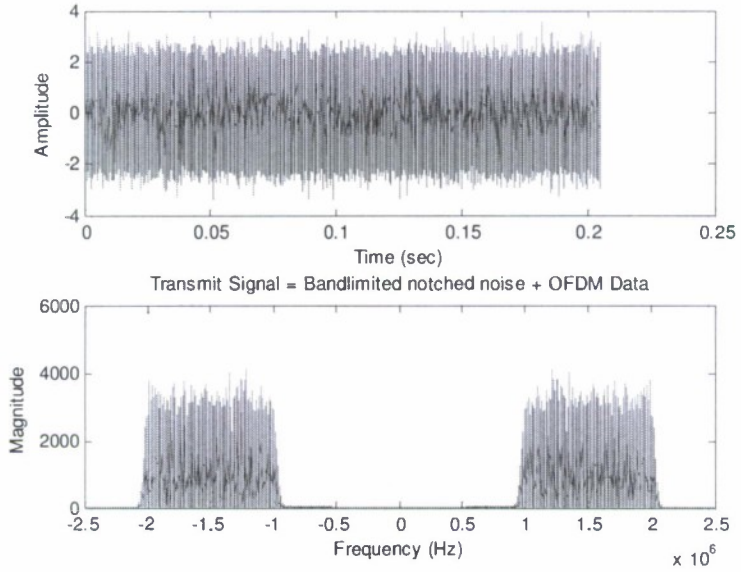


Fig. 109: Radar transmit signal, containing data (OFDM with 32 carriers with channel SNR = 2 dB) within 1.2–1.3 MHz and noise elsewhere.

*Spectrum Comparison:* Fig. 109 and Fig. 110 present the noise-OFDM-data signal and noise-BPSK-data signal respectively. The former indicates that data has been appropriately camouflaged within the noise signal and the latter indicates an unsuccessful camouflage.

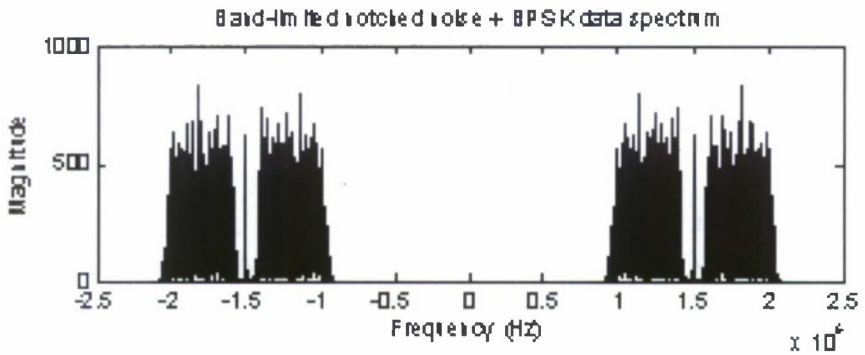

Fig. 110: Spectrum of noise-BPSK-data, carrier at 1.5 MHz.

*Camouflage and Covertness:* We show seven different power spectrum plots in Fig. 111(a)-111(g) to demonstrate that the transmitted signals do appear noise-like to the outside observer. Note from Figure 111(e) for the OFDM embedded in notched UWB noise that the spectrum appears completely random and noise-like, similar to that shown in Figure 111(c) for UWB noise. For the OFDM signal to be completely concealed within the UWB noise band, the following two conditions must be met: (1) the OFDM band must be exactly overlap the notch band so as to avoid gaps in the spectrum; and (2) the power spectral density (PSD) of the OFDM signal must be the same as that of the surrounding UWB noise so as to avoid detection. This core requirement will allow us to combine random noise radars with ad hoc

networks to develop undetectable communication bands for use by a network of radars.

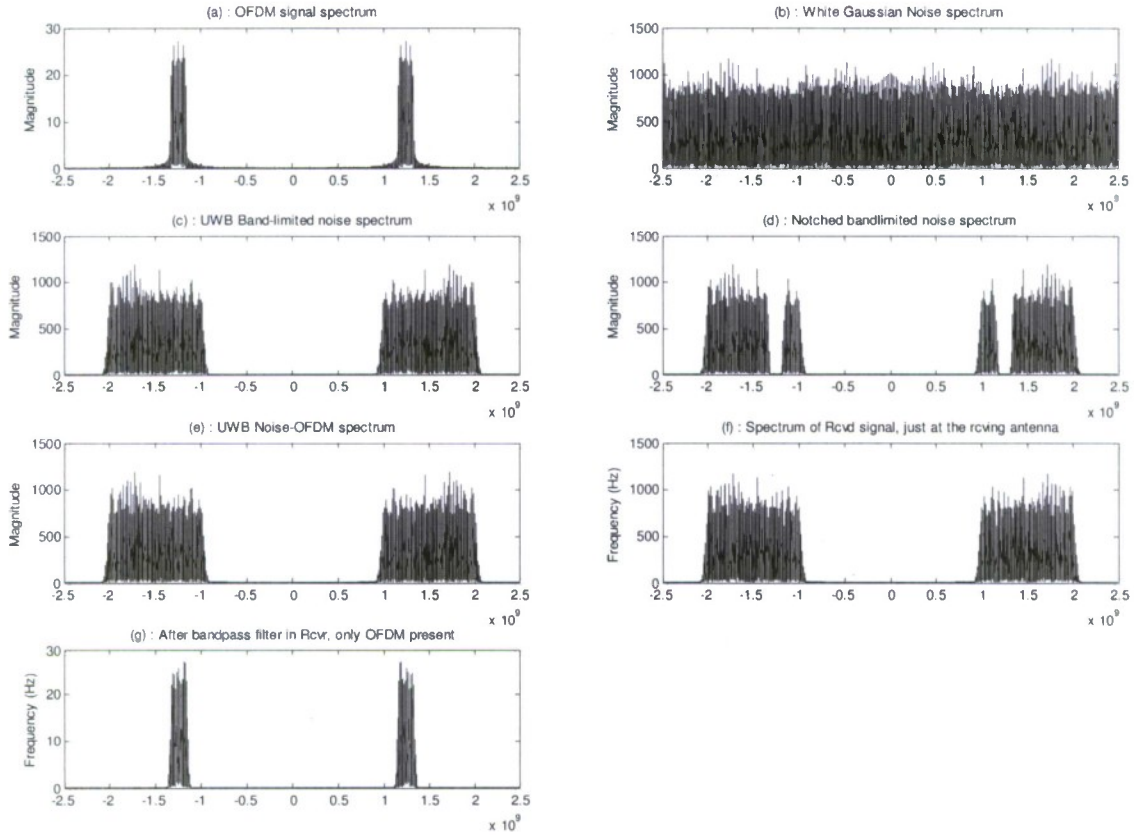


Fig. 111: Plots showing the radar sensor's spectrum at different stages of the transmitter and receiver: 1024-point FFT, 33 data sub-carriers, 1 bit per symbol, SNR = 20 dB.

We define the camouflage metric as a duple denoted as $(m_1;m_2)$ given by $(BW_{OFDM}/BW_{NOTCH};PSD_{OFDM}/PSD_{NOTCH})$ where $BW$ and $PSD$ refer to the bandwidth and power spectral density, respectively, and the subscripts $OFDM$ and $NOTCH$ refer to the respective bands. An optimum camouflage obviously occurs when this duple is $(1.0;1.0)$. While achieving this value of $(1.0;1.0)$ is idealistic, a confidence interval of around $\pm 0.2$ (for our simulations) still provides adequate camouflage to our signal. The camouflage duple can be understood better by observing the different ways in which a data-bearing OFDM signal can be embedded into the notched noise waveform.

We first consider Figure 112. It shows the resulting values for $m_1$ when the bandwidth of OFDM signals with varying number of sub-carriers is compared with the bandwidth of the notch filter in the transmitter of the radar sensor. It is clearly observed that for an system-dependent acceptable region of $\pm 0.2$ over the idealistic value of unity for $m_1$, the number of

sub-carriers required to camouflage the notch bandwidth lies between 24 and 33. Once this required number of OFDM sub-carriers is known, the power amplification factor for the OFDM signal can be chosen such that $m_2$, the PSD ratio is brought under allowable limits. This is required since an optimum value achieving perfect camouflage is when the OFDM signal PSD matches the notched noise signal PSD. We note that when $m_1 > 1.0$, then the BER of the system increases as the band-pass filter in the receiver truncates the OFDM signal around its edges. On the other hand, when $m_2 > 1$, the BER of the system does decrease, but the OFDM signal is no longer camouflaged as it towers over the surrounding noise band. When the radar sensors operate in positive SNR regions, the camouflage duple accurately quantifies the system performance. However, for systems operating in negative SNR regions, $m_2$ effectively quantifies the system performance, since in this region the complete noise-OFDM signal is under the noise floor.

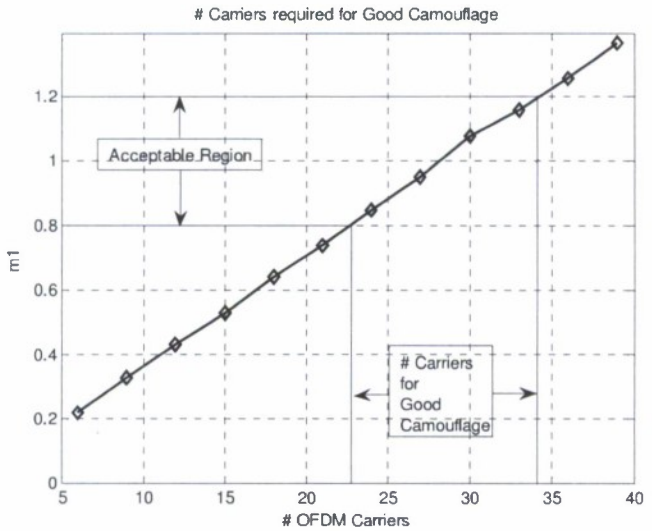


Fig. 112: Number of OFDM sub-carriers required to achieve an acceptable camouflage metric $m_1$.

To numerically emphasize the metric's usefulness, we consider Fig. 113(a) and 113(b), which present a comparison between a 30-data-carrier noise-OFDM signal and a 9-data-carrier noise-OFDM signal, respectively. The former with a camouflage metric of $(0.98;1.05)$ indicates that data have been appropriately concealed within the noise signal, while the latter with a camouflage metric of $(0.32;0.29)$ indicates an unsuccessful camouflage.

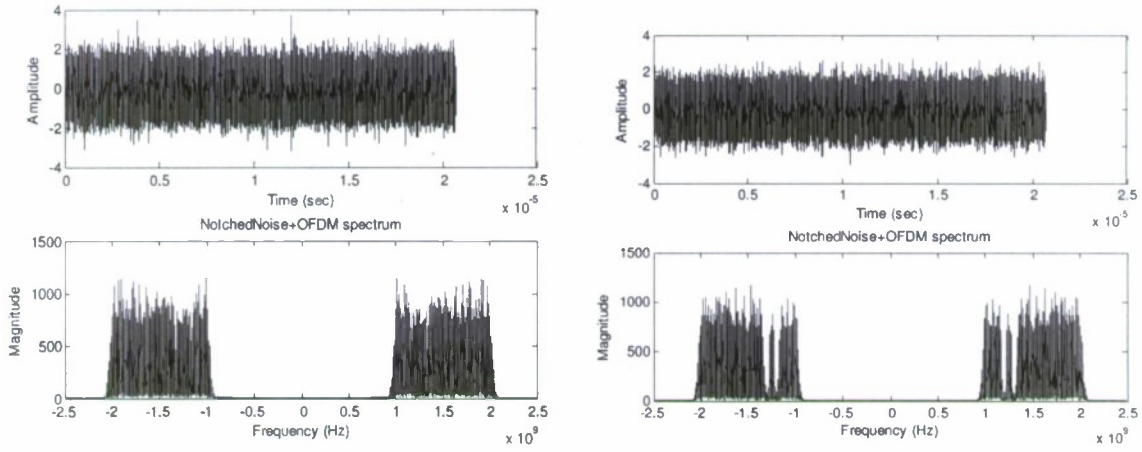


Fig. 113: Comparison of (a) 30-carrier noise-OFDM-data signal, with (b) 9-carrier noise-OFDM-data signal. The camouflage metric duple is (0.98;1.05) for case (a) and (0.32; 0.29) for case (b).

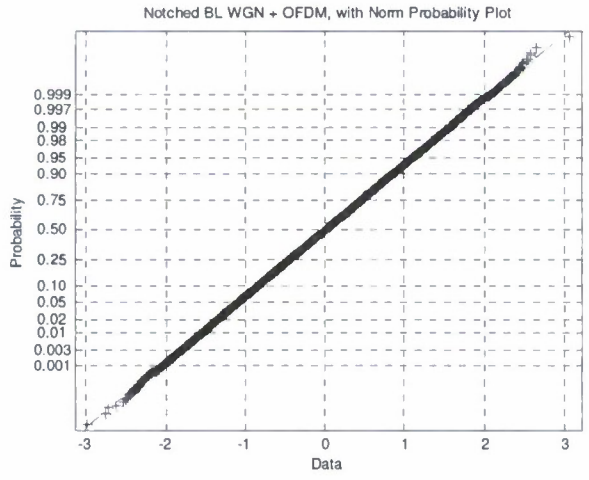


Fig. 114: Norm Probability plot of the noise-data signal in comparison to a reference Gaussian with same mean and variance.

Covertness or privacy of message communication is an important requirement in wireless radar networks. The noise-based communication platform we present supports this requirement due to the camouflage of data within the UWB noise. One test for measuring the covertness of the noise-OFDM waveform is deducing the cumulative distribution function (CDF) and noting how close it is to pure random noise. The excellent overlap in the norm probability plot in Fig. 114 between the reference band-limited white Gaussian and the noise-OFDM-data signals clearly indicates the close similarity between these two signals. Any hostile antenna capturing such a signal is likely to conclude it to be simply white noise, either generated within its own receiver or occurring due to environmental electromagnetic interference (EMI). As stated earlier, the degree of covertness however depends on the

number of sub-carriers used as well on the relative PSD of the OFDM symbol and the notched UWB noise signal. If PSD levels are not compatible, *i.e.* if $m_2$ is much different from 1, then either the OFDM signal spectrum can be seen towering over the surrounding noise signal or the unfilled notch in the noise signal spectrum will be very evident. In either case, we lose covertness associated with this system. Similarly for a lower number of sub-carriers, i.e. when $m_1 << 1$, the notch in the noise-spectrum does not get fully filled in, leading to greater detectability and hence lower covertness. Hence, appropriate power and sub-carrier selection is important to enhance system covertness.

*Characteristics of the Communication Subsystem:*

As noted earlier, the transmitting radar embeds OFDM-data symbols into the notched UWB noise frequency band and transmits the composite signal towards the target. As far as the echo is concerned, we have already shown that the transmitting radar will be able to receive it and process it for target tracking as required. In this sub-section, we consider any other radar present in the vicinity of the transmitting radar. This or these radars are potential receivers of the data that was embedded and transmitted by the transmitting radar. This receiving radar is mainly responsible for extracting the data embedded in the incoming noise-data signal. The composite transmit signal and the incoming noise-data signal can be expressed in equations (141) and (142) respectively. The communication subsystem in this radar is responsible for processing only the third term in equation (141), neglecting the delays shown in equation (142) for ease of understanding. It needs to detect the incoming frame within the channel, and then perform OFDM demodulation to extract the camouflaged data. The time domain representation of the OFDM symbol is shown below:

$$d[n] = \sum_{k=0}^{N-1} m[k] \exp\{j\omega_k n\} \tag{160}$$

In order for the receiver to perform the DFT operation on the incoming OFDM signal, it needs to have all the $N$ OFDM symbols, namely, $d[0]$, $d[1]$,...$d[N-1]$. Once all of these symbols serially come in into the receiver, they are put in parallel and passed through a DFT to extract the data symbols present on each sub-carrier.

In the case of the netted noise radar, the incoming symbols are not simple OFDM symbols, but a signal expressed as

$$S_r[n] = A' z_1[n] \exp\{j\omega_{01} n\} + B' z_2[n] \exp\{j\omega_{02} n\} + \sum_{k=0}^{N-1} m[k] \exp\{j\omega_k n\} + \xi_2[n] \exp\{j\omega_0 n\} \tag{161}$$

Therefore, this signal has to be first passed through a bandpass filter in order to extract the embedded OFDM symbol, i.e. all frequencies within $(\omega_0, \omega_{N-1})$. These are the sub-carriers that carry the data from the transmitter. The transfer function for an ideal digital bandpass filter shown in Fig. 115 is given as

$$h_{BP}[n] = \frac{\sin(\omega_{N-1} n)}{\pi n} - \frac{\sin(\omega_0 n)}{\pi n} \tag{162}$$

The desired output is then simply the convolution of $S_r[n]$ and $h_{BP}[n]$, i.e. $S_r[n] \otimes h_{BP}[n]$.

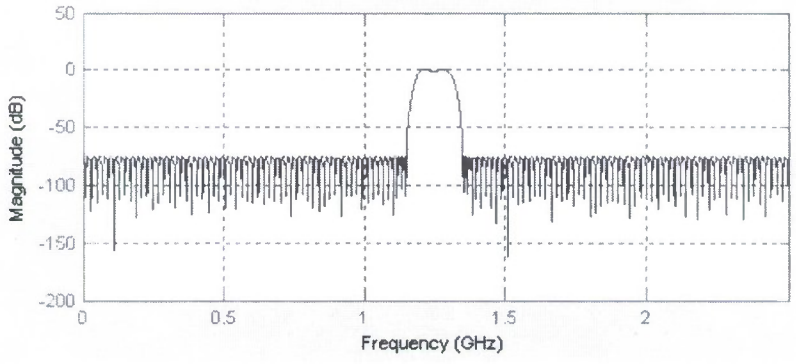


Fig. 115: FIR equiripple bandpass filter operating between 1.2 and 1.3 GHz.

Ideally, we expect that the surrounding noise is removed and a clean OFDM signal is generated as the output. However, in practice the bandpass filter in use is far from being ideal. The pass-band gain of the filter is not constant with frequency, and the roll-off bandwidths on either side are also non-ideal. Fig. 44 shows the magnitude response of a non-ideal bandpass filter designed to eliminate our noise signal and only pass through the required OFDM signal.

Fig. 116 shows a comparison plot of the OFDM signal spectra, under ideal and non-ideal filtering conditions. The top plot in Fig. 116 depicts a pure conventional OFDM signal spectrum. The bottom plot is the result of passing our noise-OFDM radar received signal through the Bandpass filter shown in Fig. 115 above. It is clearly seen that there is a significant reduction in signal spectrum around the cut-off frequencies.

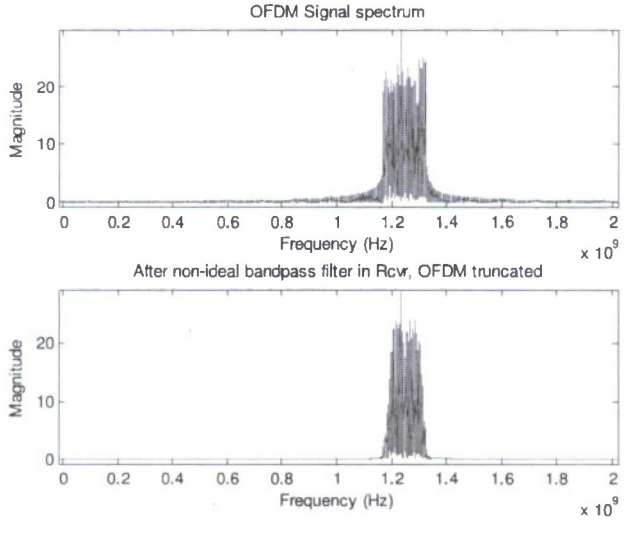


Fig. 116: OFDM spectrum truncation due to non-ideal bandpass filtering.

This truncation of the spectrum in the netted noise radar receiver, results in many issues affecting the OFDM demodulation stage. We show in later sections of this report, that inter-carrier interference and inter-symbol interference are enhanced due to this filter section. Therefore, as seen in Fig. 116, the OFDM signal in the netted noise radar is different from a conventional OFDM received signal. This calls for customized signal processing in the communications subsystem of the receiver. The next section of this report detail this analysis and present few initial methods for ICI and ISI correction based on Frame/timing synchronization.

We also present an enhanced RF version of the netted noise radar block diagram in Fig. 117. This diagram summarizes the system functionality in a concise format. It includes all the details we have seen so far in this section barring the RF processing part. Our current work assumes that we are able to generate sub-carrier frequencies directly in the UWB region.

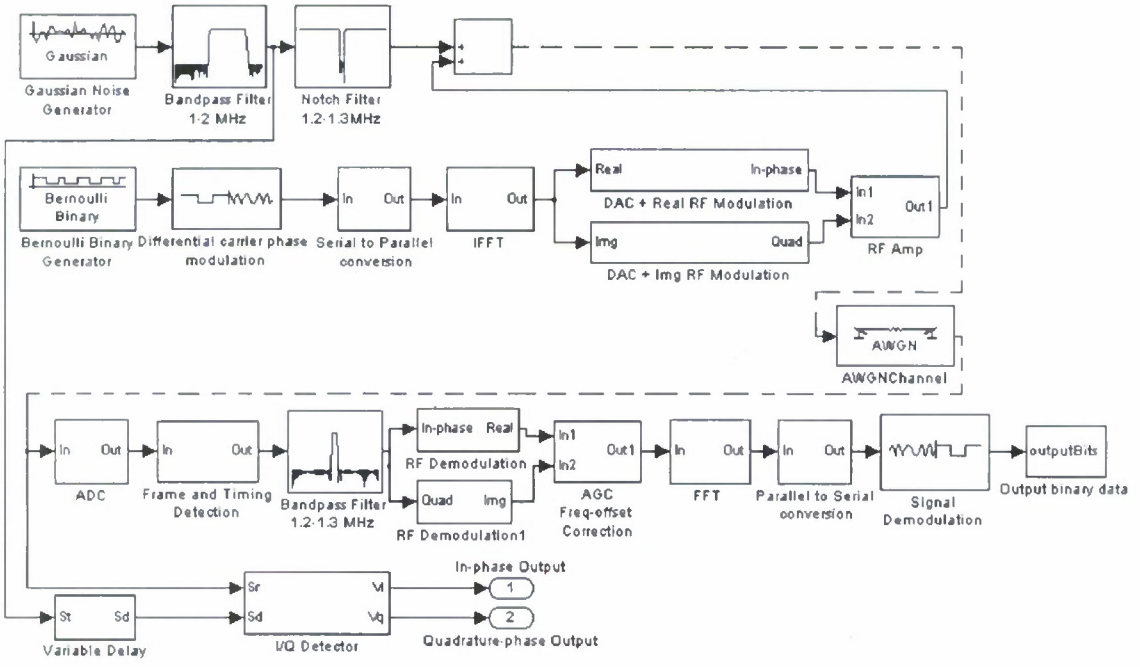


Fig. 117: Detailed block diagram of the Netted Noise Radar Sensor.

*Synchronization Requirements:*

In current defense scenarios, as much as battlespace surveillance depends on network centric operations, so are communication technologies dependent on effective synchronization mechanisms. Synchronization issues are of great importance in all digital communications systems, especially in OFDM systems. Inter-symbol interference (ISI) and inter-carrier interference (ICI) due to the loss of orthogonality among sub-carriers are some common errors caused by lack of synchronization. OFDM systems are even more sensitive to timing, carrier frequency offset, and sampling clock offset, when they are embedded within noise waveforms. Therefore, proper synchronization is an important design problem in wireless netted radar communication.

Fig. 118 compares the bit error rate (BER) performance of modulation signals embedded in noise with that of a conventional OFDM signal. Clearly, the performance of the proposed netted radar system needs to be enhanced to bring it closer to a conventional OFDM system's performance. This involves reducing the probability of bit error of the system, so that the overall reliability can be improved. To achieve this objective, proper synchronization (frame detection, timing, and frequency-offset) in the noise radar sensor needs to be achieved first and foremost.

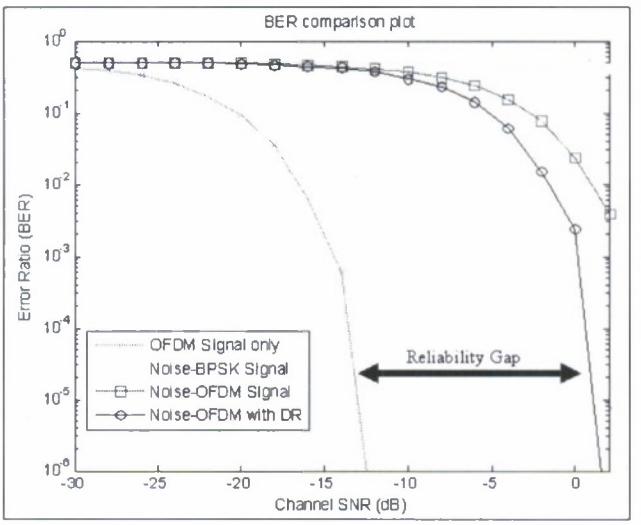


Fig. 118: BER performance of various modulation schemes.

We derive an expression that prompts that frame detection, timing estimation and frequency-offset estimation is essential in the netted noise radar sensor[54]. All these together constitute synchronization.

Consider an OFDM system with $N$ sub-carriers and a time-domain sampling rate $1/T$. Let us say that

$$D[n] = \left[ D_0[n] D_1[n] D_2[n] ..... D_{Q-1}[n] \right]^T \tag{163}$$

is the $n^{th}$ block of data to be transmitted. The number of sub-carriers used ($Q$) may be less than or equal to $N$. OFDM modulation is implemented by applying the Inverse Discrete Fourier Transform (IDFT) to this $D[n]$. Using matrix representation, the resulting $N$-point time domain OFDM signal is given by

$$d[n] = \left[ d_0[n] d_1[n] d_2[n] ..... d_{N-1}[n] \right]^T = W_Q D[n] \tag{164}$$

[54] H. Liu and G. Li, *OFDM-Based Broadband Wireless Networks: Design and Optimization*. Hoboken, NJ: Wiley, 2005.

where $W_Q$ is an $N \times Q$ sub-matrix of the IDFT matrix $W$. The columns of $W_Q$ correspond to the sub-carriers that are modulated with data.

Now, the receiver output for the $n^{th}$ block within the modulation window is given by

$$r[n] = \left[r_0[n] r_1[n] r_2[n] ..... r_{N-1}[n]\right]^T = W_Q H D[n] \tag{165}$$

where $H(i)$, $i \in [0, N-1]$ is the DFT of the channel response. In other words, each sub-carrier, with a scalar ambiguity, can be recovered by applying a DFT to $r[n]$, i.e.

$$W_Q^H r[n] = W_Q^H W_Q H D[n] = H\left[D_0[n] D_1[n] D_2[n] ..... D_{Q-1}[n]\right]^T. \tag{166}$$

Now, a truncated OFDM symbol as shown in Figure 45 will produce unwanted carrier-offset and inter-carrier interference due to the non-linear magnitude and phase responses of the bandpass filter. In this case, the receiver output for the $n^{th}$ block within the modulation window is given by

$$r[n] = X W_Q H D[n] \tag{167}$$

where $X$ is an $N \times N$ matrix representing the effects of the non-ideal bandpass filter on the transmitted OFDM symbols. Since we are trying to recover the sub-carriers by applying a DFT to $r[n]$, we have

$$W_Q^H r[n] = W_Q^H X W_Q H D[n] \neq H\left[D_0[n] D_1[n] D_2[n] ..... D_{Q-1}[n]\right]^T \tag{168}$$

since $W_Q^H X W_Q \neq I$.

Thus, the sub-carriers cannot be directly recovered since the orthogonality between the sub-carriers is disturbed due the convolution of the received signal with the transfer function of the non-ideal bandpass filter. Further analysis of this matrix $X$ is required. To recover $D[n]$, $X$ needs to be estimated. But in order to do this, $r[n]$ needs to be detected in the first place. Therefore, the first task of the receiver is to digitize the incoming signal and decide the frame/symbol boundaries. If the receiver cannot clearly identify the symbols, then ICI and ISI are inevitable.

In reference to equation (168), we recognize the necessity for a unique synchronization technique. Instead of a simple OFDM symbol going out of the transmitter, we have a wideband noise-data signal, which comprises a noise waveform in one part of the signal spectrum and an OFDM waveform in some other part. This composite signal, when received at the receiver, passes through the band-pass filter. The output cannot be directly used with

known preamble or pilot-based techniques as given in the literature for OFDM systems[55,56,57]. This conclusion is attributed to the *X* factor shown in equation (168) above. The requirement of covertness is another major deterring factor for the use of preamble-based or pilot-based estimation techniques. Therefore, in this paper we propose an accurate Frame/Timing detection mechanism for the netted noise radar. This is an incremental modification to the delay-and-correlate algorithm used in IEEE 802.11a for packet/frame detection as described in Ref. 56.

### *2. 3. 2. Noise Correlation-based Frame Timing Estimation*

OFDM systems require a reliable synchronization scheme like any other digital communication system. Binary bits are converted to symbols based on chosen modulation constellations. A subset of these symbols are taken in parallel, converted to analog form and transmitted across the wireless channel. These signals are associated with timing, frequency and phase parameters. Proper detection at the receiver requires a good estimate of these parameters. Apparently, the synchronization sequence in an OFDM system starts off with firstly coarse timing recovery/frame synchronization. Then comes coarse frequency-offset estimation, fine frequency corrections and finally, fine timing corrections. In general, frame detection is therefore the first step of this process and the later steps are heavily dependent on the accuracy of this step. As was observed in the previous section, it is also a necessary first step in the netted radar sensor. Any incorrect selection of incoming symbols will not only introduce ISI, but also cause the bandpass filter to eliminate useful data embedded in the camouflaging noise signal.

*Noise correlation-based frame timing estimation:*

This is a non-data aided RF-based noise-correlation technique for frame detection in the netted noise radar's receiver. As was seen in previous sections, the incoming signal for the noise radar is a noise-OFDM signal. Most of its spectrum (> 70%) contains UWB noise signal, with the rest containing the OFDM signal.

In this technique, we make use of the cross-correlation properties of band-limited white noise to achieve frame synchronization. This is a simple method which does not require any preamble or transmitter pre-processing in the transmitted packet. The transmitting radar generates OFDM symbols, embeds it into the notched noise signal, and transmits it towards the target. On the side of the receiving radar, the antenna output is continuously converted from analog to digital. The proposed technique is applied to this digitized antenna output for detecting the exact frame boundary of the arriving noise-data signal.

---

[55] P. Moose, "A technique for orthogonal frequency division multiplexing frequency offset correction," *IEEE Transactions on Communications*, **42**(10), pp. 2908-2914, Oct. 1994.

[56] J.-J. van de Beek, M. Sandell, M. Isaksson, and P. Ola Borjesson, "Low-complex frame synchronization in OFDM systems," *Record of the 4th IEEE International Conference on Universal Personal Communications (ICUPC)*, Tokyo, Japan, pp. 982-986, November 1995.

[57] J. Terry and J. Heiskala, *OFDM Wireless LANs: A Theoretical and Practical Guide*. Indianapolis, IN: Sams Publishing, 2001.

Fig. 119 and Fig. 120 concisely explain this noise-based correlation mechanism. There are mainly two branches here. The receiver antenna keeps receiving channel noise when there is no signal present. It passes this channel noise through branch 1 and branch 2 of the system, as shown in Fig. 120. A delayed version (Delay = 1 sample or more) of channel noise is correlated with the incoming channel noise. The output is the maximum of the absolute value of the cross-correlation result vector. The result of this cross-correlation is mostly zero or a very low level magnitude. This happens so because the different samples of the incoming white Gaussian noise are uncorrelated. A sliding window is used in the receiver for implementing this correlation. An appropriate window length is chosen (usually greater than the packet length), and is applied to both branches. Signal samples that come into this window are used for the correlation. The next instant, the earliest sample of the signal is pushed out and the latest sample is pushed in into the window, in both the branches. This is why it is called the sliding window. It is important to note here that we do not have to generate any signal in the receiver, as do some timing estimators[58].

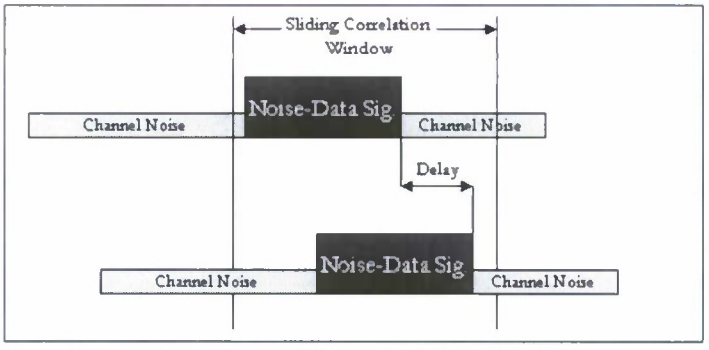


Fig. 119: Depiction of noise-correlation based sliding window on incoming data.

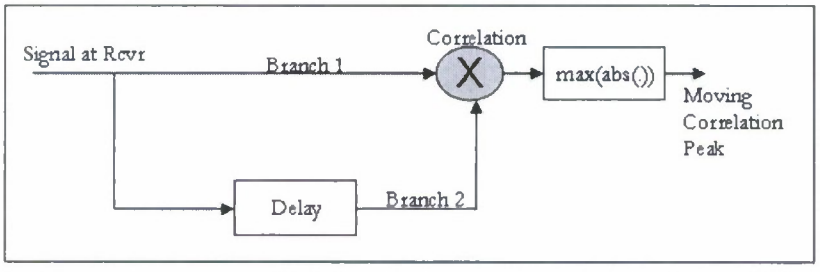


Fig. 120: Depiction of the Netted Noise Radar's Frame Timing Estimator.

When the actual noise data signal starts to come in, it is now being correlated with a delayed version of itself. From the actual mathematical implementation of correlation, we know that one input of the correlator is kept non-moving while the other input is moved against the former input. This is done one sample at a time, in correspondence with the non-moving input for obtaining the result of the correlation at various index values. During this process,

[58] T.M. Schmidl and D.C. Cox, "Robust frequency and timing synchronization for OFDM," *IEEE Transactions on Communications*, **45**(12), pp. 1613-1621, December 1997.

at a particular index value, the noise-data signal starts to overlap itself in the two branches, producing a peak value in the output. As the overlap increases, we see a linear increase in the output and as the overlap decreases we see a linear decrease in the output. There is also a time when the output is a constant value, i.e. a timing plateau exists. This occurs when the window length is greater than the noise-data signal duration. During the duration when the noise-data signal is completely inside the window, but is still moving, every correlation yields the same maximum. The sample index at which it yields the maximum will change, but the value remains the same. It is so because this same maximum value occurs when the two noise-data signals overlap completely.

From the last sample index at which this constant value exists, we can determine the first sample of the incoming noise-data signal, thus estimating the frame/symbol timing. The essential parameters in this method are the window length and the delay. Their selection decides how the output appears. With window length = packet size, the timing plateau in the output can be completely eliminated and a sharp peak indicating the exact start of the frame is observed. Results for various parameter options are also presented below. These simulations were performed on our noise-OFDM data, where the number of sub-carriers was 100, sub-carriers carrying data were 32, and the *SNR* at the receiver = 10 dB.

In Fig. 121, we can see the linear increase and linear decrease in the output that corresponds to an increasing and decreasing correlation magnitude. We also see a constant value in the output and this corresponds to the time during which the entire incoming packet is inside the sliding window. The data point shown indicates the start of the noise-data signal. Thus, by using this simple technique, we are able to achieve frame/timing synchronization for the wireless netted radar system.

Performance comparison

There are a few sliding window-based packet detection algorithms in the literature. Single window, double-sliding window, delay-and-correlate algorithm used in IEEE 802.11a (see Ref. 56) have previously presented the idea of detecting packet boundaries. In the single window technique, an incoming packet is detected as a change in the received energy level. But this technique suffers with the problem of setting an appropriate threshold level for detecting an arriving packet. To overcome this problem, a double sliding window algorithm was used. This again uses the energy of the incoming packet as a parameter, but it used a decision variable which is the ratio of the energies in two windows. Our technique is different from these techniques in two ways. First, we are working with the cross-correlation amplitude of the incoming signal as our decision parameter. Second, we are still working with a single window but without the threshold setting problem. This can be done because our output needs to have a clearly visible ramp-up and ramp-down portion for us to declare a detected packet. Incoming noise-spikes will not be able to produce this and cause drawbacks in our system.

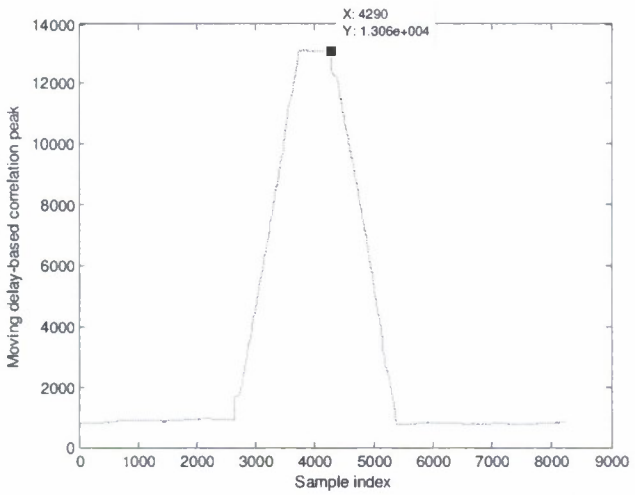


Fig. 121: Noise-data correlation output. Data points shows the frame starting point of the incoming signal.

The delay-and-correlate algorithm used for packet detection in IEEE 802.11a is a preamble-based technique, which is based on the approach provided in Ref. 25. In this method, the decision statistic is based on the ratio of the correlation of the training symbols in the preamble to the energy contained in them. Our technique is an enhanced modification of this technique. We do not use training symbols or preambles in our transmit signal, so we do not need any transmitter preprocessing especially meant for timing correction or packet detection. Next, the decision statistic in our technique is mainly based on the cross-correlation of white noise samples and the autocorrelation of our noise-data signal.

Our technique does not suffer from the timing metric plateau inherent in the method described in Ref. 58. This plateau causes a large variance in the timing estimate, causing an uncertainty in the correct detection of the start of the frame. In our technique, the timing plateau is dependent on the window length parameter. It can be adjusted (window = packet size) to get the variance of the detection estimate to zero, i.e. a single peak can be generated in the output. This peak can now be easily detected by any simple peak detector function. Two methods to reduce the uncertainty to the timing metric plateau have been presented[59], but our technique is unique since Ref. 59 also uses training symbols whereas we do not.

A standard compliant autocorrelation synchronization algorithm has been developed[60], which achieves a synchronization peak at the boundary of the short and long training symbols. Our technique compares well even to this method, in the sense that we adjust the window parameter to obtain a synchronization peak, without the use of short or long training symbols.

---

[59]H. Minn, M. Zeng, and V.K. Bhargava, "On timing offset estimation for OFDM systems," *IEEE Communications Letters*, **4**(7), pp. 242-244, July 2000.

[60]A. Fort and W. Eberle, "Synchronization and AGC proposal for IEEE 802.11a burst OFDM systems," *Proceedings of IEEE Global Telecommunications Conference (GLOBECOM)*, San Francisco, CA, pp. 1335-1338, December 2003.

We present a short summary of the improvements brought forward by our proposed methods in Table VII below.

TABLE VII: COMPARISON OF PERFORMANCE ATTRIBUTES OF THE PROPOSED METHOD WITH LITERATURE

| Method | Decision Statistic | Window length | # of complex multiplications | Preamble usage | Type of output |
|---|---|---|---|---|---|
| Proposed Method | $R(n) = \max \left\| \sum_{n=0}^{Window-Delay-1} r_n r^*_{n+Delay} \right\|$ | Large | One per received sample | Not required | No timing plateau with $W = N$; Easy peak detection |
| Double-sliding window | $m_n = \frac{\sum_{m=0}^{M-1} \|r_{n-m}\|^2}{\sum_{l=1}^{L} \|r_{n+l}\|^2}$ | Short | One per received sample | Not required | Threshold dependent |
| IEEE 802.11a method (D = 16) | $m_n = \frac{\left\| \sum_{k=0}^{L-1} r_{n+k} r^*_{n+k+D} \right\|^2}{\sum_{k=0}^{L-1} \|r_{n+k+D}\|^2}$ | Short | Two per received sample | Required | Presence of timing plateau |

$r_n$ is the $n^{th}$ sample

*Probability Analysis for BER Performance:*

In order for the receiver to perform a discrete Fourier transform (DFT) operation on the incoming OFDM signal to recover the embedded message, it needs all $N_s$ OFDM symbols, namely, $d[0], d[1], \ldots, d[N_s - 1]$. After all of these symbols serially enter the receiver, they are converted to parallel form based on $N$, $N_s$, and passed through a Fourier transform process to extract the data symbols present on each sub-carrier. In case of the radar sensor, the incoming symbols are not simple OFDM symbols, but a composite noise-OFDM signal given by

$$S_r[n] = K_2 A z_1[n] \exp\{j\omega_{o1} n\} + K_2 B z_2[n] \exp\{j\omega_{o2} n\} + K_2 \sum_{k=0}^{N-1} m[k] \exp\{j\omega_k n\} + \xi_2[n] \exp\{j\omega_o n\} \quad (169)$$

Therefore, this signal has to be first passed through a bandpass filter (BPF), which has a transfer function $h_{BP}[n]$, to extract the embedded OFDM signal, i.e. all frequencies $(\omega_0, \omega_{N-1})$. These are the sub-carriers that carry the data from the transmitter. The output of the BPF, $Y[n]$, can be expressed (as stated before) as

$$Y[n] = S_r[n] \otimes h_{BP}[n] \quad (170)$$

The BPF is designed to eliminate the noise-signal centered around $\omega_{o1}$ and $\omega_{o2}$. It also filters the channel noise component to allow through only the portion within its pass-band. Hence we can express the output of the BPF as

$$Y[n] = \alpha K_2 \sum_{k=0}^{N-1} m[k] \exp\{j\omega_k n\} + \alpha \xi_{p2}[n] \exp\{j\omega_{od} n\} \tag{171}$$

where $\alpha$ is the FIR filter response's magnitude ripple coefficient affecting the signal component, $\xi_{p2}[n]$ is the Gaussian output of the linear time-invariant band-pass filter being excited by the zero mean Gaussian noise $\xi_2[n]$, and $\omega_{od}$ is the center frequency of this pass-band. This output $Y[n]$ is then passed through a discrete Fourier transform operation to extract the individual sub-carriers of the OFDM symbols. In the noise-OFDM radar sensor transmitter, the data are BPSK modulated onto different OFDM sub-carriers. Therefore, these sub-carriers are now individually processed through a BPSK demodulation/detection mechanism to finally extract the data transmitted by RS1, namely $m[k], \forall k = 0,1,\ldots,N-1$.

We derive the bit-error-rate (BER) expression for the noise-OFDM system using a single carrier transmission model as a basis by extending the results of OFDM performance under propagation impairments[61,62]. Let us consider a sub-carrier $l$ from the different OFDM sub-carriers present in the output of the BPF in the receiver, as shown in equation (171). The sampled discrete complex baseband signal for this $l^{th}$ sub-carrier after the $N$-point DFT processing in the receiver can be written as

$$Y_l = H_l(D_l + N_l) = H_l D_l + W_l \tag{172}$$

where $D_l$ is the transmitted complex BPSK symbol, $W_l$ is the complex Gaussian noise (with mean 0 and variance $\sigma_w^2$) corresponding to the band-pass filtered channel noise, $H_l$ is the frequency domain band-pass filter transfer function on sub-carrier $l$, which is the DFT of $h_{BP}[n]$ with maximal $L$ taps

$$H_l = \sum_{m=0}^{L-1} h_{BP}[n] \exp\{-j2\pi ml / N\} \tag{173}$$

The BPF in the receiver is pre-designed for the radar sensor system, with $H_l$ corresponding to the magnitude ripple in the pass-band of the filter. It is therefore a deterministic value for each sub-carrier $l$.

---

[61] M. Krondorf and G. Fettweis, "OFDM link performance analysis under various receiver impairments," *EURASIP Journal on Wireless Communications and Networking*, vol. 2008, Article ID 145279, doi:10.1155/2008/145279, 2008.

[62] S.K. Wilson and J. M. Cioffi, "Probability density functions for analyzing multi-amplitude constellations in Rayleigh and Ricean channels," *IEEE Transactions on Communications*, vol. 47, no. 3, pp. 380–386, 1999.

The received signal on the $l^{th}$ sub-carrier $Y_l$, which is a BPSK modulated symbol, can be represented as a two-dimensional vector corresponding to its real and imaginary values as $[Y_{rl}, Y_{il}]$. Let us assume that we transmit a symbol with phase $\theta_y = \tan^{-1}(Y_{il}/Y_{rl}) = 0$. This implies

$$Y_{rl} = \alpha_l \sqrt{\varepsilon_{s,l}} + W_{rl} \tag{174a}$$

$$Y_{il} = W_{il} \tag{174b}$$

where $\alpha_l$ represents the magnitude scaling on the $l^{th}$ sub-carrier, $\varepsilon_{s,l}$ is the signal energy of the symbol being modulated onto the $l^{th}$ sub-carrier, and $[W_{rl}, W_{il}]$ represent the two-dimensional vector corresponding to the band-passed channel noise.

Because $[W_{rl}, W_{il}]$ are zero mean jointly Gaussian random variables, it follows from equation (174) that $[Y_{rl}, Y_{il}]$ are also jointly Gaussian random variables with means $E\{Y_{rl}\} = \alpha_l \sqrt{\varepsilon_{s,l}}$, $E\{Y_{il}\} = 0$, and variances $\sigma_{ry}^2 = \sigma_{ry}^2 = \sigma_{y,l}^2$. Consequently, the joint probability density function (PDF) for $[Y_{rl}, Y_{il}]$ can be written as

$$p_{Y_{rl},Y_{il}}(Y_{rl}, Y_{il}) = \frac{1}{2\pi\sigma_{y,l}^2} \exp\left\{ -\frac{(Y_{rl} - \alpha_l \sqrt{\varepsilon_{s,l}})^2 + Y_{il}^2}{2\sigma_{y,l}^2} \right\} \tag{175}$$

Since the phase of the incoming symbol is modulated with the data, the random variable of interest for finding the bit-error-rate for our system is $\theta_y$. We apply a change in variables to convert $[Y_{rl}, Y_{il}]$ to $[M, \theta_y]$ using

$$M = \sqrt{Y_{rl}^2 + Y_{il}^2} \tag{176a}$$

$$\theta_y = \tan^{-1} \frac{Y_{il}}{Y_{rl}} \tag{176b}$$

This leads us to a joint PDF

$$p_{M,\theta_y}(M, \theta_y) = \frac{M}{2\pi\sigma_{y,l}^2} \exp\left\{ -\frac{M^2 + \alpha_l^2 \varepsilon_{s,l} - 2M\alpha_l \sqrt{\varepsilon_{s,l}} \cos\theta_y}{2\sigma_{y,l}^2} \right\} \tag{177}$$

From this joint density, we can obtain the marginal density of $\theta_y$ by integrating equation (177) over the complete range of $M$, *i.e.* $[0, \infty]$, to obtain $p_{\theta_y}(\theta_y)$. Therefore, we have

$$p_{\theta_y}(\theta_y) = \int_{M=0}^{\infty} p_{M,\theta_y}(M,\theta_y)\,dM$$

$$= \frac{\exp\left\{-\alpha_l^2 \varepsilon_{s,l} \sin^2\theta_y / 2\sigma_{y,l}^2\right\}}{2\pi\sigma_{y,l}^2} \int_{M=0}^{\infty} M \exp\left\{-\frac{\left(M - \alpha_l\sqrt{\varepsilon_{s,l}}\cos\theta_y\right)^2}{2\sigma_{y,l}^2}\right\} dM \tag{178}$$

When a BPSK symbol with zero phase is transmitted, we allow for $\pm\frac{\pi}{2}$ error in deciding whether an incoming symbol falls into the range allowed for zero. Any other phase value implies a decision error. Therefore, the probability of bit-error (symbol-error also in BPSK case) for the $l^{th}$ sub-carrier is given by integrating equation (178) over this appropriate range and subtracting it from unity, as follows

$$P_b(Y_l) = 1 - \int_{-\frac{\pi}{2}}^{\frac{\pi}{2}} p_{\theta_y}(\theta_y)\,d\theta_y \tag{179}$$

For our BPSK based $l^{th}$ sub-carrier, equation (179) can be reduced to equation (180) by substituting $p_{\theta_y}(\theta_y)$ and integrating it over the given range, resulting in

$$P_b(Y_l) = Q\left(\sqrt{\frac{\alpha_l^2 \varepsilon_{s,l}}{\sigma_{y,l}^2}}\right) \tag{180}$$

Finally, the general bit-error-rate of our noise-OFDM system can be found by averaging over all the $N$ data sub-carriers with index $l$, and can be expressed as

$$P_b = \frac{1}{N}\sum_{l=-\frac{N}{2}}^{l=\frac{N}{2}} P_b(Y_l) = \frac{1}{N}\sum_{l=-\frac{N}{2}}^{l=\frac{N}{2}} Q\left(\sqrt{\frac{\alpha_l^2 \varepsilon_{s,l}}{\sigma_{y,l}^2}}\right). \tag{181}$$

For verifying the BER expression given in equation (181) against our simulation, we approximate $\alpha_l$ with its average value over all the $l$ sub-carriers denoted as $\alpha$, which is a reasonable assumption. Thus, the BER expression for the noise-OFDM system can be approximated as shown below in equation (182), where $\varepsilon_s$ denotes the OFDM signal energy in all of its sub-carriers (since for BPSK, the energies of different symbols ported on different carriers are equal) and $\sigma_y^2$ denotes the band-passed noise energy in all the $l$ sub-carriers:

$$P_b = Q\left(\sqrt{\frac{\alpha^2 \varepsilon_s}{\sigma_y^2}}\right) \tag{182}$$

Fig. 122 illustrates the calculated and simulated noise-OFDM BER versus SNR, under an AWGN channel. As seen from the plot, the results closely match each other, proving independent validation of the bit-error-rate expression.

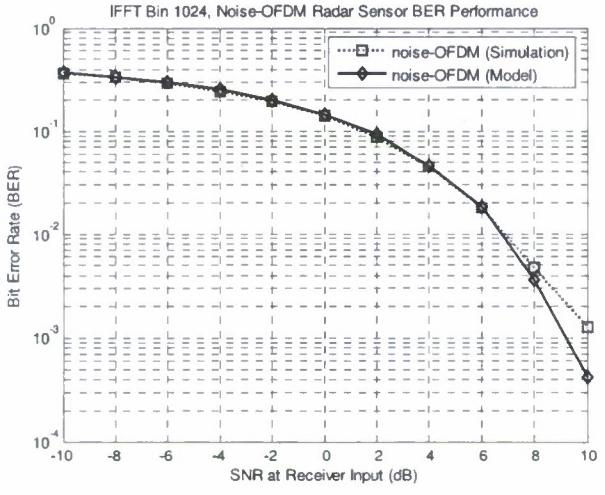


Fig. 122: Comparison of BER performance between theory and simulation.

*Message Integrity:*

Message integrity aims to protect the message from unauthorized modifications. Attacks on the integrity of messages exchanged over a wireless communication channel include typically message modification and message overshadowing (an original signal appears as noise in a much stronger attacker's signal, which is then accepted as valid by the receiver). In the noise-OFDM system, we incorporate message integrity protection with the use of what we call "Integrity Transforms" and "Integrity Carriers". From the discussion on the communication-receiver-subsystem, Fourier Transform operations are performed in the transmitter as well as the receiver. In the transmitter, inverse discrete Fourier transform (IDFT) is used to transform data from the frequency domain to the time domain. This procedure actually spreads the data in the time domain. It is almost similar to time domain encryption, with the encryption algorithm being the FFT implementation. This simple Fourier transform can be converted to an Integrity Transform by adding a secret key, known only to all radar sensors within the system, to the data sub-carriers prior to the OFDM modulation operation. At the receiver, the Fourier transform of the secret key is first subtracted from the received signal, followed by a DFT operation to regenerate the frequency domain signal onto which data are modulated. Therefore, even if the three parameters of this system were to become known to any hostile electronic system, it cannot decipher the data modulated onto the OFDM waveform since it lacks the secret key. Without the secret key, the error rate of noise-OFDM demodulation is quite high, as can be noted from the simulation presented in Fig. 123. In this plot, we compare the BER performance of a radar

sensor which possesses the secret key (friend), with other hostile systems not possessing the secret key (foe). The plot shows that with increasing SNR, the BER curve for the friend reduces as expected, while it attains a high error floor for the foe. Thus for positive SNR regions, this secret key facilitates in securing the data without the use of any application layer encryption algorithms.

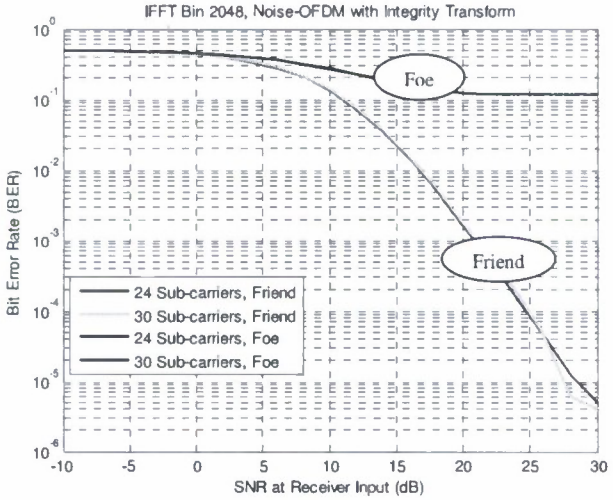


Fig. 123: BER performance of the noise-OFDM system with Integrity Transform and Data Redundancy. Friend: Known secret key, Foe: Any hostile system.

For message integrity protection, the transmitter maps a known symbol onto a specific sub-carrier, called the "integrity carrier", before the secret key is added to all the sub-carriers. This integrity carrier is also known to all radar sensors of the system. As mentioned above, the IDFT of the secret key is subtracted from the incoming signal, before it is passed through the DFT process. The output is a set of data carrying orthogonal frequencies. The integrity carrier is demodulated and the symbol output is compared with the known symbol that should ideally be present. If they match, the receiver can guarantee that the message's integrity has not been violated. Otherwise, the message has been tampered with. This conclusion can be drawn due to the spreading property of the Fourier transform operation. The known symbol is spread throughout the time domain symbol due to the Fourier transform. Hence, any integrity violation in the time domain will also affect the known symbol. The message tampering will therefore be apprehended after the DFT process in the receiver by comparing the transmitted known symbol to the received symbol. It is to be noted that we are operating under a trust model where none of the radar sensor nodes has been compromised and a sufficiently good BER exists that would allow very low errors caused by channel noise. Thus, by only adding a summation and a subtraction operation (since the IDFT of the secret key can be computed just once and stored in the radar sensor), we are able to incorporate two security measures into the system: increasing message secrecy and protecting message integrity.

*UWB-Noise-OFDM-based Multi-radar Network: Design and Analysis:*

The UWB-Noise-OFDM-based architecture is capable of communicating its data to another radar in its range, in addition to being able to perform high resolution imaging. We now consider multi-radar operation which has several defense applications. Having multiple radars talking to each other provides significant benefits in target detection and recognition by taking advantage of multi-aspect and multi-look fusion techniques[63,64]. In such situations, a number of radar sensors are required to simultaneously utilize the same radio spectrum for target detection and network communication. In such cases, if narrow-band communication is being used between two communicating nodes, the entry of additional nodes in the neighborhood will give rise to interference, causing collisions, and leading to a complete loss of communication. As an example, we present the UAV-based Perimeter Surveillance concept in Fig. 124.

The narrowband community has worked on the problem of interference minimization. It also allows all the entities in the system to communicate either on a time-shared (TDMA) or frequency-shared (FDMA) or code-shared (CDMA) basis. Current MAC protocols proposed for narrowband wireless systems like CSMA/CA, IEEE 802.11, IEEE 802.15.3 and their variations are unsuitable for the UWB system because of a number of reasons[65]:

- Clear channel assessment is necessary for CSMA/CA method of channel access. In case of UWB, clear channel assessment by energy detection is difficult with UWB-PHY because of very low power emissions
- CSMA protocol is not suitable for spread spectrum signals with high processing gain
- Voice and video, which are the targeted applications for UWB technology, cannot tolerate large transmission delays and jitter
- High channel acquisition time because of long synchronization between transmitter and receiver causes CSMA/CA to deliver poor channel utilization for short packet sizes
- Most other MACs fail to take advantage of UWB properties like localization, highly secure low power operation and large bandwidth.

We investigate a complete network stack for providing situational awareness using UWB noise radars and the concepts of ad hoc networks. We have already seen the development of the PHY (physical layer of this concept) or the point-2-point communication structure in previous sections of this report. This was designed and analyzed for just one transmitter and one receiver. But when we have several transmitting/receiving radars in our system, then it is mandatory that this system support multi-user access. Since this is a wireless channel, multi-user capability is provided by building a second layer on top of PHY. This is the medium access control layer (MAC).

---

[63] P. Bharadwaj, P. Runkle, L. Carin, J.A. Berrie, and J.A. Hughes, "Multiaspect classification of airborne targets via physics-based HMMs and matching pursuits," *IEEE Transactions on Aerospace and Electronic Systems*, vol. 37, no. 2, pp. 595-606, April 2001.

[64] Z. Li, S. Papson, and R.M. Narayanan, "Data level fusion of multi-look inverse synthetic aperture radar (ISAR) images," *IEEE Transactions on Geoscience and Remote Sensing*, vol. 46, no. 5, pp. 1394-1406, May 2008.

[65] A. Gupta and P. Mohapatra, "A survey on ultra wide band medium access control schemes," *Computer Networks: The International Journal of Computer and Telecommunications Networking*, **51**(11), pp. 2976-2993, August 2007.

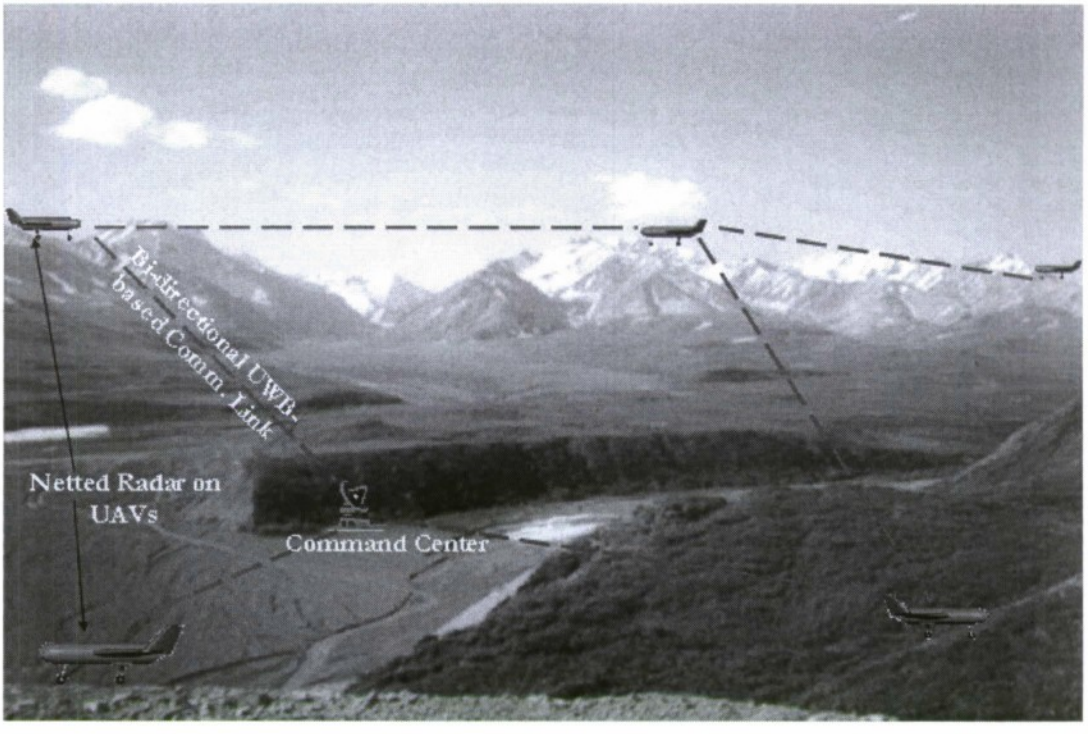


Figure 124: Concept of a UWB-Noise-OFDM-based Multi-radar UAV Network.

The main design primitives of MAC are[66]:

- *Collision avoidance*: It determines when and how a node can access the medium and send its data. Collisions are not always completely avoided in regular operation; contention-based MAC protocols accept some level of collisions
- *Energy efficiency*: Depends on the application and the type of nodes being used
- *Scalability and adaptability*: are closely related attributes of a MAC protocol that accommodate changes in network size, node density and topology. Some nodes may die over time; some new nodes may join later; some nodes may move to different locations. A good MAC protocol should accommodate such changes gracefully. Scalability and adaptability to changes in size, density, and topology are important attributes, because these networks are deployed in an ad hoc manner and often operate in uncertain environments
- *Channel utilization*: reflects how well the entire bandwidth of the channel is utilized in communications. It is also referred to as bandwidth utilization or channel capacity
- *Latency*: refers to the delay from when a sender has a packet to send until the packet is successfully received by the receiver
- *Throughput*: (often measured in bits or bytes per second) refers to the amount of data successfully transferred from a sender to a receiver in a given time. Many factors affect the

[66] W. Ye and J. Heidemann, "Medium Access Control in Wireless Sensor Networks," *USC/ISI Technical Report ISI-TR-580*, October 2003.

throughput, including efficiency of collision avoidance, channel utilization, latency and control overhead

- *Fairness*: reflects the ability of different users, nodes, or applications to share the channel equally. It is an important attribute in traditional voice or data networks, since each user desires an equal opportunity to send or receive data for their own applications

With respect to UWB networks, along with these primitives there are other design issues:

- High channel acquisition time as a result of long synchronization
- Ranging abilities
- Low power operation
- Low probability of detection and jamming
- Carrier-less pulse position modulation
- Providing a method to allow a user to decode a particular data stream
- Techniques to build the system with sufficient performance or cost advantage over existing approaches to justify the effort and investment

Also, in general we see that the following are the criteria on which MAC protocols proposed for UWB technology are measured:

- MAC functions are implemented in a centralized or distributed manner, the MAC organization is cluster based or distributed
- Implementation of quality of service functionalities
- Media access and sharing: UWB technology has been implemented as Time Hopping Impulse Radio (TH-IR), Direct Sequence UWB and Multi-band UWB. Radio access can be contention based or scheduled based on a pre-determined protocol
- Power control and efficiency is important for UWB based networks because of the requirement for low power emissions
- Ranging: UWB technology enables high precision ranging. Ranging information can be utilized for development of distance based power-aware protocols, development of positioning protocols that can help build a relative network map to enable localization aware routing and data processing, enabling dynamic transmission power control

*MAC Protocol for Noise-based Multi-radar Networks:*

The above paragraphs introduced the generic design primitives, issues and criterion involved in designing a medium access control protocol for UWB-based systems. Specifically for multiple-radar and noise-OFDM based physical layer specifications, there are further questions that the MAC protocol must resolve. We first present an initial state of the algorithm for medium access in wireless netted radars then discuss the different problems that it fails to address. We finally present a complete prototype design for MAC in wireless networked radars that resolve all issues for maximized medium access.

OFDMA Based Medium-Access Algorithm

We had presented a similar algorithm earlier for simple scenarios. However, that algorithm is not scalable to accommodate newer users and it would not re-use sub-carriers due to static allocation. Presented here under is a modified approach, the goal of which is to have all users of the system transmitting at the same time, but sharing the media through orthogonal usage of the individual sub-carriers.

The UWB frequency range is either 1-2 GHz or 3-4 GHz. A fragmental portion (<10%) of this range is notched and applied for data communication. The rest has UWB white noise. The number of users/radars in the system is varying. Multiple users need to share the same spectrum. The algorithm is as follows:

Step 1. Apply OFDMA channelization to the sub-band that is allocated for data communication and obtain orthogonal frequencies (sub-carriers) that can be allotted to different radars/users in the system. This is shown in Fig. 125.

Step 2. Choose a set of orthogonal carrier frequencies that lie in the above notched band. Each (transmitter, receiver) duple in the system, that would like to communicate is assigned a set of specific frequencies (sub-carriers) on which the duplet's data is modulated. This is the initial static assignment. But when the network topology changes (users power-down, move out of range or want to communicate with other entities), then this assignment needs to be changed to effectively utilize the medium. Not just changing the assignment, all the users in the system must also be made aware of this new assignment.

Step 3. This mapping of a duple to its transmit frequency is made known to all the users/radars in their vicinity. No two duplets use the same frequency.

Step 4. To ensure transmit covertness, every user first modulates the transmit data onto his/her assigned frequency. The user also modulates random data onto other orthogonal carriers available, which are not assigned to any other radar. This complete OFDM signal is then added to the notched band-limited noise spectrum and transmitted. This is shown in Fig. 53.

Step 5. All other duplets in the vicinity similarly create their noise-OFDM signal and transmit it out in the medium. Any radar/user in the vicinity of the transmitting radars will receive this complete noise-OFDM signal.

Step 6. The receiving radar uses OFDM demodulation to detect and decode the signal and obtains its data. The other carriers are neglected.

Step 7. Other duplets can simultaneously transmit over the same spectrum as they have no other duplet transmitting data on their assigned frequency, thus enabling multi-user access of the available UWB spectrum.

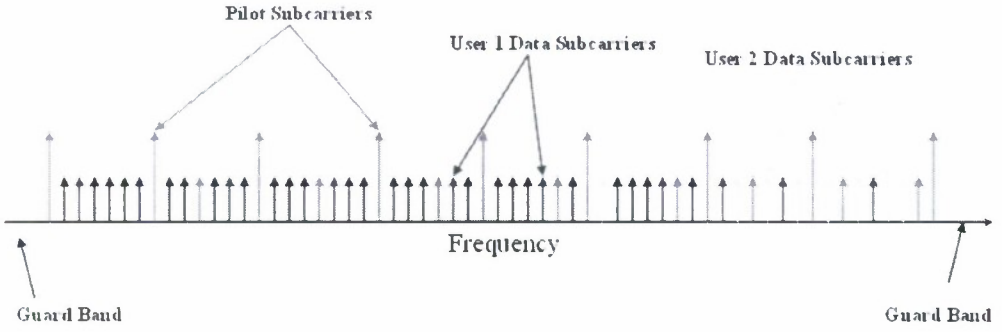


Figure 125: General OFDM symbol representation.

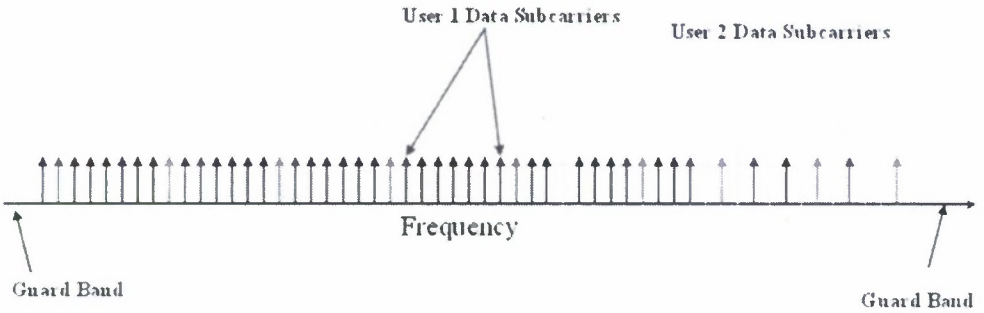


Figure 126: Netted Noise Radar case. OFDM spectrum embedded into notched UWB-noise. OFDM symbol without pilots but with dynamic sub-carrier assignment for enhanced medium usage.

The above steps provide for creating a shared point-to-point link between radars. Using this communication link and the well-known flooding algorithm or any ad hoc routing protocol (in a higher layer of the network stack), a multi-hop covert communication network can be established between the radar sensors.

The above algorithm is useful, but it does not provide for two important design attributes of any MAC protocol: scalability and adaptability. These issues are further discussed in the following two problems.

*Problem 1: Multi-radar communication using noise-OFDM*

Let us suppose that there are two radar sensors (R1 and R2) in our system to help us monitor a perimeter, as shown in Figure 127 below. By definition, these radar sensors are equipped with the capability of embedding data into their notched noise signal. R1 transmits $\alpha$ (as given by equation (141)) and R2 transmits $\beta$ (again as given by equation (141) but noise being generated from a different source). As previously stated, both the radars comprise of a tracking subsystem and a communication subsystem. The following observations can be derived from Fig. 127.

R1: Transmits α, Receives (α-e + β + β-e)
R2: Transmits β, Receives (β-e + α + α-e)

where α-e is the target echo due to R1's transmission and β-e is the target echo due to R2's transmission.

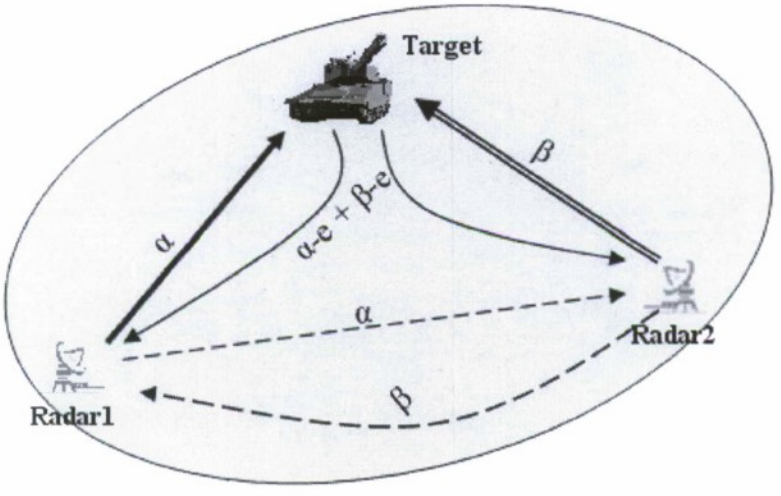


Figure 127: Multiple echo problems in a Multi-radar setup.

Consider R2. Its received signal consists of not just the target echo due to its own transmission, but also the target-echo due to the R1's transmission and R1's direct signal to it. This complete signal goes through to the tracking and communication subsystems of R2. In the tracking subsystem, the received signal is cross-correlated with a delayed replica of β in order to obtain the range information of the target. Since we are using UWB noise waveforms to construct α and β, they are uncorrelated by their construction. Hence the presence of α, and α-e does not disturb the operation of the tracking subsystem.

But when we observe the communication subsystem, it is supposed to process the signal coming from R1 to detect and demodulate the data that R1 wants to communicate to R2. Here, the received signal is passed through a band-pass filter to only allow the embedded OFDM data in α to come in to the system. Within this subsystem, the presence of β-e, and α-e can cause errors in the demodulation process of the OFDM symbol. This is because both the target echoes will have some power in the frequency band that is being used for OFDM. Therefore, it is important to make sure that the sub-carriers, on which R1 is transmitting data to R2, are not affected by the corresponding sub-carriers in the target echoes. This is an important issue that our MAC protocol will have to resolve.

*Problem 2: Dynamic sub-carrier allocation in mobile radar sensors*

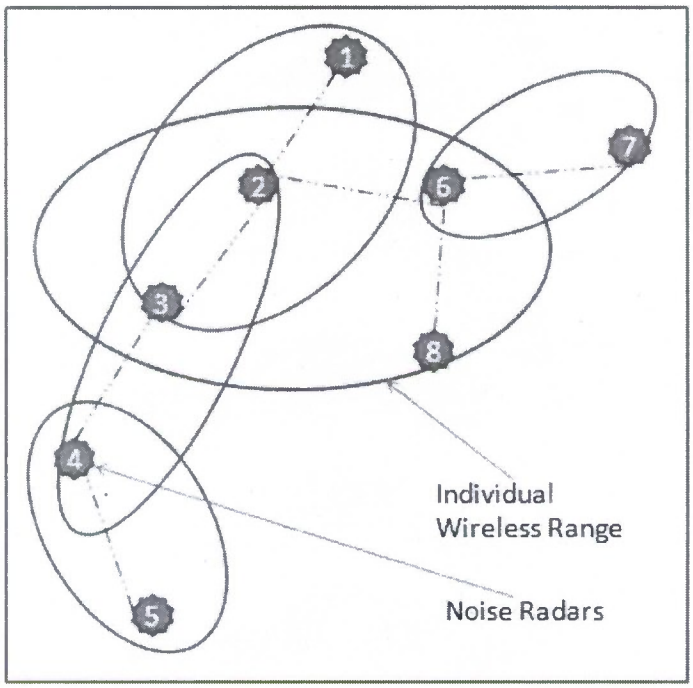


Figure 128: Requirements - {small wireless range, networked operation, spectrum sharing, covert waveforms, radar operation}, for developing a multi-hop network, effective utilization of medium/sub-carriers between the noise radars is required.

A multi-hop network of radars as shown in Fig. 128 is our primary goal. In this type of a topology, it is easy to observe that the sub-carriers in the OFDM signal need not be statically divided and allocated to a specific set of radar sensors. It is quite possible that a few radars might not have been deployed yet or that most of the radars are spatially away from each other. For example, in the above network, only radars 2, 3, 6, and 8 are required to share a given frequency spectrum. Radar 1 could possibly use the same sub-carriers as those being used by 4. This is very similar to the concept of frequency-reuse in cellular system. The only difference being that the ranges here are quite smaller compared to the size of a sector or a cell in a cellular system. In the current configuration, the available OFDM spectrum can be shared by radars 2, 3, 6 and 8. But when either of them goes down or a new radar appears, then the allocation of sub-carriers between the radars needs to be changed to accommodate the new radar. Hence we see that there is a requirement for dynamic sub-carrier allocation in the OFDM symbols that are being embedded into the notched noise spectrum[67],[68].

[67] T.C.H. Alen, A.S. Madhukumar, and F. Chin, "Capacity enhancement of a multi-user OFDM system using dynamic frequency allocation," *IEEE Transactions on Broadcasting*, vol. 49, no. 4, pp. 344-353, December 2003.
[68] J. Gross, M. Emmelmann, O. Puñal, and A.Wolisz, "Dynamic single-user OFDM adaptation for IEEE 802.11 systems," *Proc 10th ACM International Symposium on Modeling, Analysis, and Simulation of Wireless and Mobile Systems (MSWiM 2007)*, Chania, Crete Island, Greece, pp. 124-131, October 2007.

To alleviate these issues, we modify the OFDMA-based MAC algorithm to enable multi-user access with dynamic sub-carrier allocation for the embedded OFDM symbols.

*MAC Design for multi-user OFDM based Netted Radar System:*

Design Directives

- **Physical Layer Mechanism:** We are not directly using OFDM, but are embedding OFDM in notched UWB noise for providing covertness and LPI, LPD capabilities.
- **Control Carrier:** OFDM allows us to simultaneously use many orthogonal frequencies for communication. We select one frequency (a central frequency) out the many available frequencies as our control signal carrier. Slotted ALOHA[69] time division multiple access technique is employed on this carrier, to make it a control carrier. Every radar is allowed to contend for it and start using it at the start of a time slot. All signaling to establish communication between radars will happen through this carrier. All the radars will continuously be listening on this frequency for updates about the communication channel
- **Primary Index, (TxRadar, RxRadar) Duple:** Usually, sets of non-overlapping sub-carriers are allotted to users to allow for multi-user capability in down-link based OFDM systems. For our netted radar, we are not looking at a single base-station controlling the communication between itself and many subscribers. But our system is an ad hoc network of radars where we will like every radar to be able to communicate with any other radar in the system. Towards this, we have present a solution which is based on the (Transmit, Receive) duple. That is, the radars coordinate among themselves to assign a communication frequency for every 'unique' transmit radar and receive radar duple.
- **MESH Network:** This kind of a MAC will be mainly useful in a mesh kind of a network where the requirement could be that many different routes might exist between a source and destination, as is the case for battlefield deployments.

Description

As noted above, the aim is to have simultaneous communication between various radars using the same available spectrum. We use Fig. 129 to explain this further. Let us say, F1, F2 to FN are our available orthogonal sub-carriers in the 1-2 GHz range. We denote F1 as our Control Carrier, which is working on the slotted ALOHA principle.

Now Radar 2 and Radar 3 both want to send their data to Radar 1 so that it can transmit it to the base-station for further processing. Conventionally, one of them will have to talk to Radar 1 first and then the other can go ahead. But in our case, we want both of them to simultaneously be able to talk to Radar 1. Here, R2 uses the first slot to tell that it wants to talk to R1 and gives a list of the open frequencies it has at its disposal. Similar message is sent by R3 to R1. Now, R1 might be talking to many other radars in its vicinity on many other frequencies. So it selects an available frequency from the set sent by the R2 and R3 respectively and transmits the acknowledgement out to the two radars in next two slots on F1. With this, R2 knows that it received F4 for itself and R3 knows that it received F5 for

[69] http://www.laynetworks.com/Slotted%20Aloha.htm

itself. Now, both of the radars can use OFDM for simultaneous communication with R1. Similarly, R2 can setup another communication with R3 also. And since the ACK from R1 is on the control carrier, other radars in the communication vicinity can now take off F4 and F5 from their list of open frequencies. Thus multi-user communication is established in this system.

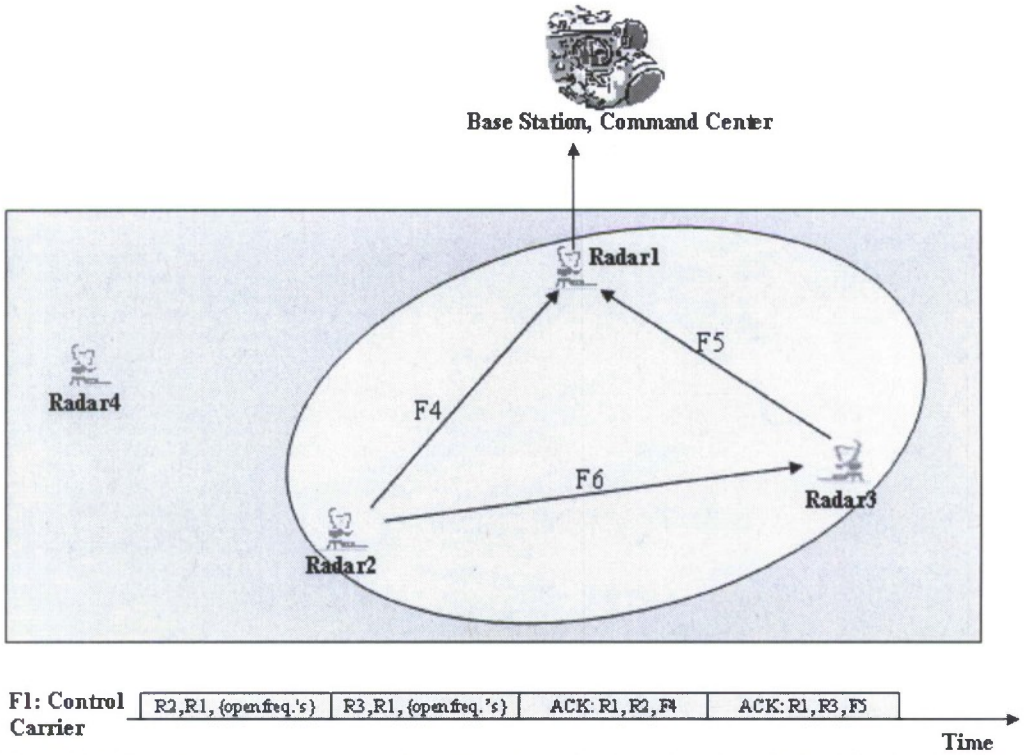


Fig. 129: Dynamic sub-carrier allocation per duplet, for the Netted Radar Sensor.

Now, this F1, F2 to FN need not be single carriers, but can be a set of contiguous sub-carriers, thus allowing high data rates for the radars.

Thus with this MAC design, we aim to achieve Scalability and Adaptability, good Channel Utilization and Fairness in our system. We are currently working on complementing the theoretical analysis of our MAC concept with concrete mathematical and simulation proofs.

*Related Work in UWB-based MAC Protocols:*

1. Most of the literature on UWB-based MAC protocols has been designed for a downlink channel only. That is, there is one single central station which will do sub-carrier allocation. It will then transmit this information to all the users in the network. And this allocation is meant for all the users to simultaneously talk to the central station only (as shown in Fig. 130). Whereas for medium access in radar sensor nets, it is the presence of more than transmitter/receiver that acts as a challenge.

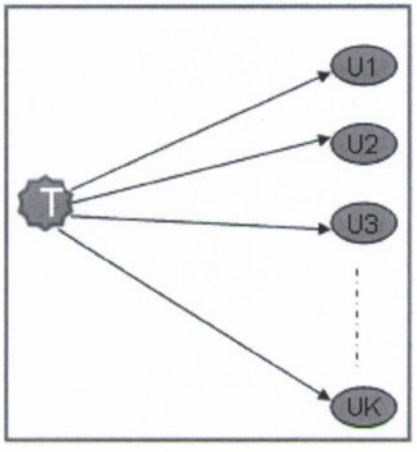


Figure 130: Downlink Channel, one Transmitter sending data to *K* users using OFDM.

2. While this has been characterized as a decentralized approach, as seen in Figure 57 above, we note that it is centralized in the transmitter. What we need is a truly decentralized dynamic sub-carrier allocation algorithm for medium access in OFDM networks
3. Another assumption in most of the literature is that the sub-carrier and bit allocation information is transmitted to each receiver via a separate control channel.
4. In order to reduce the complexity of the problem, a few of the related techniques assume that each user is allocated an equal number of partitions. This actually defeats the purpose of dynamic allocation, since using this we want to decide on the fly as to which sub-carriers should be used for which users. This is to maximize medium utilization.

- A comparison between an approach developed by Broustis et al. and our approach is provided in Table VIII.

TABLE VIII: COMPARISON OF A DOWNLINK-BASED MAC AND OUR MULTI-USER MAC

| MAC Protocol for Impulse-based Ultra-wide band Ad hoc Networks[70] | MAC Protocol for OFDM-based Ultra-wide band Radar Networks (Our approach) |
|---|---|
| Motivation for new MAC Protocol:<br>• Short pulses, pronounced effect on UWB-PHY due to multi-path delay spread<br>• No carrier, cannot use carrier-sense multiple access<br>• Wide range of UWB, effects 802.11 networks, interoperability | • All of these<br>• No known protocol in literature<br>• OFDM-based MAC introduced for netted radar |
| Conformance to FCC Regulations<br>• Effective isotropic radiated power (EIRP) <= -41.25 dbm/Mhz<br>• Peak power limitations<br>• 500 MHz of absolute bandwidth or fractional bandwidth >= 20% | • EIRP and peak power, based on the application area<br>• Satisfies fractional bandwidth requirement |
| Encoding Information<br>• Pulse position modulation<br>• 1/3 convolutional codes<br>• repetition code of 2 | • Currently using DPSK and modulating the symbols onto OFDM<br>• Source/Channel coding not considered |
| Time Hopping<br>• Control band only (used by different devices to request and reserve a band for their use) | Presence of a control carrier within the data bandwidth, thus preserving covertness |
| Effects of wireless channel impairments and their impact on the MAC protocol design<br>• Pathloss, multi-path, shadowing<br>• Cross-layer optimization | < Future Work > |
| Time synchronization<br>• Receiver/transmitter synchronization to the control band chip-times | • Noise-correlation based frame timing estimation |
| Multi-hop communications<br>• Coping with hidden terminals | OFDM-based MAC algorithm for multi-user access. No hidden terminal problems |
| Simulator requirements<br>• Network layout<br>• Frame structures<br>• Traffic characteristics<br>• Collisions and errors<br>• Mobility model<br>• Back-off and retransmission | < Future work > |
| Performance Metrics<br>• Pulse collisions<br>• Bit error rate<br>• Average packet delay<br>• Throughput<br>• For multi-band, band occupancy | < Future work > |

[70] I. Broustis, S. Krishnamurthy, M. Faloutsos, M. Molle, and J. Foerster, "A Multiband MAC Protocol for Impulse-based UWB Ad Hoc Networks," *Proceedings of IEEE Conf. on Sensors and Ad-Hoc Communications and Networks*, Santa Clara, CA, pp. 452-462, September 2005.

## 3. PERSONNEL SUPPORTED

The following professional personnel were supported by and/or associated with the research effort:

1. Ram M. Narayanan, Professor, Department of Electrical Engineering
2. Kyoung D. Kim, Graduate Student, Department of Electrical Engineering
3. Wiriyanto Darsono, Graduate Student, Department of Electrical Engineering
4. Wei-Jen Chen, Graduate Student, Department of Electrical Engineering
5. Qihe Pan, Graduate Student, Department of Electrical Engineering
6. Shrawan C. Surender, Graduate Student, Department of Computer Science and Engineering

## 4. PEER-REVIEWED PUBLICATIONS

(1) S.C. Surender and R.M. Narayanan, "Covert UWB Noise-OFDM Netted Radar: Physical/MAC Layer Design and Analysis," *IEEE Transactions on Aerospace and Electronic Systems*, submitted August 2008.

(2) W.-J. Chen and R.M. Narayanan, "Integration of Generalized Likelihood Ratio Test and Tapped Delay Line Beamforming for Ultrawideband MIMO Noise Radar," *IEEE Transactions on Aerospace and Electronic Systems*, submitted December 2008.

(3) Q. Pan and R.M. Narayanan, "Design and Performance of an RF Tag System Using Ultrawideband Noise Waveforms," *IEEE Transactions on Aerospace and Electronic Systems*, submitted January 2009.

## 5. INTERACTIONS AND TRANSITIONS

### 5. 1. Presentations at Meetings and Conferences

(1) S.C. Surender and R.M. Narayanan, "Covert Netted Wireless Noise Radar Sensor: OFDMA-Based Communication Architecture," *Proceedings of the IEEE Military Communications Conference (MILCOM'06)*, Washington, DC, doi: 10.1109/MILCOM.2006.302491, October 2006.

(2) S.C. Surender and R.M. Narayanan, "Synchronization for Wireless Multi-Radar Covert Communication Networks," *Proc. SPIE Conference on Defense Transformation and Net-Centric Systems*, Orlando, FL, Vol. 6578, doi: 10.1117/12.720220, April 2007.

(3) R.M. Narayanan, "Ultra Wide Band Noise Radars," *Proc. International Radar Symposium India (IRSI-07)*, Bangalore, India, pp. P14–P18, December 2007 (**Plenary Paper**).

(4) B.D. Paul, N.B. Sinha, R.N. Bera, and R.M. Narayanan, "Three Dimensional Processing of Digital Array MIMO Radar and its Performance Analysis," *Proc. International Radar Symposium India (IRSI-07)*, Bangalore, India, pp. 134–138, December 2007.

(5) Q. Pan and R.M. Narayanan, "An RF Tag Communications System Model for Noise Radar," *Proc. SPIE Conference on Wireless Sensing and Processing III*, Orlando, FL, Vol. 6980, pp. 698007-1–698007-12, doi:10.1117/12.777394, March 2008.
(6) W.-J. Chen and R.M. Narayanan. "A Direction Finding Algorithm for MIMO Radar System with Transmitting Diversity," *Proc. SPIE Conference on Wireless Sensing and Processing III*, Orlando, FL, Vol. 6980, pp. 69800M-1–69800M-12, doi:10.1117/12.777395, March 2008.

### 5. 2. Consultative and Advisory Functions

The PI made contact with French Air Force Commandant Jacques Raout who is working in the areas of STAP processing and noise radar at the Research Center of the French Air Force, Morpho Analysis in Signal Processing Laboratory, Salon de Provence, France. The PI is also arranging for Commandant Raout's visit to the U.S. to meet with researchers from AFOSR and AFRL, and to explore collaborative research opportunities.

### 5. 3. Transitions

None to report.

## 6. NEW DISCOVERIES AND INVENTIONS

None to report.

## 7. HONORS AND AWARDS

### 7. 1. This Project Period

None to report.

### 7. 2. Lifetime Honors

(1) Fellow of the IEEE, elected 2001 (Ram M. Narayanan)
(2) Fellow of the SPIE, elected 2004 (Ram M. Narayanan)